THE INTERACTION BETWEEN CROSS-SECTIONAL DISTORTION ~~DEFORMATION~~ AND THE FATIGUE BEHAVIOUR OF BOX GIRDER CORNER WELDS

A thesis submitted for the Degree of

Doctor of Philosophy in the

Faculty of Engineering of

The University of London

by

Khosrow Ghavami, B.Sc.(Hons.), M.Sc., D.I.C.

Imperial College of Science and Technology

London

November, 1976

ABSTRACT

This thesis is concerned with the problem of cross-sectional distortion in box girder bridges, particularly its effect on the fatigue life of corner welds. Methods for calculating distortional stresses in box sections are reviewed, and a simplified approach is developed for estimating these stresses in single-cell and multi-cell bridge structures.

A brief survey of the main parameters affecting the fatigue life of welded joints is outlined. A special type of specimen was designed to investigate the fatigue behaviour of different types of corner welds, commonly used in bridge construction, when subjected to fluctuating transverse bending stresses. The results of over one hundred tests are used to compare the performances of the various joints and to provide basic data for their design. Special attention is paid to the effects of poor fit-up between plates in fillet welded joints, and of sealing runs in butt welded joints. The statistical method used to analyse the results is given.

The fatigue lives are shown to be Log N ormally Di stributed and S-N and P-S-N curves for various fillet welded joints are statistically derived. Poor fit-up of plates significantly reduces the fatigue life of welded corners. Residual stresses are shown to affect the fatigue behaviour and failure mode of the corner joints. Finally, the significance of the presence of a fatigue crack on the distortional bending stresses in box sections is studied using the finite element method.

ACKNOWLEDGEMENTS

The research work presented in this thesis was carried out in the Structures Section of the Civil Engineering Department of Imperial College, University of London.

The author wishes to express his deepest gratitude for the active supervision and encouragement given throughout the work by his supervisor Dr. P.J. Dowling, Reader in Steel Structures. The author also gratefully acknowledges the support given by Professor B.G. Neal, Professor of Engineering Structures. The investigation was begun under the general direction of the late Professor S.R. Sparkes, formerly Professor of Engineering Structures.

The author also thanks his friends and colleagues for all their help, particularly Dr. K.R. Moffatt for so freely providing his F.E. computer programme.

Thanks are also due to the Technical staff of the Structural Engineering Laboratory led by Mr. J. Neale, and in particular to Mr. R.A. Mason, a former member of staff who welded all of the specimens, to Mr. J. Finn who helped with the experimental work, and to Mr. F. Winser for machining the specimens.

Special thanks are due to Miss C.D.M. Collins for typing the manuscript and to Miss J. Gurr for preparing the photographs.

The author wishes to record his gratitude to the Bridges Engineering Standard Division of the Department of the Environment (DoE) and to the Constructional Steel Research and Development Organisation (CONSTRADO) for their sponsorship of the experimental investigation.

Finally, but in no way least, the author is deeply grateful to his fiancée, Ursula Schüler, for preparing the drawings and for the extreme patience and understanding she has shown during the course of the study.

CONTENTS

		Page No.
ABSTRACT		3
ACKNOWLEDGEMENTS		4
CHAPTER ONE:	INTRODUCTION	14
1.1	GENERAL	14
1.2	BACKGROUND AND OBJECTIVES OF THIS RESEARCH	15
1.3	THE FATIGUE PROBLEM	16
1.4	SCOPE AND PRESENTATION OF THE THESIS	17
CHAPTER TWO:	CROSS-SECTIONAL DISTORTION DUE TO ECCENTRIC LOADING IN BOX GIRDER BRIDGES	20
2.1	GENERAL	20
2.2	SINGLE CELL BOX GIRDER UNDER ECCENTRIC LOADING	20
2.3	AVAILABLE METHODS OF ANALYSIS	22
	2.3.1 Richmond Displacement Solution	22
	2.3.2 Beam on Elastic Foundation Analogy	24
	2.3.3 The Finite Element Method	30
2.4	COMPARISON OF AVAILABLE METHODS	31
2.5	CALCULATION OF DISTORTIONAL STRESSES IN PRACTICAL BOX GIRDER BRIDGES	32
	2.5.1 Details of Actual Box Girder Bridges	32
	2.5.2 Load Distribution in Multibox Systems	32
	2.5.3 Simplified Design for Distortional Effects	34
2.6	SUMMARY	35

		Page No.
CHAPTER THREE:	REVIEW OF FATIGUE BEHAVIOUR OF WELDED JOINTS	37
3.1	GENERAL	37
3.2	BRIEF HISTORICAL NOTE	37
3.3	MAIN FACTORS AFFECTING FATIGUE BEHAVIOUR	38
	3.3.1 Effect of Testing Speed	38
	3.3.2 Effect of Elapsed Time	39
	3.3.3 Effect of Steel Type	40
	3.3.4 Effect of Weld Defects	41
	3.3.5 Effect of Residual Welding Stress	43
	3.3.6 Effect of Size and Shape	45
	3.3.7 Effect of Geometrical Stress Concentrations	46
3.4	REVIEW OF TESTS ON WELDS SUBJECTED TO TRANSVERSE BENDING	47
3.5	SUMMARY	50
CHAPTER FOUR:	DETAILS OF FATIGUE EXPERIMENTS	51
4.1	INTRODUCTION	51
	4.1.1 General	51
	4.1.2 Main Factors Affecting Fatigue Life of Weld Detail	51
	4.1.3 Stresses at the Joints	52
4.2	TEST PROGRAMME	52
	4.2.1 Objectives of Test Programme	52
	4.2.2 Selection of Experimental Approach	53
	4.2.3 Types of Welded Joints Tested	54
	4.2.4 Loading Conditions	56

		Page No.
4.3	DETAILS OF SPECIMEN	56
	4.3.1 Design of Specimens	56
	4.3.2 Specimen Designation	57
	4.3.3 Fabrication of Specimens	58
4.4	RESIDUAL STRESS MEASUREMENTS	63
4.5	DETAILS OF TESTS	63
	4.5.1 Testing Equipment	63
	4.5.2 Fatigue Testing Procedure	65
	4.5.3 Tests for Mechanical Properties of Materials	68
4.6	THEORETICAL STRESS ANALYSIS OF SPECIMEN	69
	4.6.1 Calculation of Deflections and Nominal Stresses in Typical Specimen	69
	4.6.2 Calculation of Nominal Bending Stress in Fillet Weld Throat of Specimens BESFWI and BESFGI	71
	4.6.3 Comparison between Analytical and Experimental Results	72
CHAPTER FIVE:	STATISTICAL ANALYSIS OF FATIGUE EXPERIMENTS	74
5.1	INTRODUCTION	74
5.2	INDEPENDENT AND DEPENDENT VARIABLES	75
5.3	POPULATION AND SAMPLE	75
5.4	BASIC ASSUMPTIONS	77
5.5	THE FREQUENCY DISTRIBUTION	77

		Page No.
5.5.1	General	77
5.5.2	Normal Gaussian Distribution	78
5.5.3	Transformation of Data to Logarithm Normal Distribution	80
5.5.4	Normal Probability Paper	80
5.5.5	χ^2-Test for Goodness-of-Fit	81
5.6	CONFIDENCE INTERVAL OF THE MEAN AND VARIANCE	83
5.6.1	General	83
5.6.2	Confidence Interval of the Mean	83
5.6.3	Confidence Interval of the Variance	84
5.7	COMPARISON OF SAMPLE VARIANCES AND MEANS	85
5.7.1	General	85
5.7.2	Comparison of Two or Several Variances	85
5.7.3	Comparison of Several Means	87
5.8	REGRESSION ANALYSIS	88
5.8.1	General	88
5.8.2	Assumptions of the Regression Analysis	88
5.8.3	Estimate of the Regression Line	89
5.8.4	Standard Error of a Prediction of a Further Observation	92
5.8.5	Comparison of Two Regression Lines	93
5.9	P-S-N CURVES	96
5.10	APPLICATION OF ABOVE ANALYSIS TO PRESENT TESTS	98

Page No.

CHAPTER SIX:	EXPERIMENTAL RESULTS AND DISCUSSION	99
6.1	INTRODUCTION	99
	6.1.1 General	99
	6.1.2 Statistical Factors	100
6.2	FATIGUE FAILURE OF THE SPECIMENS	101
	6.2.1 Failure Criterion	101
	6.2.2 Modes of Failure	102
	6.2.3 Detection of Failure	103
6.3	MATERIAL	103
6.4	FATIGUE TESTS ON DOUBLE FILLET WELDED CORNERS	104
	6.4.1 General	104
	6.4.2 Test Series BEDFW	104
	6.4.3 Test Series BEDFG	110
6.5	FATIGUE TESTS ON SINGLE FILLET WELDED CORNERS	115
	6.5.1 General	115
	6.5.2 Test Series BESFW	116
	6.5.3 Test Series BESFG	119
	6.5.4 Test Series BESFWI	123
	6.5.5 Test Series BESFGI	129
6.6	SUMMARY OF THE STATISTICAL ANALYSIS OF THE FILLET WELDED JOINTS	131
6.7	DISCUSSION OF THE RESULTS	134

Page No.

6.8	FATIGUE TESTS ON BUTT WELDED CORNERS	136
	6.8.1 General	136
	6.8.2 Test Series BEVBS	136
	6.8.3 Test Series BEVB	137
	6.8.4 Test Series BESBS	139
	6.8.5 Test Series BESB	140
	6.8.6 Comparison of the Results of Different Butt Welds	141
CHAPTER SEVEN:	EFFECT OF RESIDUAL STRESS ON FATIGUE	142
7.1	INTRODUCTION	142
7.2	CONTROL TEST SERIES	143
	7.2.1 General	143
	7.2.2 Measurement of Residual Strains	143
	7.2.3 Analysis of Results of Test Series BESFWIR	145
7.3	OTHER TEST RESULTS	148
7.4	DISCUSSION IN INFLUENCE OF RESIDUAL STRESS ON FATIGUE BEHAVIOUR	149
7.5	SUMMARY	151
CHAPTER EIGHT:	EFFECTS OF CORNER CRACKS ON BOX DISTORTIONAL BEHAVIOUR	153
8.1	APPLICATION OF PRESENT FATIGUE DATA TO DESIGN	153
	8.1.1 General	153
	8.1.2 Cumulative Damage	153
	8.1.3 Fatigue Damage to Corners of Closed Sections	156

		Page No.
8.2	DESCRIPTION OF ANALYTICAL APPROACH	157
	8.2.1 Assumptions	157
	8.2.2 Method of Analysis	158
	8.2.3 Linkage Elements	158
8.3	EXAMPLE BOXES	159
	8.3.1 General	159
	8.3.2 Details of Loading and Cases Analysed	161
8.4	PRESENTATION AND DISCUSSION OF THE RESULTS	162
8.5	SUMMARY	169
CHAPTER NINE:	CONCLUSIONS AND RECOMMENDATIONS FOR FURTHER RESEARCH	170
9.1	CONCLUSIONS RELATING TO ESTIMATION OF DISTORTIONAL STRESSES	170
9.2	MAIN CONCLUSIONS RELATING TO FATIGUE INVESTIGATION	171
9.3	CONCLUSIONS RELATING TO EFFECT OF CRACKS ON DISTORTIONAL BEHAVIOUR	172
9.4	RECOMMENDATION FOR FURTHER RESEARCH	173

		Page No.
REFERENCES		175
APPENDIX 2-I	PARAMETRIC STUDY OF CROSS-SECTIONAL DISTORTION OF SINGLE CELL BOX GIRDER	189
APPENDIX 4-I	CALCULATION OF BENDING STRESSES FOR SPECIMEN TYPE B	196
APPENDIX 4-II	CALCULATION OF BENDING STRESS IN FILLET WELDED THROAT FOR SPECIMEN SERIES BESFWI AND BESFGI	203
APPENDIX 6-I	A TYPICAL CALCULATION OF THE COMPARISON OF TWO REGRESSION LINES	206
NOTATIONS		210
TABLES		216
FIGURES AND DRAWINGS		263
PLATES		352

CHAPTER ONE

INTRODUCTION

1.1 GENERAL

There has been a considerable amount of research in recent years into the behaviour of steel girder bridges. This research - largely stimulated in the wake of a series of major box girder failures - has for the most part been concerned with the unserviceability and collapse limit states of such structures. Relatively little attention has been paid to the limit state of fatigue despite the fact that box girder bridges are generally all-welded structures subjected to repeated loading over a design life of 120 years.

Although there is little evidence to-date to suggest that fatigue is a serious problem in steel box girder bridges - the same could be said with respect to the static strength of these bridges shortly before the series of accidents referred to previously occurred. Furthermore, as fatigue is very much a time dependent phenomenon, the argument that no evidence of fatigue failure has been found to-date holds little weight when it is considered that the majority of modern steel box girder bridges have been built within the last thirty years - that is they have been in service for only about twenty five per cent of their design life.

It is thus clear that an understanding of the fatigue behaviour of welded joints - particularly those peculiar to box construction is highly desirable and it is in this spirit that the work described in this thesis is presented.

1.2 BACKGROUND AND OBJECTIVES OF THIS RESEARCH

Following an earlier interest in the elastic response of box girders at Imperial College[1.1, 1.2] attention was focussed on the cross-section distortional behaviour[1.3]. Evidence was accumulated to suggest that in certain circumstances the transverse bending stresses at the corner of boxes could be significantly large, and very often reversible under service loading in bridges. The author of this thesis played an active part in the formulation of design rules for the Merrison Committee relating to the calculation of these elastic transverse bending stresses[1.4] - and indeed the second chapter describes in summarised form some of this work.

Following on from this research attention was switched to the fatigue response of the welded joints which are generally located at the box corners - the precise position where the reversible transverse distortional bending stresses are at a maximum. The major part of the thesis is concerned with this aspect of the research program.

Having gathered experimental information on the fatigue behaviour of box corner welds the question was posed as to what the significance was of any cracking which might occur at the corner of steel boxes due to fatigue. The second last chapter of the thesis goes part way to answering this question by studying the interaction between fatigue cracking and structural response.

1.3 THE FATIGUE PROBLEM

Box corner welds are subjected to a complex stress system, comprising combined longitudinal shear and direct stress caused by the overall flexure in the direction of span and transverse bending stresses caused by the cross-sectional distortion of the box. These secondary transverse distortional bending stresses are almost exclusively caused by live loading in the case of a box used in bridge construction. Where significant restraint is present against transverse distortion, e.g. when closely spaced diaphragming is provided between supports, the transverse bending stresses will be small at the box corner. However, where widely spaced diaphragming is used, or where such stiffening is omitted altogether, these so-called secondary stresses may in effect be the primary stress system limiting the fatigue life of the welds and thus determining both the type and size of weld which must be used in design.

An example of small scale undiaphragmed boxes used frequently in bridge construction are the closed stringers of orthotropic deck construction. On a larger scale, undiaphragmed open top composite boxes (e.g. 2m x 2 m) are now used in bridge construction on relatively short spans in the United States and Canada, where they have proved to be economical. The limiting criterion determining the maximum dimensions of these boxes was the possibility of fatigue failure occurring at the box corner welds during the life of the bridge. Moreover, the increasing tendency for engineers to design bridges with less stiffening to keep down the costs of workmanship and fabrication, which may well be the future trend following inflation and the Merrison Rules, will be inhibited unless reliable

information concerning the fatigue behaviour of the welded joints is available.

1.4 SCOPE AND PRESENTATION OF THE THESIS

This thesis is concerned with the fatigue behaviour of different corner welds as used in the box girder bridges. Such bridges are generally subjected to transverse distortional bending stresses which are caused by deformations of the cross-sections due to eccentric loading. Where the degree of distortion changes along the length of the box, in-plane bending of the walls takes place in such a way as to cause warping of the cross-section. Chapter 2 deals with the distortional aspect of the box girder bridges and with the development of a simplified method for calculating the transverse distortional bending and distortional warping stresses.

Chapters 3 to 7 inclusive are concerned with the experimental and analytical investigation of the different types of weld used in box girder constructions. The fatigue behaviour of welded joints was reviewed generally with the purpose of identifying the main factors affecting behaviour and, in particular, the fatigue behaviour of corner welded joints subjected to bending. A short account of this review is given in Chapter 3. It was found that there was no systematic study of the behaviour of different types of corner welded joints under cyclic transverse bending reported in the literature. A special specimen which could closely represent the cross-sectional deformation of a box was designed. A description of different types of weld together with the manufacturing and fatigue testing procedure used throughout the investigation is given in Chapter 4.

All the tests connected with the fatigue behaviour of fillet corner welds were performed using statistically controlled experiments. This procedure allowed the formulation of a suitable mathematical relationship, relating to the fatigue life of each different type of weld detail and the applied stresses, to be made, and also made it possible to derive this relationship with different probabilities of failure. The derived mathematical equations could be compared with the considered confidence limits using such a statistical approach. In Chapter 5 the statistical method used in the analysis of experimental results is described. It is included within the main body of the text, rather than in an Appendix, for the convenience of the reader who may not be familiar with the concepts and terminology used in the following main Chapter.

To accomplish the objectives of this investigation, a total of 144 specimens were fabricated and tested during the research programme. From this total, 114 specimens were manufactured with different types of fillet welded joints. With the special design of the specimen, 146 results for fillet type welds were obtained and used for the derivation of design formulae. The number of specimens for each type of fillet weld corner was between 17 and 20. A total of 22 experiments was carried out on two types of butt corner welds with and without sealing runs. This may be regarded as a pilot study on the fatigue behaviour of butt corner welds subjected to transverse bending. In Chapter 6 the experimental results are presented and discussed. A subsidiary series of experiments was carried out to study the effect of residual welding stresses on fatigue behaviour, particularly in relation to the change of

failure mode. The results are discussed in Chapter 7.

The significance of fatigue cracks in welded joints at the corners of closed sections, such as those in a large-scale box girder or in smaller short span boxes, has been briefly studied with the objective of establishing the effect of the local reduction in distortional stiffness caused by the crack on the transverse bending stresses at the root of the crack. The finite element method, with the application of a special linkage element at the corners of the box sections, has been used for this investigation. The results are described in Chapter 8.

Finally, the conclusions drawn from this research and the suggestions for further research are summarised in Chapter 9.

CHAPTER TWO

CROSS-SECTIONAL DISTORTION DUE TO ECCENTRIC LOADING IN BOX GIRDER BRIDGES

2.1 GENERAL

Box girder bridges when subjected to eccentric loading undergo deformation of the cross-section. This behaviour causes longitudinal stresses due to non-uniform warping and transverse distortional stresses. The value of these stresses can be determined accurately with the aid of a computer using advanced methods of structural analysis such as finite element or folded plate techniques. Such methods are generally demanding in both computer time and cost.

The objectives of the investigation were to determine the level of distortional stresses likely to occur in practical box girder bridges and for this purpose to develop an approximate simple method of analysis. The results of this investigation together with a critical resume of available analytical methods for calculating distortional stresses in box girder bridges are presented in this Chapter.

2.2 SINGLE CELL BOX GIRDER UNDER ECCENTRIC LOADING

In the design of bridges the type of live loads considered in specifications are uniformly distributed live loads and standard axle loads which are a particular configuration of point loads as shown in Fig. 2.1a. The structural action of a box under such loads can best be understood by considering the response in stages.

If it is assumed at first that the webs are supported along the length of the box then the load is transferred to the webs by bending of the top flange. This bending is associated with transverse flexure of the walls of the box girders, and induces transverse bending stresses which can be calculated by simple frame analysis. When the assumed supports under the webs are removed the effects of so doing can be studied by replacing the load applied over the flange width by reactions P_1 and P_2 which are statically equivalent to the applied load at the positions of intersection of the top flange and the web. This load in turn can be decomposed into two force systems as shown in Fig. 2.1b. The symmetrical component of the load system causes vertical bending of the entire cross-section. The stresses for this component of load can be calculated by conventional flexural beam theory, accounting for shear lag with the use of effective breadth [2.1]. The antisymmetrical component of the load system causes shears which twist the box section (torsional load). The torsional load itself is equivalent to the two load systems shown in Fig. 2.1c. The pure torsional component consists of P_T forces in different plates which equilibrate the applied torsion of the antisymmetrical load system and the distortional component is a self-equilibriating pure shear system P_D which in combination with the pure torsional component balances the externally applied antisymmetrical loads at the webs. Fig. 2.1d shows the deformation of the cross-section of the box girder under different load components.

It is not strictly correct to separate the torsional and distortional components of the loading [1.4] but it has been shown that the effects of the interaction between the torsional and distortional components of loading for the practical range of medium span bridges are negligible. Based on this assumption the effect of each system of forces can be studied independently. Only the effect of the distortional loading component is considered in this Chapter.

2.3 AVAILABLE METHODS OF ANALYSIS

2.3.1 Richmond Displacement Solution

This method of analysis is based upon earlier work by Reissner [2.2] and Ebner [2.3]. The box is represented by four longitudinal booms and four walls, as shown in Fig. 2.2. It is assumed that the booms carry longitudinal bending forces only and the walls carry only the shearing effects. The frame stiffness of the box is neglected and distortional loading is resisted only by diaphragms. The box is thought of as a number of cells between diaphragms. The unit load method is used to derive the following equation

$$\frac{1}{E}\{S\}_{(i-1),i} = [Y_{AA}]_i \{\Delta\}_{i-1} + [Y_{AB}]_i \{\Delta\}_i$$

$$\frac{1}{E}\{S\}_{i,i} = [Y_{BA}]_i \{\Delta\}_{i-1} + [Y_{BB}]_i \{\Delta\}_i \qquad (2.1)$$

where S is a column matrix of end forces, Δ is a column matrix of displacements and y is the stiffness matrix.

The properties of the diaphragm which is assumed to be acted upon by distortional forces, $\bar{V}_i$, is defined by the relationship

$$\frac{1}{E}\ \bar{V}_i = v_i d_i \qquad (2.2)$$

where d_i is called the idealised thickness (or the distortional stiffness) of the diaphragm. The diaphragm can be a plate, a braced frame, or a stiff-jointed frame. For a plate diaphragm of uniform thickness "t_i" the expression for d_i of the cross-section shown in Fig. 2.2 is

$$d_i = \frac{G}{E} \cdot \frac{8C}{B} \cdot t_i \qquad (2.3)$$

The derivatives of equation (2.3) for a trapezoidal section are given in Ref. (2.4).

The external loads in this method are applied only at diaphragm positions. When loads are applied between diaphragms they are replaced by fixed end moments and forces at diaphragm positions. Now the equilibrium conditions at the diaphragm must be satisfied. Equation (2.4) relates the external loads at the diaphragm to the internal forces.

$$\{\bar{S}\}_i + \{S\}_{i,i} + \{S\}_{i,(i+1)} = \{P\}_i \qquad (2.4)$$

where $\{\bar{S}\}_i$ is the column matrix $\{0, \bar{V}_i, 0\}$, and $\{P\}_i$ is the column matrix of the load. These two steps are repeated for each cell and diaphragm respectively and together give a set of linear simultaneous equations, which are solved for the displacements. The

displacements then are substituted back into equations (2.1) from which the internal forces are found and hence stresses.

A computer program "RDISP" [1.4] using the above method was used to analyse the box given in Fig. 2.7 for point load and uniformly distributed loads.

2.3.2 Beam on Elastic Foundation Analogy

The first investigation using Beam on Elastic Foundation (BEF) theory was concerned with the study of stresses and deflections of rails resting on elastic soils [2.6]. It was Vlasov [2.7] who first suggested the analogy between the response of a beam on elastic foundation and that of a box girder under distortional loading. Wright et al [2.8, 2.9] developed the BEF method for single cell box girder including the effects of longitudinal and transverse stiffeners in the plates. It has been shown that section parameters [1.4, 2.8, 2.9, 2.10] defined by the BEF analogy may be used to define accurately the magnitude of the transverse distortional bending and warping stresses for both point and uniformly distributed loading. This method accounts for the effects of rigid and deformable interior diaphragms, non-prismatic section, continuity over intermediate supports and for any arbitrary end conditions. In the following section the analogy between the differential equation of the BEF and that corresponding to the response of a box girder to eccentric loading is examined.

The Analogy between Differential Equations: A straight beam with a bending rigidity of EI_b is supported by a Winkler type elastic foundation of modulus K and by regularly spaced elastic supports of stiffness Q as shown in Fig. 2.3a. When the beam is

subjected to a distributed load the differential equation describing the deflection of the beam is given by the following equation

$$EI_b \frac{\partial^4 w}{\partial x^4} + kW = p(x) \qquad (2.5)$$

where p(x) is the applied load along the longitudinal x axis of the beam. Introducing the notation

$$\beta = \sqrt[4]{\frac{k}{4EI_b}} \qquad (2.6)$$

which is a function of the foundation modulus "K" and flexural stiffness of the beam, the equation (2.5) becomes

$$\frac{\partial^4 w}{\partial x^4} + 4\beta^4 w = p(x) \qquad (2.7)$$

The differential equation describing the response of a box girder with deformable cross-section subjected to antisymmetrical component of loading is (2.8)

$$EI_c \frac{\partial^4 W}{\partial x^4} + KW = p(x) \qquad (2.8)$$

where I_c is the cross-sectional property related to warping of the box

K is a measure of the deformation stiffness of the box/unit length (distortional stiffness)

W is a measure of distortional deflection of the box as shown in Fig. 2.4a

p(x) is the applied distortional component of load along the longitudinal x-axis of the box.

The similarity between equations (2.8) and (2.5) is evident. Therefore solutions to the differential equation of the BEF can be directly applied to that of box girder.

The basic assumptions in deriving equation (2.8) which is derived in terms of vertical deflection w at the top of the box web (Fig. 2.5b) are that,

(a) the response is linearly elastic,

(b) the corners of the box have rigid joints,

(c) the warping stress distribution is linear,

(d) the shearing strains due to distortion of the cross-section are negligible,

(e) transverse axial strains due to transverse axial forces are negligible,

The actual deflection of the cross-section due to distortion is directly proportional to the change of the diagonal length, as shown in Fig. 2.5a. However, Wright's[2.8] formulation which leads to equations (2.8) has been used in this investigation.

Relationship between Box Girder and BEF Properties: The relationship between box girder and BEF properties for a trapezoidal box girder is considered in the following.

1. The BEF has a foundation modulus "k" proportional to the distortional stiffness "K" of the box girder. Distortional stiffness of a box is calculated by considering a unit length of the box girder and subjecting it to the unit distortional component of the load.

From conditions of skew symmetry, there is only one redundant force "V" which is the vertical shear normal to the middle surface of the bottom plates. The redundant force can be determined by solving equation (2.9) which is derived using the influence coefficient method

$$\delta_{11} V + \delta_{10} = 0 \tag{2.9}$$

The coefficients δ_{11} and δ_{10} are determined by the force method and hence the value of "V" is found to be

$$V = \frac{\frac{1}{D_C}\left[(2B_T + B_B)\ B_T.B_B.C\right] + \frac{1}{D_T}(B_B.B_T^3)}{(B_T + B_B)\left[\frac{B_T^3}{D_T} + \frac{2C\left[B_T^2 + B_T.B_B + B_B^2\right]}{D_C} + \frac{B_B^3}{D_B}\right]} \tag{2.10}$$

where B_T and B_B, C, D_T, D_B and D_C are shown in Fig. 2.6. The deflection of the box cell under a unit generalised distortional load can now be found and is given by equation (2.11)

$$\delta_1 = \frac{B_T.B_B}{24(B_T+B_B)}\left\{\frac{C}{D_C}\left[\frac{2B_T.B_B}{(B_T+B_B)} - V(2B_T + B_B)\right] + \frac{B_T^2}{D_T}\left[\frac{B_B}{(B_T+B_B)} - V\right]\right\} \tag{2.11}$$

Thus the property of the cell analogous to k of the BEF is

$$K = \frac{1}{\delta_1} \tag{2.12}$$

2. The analogous BEF has a flexural stiffness EI_b proportional to the warping stiffness of the box cell. The approximate cross-section properties of the box for bending about the horizontal axis is given by equation (2.13)

$$I_b \approx \frac{I_c}{4} \qquad (2.13)$$

where I_c is the moment of inertia of the cross-section of the box about its horizontal axis. The exact expression for I_b is given in Ref.[2.8]. The comparison of the I_b of equation (2.13) with the exact values as given in Appendix 2-I Table I-2 has shown that equation (2.13) leads to sufficient accuracy for the practical range of box girders considered in this investigation.

3. The BEF analogy is extended to include various cross-bracing diaphragms and support conditions which are shown in Fig. 2.3b. A diaphragm rigid in shear but free to warp is analogous to a pinned support, a diaphragm flexible in shear and warping is analogous to both vertical and rotational elastic supports and finally a diaphragm rigid in shear and warping is analogous to a fixed-end support of the BEF. The equations for calculating the diaphragm stiffness of different types of diaphragm can be found in Ref.[2.8, 2.10]

4. The panel length between supports of the BEF is the same as the panel or span length of the box girder.

5. The point load or distributed loads on the BEF correspond to point or distributed torsional loads on the box girder.

Solutions for the Analogous BEF: Once the properties of the analogous BEF have been determined, the differential equation given by equation (2.7) can be solved by one of the established methods. The BEF solution is obtained in terms of deflections and moments. The deflection of the analogous BEF is proportional to the distortional deflection "W" of the box cell. Hence the transverse distortional bending stresses "σ_{DB}" are obtained from the "W" of the analogous BEF.

The maximum transverse distortional bending stresses occur at the corners of the box cell and they are calculated by the following equations

$$\sigma_{DB} = K.F_d.W \tag{2.14}$$

where K is the distortional stiffness

and

$$F_d = \frac{B_T}{2Z}\left[\frac{B_B}{B_T + B_B} - V\right] \qquad \text{at the top of the web}$$

$$F_d = \left[\frac{B_B}{2Z} \cdot V\right] \qquad \text{at the bottom of the web}$$

where Z is the section modulus of the plate in question per unit length in the span direction of the box.

B_B, B_T are given in Fig. 2.6 and V is given by equation (2.10).

The moments in the analogous BEF are proportional to the distortional warping stresses "σ_{DW}" in the box cell, and the value at the intersection of bottom flange and web can be calculated by equation (2.15)

$$\sigma_{DW} = \frac{B_B \cdot \psi_b \cdot M}{2I_b} \qquad (2.15)$$

where I_b and B_B were defined earlier and

M is the BEF moment

ψ_b is a displacement coefficient for the bottom flange plate the expression for which is given in Ref. (2.8).

The warping stresses at the top corners of the box can be found from equation (2.15) and the requirement that the warping stresses at a section are self-equilibriating.

The box girder given in Fig. 2.7 was analysed using this method for point load and uniformly distributed load.

2.3.3 The Finite Element Method

The FE method was used as the third method of the analysis. The results of the analyses obtained using the two previous methods were compared with those from the extensional-flexural solutions using an element specially developed for box girder analysis (2.1, 2.11). In the next section the idealisation of the test example by this method is described.

Finite Element Idealisation of the Test Example: The box girder shown in Fig. 2.7 was analysed by the FE method for two load cases, i.e. vertical point load at midspan and a uniformly distributed vertical line load above the web.. Each load case was analysed as a vertical antisymmetrical load with its torsional and distortional components considered separately. The load was applied at the

cross-sectional nodes. The cross-sectional nodal positions and FE meshes used in the analysis are shown in Fig. 2.8. Because of the asymmetry of the loading it was possible to analyse only a quarter of the box with resultant savings in computer time. The plates of the support diaphragms were replaced by bracing of equivalent stiffness so that extra nodes needed to define the diaphragms were not necessary. The stiffened plates were replaced by orthotropic plate elements which reproduced the correct transverse flexural stiffness and longitudinal in-plane stiffness. Appropriate boundary conditions were applied along the longitudinal centre line and at midspan to obtain the correct antisymmetrical behaviour.

2.4 COMPARISON OF AVAILABLE METHODS

In previous sections the three different analytical methods used to analyse the selected box shown in Fig. 2.7 were summarised. The stresses obtained by the three methods were non-dimensionalised against the maximum Bredt shear stress occurring in the box under the torsional component of the loading case being considered. The results of the analysis obtained from each method for point load and UDL are given in Figs. 2.9 and 2.10 respectively. The BEF method shows good agreement with the FE result. (The BEF method also was compared with model test results, the results of which are given in Ref.[1.4].) Richmond's displacement solution also gave reasonable agreement with the FE method, but subsidiary calculations are necessary to obtain σ_{DB} stresses and are only possible when fictitious diaphragms are incorporated into the analysis to represent the frame stiffness of the box. The computer time and storage needed by each program for the analysis of the box under

study is given in Table 2.1. The BEF program is seen to be the most economical.

2.5 CALCULATION OF DISTORTIONAL STRESSES IN PRACTICAL BOX GIRDER BRIDGES

2.5.1 Details of Actual Box Girder Bridges

As a result of the above comparison the BEF method was used to analyse practical box girder bridges to establish a simplified method of analysis for calculating "σ_{DB}" and "σ_{DW}". To achieve this objective details of the 26 recent steel box girder bridges listed in Table I.1 were studied. The cross-sectional properties of the boxes studied are given in Table I.2. As can be noted, most of the bridges are of multibox construction. A formula is derived in the following section which can be used to calculate the most critically loaded cell of a multicell bridge. This cell can subsequently be analysed by the BEF method which strictly applies only to a single cell.

2.5.2 Load Distribution in Multibox Systems

In this section a method is proposed for evaluating the distribution of torsional component of loads in multibox system. This method is based on the procedure suggested by Wright[2.9].

If the distribution of the torsional component of the load in multibox systems can be determined, the distortional stresses may be calculated separately for each cell. In Fig. 2.11 the procedure for evaluating the distribution of torsional component of the load in multibox systems is illustrated. The bridge deck

is assumed to act as a continuous beam in the transverse direction over rigid supports at web positions and the support reactions are calculated for loads applied to the deck. Then, on the assumption that there is a negligible contribution of the webs to the bending stiffness, the flexural component of the loading is subtracted from the support reactions to give the torsional component. The direct torsional load acting on each cell is then obtained by beginning at one side of the cross-section and indicating the torsional load on each cell across the width for no change in the total force at any flange-web intersection. Where there is no cell the direct torque is reassigned to adjacent cells. The most critically loaded cell may then be analysed by the BEF analogy. The complex interaction between deformation of the cross-section and torsion in the multibox girder is neglected. (Wright [2.10] has established that conservative results are obtained using this assumption.)

Based on this method a large range of carriageway layouts and arrangements of box girders was analysed with a view to relating the torsional loading to the numbers of boxes and traffic lanes. A computer program, using the stiffness method, was developed to analyse all practical combinations of numbers of boxes and lanes from a two-lane carriageway supported on two boxes, to an eight lane carriageway with a central reservation supported on eight boxes.. The torsional loading on the most critically loaded box for any combination of numbers of boxes and traffic lanes was established for HA and HB loading and the torsional moments are tabulated in Tables 2.2 and 2.3 The values were also plotted graphically and the following interaction formula was then obtained:

$$R = \frac{0.35\ N_L}{1 + 0.5\ (N_B \cdot \frac{B_T}{L})} \qquad (2.16)$$

where N_L is the number of lanes

N_B is the number of boxes

B_T is the top width of one box

L is the total width of bridge deck

R is the ratio of antisymmetrical load acting above one web of the most critically loaded box to the total load in one lane, e.g. for HA uniformly distributed load:

$$P = R.W_L \qquad (2.17)$$

where P is the antisymmetrical load/unit length

W_L is the distributed load/unit length in one lane.

This formula (or the values given in Tables 2.2 or 2.3, whichever is the higher) together with the BEF method can be used for the initial design of multibox system to obtain an appreciation of the magnitude of distortional effects without the need to use expensive load distribution techniques.

2.5.3 Simplified Design for Distortional Effects

The various parameters based on BEF analogy which influence the distortional behaviour of a steel box girder are given in Appendix 2-I. A parametric study was carried out and reported elsewhere[1.4] which resulted in a simplified design procedure to

account for the effects of distortion in a steel box girder. The torsional loading is determined for each box in the cross-section either from a global analysis of the structure or from Tables 2.2 and 2.3 and/or equations(2.16) and (2.17). The dimensionless span length, βL, is greater than 2.5 for almost all practical steel box designs so if internal diaphragms are for the moment neglected each box can be analysed as a separate infinite BEF for which a simple solution exists. This gives an upper bound to the distortional stresses and if these values are within acceptable limits no further calculations are necessary. If the stresses are above these limits, diaphragming or redesign is necessary and alternative treatments depend on whether the transverse bending stresses or the warping stresses are critical. This procedure has been incorporated in the relevant Merrison Design Rules for steel box girder bridges.

2.6 SUMMARY

The investigation presented in this chapter was concerned with the study of distortional behaviour of box girder bridges under eccentric loading. The investigation led to the development of a simple method for the calculation of the transverse distortional bending and distortional warping stresses in box girders.

It was found that the peak transverse distortional bending stresses σ_{DB} may be high [1.4, 2.9] and that these stresses could be of primary importance when fatigue life of the box corner weld is considered. Very little fatigue data was available to assess the performance of a box corner weld subjected to repeated bending. It was considered that the fatigue performance of corner welded joints

needed to be investigated further. The results of the fatigue investigation of welded joints subsequently carried out for this purpose are described in the following chapters and are the main concern of this thesis.

CHAPTER THREE

REVIEW OF FATIGUE BEHAVIOUR OF WELDED JOINTS

3.1 GENERAL

It has been estimated that some 80-90 per cent of the failures in welded structures, subjected to repeated loading, are attributable to fatigue failure[3.1]. The high incidence of such failures can partly be attributed to the fact that some designers do not consider fatigue as a design criterion, but it must also be admitted that present knowledge is not adequate for the engineer to estimate accurately the fatigue life of all types of welded structures.

In this chapter a selection of literature on this subject is reviewed with the purpose of identifying and explaining some of many variables which can influence the fatigue strength of welded structures and determining the most important factors on the fatigue strength of the weldment.

3.2 BRIEF HISTORICAL NOTE

The first fatigue failure was noted in rolling stock and track and registered by railway engineers as early as 1843[3.2]. As the cycles of loading due to traffic increased and bridge engineers became more aware of the effect of repeated loading fatigue cracks were also found in bridge structures.

In 1852 Wöhler initiated a series of fatigue tests to find out how various materials responded to different ranges of cyclic load[3.2]. Although only material and strain amplitude were considered as variables in his investigation, Wöhler soon realised that other factors had some influence on the fatigue results. Since then many fatigue test results

have been published on different aspects of fatigue behaviour[3.2]. Several controlled fatigue tests on bridges have also been conducted on site. In 1929 a 30 ft span bridge which was subjected to cyclic load by Bernhard reached failure at a small number of cycles. The more recent investigation carried out by the Bridge Design Division of the Transport and Road Research Laboratory (TRRL)[3.3] on in situ orthotropic plate bridge decks has shown the need for research into this type of bridge construction. The results of such in situ tests do not lead to quantitative recommendations concerning the fatigue, but serve to illustrate the gravity of the problem in actual structures.

Although a complete review of literature concerning fatigue would be impractical due to the extent of the published literature, it was felt that an over-generalisation for the sake of brevity would be equally unsatisfactory. It is not suggested that the references mentioned are the only ones, or necessarily the best ones, on each specific topic; they merely have been chosen to illustrate those aspects of the problem which are related to the investigation presented and discussed in this thesis.

3.3 MAIN FACTORS AFFECTING FATIGUE BEHAVIOUR

The main factors which could be expected to influence the fatigue behaviour of welded joints are reviewed in the following sections.

3.3.1 Effect of Testing Speed

Since the specimens tested in the laboratory are subjected to higher frequencies of loading than the loads to which actual structures such as bridges are subjected, the speed effect on the experimental results in the laboratory must be considered. In addition, the prototype

structures are not subjected to continuous cyclic loading as takes place in the laboratory specimens. Most of the experimental results concerning this aspect of fatigue are done on small polished specimens. Available results in the literature tend to show that there is very little or no speed effect for frequencies between 200 c/min. and 12,000 c/min. The American Society for Testing and Materials (ASTM) Task Group[3.6] has found that the speed effect is small for frequencies between 200 c/min. and 7,000 c/min. but does not give clear statements for frequencies lower than 200 c/min. The test results at room temperature of investigators[3.4] who studied this aspect of fatigue are summarised in Fig. 3.1. Their experiments refer to frequencies between 600 c/min. and 12,000 c/min. They found that there was no appreciable speed effect on the fatigue results. The evidence concerning a speed effect at frequencies below 200 c/min. in the reviewed literature is not clear cut. However, Forrest and Tapsell[3.5], using 0.17 per cent carbon steel, have shown that the stress for a given endurance is 10 per cent lower at 10 c/min. than at 2,000 c/min. It seems that there is some speed effect for speeds lower than 200 c/min. It is of course practically impossible to determine the fatigue limit at very low speed due to the time involved.

3.3.2 Effect of Elapsed Time

In the investigation done at The Welding Institute[3.7] on fifteen specimens of non-load-carrying longitudinal fillet welds, which were fabricated at the same time and were tested after welding, insignificant differences in terms of design stresses have shown up after 14 and 24 months. Similar results obtained by Fisher[3.8,3.9] have confirmed that there is no elapsed time effect on fatigue behaviour.

3.3.3 Effect of Steel Type

Different structural steels used in welded bridge constructions range from mild steel to high strength alloy steels. There is a great variation in the chemical composition and mechanical properties of these materials. Fatigue experiments carried out on small polished specimens without notches, made from different materials, have shown quite different behaviour at high cyclic load. A relationship between tensile strength of the basic materials and the fatigue limits obtained from small laboratory specimens was derived [3.10].

However, it has been found that in steel specimens which contain stress concentrations (caused by notches, holes, voids and other defects) this relationship no longer exists. The relationship between the endurance limit and ultimate tensile strength of various steels for smooth polished specimens and severely notched specimens is illustrated in Fig. 3.2. This diagram is originally due to Bullen and has been reproduced many times [3.25]. It can be seen that in specimens which are severely notched the fatigue lives are relatively constant regardless of the ultimate tensile strength of the material. It has been also shown that with welded specimens U.T.S. has virtually no effect on their fatigue behaviour [3.1]. Experimental studies carried out on welded steel beams [3.8, 3.9] fabricated from various structural steels with different tensile properties also indicated that there were little differences in the fatigue behaviour of the beams. This fact can be attributed to the existence of defects which form stress concentrations in real structures. The existence of the defects and their formation in welded joints are discussed in the following sub-section.

3.3.4 Effect of Weld Defects

The existence of slag intrusions, undercut and their shapes were studied by Signes et al.[3.11] at the toe of manual metal arc fillet welds in high tensile steel. Watkinson et al.[3.12] found that slag intrusions are formed when welding processes other than manual metal arc welding are used. The explanation for this phenomenon is that normally during welding non-metallic parts of the weld, i.e. slag, float to the surface of the molten weld metal before it has been cooled sufficiently to solidify. However, at the external boundary between the weld pool and the solid parent material, a part of the weld metal, while being soft, is not liquid and the slag of the weld cannot float to the surface. It has been observed that the slag intrusions are needle shaped with root radii of about 0.0025 mm and sometimes reach a depth of 0.43 mm below the surface at the toe of the weld. Furthermore, it was found that some undercut always exists at the toe of the weld with a depth of at least 0.076 mm. Usually the slag intrusions are situated at the bottom of the undercut. In other words, crack-like defects of the order of 0.15 mm depth below the surface of the parent material exist at the toe of a weld. These defects are situated in regions of already high geometrical stress concentration and so the actual stress at the tip of the defects is very high. In most welded joints the fatigue crack starts from such points.

The fatigue behaviour of a welded joint is generally very sensitive to defects. It has been shown by Hempel et al.[3.13] that a very dense porosity can decrease the fatigue strength of a mild steel butt weld to less than 1/3rd of the fatigue life of a relative defectless similar butt weld. Tests carried out on transverse butt weld[3.14] in

HY-80 steel, with the weld reinforcement removed, showed that 1 per cent porosity reduced the fatigue life at 10^5 cycles by 18 per cent and for the case with 5 per cent flaw area the fatigue life was reduced by 45 per cent. These defects are points of stress concentration and provide locations for crack initiation. Efforts have been made to correlate the fatigue life with defect size. For example, techniques have been developed recently for the production of slag inclusions of a reproducible shape and size[3.15] defects, thus permitting systematic investigations of the effect on fatigue behaviour to be made. In Fig. 3.3 the results obtained by Matting and Neitzel[3.15] show the effect of different defects on the life of welded joints. It can be noted from Fig. 3.3 that restart has the least effect, and the highest effect is because of undercut. Investigations carried out by Thielsch[3.26] on weld surface contour variations has shown that an undercut of about 0.89 mm depth can reduce the fatigue life of mild steel welds by almost 50 per cent for pulsating tensile fatigue.

Another defect which may occur in most fillet welded joints is the existence of gaps between the plates due to distortion of the material during welding and the general difficulties of achieving good fit-up. This defect has been examined in the context of fatigue for stiffened plates[3.33] on the specimen types shown in Fig. 6.33. The obtained results showed that, for single fillet welds, when the stiffener carried a direct stress and the plate a bending stress the mode of failure is influenced by the presence of a gap between the two members. However because of insufficient results obtained no definite conclusions concerning the effect of the gap on fatigue life of the welded joints was made. In this investigation the effect of the gap between two plates on the fatigue life of welded corner joints receives special attention.

3.3.5 Effect of Residual Welding Stress

When steel components are connected by welding it is inevitable that in the cooling process a system of self-equilibrating tensile and compressive stresses will be locked into the structure. It is only if a plate is uniformly heated and allowed to cool so that thermal expansion and contraction can take place freely that there are no residual stresses. But if while the plate is hot it is firmly attached to another plate by welding, the shrinkage which would otherwise occur by cooling is prevented to some extent and locked in stresses are produced in the welded structure. The weld material itself contributes to this process in that as soon as the weld material solidifies, it attempts to shrink, but as it is firmly attached to the adjacent plates and cannot shrink freely, stresses are produced in the weld. The state of stress induced is very dependent on the temperature distribution throughout the joint, on the rate at which the welded joint loses heat, and the degree of restraint provided by the surrounding material. An idealised distribution of such stresses in a simple weldment is shown in Fig. 3.4. It will be noted that near the weld a zone of tensile yield stress of width 'c' exists[3.16,3.17].

The effect that these stresses may have on the fatigue behaviour of a welded structure has been a controversial subject for many years. Conflicting claims were made for the effect of residual stress on fatigue behaviour in the literature until the middle 1950's[3.20]. For example, Ros [3.27] and Hebrant[3.28] considered that residual stresses had very little effect on the fatigue strength of the welded structure as compared with the geometry. He suggested that in a good weld the residual stress can be ignored completely. However, later it was shown[3.29] that tensile

residual stresses had a substantial effect in small notched specimens. Dugdale[3.29] stated that tensile residual stresses reduced the fatigue strength of notched base metal specimens. He also suggested that a similar effect should be expected on the fatigue strength of welds, where a notch condition exists at the edge of the weld reinforcement or at the defects in the weld.

It has been shown that when residual stresses are present the stress range has an important effect on the fatigue behaviour[3.18,3.19,3.20]. Figure 3.5 shows the effect of the residual stress on the fatigue strength at 2×10^6 cycles of fillet welded mild steel specimens. It can be noticed that the effects of residual stress become bigger as the applied stress cycles has a greater compressive component[3.1]. In the test programme carried out by Fisher[3.9] on relatively large beams with welded cover plates the fact that in most practical welded structures,which contain high tensile residual stresses in the vicinity of the welds,the dominant variable is stress range has been to a large extent demonstrated. However, this investigation can be criticised because of the small compression stresses considered in the specimens tested. Nevertheless, in recent years, many investigators have concluded that fatigue life of a welded structure depends only on the stress range. However, if for some reason the residual stress in a welded structure is low or non-existent, (this could happen as a result of stress relief processes or because the joint is too small to provide the restraint required to form significant residual stresses) a joint subjected to a partially compressive stress cycle could have a higher fatigue life, because the compressive part of the cycle will be largely non-damaging.

3.3.6 Effect of Size and Shape

Most of the published work concerning the effects of size and shape of specimen on fatigue behaviour has been concerned with polished laboratory specimens of simple geometrical shapes and rarely with structural members or connections. This review is mainly concerned with the size and shape effect on the fatigue behaviour of specimens subjected to cyclic bending stresses. Blatherwick and Lazan[3.21] have shown that both size and shape of a specimen, particularly under non-uniform stress, affect its fatigue strength. Results of the experiments carried out on different specimens subjected to bending[3.22] have shown higher fatigue strength for small specimens than for somewhat larger specimens subjected to the same extreme fibre bending stresses. The higher fatigue lives in these experiments have been related mainly to the differences in stress gradients resulting from the different distances from the neutral axis to the extreme fibre. Hence in bigger specimens a larger volume of material is subjected to a stress nearly as high as the surface stress. A summary of the results of the size effect phenomenon on fatigue lives, and its relation to the stress gradients is presented in Fig. 3.6. As it can be seen in the case when there is no stress gradient in the specimen, no size effect is observed in axially loaded plain specimens (Case 1). Tests on specimens subjected to bending (Case 2) and notched specimens (Case 3) show a distinct size effect.

In addition to the effect of size and shape of the cross-section of the specimen, it has been found that the fatigue behaviour of welded joints is affected by the manner of loading. The results of the experiments on a butt weld, carried out by Christopher[3.23] on different types of specimen are given in Fig. 3.7. The fatigue life of a corner weld has shown the lowest fatigue performance in comparison to the other results[3.23].

3.3.7 Effect of Geometrical Stress Concentrations

It is well known that fatigue cracks start at the position of a stress concentration. Geometrical stress concentration is a consequence of discontinuity, or change in shape, either by decreasing (see Fig. 3.6, Case 3) or increasing the cross-sectional area as shown in Fig. 3.9. Neuber[3.24] has provided information that facilitates the evaluation of the theoretical peak stresses in many types of notched members. It has been shown that if a flat specimen is locally reinforced with a weld spot this spot produces a local increase in stress over the uniform stress in the non-reinforced bar. This fact is very important in welded joints.

Sanders et al.[3.30] used specimens of the form shown in Fig. 3.8a to investigate the effect of weld radius and the flank angle on fatigue behaviour, Fig. 3.8b. The results have shown that any measure to reduce the severity of geometrical discontinuity represented by the weld reinforcement, and hence the stress concentration at the toe of the weld, tends to increase the fatigue strength of the welded joints.

Stress concentrations in fillet welded joints have been determined for lap joints made with transverse fillet welds. In Table 3.1 the photoelastic results for fillet welded details shown in Fig. 3.9 found by different researchers are given. It is interesting to compare the differences in results obtained by different investigators. The stress concentration factor "K_t" in the table relates the maximum stress to the nominal stress at the point of interest as given by equation (3.1)

$$K_t = \frac{\sigma_{max}}{\sigma_{nom}} \qquad (3.1)$$

The value of the K_t for idealised fillet weld profiles on pure tension has been found to vary between 1.3 and 8 and for butt welds K_t varies between 1.1 and 2.5.

Much of the reported work is unsatisfactory as attempts are made to define absolute stress concentration factors at locations where sudden changes in section occur. At such locations there are often singularities and the figures arrived at are dependent on the degree of mesh fineness in the case of numerically derived values and the accuracy of measurements in the case of experimentally derived values. The stress concentration at the discontinuity is infinite and figures provided only have a qualitative significance as assessing the degree of fatigue performance of practical details in the "as welded" state.

Because of the irregular nature of the stress concentration in real structural joints, a precise theorètical evaluation of the stress concentration is not possible. Knowledge of the ideal theoretical stress concentration factor for a particular idealised type of joint again can only give some indication of the types of joint that are likely to have good and bad fatigue strength. It is more likely that the real usefulness of finding the local stress distribution is that it gives some idea of the stress gradient in the surrounding stress field and thus it must influence the propagation of cracks, and therefore fatigue life.

3.4 REVIEW OF TESTS ON WELDS SUBJECTED TO TRANSVERSE BENDING

During the last decade the fatigue behaviour of welded joints in orthotropic bridge decks with trapezoidal cross-section stiffeners has been investigated. The welded joint between the deck plate and the longitudinal stiffener is subjected under service loading mainly to transverse bending stress. Both single fillet and butt welds have been

used in this type of deck; fillet welds are preferred from the point of view of ease and cost of fabrication.

Fatigue tests carried out on four full-sized orthotropic bridge decks with trapezoidal stiffeners are reported by Davis and Toprac[3.31]. Two of the trough stiffeners used in their study had flanges bent parallel to the deck plate at the top of the sloping walls which were welded to the deck plate with fillet welds. The two remaining test specimens were carried out on more conventional unflanged stiffeners which were butt welded to the deck. The results of the experiments showed that fillet weld used in the flanged specimen had a very low fatigue life when compared with the butt welded joints. This work was very limited in scale and could be criticised on several points. However the results of the investigation highlighted the need for a more systematic study on the fatigue behaviour of single fillet welded joints as used in orthotropic steel bridge decks.

A series of tests were recently carried out, at the Welding Institute[3.34], on single fillet welded connections between the trapezoidal stiffeners and the deck plate in orthotropic bridge decks under transverse bending. It has been found that the joint is load-carrying and the most likely mode of failure is by crack propagation from the weld root through the throat under the action of a bending moment in the stiffener. The effects of the residual welding stress was studied by spot heating the welded joints. The results showed that the applied stress ratio had little effect on the fatigue life for weld failure. The results also indicated that for the specimen geometry the fatigue life of the weld detail was approximately the same for all modes of failure. This is a rather surprising result as the conditions of the weld at the toe and root of

the weld are quite different. (It is generally recognised that the irregularity at the root of the weld is much worse than at the toe.)

Studies were made by Seim and Ferwerda [3.32] on the deck-to-rib welded connections to determine the fatigue behaviour of full penetration butt welds with back-up plate and 80 per cent partial penetration butt welds both with and without reinforcement. (The experiments were carried out at stress ratios of zero and -1.0) The results showed a very wide scatter. It was concluded that the fatigue life of 80 per cent partial penetration welds is 13 to 23 per cent less than for 100 per cent (or full) penetration welds. The investigation suggests that the stress ratio is an important factor and gives different graphs for $R^*= 0$ and $R^*= -1.0$. This result shows that the magnitude of residual stress is low in these test specimens. No measurements were made concerning the residual welding stress. It is suggested that the weld reinforcement in this type of weld may increase the fatigue life of butt welds. It is also mentioned later that the increase of fatigue life may be due to weld quality and that the number of specimens tested is insufficient to give conclusive evidence.

No comparative study on the fatigue life of different types of fillet welded corner joints subjected to transverse bending was found in the literature.

*R = Stress ratio

3.5 SUMMARY

Literature relating to the effect of different variables on the fatigue behaviour of welded joints has been reviewed. The testing frequency, elapsed time and type of steel have been found to have no, or relatively small, effect on the fatigue behaviour of welded joints. The main factors affecting the fatigue behaviour and scatter in fatigue experimental results are the existence of different defects in a welded joint and the geometrical stress concentration. It was found that for welded joints containing high tensile residual welding stresses and subjected to cyclic tensile stress, the effect of residual stress on their fatigue life is small. However, under a stress cycle in which the nominal applied stresses are partially compressive the residual stresses have significant influence on their fatigue behaviour[3.1,3.20]. It was found that different types (see Fig. 3.7) of specimen tested in the laboratory show different fatigue behaviour under cyclic loading. No systematic comparative study concerning the fatigue behaviour of welded joints subjected to high cyclic transverse bending was found in the reviewed literature.

CHAPTER FOUR

DETAILS OF FATIGUE EXPERIMENTS

4.1 INTRODUCTION

4.1.1 General

The experimental studies described in this section were concerned with the behaviour of welded details subjected to the transverse bending stresses which occur in box girders used in bridge construction.

As has been shown in Chapter 3, there is little reliable data on which a proper assessment of the significance of repeated transverse distortional bending stresses can be based.

To rectify this, the results of the experimental study described in this Chapter are used in Chapter 6 to compare the fatigue performance of various practical details and provide information on which their design can be based. Poor fit-up of components which may influence considerably the fatigue life is given special attention.

4.1.2 Main Factors Affecting Fatigue Life of Weld Details

At welded joints subjected to repeated loading, microscopic cracks are initiated due to the presence of discontinuities and due to small sharp slag inclusions or undercuts [3.11]. The continuation of the repeated loading enlarges these cracks into macroscopic cracks which propagate and lead to structural failure. In this process, known as fatigue crack propagation, the behaviour depends mainly on the type of weld details used and the stresses to which they are subjected.

Factors such as type of steel, speed of loading, rest period, and surface finish, have very small effects on the fatigue behaviour of welded structures as stated in Chapter 3.

4.1.3 Stresses at the Joints

The nominal stresses at the joints of a welded structure depend on the applied loading and the geometry of the joint and may be evaluated by simple analytical methods. However, additional stresses are present at welded joints. These are stress concentrations caused by discontinuities at the joints and due to defects in the weld, and residual stresses resulting from the welding process. Each of these may significantly influence the fatigue resistance of the welded joints. The effect of stress raisers is to accelerate the process of fatigue crack propagation.

4.2 TEST PROGRAMME

4.2.1 Objectives of Test Programme

The general objective of the experiments in this research work was to establish the fatigue life of box corner welded joints when subjected to transverse bending stresses. It was required that the influence of the fit-up and manner of loading on the fatigue performance of fillet welded joints be given special attention and that the results should be analysed statistically. By studying and comparing the results with related experiments and analytical methods it was hoped to draw conclusions for practical use in the fatigue design of welded joints subjected to transverse bending especially in the context of cross section distortional effects.

The test results were to be used to achieve the following detailed objectives:

(a) to compare the fatigue performance of the different weld types tested, classify them according to their performance, and provide design information for each type;

(b) to review the existing design methods and compare them with the results of this investigation;

(c) to develop a mathematical relationship describing the fatigue behaviour of the different welded joints in terms of the number of cycles and stress ranges;

(d) to study the effect of poor fit-up of components, stress concentrations, residual stresses in welds on fatigue behaviour of the welded joints.

4.2.2 Selection of Experimental Approach

The fatigue behaviour of a structure may be studied by one of the following three experimental methods: (a) the actual structure method, (b) the full-scale or scaled model method, and (c) the small specimen method.

In method (a) strain measurements, made at the critical parts of the structure on site, must be carried out over an extremely long period of time. Measurements made in this way usually represent the total effect of several factors influencing the structure simultaneously, and therefore, the accuracy of the analysis of the observations is dependent upon the degrees to which these various factors can be isolated and quantified. An additional difficulty in interpreting the results is the extent to which design assumptions are not realised in actual structures.

Method (b) involves laboratory experiments carried out on models of a structure preferably at full scale. Models are subjected to repeated loading in a manner representative of actual conditions. This method is a desirable one insofar as it reproduces the actual conditions as closely as is possible in a laboratory, but the high costs of the testing equipment and specimen preparation limit its application.

In Method (c) a number of small specimens are subjected to repeated stress cycles of known magnitudes. In the present research programme, method (c) was used because of two main considerations. Firstly, the cost of the experiments using this method was much lower as compared to method (b) and, secondly, owing to the controlled laboratory conditions, the experimental results could be analysed more accurately for selected variables. In the present study the main variables chosen were joint detail and loading.

4.2.3 Types of Welded Joints Tested

Joint details used in several recently constructed steel box girders were obtained from the Bridge Engineering Section of the Department of the Environment (DoE) and the Constructional Steel Research and Development Organisation (CONSTRADO). Details from other research papers on box girder and orthotropic bridges were also studied. The most commonly used welded corner details were chosen for the purpose of this investigation.

Of the two main types of welds, fillet welded joints are generally more economical than butt welded joints. Although butt welded joints usually require less welding the edge preparation makes them more expensive than fillet welded joints. Normally it is only because of strength considerations that butt welds are used in preference to fillet welds.

The welded joint details considered in the investigation are:

(1) Double fillet welded corners with good fit-up (Series BEDFW*)

(2) Double fillet welded corners with poor fit-up (Series BEDFG)

(3) Single fillet welded corners with good fit-up subjected to maximum tensile stress at the toe of the weld (Series BESFW)

(4) Single fillet welded corners with poor fit-up subjected to maximum tensile stress at the toe of the weld (Series BESFG)

(5) Single fillet welded corners with good fit-up subjected to maximum tensile stress at the root of the weld (Series BESFWI)

(6) Single fillet welded corners with poor fit-up subjected to maximum tensile stress at the root of the weld (Series BESFGI)

(7) V-butt weld with sealing run (Series BEVBS)

(8) V-butt weld without sealing run (Series BEVB)

(9) Single bevel V-butt weld with sealing run (Series BESBS)

(10) Single bevel V-butt weld without sealing run (Series BESB)

---

*For specimen designation see Section 4.3.2.

The first six series, i.e. all the fillet welded joints, were studied in the greatest detail.

4.2.4 Loading Conditions

The test loading conditions were chosen on the basis of stress range being the dominant loading variable for welded joints.

4.3 DETAILS OF SPECIMENS

4.3.1 Design of Specimens

An important consideration in the selection of the specimen was to reproduce, as accurately as possible, the real pattern of stresses in the weld metal and the zones adjacent to the weld in bridge box girders caused by cross-sectional distortion. Due to a lack of adequate information, it has been common practice until now to base fatigue calculations on the behaviour of specimens which do not accurately reproduce real conditions. The specimens used in this present programme are different from any used before and are considered to represent more closely the transverse stresses caused by box girder cross-sectional distortion. It was necessary to provide specimens which were large enough to allow plates of a practical size and realistic welding details to be used.

Two types of specimens which were considered are shown in Fig. 4.1. Type A specimen which was similar in shape to the cross-section of a box girder, and easier to manufacture, was considered initially but its suitability was in doubt because of the complicated concentration of stresses which could exist at the upper and lower corners where the load was applied through the grips. It was

anticipated that the upper and lower welds might fail in fatigue before the side welds under study. Early tests carried out on specimens of Type A confirmed that suitable results were not easily obtainable. The problem was solved by using Type B specimens. Overall dimensions of the specimen and the grippings were so designed to fit in the testing rig. In Drawing 4.1 the exact dimensions of the specimen are shown. Drawing 4.2 shows the specimen with its specially designed grips to fit the Vibrophore testing machine. The dimensions of the grips are given in Drawings 4.3 and 4.4. A general view of the specimen fixed in the Vibrophore testing machine is shown in Plate 4.1.

4.3.2 Specimen Designation

The designation system used is such that it contains a complete description of the specimen geometry and type of weld.

The first two parts of the designation denote the plate type used in the specimen, i.e. bent plates or plates which are welded at the upper and lower of the specimen where it is gripped to the Vibrophore. The third part corresponds to the type of weld under consideration, e.g. double fillet, single fillet, etc. The fifth letter indicates the fit-up of components at the welded joints, i.e. fillet weld without gap or with gap between plates. The letter I shows the position of the weld. The number following the letter indicates the specimen number of the particular series. For example, specimen BESFGI3 may be identified as follows:

BE	SF	G	I	3
Bent End	Single Fillet	With Gap (a poor fit-up)	Weld on Inside	Specimen Number in Series

The weld types and conditions are designated as follows:

(a) Weld Types

DF - Double Fillet Weld

SF - Single Fillet Weld

VB - V-butt Weld

SB - Single Bevel butt Weld

(b) Joint Details

W - Fillet Weld without gap (good fit-up)

G - Fillet Weld with gap (poor fit-up)

S - Sealing Run

I - Inside

4.3.3 Fabrication of Specimens

General: To prepare Type B specimens steel plate, 2500 mm x 1250 mm, was flame-cut to size 1200 mm x 585 mm and these smaller plates were then bent transversely in the direction of the rolling of the steel plate to the shape shown in Fig. 4.2. Each was cut into three equal pieces to make the welding operation in the inner side of the frame possible. After the edges of the bent plates were prepared by machining, each pair of bent plates was fixed together by tack-welds at the two ends and the points of the joints where the specimen were to be cut. Then the

corners were welded completely as shown in Fig. 4.3. After completion of the welding and cooling of the long specimen it was sawn into four specimens. These small specimens were machined and ground to the final size. The sides of the specimens at the welded joints were polished with a fine grade of emery paper. Eight tensile specimens were also prepared from each plate to find the mechanical properties of the plate material. To ensure unformity of welding at the two corners, welding runs were made alternately at one corner and then the other. Details of the final weld sizes and gap sizes are given in Chapter 6.

Double Fillet Welded Corners(BEDFW): The welding was carried out with the specimens corners in the horizontal position. The root runs were made by a Vitemax electrode of 5 mm diameter and 254 mm length resulting in an average of 290 mm run in 83 secs (i.e. a speed of 2.494 mm/sec). The electric power was open circuit with a voltage of 100 volts, producing a welding current of 235 amps. The capping runs were carried out by a rod of the same size as above and with an open circuit of 100 volts but a welding current of 215 amps. The size and shape of the final weld is shown in Fig. 4.4.

Double Fillet Welded Corner with Poor Fit-up(BEDFG): The welding procedure was similar to that of specimen type BEDFW, the only difference being that a gap was introduced between the plates. The average welding speed of the root run was 3.6 mm/sec, the first run was 3.76 mm/sec and the second runs were 3.44 mm/sec. After several trial weldings a satisfactory method of producing 1 mm gaps was devised. Spacing strips of 1.2 mm thickness were prepared and placed between the edge of the plates and then the two bent plates were fixed by tack welds. Afterwards

strips were removed and the corners welded. The gaps generally shrank after welding from 1.2 mm to 1.0 mm, see Fig. 4.5. After completion of the specimens fabrication the actual sizes of the gaps were measured.

Single Fillet Welded Corners(BESFW): The welding procedure was similar to that of specimen type BEDFW, the only difference being that the weld was deposited on one side only and the welding was carried out with the specimen corners in the flat position. The speed of the welding for most of the specimens was measured, and the average speeds for different weld runs were as follows: the speed for the root run was 3.22 mm/sec, the first run 3.32 mm/sec, and the second run 3.419 mm/sec. The size and shape of the final weld is shown in Fig. 4.6.

Single Fillet Welded Corners with Poor Fit-up(BESFG): The welding procedure was similar to that of specimen type BESFW, with the average of the weld speeds of 3.274 mm/sec for the root run, 3.359 mm/sec for the first, and 3.314 mm/sec for the second capping run. The main difference compared with BESFW was the 1 mm gap between two plates as shown in Fig. 4.7. The gap was maintained in the same way as described for the specimen type BEDFG.

Single Fillet Welded Corners with Good Fit-up Subjected to Maximum Tensile Stress at the Root of the Weld(BESFWI): This specimen was designed so that the maximum tensile stress could be applied at the root of the weld without changing the direction of loading. The welding procedure for this series was similar to that of specimen BESFW, the only difference being that the weld was deposited inside the corners as shown in Fig. 4.8.

Single Fillet Welded Corners with Poor Fit-up Subjected to Maximum Tensile Stress at the Root of the Weld(BESFGI): The welding procedure was similar to that of specimen series BESFWI, the only difference being the gap between the plates. The gap was maintained in the same way as described for the specimen series BEDFG. The specified dimensions of the weld and its sequences of welding runs are shown in Fig. 4.9.

V-butt Welded Corners with Sealing Run(BEVBS): Before establishing the final process of welding to be employed in the actual tested specimens, several trial welding processes on simple specimens were carried out. The conditions of the welds were inspected by the destructive method until a satisfactory process was obtained. In this process the welding was first carried out with the specimen corners in the horizontal position. The root runs were made by a Vortic Marine electrode of 3.25 mm diameter with an average welding speed of 2.0 mm/sec. The arc welding was open circuit with a voltage of 100 volts producing a welding current of 127 amps. Sealing runs were carried out by the same type of welding electrode and the procedure was as above. The three filling runs were carried out with specimen corners in the flat position and the weld was made by a Radian electrode of 4 mm diameter. Speeds of the capping welds in the trial weld were 2.509, 3.427 and 3.315 mm/sec. The electric power was open circuit with a voltage of 100 volts and the current of 160 amps. The edge preparation and the welding sequence is shown in Fig. 4.10. The edges of the specimens were machined to the required shape and the slag at the root of the weld was cleaned, by air chisel, before the sealing run was carried out.

V-butt Welded Corners without Sealing Run(BEVB): The edge preparations and welding procedures were similar to those of Series BEVBS, the only difference being that the slag at the root of the weld was not chiselled out and the sealing run was not deposited. A typical detail of this series with its sequences of welding is shown in Fig. 4.11.

Single Bevel V-butt Welded Corners with Sealing Run(BESBS): As for Series BEVBS, the final welding process was established after several trial weldings on simple specimens. In the welding process which was finally adopted the root runs were made by Vortic Marine electrode 3.25 mm with an average speed of 1.839 mm/sec in the horizontal position. The arc welding condition, edge preparation, and cleaning of the slag at the root of the weld were the same as for Series BEVBS. The sealing run was carried out with 3.25 mm Radian electrode with a speed of 2.818 mm/sec. The three filling runs were carried out with the specimens'corners in the flat position. The first runs were made with a 3.25 mm electrode, and an average welding speed of 2.583 mm/sec. Second runs with 5 mm Radian electrode and an average welding speed of 2.45 mm/sec, and third runs with 4 mm Radian electrode and an average welding speed of 1.866 mm/sec, were laid down. The arc welding was open circuit with a voltage of 100 volts producing welding currents of 127 amps, 215 amps and 160 amps respectively on the first, second and third runs. The edge preparation and the welding sequences are shown in Fig. 4.12.

Single Bevel V-butt Welded Corners without Sealing Run(BESB): The edge preparations and welding processes were similar to those of specimen Series BESBS, the only difference being that the slag at the root of the weld was not chiselled out and the sealing runs were not deposited. The edge preparations and the welding sequences are shown in Fig. 4.13.

4.4 RESIDUAL STRESS MEASUREMENTS

The longitudinal and transverse residual stresses due to welding were measured by the non-sectioning method using a mechanical extensometer of the Demec type with a gauge length of 50.8 mm (2 in). In this method pairs of small holes of about 1 mm diameter were made at a number of points along and across the plate close to the weld corners. The positions of the Demec gauges were arranged as shown in Fig. 4.14. No gauges were located in the immediate zone of the welds.

Readings were taken before and after welding. In some specimens readings were also taken after sawing the long specimens into four and also after machining the short specimens into the final sizes ready for testing. This was done to check the longitudinal residual stress release. The final result gave the residual stresses in the main body of the specimen. Measurements were made on both faces of the plates. Each reading was made three times and then averaged. The results are given in Chapter 6.

4.5 DETAILS OF TESTS

4.5.1 Testing Equipment

Testing Machine: A Vibrophore high frequency fatigue testing machine type 2HPF421 of maximum capacity 10 tonne and 2 tonne dynamometers manufactured by the Amsler Co. was used. The machine operates electro-magnetically at the resonant frequency of the vibrating parts. The system consists of two masses connected through the specimen and a dynamometer in series. The load was measured by a dynamometer using an optical system. The load range, before initiation of the visible fatigue crack, was controlled automatically by a photoelectric device.

Instrumentation: Other instrumentation and equipment used included foil strain gauges manufactured by Showa type F-8 (8 mm length with gauge factor 2.12) with a fatigue life of 10^7 cycles at 3000 microstrain; dial gauges of .0001 in division, to measure the overall deformation of the specimen during static loading; magnifying glass x5, and Magnaflux flow finder to detect the appearance of the visible crack. A specially designed photographic system was used to record the crack propagation of the specimen at different stages from the time when the first crack appeared up to the time of failure. Since the Vibrophore is mounted on a spring loaded concrete block, the camera system had to be attached to the frame of the Vibrophore away from the concrete block and the floor. As cracks could appear on either side of the specimen, one optical bench was moved round for each position. Part of a Leitz Aristophot was removed from the stand and suspended horizontally and upside down from brackets on the two optical benches. Movements on the saddles in x and y directions enabled the crack to be kept in the field of view. A diffuse vertical illuminator was made using a cleaned half plate glass, an opal perspex screen and Anglepoise lamp. A close-up of the camera systems is shown in Plate 4.2. A double beam oscilloscope type CD1014.2 manufactured by Solatron was used to check the strain ranges at the points of measurements (see Plate 4.1) during application of the cyclic load. A stroboscope type PR9103 manufactured by Philips was used to calibrate the frequency of the test.

4.5.2 Fatigue Testing Procedure

General: To obtain the strain, and hence the stress, distribution in the specimens experimentally, one specimen each of the test Series BEDFW, BESFW and BEVBS was fitted with sixteen strain gauges at the positions shown in Fig. 4.15, and subjected to static loads of 0.2, 0.5 and 1.0 tonne (0.1968, 0.492 and 0.984 tonf). The vertical deflection of the specimens at the points of application of the load was also measured. Theoretical calculations and a comparison with experimental results are given in Section 4.6. The uniformity of the strains along the toe of the weld was also checked in two of the specimens. The specimens were then subjected to repeated loading until fatigue failure was reached.

The remainder of the specimens were tested with four strain gauges fitted at the points 1, 2, 3 and 4 as shown in Fig. 4.15. The applied loads were chosen in such a way that they caused a minimum tensile stress of +69.3*N/mm^2 (+4.5 tonf/in^2) at the toe of the weld. A few tests were also carried out with zero minimum stress to investigate the effect of residual stresses on fatigue behaviour.

Although an attempt was made to keep the temperature in the laboratory constant, it varied between 18^o - 25^{o}C. The order of testing for each series was randomised so that the effect of uncontrolled variables such as temperature or humidity could be included as a random error in the analysis of the test results. Thus any systematic bias due to these effects on the controlled variables was prevented.

The Vibrophore was calibrated carefully once before the start of the investigation and once again during the investigation period.

---

*The sign convention in this thesis is: (+) tension (-) compression.

Alignment of Specimens in Vibrophore: The points of application of the load in the specimen before testing were machined (about .01 in) so that a uniform load could be applied to the specimen, see Drawing 4.1. To check the uniformity of the strain distribution along the joint, strain gauges were fitted along the toe of the weld at predetermined positions for specimens Series BEDFW and BESFWI. The strain gauges were fitted opposite each other, both on the tension and compression sides. The results of the measured strain distribution for 0.5 tonne and 1.0 tonne applied load for both specimens are shown in Fig. 4.17 and 4.18. The results indicate that though the strain distribution along the welds was not perfectly uniform, the differences were nevertheless small. The mean value of the three measured strains on each side of the specimen was compared with the measured value of the strain at the centre, to find the accuracy of the measurement if only the strain gauges at points 1, 2, 3 and 4 were used. For the specimen BEDFW the differences were between 0.74-3.9 per cent and for the specimen BESFWI the differences were of the order of 0.9 to 8.3 per cent. The higher differences in the latter specimen may have been due to the irregularities at the root of the weld.

To verify the variation of strains on another type of specimen a simple T-type specimen with the same material and width as used in the other specimens was designed and strain gauges were fitted along the weld as shown in Fig. 4.19. This specimen was subjected to tension. The variation of the surface strains for this specimen was of the same order as for specimen Series BEDFW. The differences between the average strains along the weld on each side of the specimen and the strain at middle of the specimen were of the order of 0.8-2.6 per cent.

These tests thus give enough evidence to show that the strain gauges fitted at the middle width of the specimen close to the weld give a sufficiently accurate estimate of the average strain distribution along the weld.

Testing procedure: Before the application of the cyclic load, the minimum, mean and maximum static loads of the chosen strain range were applied to the specimen and the corresponding strain gauge readings were taken. The loading was then set to the mean value, and the cyclic loading of the relevant range was started. The machine was preset to stop automatically at the occurrence of a flaw. When the machine had stopped, the mean load and strain readings were checked and the specimen was examined with the aid of a magnifying glass or Magnaflux dye penetrants to detect whether a flaw had actually occurred. Normally a change in strains and mean load were observed after the initiation of a macrocrack in the specimen. The number of cycles, the mean load reading, and the crack length were recorded and the machine was allowed to continue automatically at the new mean load, but with the same strain range until the preset number of cycles was reached. Then the machine was operated manually. It should be noted that during fatigue fracturing of the specimen it was not possible to keep the strain range exactly constant although care was exercised to achieve this objective. This procedure was continued for several intervals of cycles until complete fracture. Whenever the machine stopped and the load and strain readings together with a visual inspection of the specimen did not indicate the existence of a crack, the machine was reset to the applied load range and the

procedure was repeated. The stoppage of the machine in such case could have been due to a change in the mains voltage. In most of the specimens the actual strains during the application of the cyclic load were measured by connecting the strain gauges to the Double Beam Oscilloscope. The response on the screen of the oscilloscope gave an almost perfect agreement with the measured static strains. The loading frequency of the machine was about 42 Hz and was calculated by using the counter in the control deck of the Vibrophore. This value in turn was checked independently by a Stroboscope which gave a frequency of 41-41.5 Hz.

4.5.3 Tests for Mechanical Properties of Materials

Tensile specimens were prepared according to BS18, part 2 to determine the mechanical properties of the parent material in an Amsler hydraulic multi-range testing machine type 10sZOA52 for tensile and compression tests. The deformation was measured with 4 in extensometer transducer and the two outputs were fed into an X-Y plotter. The rate of the deformation up to the time of strain hardening was controlled. Strain rates of about 0.03 per cent per minutes were applied in the elastic range, increasing to about 1.2 per cent per minute after the first yield had occurred. To determine the static yield load, the cross-heads of the machine were stopped at strains of 0.25, 0.5 and 0.8 per cent, but the load and extension recordings continued. The dynamic yield load prior to the halting of the cross-heads was registered at each stop. The same procedure was used to establish the mechanical properties of the filler material. Small specimens were made from the weld and were tested in the Instron universal testing machine. A typical load extension curve is shown in Fig. 4.20 and the test results are given in Table 6.1.

4.6 THEORETICAL STRESS ANALYSIS OF SPECIMEN

4.6.1 Calculation of Deflections and Nominal Stresses in Typical Specimen

In this section the nominal theoretical static stresses at the toe of the weld, and the deflections of the specimens used in the experiments are calculated. The theoretical results are compared with the value obtained from the test specimen which was fitted with sixteen strain gauges. Nominal bending stress in the throat of a single fillet welded joint is also derived.

The system under consideration is indeterminate to the third degree. The specimen is symmetrical along its vertical and horizontal axes and subjected to symmetrically located forces as shown in Fig. 4.21. By taking advantage of symmetry, the degree of indeterminancy is reduced to one and the analysis is carried out by the flexibility method. This is done by cutting the specimen hypothetically through the axes of symmetry in vertical and horizontal directions as shown in Fig. 4.22a. The applied load and the unit force are applied to the basic system and their corresponding bending moments are found. The results are shown in Figs 4.22c and 4.22b. The simple compatability equation of the system is

$$\delta_{11} x_1 + \Delta_{1p} = 0 \qquad (4.1)$$

To solve this equation for x_1 the quantities δ_{11} and Δ_{1p}, the values of displacement due to the unit bending moment and applied load respectively, can be determined by any of the conventional methods. Here the moment-area method is used. Assuming the upwards deflection to be positive and using the notation for the dimensions of the specimen as given in Fig. 4.22, the equations for the value of δ_{11} and Δ_{1p} are:

$$\delta_{11} = \frac{d}{2EI_1} + \frac{(\ell_1 - d)}{2EI_2} + \frac{\ell_2}{EI_3} \qquad (4.2)$$

$$\Delta_{1p} = -\left[\frac{Pd^2}{16EI_1} + \frac{P(\ell_1^2 - d^2)}{16EI_2} + \frac{P\ell_2(\ell_1 + b)}{4EI_3} \right] \qquad (4.3)$$

Substituting the values of δ_{11} and Δ_{1p} calculated by Equations (4.2) and (4.3) into Equation (4.1) the value of x_1 is calculated. Knowing the value of x_1 the final bending moments in the specimen can be calculated easily for any value of P. The bending moments of the specimen at points A, B and C (see Fig. 4.22a) are given by the following equations:

$$M_A = X_A = - \frac{\Delta_{1p}}{\delta_{11}} \qquad (4.4)$$

$$M_B = M_A - P \frac{\ell_1}{4} \qquad (4.5)$$

$$M_C = M_A - \frac{P}{2} \left(\frac{\ell_1}{2} + b \right) \qquad (4.6)$$

The axial force in the specimens' elements is given by:

$$N = \frac{P}{2 \cos 45^\circ} = \frac{P}{\sqrt{2}} \qquad (4.7)$$

Knowing the bending moments at points C and B the shear force at point C can be calculated. The theoretical deflection of the specimen at the point of application of the load is obtained from Equation (4.3). The detailed theoretical calculations of stresses and hence strains at different points and the deflection of the specimen at the point of

application of load for specimens Series BESFW and BESBS are given in Appendix 4.I. These theoretical results are compared with the experimental values in Section 4.6.3.

4.6.2 Calculation of Nominal Bending Stress in Fillet Weld Throat of Specimens BESFWI and BESFGI

Only the welded corners of the specimen from the points of contra-flexures, as shown in Fig. 4.28, need to be considered to calculate the nominal stresses in the throat of a single sided fillet weld. To calculate the bending stress in the weld, the detail of the geometry of the weld joint must be considered. The bending moment at the root of the weld for specimens Series BESFGI is

$$M_{A'} = P\left[L - (t + \delta)\right] \tag{4.8}$$

and the bending moment for type BESFWI then is obtained by putting $\delta = 0$ which leads to

$$M_E = P\left[L - t\right] \tag{4.9}$$

The ratio of the nominal stress at the root of the weld to the stress at point B' is

$$R_{A'} = \frac{\sigma_E}{\sigma_{B'}} = 4\left(\frac{t}{\ell}\right)^2 \left[\frac{L - (t + \delta)}{2(L - \ell) - t}\right] \tag{4.10}$$

and the ratio of the bending moments at points E and B' is

$$R_M = \frac{M_E}{M_{B'}} = \frac{\left[L - (t + \delta)\right]}{\left[L - (t/_2 + \ell)\right]} \tag{4.11}$$

The detailed calculation of the stresses in the weld throat is given in Appendix 4.II.

4.6.3 Comparison between Analytical and Experimental Results

The analytical and experimental results of stresses in the frame for the applied load p = 1 tonne (0.984 tonf) are shown in Fig. 4.25 to 4.27. The stresses calculated from measured strains in the single fillet welded specimen type BESFW8 are slightly lower than the theoretical results, the difference between measured (161.931 N/mm^2) and calculated (175.621 N/mm^2) stress being less than 8.5 per cent.

Calculations for the butt welded specimen BESBS are also given in Appendix 4.I. The analytical and experimental stress distribution across the thickness of the plate at the weld toe is as shown in Fig. 4.24. The analytical results at point C' are:

$$\sigma_t = \sigma_B - \sigma_N = 148.2 - 6.8 = 141.2 \text{ N/mm}^2 \ (9.2 \text{ tonf/in}^2)$$

$$\sigma_c = \sigma_B + \sigma_N = 154.5 \text{ N/mm}^2 \ (10.03 \text{ tonf/in}^2)$$

compared with the experimental results for the same applied load, which are:

$$\sigma_t = 144.4 \text{ N/mm}^2 \ (9.4 \text{ tonf/in}^2)$$

$$\sigma_c = 158.9 \text{ N/mm}^2 \ (10.3 \text{ tonf/in}^2)$$

The agreement between theoretical and experimental results for butt welded specimens is better than that for single fillet welded specimens as corner conditions conform more closely to those assumed in the analysis.

It should be noted that the corners of the specimen are predominantly subjected to bending stresses (151.1 N/mm^2) rather than axial stresses (6.8 N/mm^2).

CHAPTER FIVE

STATISTICAL ANALYSIS OF FATIGUE EXPERIMENTS

5.1 INTRODUCTION

Statistical analysis is an essential tool in the planning and interpretation of fatigue-test results. This is because of the very wide scatter obtained in fatigue testing[5.1,5.2,5.3,5.4]. It is also well established that the observed strengths of materials are considerably different from those determined theoretically. The reason for this discrepancy has been attributed to the fact that the real materials contain defects, flaws, or weak points. In welded details these defects are in the form of undercuts, slag inclusions, flaws or voids. In the statistical analysis of failure, it is assumed that these defects are randomly distributed and are of a random nature. By applying statistical analysis to fatigue data,not only the estimate of the mean line of the results will be established, but also some knowledge of the variance of that estimate will be gained. With this additional information the fatigue life of the particular detail can be found for a specified probability.

As the theory of statistics is based on the theory of probability, a short account of the fundamental concepts of probability and statistics appropriate to the analysis of fatigue data is given in this chapter.

5.2 INDEPENDENT AND DEPENDENT VARIABLES

When there are two variables in an experiment, as in this investigation, the variable determined by the experimentalist, i.e. the stress range, is called the "independent variable". The resulting value is the "dependent variable", i.e. the number of cycles to failure which depends on the selected value of the independent variable. The dependent variable is subjected to a certain amount of variation or scatter caused by imperfections. The probability distribution of this variation will be considered in this investigation. The independent variable, that is the stress range, is denoted by "X" and the dependent variable, the number of cycles, is denoted by "Y".

5.3 POPULATION AND SAMPLE

The hypothetical collection of all specimens prepared in a particular way, which could be tested, is called the "population". The prime parameters of the population are the arithmetic mean and variance which are denoted by "μ" and "σ^2". Any collection selected from the population is called the "sample". Any sample has a mean denoted by $\bar{y}$ and variance denoted by s^2. The sample mean is calculated by Equation (5.1)

$$\bar{y} = \frac{\sum_{i=1}^{n} y_i}{n} \tag{5.1}$$

and the sample variance is defined by Equation (5.2)

$$s^2 = \frac{1}{(n-1)} \sum_{i=1}^{n} (y_i - \bar{y})^2 \tag{5.2}$$

where y_i - is each individual observation

n - is the number of observations at each stress level

$(y_i - \bar{y})^2$ - is the square of the deviation of the observed values from the sample mean

The positive square root of the sample variance is defined as the "standard deviation" and denoted by "S"

$$S = \sqrt{\frac{\sum_{i=1}^{n} (y_i - \bar{y})^2}{(n - 1)}} \qquad (5.3)$$

The standard deviation is in the same units as the original measurements and represents the spread of the results. The denominator in Equations (5.2) and (5.3) is called the number of degrees of freedom of the estimate. Since in the statistical analysis of the fatigue data, the population mean and variance are not known, the sample mean and variance are used for their estimation, so that the value of (n-1) degrees of freedom is used instead of n.

It is sometimes much more useful to measure the spread of the results in relative terms, i.e. dividing the standard deviation by the sample mean. This ratio is called the coefficient of variation and is represented by Equation (5.4)

$$K_V = \frac{S}{\bar{y}} \qquad (5.4)$$

The advantage of using K_V compared to S is that it is independent of the units in which the variation is measured.

5.4 BASIC ASSUMPTIONS

It is assumed firstly that the observations are random from a population of all possible fatigue lives (y_{ij}) for each stress range (x_i) used. The validity of this assumption may be verified by the proper randomisation of the experiment using the table of random numbers. This method ensures that the influence of variability in the experiments is reflected in the test data.

The second assumption is that the fatigue lives or their transformations are distributed as Normal Gaussian Distributions. A Normal Gaussian Distribution and its validity to the fatigue data will be discussed in the following section.

5.5 THE FREQUENCY DISTRIBUTION

5.5.1 General

The experimental data can be represented graphically by plotting the number of cycles along the horizontal scale and the number of cases to failure on the vertical scale. The frequency distribution may be estimated using such a graph. In the limiting case the frequency curve can be given by Equation (5.5)

$$p = f(y) \tag{5.5}$$

where p equals the frequency of occurrence of a result. As only a limited number of test results are available, it cannot be certain that the histogram obtained will exactly represent the true relationship between p and y. The hypothetical shape of the frequency distribution and its function, with which the experimental data will later be found to conform closely, must be assumed and verified. This assumption must be made before starting the statistical analysis.

5.5.2 Normal Gaussian Distribution

One of the distributions which has been found to give an adequate fit to different types of data is the Normal Gaussian Curve, given by Equation (5.6)

$$f(y) = \frac{1}{\sigma\sqrt{2\pi}} \exp\left[-\frac{1}{2}\left(\frac{y-\mu}{\sigma}\right)^2\right] \qquad (5.6)$$

In Fig. 5.1 the general shape of this function is shown. This curve is symmetrical about the population mean value "μ" and approaches the y axis asymptotically to the left and right of the mean (i.e. at $y = -\infty$ and $y = +\infty$; $f(y) \to 0$).

The area under the Normal Distribution Curve represents the cumulative normal distribution which is the integral of Equation (5.6). Since the sum of all probabilities is equal to unity (or 100%) Equation (5.7) must be true

$$\frac{1}{\sigma\sqrt{2\pi}} \int_{-\infty}^{+\infty} \exp\left[-\frac{1}{2}\left(\frac{y-\mu}{\sigma}\right)^2\right] dy = 1. \qquad (5.7)$$

In Equation (5.7) the y values are considered to vary between $-\infty$ and $+\infty$ and yet in this investigation the observed values cannot extend so far from the mean. Furthermore, negative values of y have no physical meaning in the high cyclic fatigue life zone. To explain this peculiarity it must be remembered that the Normal Distribution Curve is used as an approximation to physical observations, and the mathematical equation is only valid between finite limits. For example, in the case of $(\mu \pm 3\sigma)$, the area under the curve is 99.74 per cent of the total area.

It follows that the probability of the dependent variable being less than or equal to any specified value is the area under the Normal Distribution Curve from "$-\infty$" to the specified value as given by Equation (5.8a)

$$P(y \leq y_1) = \frac{1}{\sigma\sqrt{2\pi}} \int_{-\infty}^{y} \exp\left[-\frac{1}{2}\left(\frac{y-\mu}{\sigma}\right)^2\right] dy. \qquad (5.8a)$$

and Equation (5.8b)

$$P(y_1 \leq y \leq y_2) = \frac{1}{\sigma\sqrt{2\pi}} \int_{y_1}^{y_2} \exp\left[-\frac{1}{2}\left(\frac{y-\mu}{\sigma}\right)^2\right] dy \qquad (5.8b)$$

represents the proportion of the results found between y_1 and y_2.

Equation (5.6) can be simplified by writing it in terms of the deviation of y from $\mu = 0$ and $\sigma^2 = 1$. This is done by making the transformation

$$U = \frac{y-\mu}{\sigma} \qquad (5.9)$$

Hence (5.6) becomes

$$f(u) = \frac{1}{\sqrt{2\pi}} \exp\left(-\frac{u^2}{2}\right) \qquad (5.10)$$

Equation (5.10) is known as the Standardised Form of the Normal Probability Curve, and the variable expressed in the form of Equation (5.9) is said to be in the standard form. The integration of Equation (5.10) cannot be performed explicitly, but the definite integral has been tabulated for a wide range of values of U and most statistical tables have been prepared for this form of distribution[5.5, (5.6, 5.7)].

5.5.3 Transformation of the Data to Logarithm Normal Distribution

The frequency distribution of the fatigue life departs from normality, so that it would not be safe to apply the common statistical tests[5.3,5.8,5.9]. It is found that the logarithm of the fatigue life gives a frequency distribution which approximates that of the cumulative normal distribution. To estimate the normality of the original results or their transformation the normal probability paper and χ^2-test for goodness-of-fit, as explained in the following sub-sections, can be used.

5.5.4 Normal Probability Paper

In Fig. 5.2, the cumulative distribution function of the Gaussian Normal Distribution is plotted. After a transformation of the vertical scale, f(u) will be plotted as a straight line. Graph paper with such a scale is called Normal Probability Paper.

Since the area under a standardised normal curve between the mean and a standard deviation is equal to 34.13 per cent of the total area under the curve, the standard deviation can be estimated from the graph by finding the difference in abscissa between the mean and the point whose ordinate is (50-34.13) = 15.87 per cent or between the mean and the 84.13 per cent point as shown in Fig. 5.3.

To find the approximate distribution of the fatigue results using probability paper, several methods of plotting positions have been proposed. One method suggested by Weibull and Gumbel[5.8] is that the data should first be arranged in the order of magnitude so that

$$y_1 \leq y_2 \leq y_3 \leq \ldots\ldots \leq y_n \qquad (5.12)$$

then at each point the observed cumulative frequency is calculated using Equation (5.13)

$$p(y_i) = \frac{\text{Number of observation} \leq y_i}{(n + 1)} \tag{5.13}$$

It is found that in most cases Equation (5.13) leads to a biased estimate of the population parameters[5.8]. An improvement was introduced by Blom[5.10] in Equation (5.14)

$$p(y) = \frac{i - 3/8}{n + 1/4} \tag{5.14}$$

which gives an unbiased estimate of the population.

5.5.5 χ^2-test for Goodness-of-Fit

To estimate the normality of the data at the specified significance level, the statistic called the χ^2-test for goodness-of-fit may be applied. To carry out this test, the data is divided into K groups. Each group must be arranged so that it contains at least five experimental results[5.5]. If n experiments are performed the number of groups, which is an integer number, can be calculated by the following inequality

$$K \leq \frac{n}{5} \tag{5.15}$$

The expected or theoretical frequency "E" and the observed frequency "O" are found. The agreement between the observed and expected values must be considered by using Equation (5.16)

$$\chi^2 = \sum_{i=1}^{K} \frac{(O_i - E_i)^2}{E_i} \qquad (5.16)$$

It must be noted that in Equation (5.16) only the number of groups is considered. The calculated value of χ^2 is then compared with those values given in χ^2 tables for different numbers of degrees of freedom. The number of degrees of freedom is calculated as K - (r+1), where "r" is the number of degrees of freedom for each parameter of the normal distribution estimated from the sample. In this investigation r equals 2, since μ and σ^2 are the estimated values. If the calculated value of χ^2 is much smaller than the theoretical value, "$\chi^2_{(1-\alpha)/d.f.}$", the hypothesis that the data is normally distributed at the significance level α can be accepted.

As experimental results in this investigation at each stress level are not enough, the transformation of the data is achieved by using Equation (5.9) for each stress range by substituting

$$y = \log N; \quad \mu = \overline{\log N} \quad \text{and} \quad \sigma = S$$

hence

$$U = \frac{\log N - \overline{\log N}}{S} \qquad (5.17)$$

After this transformation of results to the standardised probability curve, the χ^2-test is then performed using the calculated U-values and those given in the tables of statistics.

5.6 CONFIDENCE INTERVAL OF THE MEAN AND VARIANCE

5.6.1 General

In normally distributed data for which the true values of the parameters of the population (i.e. μ and σ^2) are not known, sample mean and variance are the best estimated values of the population parameters. However, it is desirable to find an interval estimate for these parameters. This interval estimate which is called the confidence interval is constructed so that we have a certain confidence that the unknown parameters of the population are contained within this interval in a stated proportion of time 'γ' called the "confidence level". In this case there is a risk of $(1-\gamma)$ that the interval does not contain the population parameters. For this reason the confidence level must be decided before the computation of the confidence interval. The greater the confidence level is the wider the confidence interval.

5.6.2 Confidence Interval of the Mean

In the computation of the confidence interval for the mean, the "standard error factor" must be considered. That is to say if random samples, size n, are taken from a normal distribution with mean "μ" and variance "σ^2", the confidence interval for the population mean, allowing for the standard error, has the limits given in the following Equation

$$\bar{y} + t_{\beta_{1,(n-1)}} \left(\frac{S}{\sqrt{n}}\right) \leq \mu \leq \bar{y} + t_{\beta_{2,(n-1)}} \left(\frac{S}{\sqrt{n}}\right) \qquad (5.18)$$

where $\beta_1 = (1-\gamma)/2$

and

$\beta_2 = (1+\gamma)/2$

and the value of t which represents the t-distribution depends on the number of degrees of freedom. In the case of small numbers of data the use of the t-distribution is restricted to the Normal Gaussian Distribution. In cases of a non-normal distribution the use of the t-distribution is justified if the number of data in a sample is sufficiently large.

5.6.3 Confidence Interval of the Variance

The following theorem is applied to find the confidence interval of the variance. If repeated random samples, size n, are taken from a normal distribution with variance σ^2, the statistic 'S^2', will vary from sample to sample. This forms a distribution called the χ^2-distribution given by Equation (5.19)

$$\chi^2 = (n-1) \frac{s^2}{\sigma^2} \tag{5.19}$$

Rearranging Equation (5.19) the confidence interval for the variance can be found. It has the limits given by the following inequality

$$\frac{s^2}{(\chi^2/\text{d.f.})_2} \leq \sigma^2 \leq \frac{s^2}{(\chi^2/\text{d.f.})_1} \tag{5.20}$$

The values of χ^2/d.f. are read from the table of statistics for a different number of degrees of freedom using the percentiles $100\beta_1$ and $100\beta_2$.

5.7 COMPARISON OF SAMPLE VARIANCES AND MEANS

5.7.1 General

Two or several sets of data are usually compared with each other by their means. However, before comparison of the means is made, it is necessary to examine whether or not the variances are significantly different. In the case where variances are not significantly different, it is possible to conclude that the population from which the samples were chosen has a common variance. In the following section, methods of comparing variances and means of samples will be discussed.

5.7.2 Comparison of Two or Several Variances

If two random samples, size n_1 and n_2 are selected from a normally distributed population with variance "σ^2", and their sample variances are S_1^2 and S_2^2, the ratio S_1^2/S_2^2 is expected to be close to unity, provided the number of experiments is large. It is shown that for the repeated samples of a population their ratio will follow the statistic called the "F-test" which is given by Equation (5.21)

$$F = \frac{S_1^2}{S_2^2} \tag{5.21}$$

where S_1^2 is the larger variance. To see whether the observed ratio S_1^2/S_2^2 is significantly larger than 1.0, it is compared with the upper percentage point of the F-distribution which is given in the table of statistics and expressed as $F_{(1-\alpha/2),(\gamma_1,\gamma_2)}$ where $\gamma_1 = (n_1-1)$ degrees of freedom in the numerator and $\gamma_2 = (n_2-1)$ degrees of freedom in the denominator. If the calculated value of F is smaller than the theoretical value, the hypothesis that the variances are equal is accepted at the 100α percent level of significance.

The F-test is only used to compare two variances. To test the equality of more than two variances, the BARTLETTS test [5.5,5.8] which is a special application of the χ^2-distribution may be applied. The value of χ^2 is calculated by the following equation

$$\chi^2 = \frac{1}{C}\left[f \ell n\ s_w^2 - \sum_{i=1}^{K} f_i \ell n\ s_i^2\right] \qquad (5.22)$$

where $f_i = n_i - 1$

$$f = \sum_{i=1}^{K} f_i$$

and

$$C = 1 + \frac{1}{3(K-1)}\left[\sum_{i=1}^{K}\frac{1}{f_i} - \frac{1}{f}\right]$$

The term s_w^2 is the combined (or pooled) variances within the samples, and is calculated using Equation (5.23) on the assumption that the variances of the K-samples are not significantly different.

$$s_w^2 = \frac{\sum_{i=1}^{K} f_i s_i^2}{f} \qquad (5.23)$$

When all samples are of the same size n, Equation (5.22) simplifies to

$$\chi^2 = \frac{(n-1)}{C}\left[K \ell n\ s_w^2 - \Sigma \ell n\, s_i^2\right] \qquad (5.24)$$

If the value of χ^2 computed either using Equations (5.22) or (5.24) is smaller than $\chi^2_{(1-\alpha),\,(K-1)}$ then the variances are not considered to be significantly different at the 100α percent level of significance and vice versa.

5.7.3 Comparison of Several Means

When the variances of K-samples are not significantly different the pooled variance of the K-samples is calculated by Equation (5.23). It is now intended to compare the means of the samples, using the F-distribution, to establish whether their means differ significantly or not.

The variance within the limits of the samples is calculated by the following Equation:

$$s_m^2 = \frac{\sum_{i=1}^{K} n_i (\bar{y}_i - \bar{y}_t)^2}{(K-1)} \qquad (5.25)$$

where $\bar{y}_t$ is the mean of all the samples' data considered and calculated by Equation (5.26)

$$\bar{y}_t = \frac{\sum_{i=1}^{K} \sum_{j=1}^{n_i} y_{ij}}{\sum_{i=1}^{K} n_i} \qquad (5.26)$$

y_{ij} is the j^{th} data from the i^{th} sample and $\bar{y}_i$ is the mean of the i^{th} sample. The theoretical value of the F-distribution is compared with the calculated value of F given by Equation (5.27)

$$F = \frac{s_m^2}{s_w^2} \qquad (5.27)$$

This is compared with the theoretical value of $F_{(1-\alpha),\ (\gamma_1,\gamma_2)}$ for $\gamma_1 = (K-1)$ and $\gamma_2 = \sum_{i=1}^{K} n_i - (K)$ degrees of freedom. If F is smaller than the theoretical value, the means are not considered to be significantly

different at 100 α percent level of significance.

When only two samples' means need to be compared the t-test given by Equation (5.28)

$$t = \frac{\bar{y}_1 - \bar{y}_2}{S_w \sqrt{\frac{1}{n_1} + \frac{1}{n_2}}} \qquad (5.28)$$

is applied, where S_w is calculated using Equation (5.23) for two samples.

If the calculated value of t is smaller than the theoretical $t_{(1-\alpha/2),(\gamma)}$, where $\gamma = (n_1 + n_2 - 2)$ degrees of freedom, the means are considered to be not significantly different at 100α percent level of significance.

5.8 REGRESSION ANALYSIS

5.8.1 General

In previous sections the statistical theory of one variable, without reference to the behaviour of any other variable, was discussed in the context of fatigue tests. In this section the statistical method, called "regression analysis", which describes the relation between two variables with specified confidence limits and probabilities is considered.

5.8.2 Assumptions of the Regression Analysis

The stress-fatigue life relation of the S-N curve may be described by linear regression analysis. The computations of the regression coefficients require no assumptions concerning the observations other than the linearity of the relation between variables.

However, the computation of confidence intervals, percentiles of survival, and statistical tests using the regression analysis require the acceptance of certain assumptions. These are:

1. The observed value of y_i ($\log N_i$) is a random observation from a population of all possible y_i for each x_i (σ_i or $\log\sigma_i$) used.

2. The observed values of fatigue lives or their transformed lives to the assigned value of stress level are normally distributed.

3. The fatigue lives (or their transformations) for all values of the stress range have a common standard error of variance.

The first assumption may be verified by the proper randomisation of test sequences. The second and third assumptions can be verified by using the techniques described in section (5.5).

5.8.3 Estimate of the Regression Line

The most satisfactory method to determine the best fit-up line consists of the application of the theory of least squares to the determination of the coefficients in the linear equation (5.11). By definition, the sum of the squares of the deviations of the individual values of y (logN), from those predicted by the line is the minimum. The reasons why this method, at least theoretically, is preferable to other methods are as follows:

1. It gives the most probable linear relationship between y and x if the deviations of the individual observations from the line, in the y-direction, are assumed to be normally distributed.

2. The probable error (standard error) of the estimate of y (logN) from the line of regression is less than from any other straight line.

Let the line of regression y on x be given by

$$Y = a + bX \tag{5.29}$$

The capital letter is introduced to denote the predicted or mean value of the dependent variable, and the small letter is used to denote an observed value. By definition, the quantity $Q = \Sigma (y_i - Y)^2$ must be a minimum. This leads to the two conditions

$$\left.\begin{aligned} \frac{\partial Q}{\partial a} &= 0 \\ \text{and} \\ \frac{\partial Q}{\partial b} &= 0 \end{aligned}\right\} \tag{5.30}$$

These two conditions give the two equations for a and b.

Hence

$$b = \frac{n\Sigma(x_i y_i) - \Sigma x_i \, \Sigma y_i}{n \, \Sigma(x_i)^2 - (\Sigma x_i)^2} \tag{5.30a}$$

the quantity "b" is called the "regression coefficient" of y upon x

and

$$a = \bar{y} + b\,(x - \bar{x}) \tag{5.30b}$$

The line of regression can thus be written

$$Y = \bar{y} + b\,(x - \bar{x}) \tag{5.31}$$

Choice of the Linear Function: To establish the best mathematical equation relating the fatigue life to the stress range two transformations have been applied to linearise their relations. These are:
the logarithmic equation,

$$\log N = \log A + B \log \sigma_R \tag{5.32}$$

or

$$N = A\sigma_R^B$$

and the semi-logarithmic equation,

$$\log N = A + B\sigma_R \tag{5.33}$$

or

$$N = 10^{(A + B\sigma_R)}$$

The selection of the best equation is made by calculation of the correlation coefficient. If the correlation coefficient is close to unity there is good correlation between the actual and the predicted results,i.e. the fitted regression line is a good fit.

Correlation between Predicted and the Experimental Results: The precision of the regression Equation (5.31) depends on the number of experiments, on the extent of the scatter about the regression line and on the range of values of $x(\sigma_R$ or $\log\sigma_R)$ variables.

It is shown that the total variation of all the observations (y or logN) about their weighted mean consists of two parts as given in the following Equation (5.34)

$$\Sigma(y_i-\bar{y}_t)^2 = \Sigma(y_i-Y_i)^2 + \Sigma(Y_i-\bar{y}_t)^2 \qquad (5.34)$$

where $\Sigma(y_i-Y_i)^2$ is called the residual variation, and $\Sigma(Y_i-\bar{y}_t)^2 = b^2\Sigma(X-\bar{X})^2$ is called the explained variation.

When all the results fall on the regression line the value of the residual variation is zero; i.e. the correlation between the predicted and the experimental results is perfect. In this case the ratio

$$R^2 = \frac{\Sigma(Y_i-\bar{y}_t)^2}{\Sigma(y_i-\bar{y}_t)^2} = 1$$

As the residual value increases, the explained variation decreases so the value of R^2 becomes smaller. In the limit when there is no correlation between y and x, the value of R^2 is zero. The square root of R^2 is called the correlation coefficient and is given by

$$R = \pm\sqrt{\frac{\Sigma(Y_i-\bar{y}_t)^2}{\Sigma(y_i-\bar{y}_t)^2}} \qquad (5.35)$$

5.8.4 Standard Error of a Prediction of a Further Observation

When the mathematical equation used for the prediction of the S-N is regarded as satisfactory, the coefficients of the equation are still subject to error because they are estimated from a limited number of experimental data. The variation of the test results about

the predicted line can be calculated from Equation (5.37)

$$S_R^2 = \frac{\sum_{i=1}^{n} (y_i - Y_i)^2}{(n-2)} \qquad (5.37)$$

The square root of S_R^2, called the "standard error of estimate", gives the scatter of the data about the predicted line. Using Equation (5.37) for S_R the confidence limits of the predicted value are then given by Equation (5.38)

$$Y_{C.L} = Y_K \pm t.S_R \sqrt{\left[\frac{1+n}{n} + \frac{(X_k - \bar{x}_t)^2}{(x_i - \bar{x}_t)^2}\right]} \qquad (5.38)$$

where t is the value obtained from tables of t-distribution for (n-2) degrees of freedom corresponding to a pre-assigned confidence level. As can be seen from Equation (5.38) the resulting confidence limits are hyperbolic, with the closest point at the mean value. The error increases as the independent variable moves further away from the mean value (see Fig. 5.4).

5.8.5 Comparison of Two Regression Lines

After the determination of the regression lines for each series of the experimental results, they can be compared with each other to find whether they are identical or not. To achieve this objective the two variances about the regression lines are first compared as described in Section 5.7.2, and then the t-distribution is used to compare the slopes of the regression lines. In comparing the two variances about their regression lines the following cases may occur:

CASE A: When the two variances about their regression lines are significantly different, the t-test can be used to compare the slopes of the lines. The calculated value of t for this case is given by Equation (5.39)

$$t = \frac{b_1 - b_2}{S_R\sqrt{\frac{1}{h_1} + \frac{1}{h_2}}} \tag{5.39}$$

where S_R is calculated for each series of data by Equation (5.37) and

$$h_1 = \sum_{i=1}^{K} n_i (x_i - \bar{X}_1)^2$$

$$h_2 = \sum_{i=1}^{K} n_i (x_i - \bar{X}_2)^2$$

This value of t is compared with t_β for f-degrees of freedom given by the following expression

$$f = \left[\frac{C^2}{(N_1-1)} + \frac{(1-C)^2}{(N_2-1)}\right]^2 \tag{5.40}$$

where,

$$C = \frac{\frac{S_R^2}{N_i}}{\sum_{i=1}^{2} \frac{S_{Ri}^2}{N_i}}$$

If $t \leq t_\beta$ then the slopes are not significantly different and the two lines may be parallel or identical. The identity of

the two lines can be tested by Equation (5.41)

$$t = \frac{D - E}{S_r \left[\frac{1}{(\bar{X}_1 - x_2)^2} \left(\sum_{i=1}^{2} \frac{1}{N_i} \right) + \left(\sum_{i=1}^{2} \frac{1}{h_i} \right) \right]^{1/2}} \tag{5.41}$$

where

$$D = \frac{a_1 - a_2}{\bar{X}_1 - \bar{x}_2}$$

$$E = \frac{b_1 h_1 + b_2 h_2}{h_1 + h_2}$$

The computed value of t is compared with the value of t_β for $(N_1 + N_2 - 3)$ degrees of freedom. If $t \leq t_\beta$, the regression lines are significantly different at the 100β significant level.

CASE B: In this case the two variances about their regression lines are not significantly different. The pooled variance of the two series S^2_{RP} is calculated from Equation (5.42)

$$S^2_{RP} = \frac{\sum_{i=1}^{2} (N_i - 2) S^2_{Ri}}{\sum_{i=1}^{2} (N_i - 2)} \tag{5.42}$$

where S^2_{Ri} is calculated from Equation (5.37) for each set of data.

Then the slopes of the two lines are compared by the substitution of the S^2_{RP} for S^2_{Ri} which leads to the following equation

$$t = \frac{b_1 - b_2}{S_{RP}\sqrt{\frac{1}{h_1} + \frac{1}{h_2}}} \tag{5.43}$$

This value is compared with t_β for $\sum_{i=1}^{2} (N_i-2)$ degrees of freedom. If the slopes are not significantly different, the two lines could be considered parallel or identical. The identify of the two lines is tested, as for Case A, by substituting the value of S_r^2 as given by Equation (5.44) in Equation (5.41)

$$S_r^2 = \frac{\sum_{i=1}^{2} (N_i-2)\ S_{Ri}^2 + H}{(N_1 + N_2 - 3)} \tag{5.44}$$

where

$$H = \frac{(b_1-b_2)^2}{\frac{1}{h_1} + \frac{1}{h_2}}$$

If the computed value of t is smaller than the value of t_β, as given in the table of statistics for $(N_1 + N_2 - 3)$ degrees of freedom, then the regression lines are not significantly different.

5.9 P-S-N CURVES

The regression equation describes the relationship between the two variables x and y where "Y" is the 50 per cent probability line, i.e. there is a 50 per cent possibility that the failure due to fatigue at a given stress range may happen at a number of cycles

equal to or less than the number of cycles given by the regression equation. To find the lower or higher probability curve the distribution function of the dependent variable must be known. In S-N testing of the fatigue results it is found that a "log-normal" distribution of number of cycles fits the results with good accuracy. Taking this fact into account, the relationship between the probabilities,stress range and number of cycles, can be established by using the cumulative normal distribution function as given in Equation (5.45)

$$P = \frac{1}{S_R \sqrt{2\pi}} \int_{-\infty}^{y_p} \exp\left[-\frac{1}{2} \left(\frac{y-Y}{S_R} \right)^2 \right] dy \qquad (5.45)$$

where Y - is the predicted S-N line

S_R^2 - is the variance about the regression line.

The y_p value corresponding to a probability level "p" is then obtained from

$$y_p = Y \pm U_p \cdot S_R \qquad (5.46)$$

where U_p is the "normal deviate", which is tabulated in most statistical books. By applying Equation (5.46) a complete relationship between probability, number of cycles, and stress can be established.

5.10 APPLICATION OF ABOVE ANALYSIS TO PRESENT TESTS

To analyse the fatigue data statistically a computer program was developed. The statistical analysis and discussion of the experimental results are given in Chapter Six.

CHAPTER SIX

EXPERIMENTAL RESULTS AND DISCUSSION

6.1 INTRODUCTION

As stated previously special emphasis was laid on the fatigue behaviour of fillet welded joints as an examination of previous studies has shown that welded joints of this type have a much lower fatigue strength than butt welded joints. However, some tests were carried out on butt welded joints and V-butt welds were found to have a good performance under fatigue loading. The test results obtained for butt welds have not been subjected to statistical analysis because of the very small number of specimens tested.

In all experiments the controlled stress levels were selected as being the nominal flexural stresses in the base metal of the tension side at strain gauges number 3 and 4 as shown in Fig. 4.15. The testing procedure adopted was as described in Chapter 4. The results and evaluation of the experimental analysis of the data are summarised in this chapter for each type of welded joint. Crack initiation and propagation are discussed and where possible the results are compared with those of other relevant research work.

6.1.1 General

The determination of the fatigue life, may be divided in general into two phases: (a) determination of the finite fatigue life, and (b) determination of the mean fatigue limit. This investigation was concerned mainly with relatively high cyclic

finite fatigue life of welded corner joints and particularly the effect of poor fit-up behaviour. However in some test series the specimens did not fail in the low stress range within the range of cycles to which they were subjected.

6.1.2 Statistical Factors

Most tests were carried out randomly using the table of random numbers, but in some cases this procedure could not be followed. At the beginning of some test series one or two experiments were carried out at a high stress level to establish the required stress range to be applied to the rest of the specimens in that series.

The minimum number of tests required for the determintion of the P-S-N curves depends on the scatter of the results and on the confidence level desired. BS 3518 part 5 1962 [6.1] and ASTM Committee E-9 on Fatigue [6.2] recommend that at least five or six specimens must be tested at each stress level to determine the P-S-N curves. To verify any statistical hypothesis, a level of significance must be selected. In this study the values of 5 and 10 percent levels of significance are considered in the statistical analysis.

In the initial program, it was planned to test sixteen specimens in each series at three different stress levels. This would have given between 10 - 12 results at each stress level, had both joints failed. But, due to small differences in the welds on both sides (such as weld size, slag inclusion, undercuts or other defects), only one of the welds failed in some specimens. On account of this the number of specimens in each fillet welded joint series was increased to about twenty.

6.2 FATIGUE FAILURE OF THE SPECIMENS

6.2.1 Failure Criterion

Generally, fatigue failure of welded joints can be defined as a progressive failure of a component or part of a structure under repeated loads. To give a single comprehensive criterion of failure which is applicable to all types of detail under various conditions is not possible. In plotting the experimental fatigue results, researchers have used different criteria of failure for their S-N curves. In certain investigations[3.8, 3.32] the plotted points are those of the first visual cracks in the specimens and in others the results are related to the final fatigue failure of the specimens[3.33]. The former is usually used for full-scale specimens and the latter for small specimens.

In this work the propagation of the crack was observed and registered in cases where the crack initiated and propagated from the toe or surface of the weld. Usually a change in the measured strains was recorded when the fatigue crack initiated, but in test series BESFWI the change of strain was small for a long crack. The final failure was not considered to be suitable, because of the difficulty of operating the machine manually during the fatigue crack propagation process. It was therefore not possible to maintain the exact value of the required strain range during this stage. After the completion of several tests a suitable criterion of fatigue failure was considered to be the appearance of about 1 mm long crack on the side of the specimen as shown in Plates 6.1 and 6.2.

6.2.2 Modes of Failure

Three main modes of fatigue failures were observed in all tests. These were,

1. A toe fatigue fracture (for simplicity referred to as Type 1, and shown in Fig. 6.1(a)) which is a fracture in which the crack initiated from the toe of the weld and propagated mainly through the parent material (see Plates 6.1 and 6.2).

2. A weld surface fracture (referred to as Type 2 and shown in Fig. 6.1(b)) which is a fracture in which the crack initiated from the surface of the weld and propagated through the weld throat (see Plate 6.19).

3. A root fatigue fracture (referred to as Type 3 and shown in Fig. 6.1(c)) which is a fatigue fracture in which the crack initiated from the root of the weld and propagated through the weld throat (see Plates 6.23 and 6.24).

Two zones, a fatigue fracture zone and a rupture zone as shown in Figs. 6.2(a) and (b), were clearly evident when the fractured surface of the failed specimens was inspected. In most cases of fatigue fracture zone the origin of the crack initiation could be clearly identified. It was found that the size of the fatigue fractured zone was generally related to the level of the stress - the lower the stress range the greater the fatigue fractured zone.

6.2.3 Detection of Failure

In the first instance a specimen of series BEDFW was tested without polishing the sides. The resulting crack on the side of the specimen was of the form shown in Plate 6.3. As can be seen, the crack was observed at different points, some of which could be related to the roughness of the surface. Moreover, depending on the angle of the light and shadows produced by the roughness of the surface, it was difficult to observe the pattern of the propagated crack on the side of the specimen. Therefore, the sides of the specimens at the welded joints were polished before testing. This was also necessary to reveal the structural details of the welded joints using etching techniques. As can be seen in Plate 6.4 the polishing produced satisfactory results and the remaining experiments were carried out on polished specimens.

A 5 percent nital solution, i.e. 5 percent nitric acid and 95 percent alcohol, was used for etching the weld joints. The weld metal and the heat affected zones of the parent material were seen clearly after etching. This technique was used throughout the experiments.

6.3 MATERIAL

The material used for the test specimens was structural mild steel to BS15 Grade 43A of 12 mm and 12.7 mm thicknesses. The mechanical properties and chemical analysis of the parent materials as supplied by the steel manufacturer and the results obtained in the laboratory are given in Tables 6.1(a) and 6.2. The mechanical properties of the weld as determined on small specimens made from the deposited weld are also given in Table 6.1(b).

6.4 FATIGUE TESTS ON DOUBLE FILLET WELDED CORNERS

6.4.1 General

Two series of tests were carried out on double fillet welded corner joints. These were test series BEDFW and BEDFG. Test series BEDFW was performed to provide an experimental relationship between the applied stress range and the probable fatigue life of a double fillet welded corner with good fit-up between the plates.

The existence of gaps (poor fit-up) in welded box sections seems to be an inevitable consequence of manufacturing and fabrication tolerances. To investigate the effect of poor fit-up between the plates on the fatigue behaviour of double fillet welded corners, test series BEDFG was carried out. The results of these two test series and their comparison with each other are discussed in this section.

6.4.2 Test Series BEDFW

After manufacturing the test specimens, the actual sizes of most welds were measured. The leg lengths of the welds varied between 7.0 to 13.5 mm and the size of the weld throat ranged from 6.0 mm to 7.5 mm. The average leg length based on 18 samples was 9.6 mm and the mean value of the weld throats was 6.3 mm. All the welds were inspected prior to fatigue testing. At the root of most of the welds a lack of penetration of about 0.5 - 1.5 mm and in some places voids of about 0.5 mm or less were observed, see Plates 6.4 and 6.6.

In one of the long specimens, Fig. 4.14, the residual stresses were measured and the results are given in Table 6.3. They indicate the presence of bending residual stresses perpendicular to the direction of the weld and large tensile residual stresses along the weld, in the vicinity of the filler material. During the application of cyclic load to the specimens subjected to high stresses some permanent deformation was observed which could indicate that the residual stresses were redistributed.

Specimens in these series failed with a Type 1 fatigue fracture, of two varieties "a" and "b". In type "a" the fatigue crack started from one point at the toe of the weld as shown in Fig. 6.1 and propagated through the filler material, usually about 0.5 - 1 mm, then propagated through the heat affected zones (HAZ) and continued through the parent material as shown in Plates 6.4 and 6.5. In some cases the crack propagated directly through the HAZ and then through the parent material, see Plate 6.6. In type "b" cracks originated from two or more points and propagated in the same manner as those in "a". These differences may be related to the position of the defects at the toe of the weld. The condition of the weld before testing for specimen BEDFW-3 is shown in Plate 6.7. The propagated crack along the toe of the weld on both sides of the same specimen is shown in Plates 6.8 and 6.9.

The effect of residual locked-in stresses was studied in detail on specimen series BESFWIR. (The experimental and analytical results of this study are given in Chapter 7.) It was found that in cases where $\sigma_s < \sigma_y$ the combined effect of locked-in and applied stresses must be considered in the interpretation of results.

The average of the transverse locked-in stresses on the outside face of the specimen close to the weld was between 64 - 84 N/mm^2 compression stress (see Parts I and IV of the specimen as given in Table 6.3), and the locked-in stress inside the specimen ranged between 91 and 100 N/mm^2 tensile stress. It was clear that the stresses at the toe of the welds at the locations of strain gauge numbers 3 and 4 would be subjected to tensile fluctuating stresses.

In specimens subjected to low stress levels, when the fatigue crack propagated to half of the plate thickness, a crack appeared on the compression side of the specimen (see Plate 6.6). Both cracks then propagated to meet somewhere about 9 - 10 mm from the tension side*. This phenomenon is related to the existence of the residual welding stresses in the specimen. In specimen BEDFW-6 (see Table 6.4), which was subjected to a stress range of 169.3 N/mm^2 with σ_{min} = 0.0, the first visual crack was seen on the compression side of the specimen after 2.179×10^6 cycles. This crack propagated in the same manner as in other specimens of this series, i.e. Type 1 fatigue fracture. The fatigue life of this specimen is higher compared with other specimens within the same applied stress range. Assuming that the magnitude of the residual welding stress in this specimen can be as those given in Table 6.3 then it follows that the side of the specimen with SG-1 is in fact subjected to fluctuating tensile stress. The fracture surface of specimens BEDFW-10 and BEDFW-6 are shown in Plates 6.10 and 7.4 respectively. It should be noticed that in both specimens the fatigue cracks propagated with a

---

*Tension side of the specimen due to applied load.

semi-elliptic crack front shape across the plate width and through the plate thickness. It was also noted that the pattern of the crack propagation through the plate was not at right angles to the plate surface, as might be expected by first considering the direction of the nominal stress, but that the path of the crack was inclined to the surface. This reflects the direction of the maximum principle tensile stress in the region near the weld which is at right angles to the path of the crack.

The increase in fatigue life of the specimen from the time of the first visible crack on the side up to the final failure of the specimen varied between 1.5 to 33.7 percent. This variation in most cases depended on the applied stress range, the higher the load the shorter the final failure process. The stress range, the mean stress readings due to applied load at the tension side of the specimen, the number of cycles corresponding to the appearance of the first visual side crack, and the number of cycles related to the final fatigue failure of the specimens are all given in Table 6.4.

To show the Log Normal Distribution of the data graphically stress curves were first plotted. In Fig. 6.3 the P calculated by equation (5.14) is plotted against logN for each stress level separately. For stress ranges 169.3 N/mm^2 and 138.15 N/mm^2 the results follow a straight line. The result seems to depart from the Normal Distribution at stress range 107.0 N/mm^2. The χ^2-test for goodness-of-fit was also carried out. The result is given in Table 6.28. The test was passed at 5 percent and 10 percent level of significance. In the light of the results of these two statistical tests it may be concluded that the transformed fatigue lives into logN are normally distributed.

A regression analysis was carried out using two different functions of $\log N = f(\log\sigma_R)$ and $\log N = f(\sigma_R)$. The log-log function showed a better correlation factor, as can be seen in Table 6.33. In Fig. 6.4 the cumulative frequency distribution of errors is plotted. A straight-line relationship holds between e_i and P. The mean fatigue life with its 95 percent confidence limit is shown in Fig. 6.5 and the mean fatigue life with various probabilities of failure is given in Fig. 6.6.

The results of the tests which did not fail at the low stress range were not included in the statistical analysis.

Comparison with Relevant Results: This type of welded joint would normally be designed as a Class F welded detail according to the fatigue clause in BS 153, part 3B [6.3] or to the recent fatigue clause in the Merrison report, part III [6.4]. The test results therefore were compared with corresponding design curves given in the latter reference as shown in Fig. 6.5. It can be noted that the test results showed a higher fatigue life than a Class F weld detail. On the same graph Class D and C of reference [6.4] and Class D for welded joints according to reference [6.5], is shown. Class D of the Merrison report is the closest prediction line although at a high stress level it gives a conservative prediction. (The mean fatigue strength of the test series BEDFW was ≈ 142 N/mm^2 in comparison with ≈ 125 N/mm^2 for Class D of Merrison report at 2×10^6 cycles.) It is possible that the reason why the design curves for this type of welded joint give conservative predictions is that they are based on axially loaded specimens but not specimens subjected to bending. An extensive study was carried

out on welded I-beams subjected to bending. The stress gradient in the flanges of the I-beam are so small that it is possible to assume that the welds are subjected to axial stresses. However such an approximation cannot be valid in the design of welded corners of box sections subjected to transverse bending.

It was of interest to compare the results of the present study with other fatigue investigations similar to this work. Most of the available past work on double fillet welded joints was carried out on T or cruciform specimens under axial load and some under bending. As was discussed in Chapter 3 (see section 3.3.6) both stress gradient and shape of the specimen significantly affect the fatigue behaviour of the welded joints. The investigations most relevant to this work were the knee-joint tests carried out by Christopher[3.23]. Unfortunately those experiments were concerned with low cycle fatigue life of welded joints. It was thought that from the many reviewed investigations concerning fatigue behaviour of double fillet welds on cruciform specimens, the most relevant results were those obtained by Evans and Jones [6.6]. In Fig. 6.5 the results of the experiments carried out on the specimens shown in Fig. 6.32 are given. The experiments were carried out in Amsler Vibrophore machines and the specimens were subjected to bending stress at zero mean stress. It is reported that the specimens were undercut at the weld toe as a result of grinding. The design stresses given are the nominal stresses based on nominal plate thickness. The design ratio of the weld height to plate thickness in Evans and Jones' study is 0.75 which is close to 0.78 of this investigation. The fatigue failure in their study is also of Type 1. Unfortunately the

criteria of failure and the magnitude of residual stresses are not given. The results related to only tensile part of the applied cyclic stress and that related to the applied stress range is plotted in Fig. 6.5. As it was noted at low stress level, if only the tensile applied stress is considered, their results fall in the scatter band of this investigation, but at stress level $\sigma_R = \pm$ 100 N/mm^2 the applied stress range gives similar result. These differences may be related to the existence of residual stresses or the plastic deformation at the toe of the weld due to the undercuts.

6.4.3 Test Series BEDFG

The gap of 1 mm width was thought to be representative of the poor fit-up likely to occur in practice. The actual sizes of the gaps were measured before testing at the ends of the specimens. Their widths varied between 0.6 mm to 1.3 mm with an average of 0.83 mm. The length of the gaps, i.e. "Wg", varied in the range 8.5 to 13.7 mm with an average of 9.8 mm. The general shape of the gaps also varied from one specimen to another. In Plates 6.12 to 6.14 the variation of the shape and size of the gaps can be seen. The dimensions of the weld were measured with tolerance limits of ±0.25 mm at nine points along the weld. The results of the measurements for specimens BEDFG-9 for both weld corners are given in Tables 6.5a and 6.5b. In Plate 6.12 a propagated crack through the thickness of the plate for the same specimen is shown. The first crack 22 mm long was seen along the toe of the weld on the side with SG-3, 15 mm from point 1.0 (see diagram of the Table 6.5a) after 1.225 million cycles. Then a crack, 31 mm long, was observed on the side with SG-4 along the toe and 27 mm away from point 1. The crack on the side with

SG-3 propagated until final failure while the fatigue crack on the other side was propagating very slowly. At the final stage when the joint on the side with SG-3 failed, the length of the crack along the weld on the other joint of the specimen was 69 mm. It was noted that in both welds the cracks started to propagate where the leg length of the weld along the direction of the weld was the smallest. The fracture surfaces of both cracks were inspected and a fatigue failure of Type 1b was seen on the side with SG-3 and a fracture surface of Type 1a was observed on the side with SG-4. The leg length of the weld in the y-direction, i.e. y_1 and y_2 varied between 8 mm and 12.6 mm. The mean value of the leg length in the same direction was 10.13 mm. The leg length of the weld in the x-direction varied between 7.5 mm and 13.3 mm with a mean of 10.6 mm, and the size of the weld throat ranged from 7 mm to 9.2 mm with an average of 7.96 mm. All the above calculations were based on 26 measurements.

In one of the long specimens (see Fig. 4.14) the residual welding strains were measured with a Demec extensometer after the completion of the weld and the corresponding stresses are given in Table 6.6. They all indicate the presence of high tensile residual stresses along the direction of the weld. The tensile zone adjacent to the weld seems to be wider in this series of specimens than in specimen series BEDFW. The level of the residual locked-in stresses transverse to the direction of the weld may be considered to be of the same magnitude as for series BEDFW. This limited data shows that the existence of a gap in the corner fillet joint may have a large effect on the magnitude of the longitudinal tensile residual zones adjacent to the filler material. Similar measurements were taken when the specimens were ready to be tested to find the changes

of residual stresses due to cutting of the long specimens. The calculated stresses are given in Table 6.7. It was noted that the magnitude of the longitudinal locked-in stresses was changed substantially, but that related to the transverse locked-in stress changed little (see Tables 6.6 and 6.7). Although great care was taken with the Demec readings, the measurements showed some inconsistency. (After the first reading and before cutting the long specimens, the points where the readings were taken were covered to protect them,e.g. from dust particles and some other variables). The assumption that the magnitudes of the transverse locked-in stresses in both test series BEDFW and BEDFG are almost the same is based on the recorded mean values of the transverse strains close to the weld.

The specimens in series BEDFG failed because of Type 1 fatigue failure with the sub-types "a" and "b" as for test series BEDFW. In Plates 6.12 to 6.14 the propagated crack on the side of specimens are shown. An examination of the fractured surface in these specimens shows that they have propagated with a semi-elliptic crack front shape across and through the plate thickness.

The fatigue life of the specimens from the time of first visual crack at the toe of the weld until final fatigue failure of the specimens was between 35 - 73 percent of the total fatigue life. The fatigue life from first side crack up to final failure was 7.2 - 36.9 percent of the total life. When the crack propagated along the toe of the weld in specimens BEDFG-4 and BEDFG-11 the tests were terminated to observe the shape of the fatigue fractures at this stage and to find the ratio of a/b (see Fig. 6.2). The ratio of a/b was in the order of 1/6. Specimen BEDFG-3 was subjected to a stress

range of 169.3 N/mm^2 with zero minimum stress. The first visual side crack appeared on the compression side of the specimen after 0.764×10^6 cycles and propagated in the same way as in other specimens of this series. At 0.942×10^6 cycles a crack appeared on the side of the second welded joint. As can be noted the fatigue life of this specimen is of the same magnitude as for other specimens which were subjected to the same stress range. In some of the specimens subjected to low stress levels when the fatigue crack propagated to more than half of the plate thickness a crack appeared on the compression side of the specimen and from then on both cracks propagated. This process was photographed for specimen BEDFG-15, and the result is shown on Plates 6.13 and 6.14.

A summary of the experimental results for test series BEDFG is given in Table 6.8. In Fig. 6.7 the probability of failure calculated by Equation (5.14) is plotted against logN for each stress level separately to see whether the data are normally distributed. As can be seen all the data form a straight line. The χ^2-test for goodness-of-fit was calculated and the result is summarised in Table 6.30. The test passed at 5 and 10 percent level of significance. It is clear that the transformed fatigue lives into logN for this test series are normally distributed.

A regression analysis was carried out for two functions, as given by Equations (5.32) and (5.33). Both transformed functions gave a good correlation between stress range and number of cycles, the value of the R is given in Table 6.33. The log-log function was accepted as for the other test series. In Fig. 6.8 the CFD of errors of test series BEDFG is plotted. A straight line relationship holds between e_i and P except at the extreme points of the line.

The mean fatigue life with its 95 percent confidence limits is shown in Fig. 6.9 and the mean with different probabilities of failure is given in Fig. 6.10.

Comparison with Relevant Results: This type of joint would normally be designed as a Class F or sometimes as a Class G welded detail, according to different standards [6.3, 6.4]. The results obtained in this investigation correspond to a Class D detail [6.4] as shown in Fig. 6.9. The mean fatigue strength of test series BEDFG at 2×10^6 cycles is 125 N/mm^2 which is identical to that of a Class D detail of the Merrison report. On the same graph the predicted line for test series BEDFW is represented. A comparison of these two results shows that the existence of a gap in a double fillet corner joint subjected to bending affects the fatigue behaviour at high bending stress ranges. The means of the two test series were compared statistically and the results are given in Table 6.32. The result has shown that at $\sigma = 169.3$ N/mm^2 the means of the two test series are significantly different but at the two lower stress ranges the t-values are in the zones of uncertainty. The two predicted lines were also compared statistically. The results showed that the two variances about the regression lines and their slopes are not significantly different but the two predicted lines are significantly different. The results of the comparison are given in Table 6.34. From the results of the two test series it is possible to conclude that the poor fit-up has its maximum effect on the fatigue behaviour of a double fillet weld at high stress. (The detailed calculation of the comparison of the two regression lines is given in Appendix 6.I.)

In Fig. 6.9 the results of the experiments carried out on specimens shown in Fig. 6.33 by Maddox [3.33] and identified as 6D and 7D are also included. The fatigue failure type in these specimens was the same as for test series BEDFG. It can be seen that the present results indicate a lower fatigue life. This may reflect the shape effect of the specimens and the manner of loading. Referring to Fig. 3.7 it was noted that the knee bend specimens give much lower fatigue life than three point and four point bend Tee-butt weld. Differences may also be expected as a result of the difference in applied stress ratio (R = -4 in comparison with positive R value in this investigation) and differences in the definition of failure. The failure criterion used for test series 6D and 7D was propagation of crack through the plate thickness. In general the results of this investigation tend to be more pessimistic than those obtained by Maddox.

6.5 FATIGUE TESTS ON SINGLE FILLET WELDED CORNERS

6.5.1 General

Four series of tests were carried out on single fillet corner welds. These were test series BESFW, BESFG, BESFWI and BESFGI. Test series BESFW was intended to investigate the fatigue behaviour of single fillet corner weld with good fit-up between the plates. The results were compared statistically with test series BEDFW. Test series BESFG was carried out to establish the effect of poor fit-up on single fillet corner welds by comparing the results with test series BESFW. Test series BESFWI and BESFGI aimed to find the fatigue life of single fillet corner welds when maximum tensile stress occurs at the root of the weld and there is poor fit-up.

6.5.2 Test Series BESFW

As for all other test series the actual dimensions of the welds were measured before testing. The leg length of the weld varied between 8.5 - 11 mm with a mean of 9.76 mm based on 15 measurements. The throat of the weld varied between 6.7 - 8.9 mm with the average of 7.2 mm. In some of the specimens a shallow groove existed on the surface of the weld marking the boundary between two capping runs. The depth of the grooves and shapes of the weld are shown in Plates 6.15 and 6.16, and the line of the groove can be seen in Plate 6.17. The depth of the groove was less than 1 mm.

This groove must have caused a significant stress concentration. At the start of the experiment it was anticipated that the fatigue crack might have initiated either at these points of high stress concentration on the surface of the weld or at the toe of the weld. In the event, none of the specimens failed in the former way. All the specimens failed due to Type 1 failure, with the two types as described for test series BEDFW and BEDFG but with different crack patterns through the plate thickness as shown in Plates 6.15 and 6.16. The observed pattern of the fatigue crack through the plate thickness depended much on the magnitude of the applied load. For cases of high stress ranges the crack generally propagated through the plate almost in a semi-circular fashion as shown in Plates 6.16 and 7.2 In cases with a low stress range the crack mostly propagated almost linearly through the plate, as shown in Plate 6.15. The differences in the pattern of the crack may be related partly to the fact that at high applied load some indentation might have occurred at the places shown by "X" on Plates 6.16 and 7.2, and partly because a small gap

may have existed at the joint. The fatigue fracture surface of the failed specimens showed a smaller smooth fracture zone in comparison with test series BEDFW and BEDFG as can be seen in Plate 6.18.

The measured residual welding stresses in one of the long specimens are given in Table 6.9. It was noted that the magnitude of the transverse locked-in stresses was quite different in comparison with test series BEDFW and BEDFG and that they were of the opposite sign. Specimen BESFW-11 (Table 6.10) was subjected to a stress range of 107.8 N/mm^2 with minimum zero stress. The mode of failure in this specimen was the same as for other specimens and the fatigue life fits within the scatter band of the whole population. To provide some additional information about the failure process in this test series, the weld toe regions of specimen BESFW-17 were dabbed with a flaw detector dye penetrant when the first fatigue crack appeared on the toe of the weld. The test was halted at this stage for about 15 hours and then the test was carried out until the crack had propagated along the weld toe. The dye penetrant was dabbed and the test was terminated. The fracture surface was then examined to find the ratio of minor axis to the major axis of the semi-elliptic shape at different stages of the fatigue test. The semi-elliptic shape of crack front was clearly observed but lines marking different stages of the test were not recognisable.

A summary of the fatigue test results is given in Table 6.10. In Fig. 6.11 the Cumulative Frequency Distribution of logN at each stress level is plotted. The results lie almost on a straight line on P-logN. It was noted that the slope of the P-logN at σ_R = 77 N/mm^2 is smaller, i.e. the variance of the result is higher compared with the two other P-logN lines. The test of common variances showed that

these differences are not significant. The result of the calculation is given in Table 6.33. The χ^2-test for goodness-of-fit was calculated and passed at 5 percent and 10 percent level of significance. The result is given in Table 6.30. The regression analysis of data on a log-log function gave a high correlation factor (see Table 6.33). The mean fatigue life with its 95 percent confidence limits is shown in Fig. 6.13. The CFD of errors is plotted in Fig. 6.12. The results follow a straight line in the middle. All the results show that the logN of the results is normally distributed. In Fig. 6.14 the mean fatigue life is shown with different probabilities of failure.

Comparison with Relevant Results: In Fig. 6.13 the predicted lines for Class F proposed by Halse and Smith [6.5] are shown. As can be noted the lower band of the scatter coincides with the proposed Class F. The regression lines for this test series were compared statistically with test series BEDFW and BEDFG. A summary of the results is given in Table 6.34. As can be noted the variance of the regression lines compared with BEDFW and BEDFG are not significantly different, but the slopes of the lines are significantly different. The objective of the investigation was to establish the fatigue life of the joints under investigation for relatively high cyclic load. As the fatigue life for this test series at high stress range was low, the next stress range considered was 107.0 N/mm^2 rather than 138.6 N/mm^2. In the same graph the results of tests on specimens shown in Fig. 6.33 with single fillet welds are shown [3.33]. The results fall in the scatter band of this investigation.

The results obtained in this investigation on test series BESFW show that this type of welded joint may be represented as Class F of the Interim Design Rules [6.4].

6.5.3 Test Series BESFG

As for test series BEDFG a gap of 1 mm nominal width was introduced between the two plates at the welded joints. The variation of the gap "W_g" width was between 0.46 mm to 1.5 mm with an average of 1.01 mm and the length of the gap "L_g" ranged between 8.9 mm to 12.5 mm with a mean value of 10.5 mm based on 28 measurements. The summary of the measured dimensions for this test series is given in Table 6.11. It must be mentioned that the figures are the mean of the results at each weld. As can be noted, the leg length of the weld in the y_1 direction had varied in the range of 9.8 - 12.5 mm. The mean value of the result was 11.21 mm which at first seems higher than the designed size of the weld but if the size of the gap is not considered the correct size of the leg length is achieved. In Plates 6.19 and 6.20 the general shape of the weld and gap for two of the specimens of this test series is shown.

A summary of the measured residual stresses for one of the long specimens after the completion of the welding and before testing of each individual specimen are given in Tables 6.13 and 6.14 respectively. It was noted that the magnitude of the residual stresses transverse to and along the weld in this series (see Table 6.13) is slightly smaller than those recorded in test series BESFW (see Table 6.9). After the test was terminated on specimens BESFG-18 and BESFG-19 they were cut at the mid-point, as described in Chapter 7, to measure the magnitude of the locked-in stresses transverse to the weld. The results are given in Table 6.12. These values are of the same magnitude as those given in Table 6.14.

A summary of the fatigue test results and types of fatigue failure is given in Table 6.15. As can be seen, 76 percent of the welded joints of this test series failed due to type 2 fatigue failure. The crack initiated mostly from the small needle shape groove at the surface of the weld and propagated along the groove line referred to previously. In some of the specimens the crack initiated from only one point on the surface of the weld and then radiated from this area with a semi-elliptic crack front shape through the weld throat towards the root of the weld, but in most of the specimens the crack initiation occurred at two or more points along the groove. Plate 6.21 shows the fracture surface of specimen BESFG-6. This test was stopped at the stage when the cracks joined together at the surface of the weld with the first visible crack on one side of the specimen. It can be seen that all three cracks propagated with a semi-elliptic crack front shape. The same procedure was carried out for specimens BESFG-3 and BESFG-17. Plate 6.19 shows a typical Type 2 fatigue crack through the weld throat in this series. The fatigue crack in specimen BESFG-5 was initiated at the toe of the weld after 130,000 cycles on the side SG-3, at 0.148×10^6 cycles a crack of Type 2 was seen also on side SG-3 and a crack of Type 1 on side SG-4. Then the Type 2 crack propagated through the weld throat until final failure; but the Type 1 crack did not propagate further. This suggests that the magnitude of the stresses at the toe of the weld and at the surface at the points of stress concentration may have been almost identical. The fatigue life of this specimen was shorter than the fatigue lives of other specimens tested in the same stress range. This could be attributed to the size of the gap. As can be noted from Table 6.11 the depth of the gap in this specimen is larger than normal.

Specimen BESFG-12 failed due to Type 1 failure. The propagated crack for this specimen is shown in Plate 6.20. When the crack propagated almost along the entire length of the toe of the weld on side with SG-3 at 732,000 cycles, two cracks of the length 28 and 23 mm were observed on side with SG-4. This crack did not propagate much further after this stage. After final failure the weld was examined carefully and two cracks of length 6 mm and 2 mm of Type 2 were also seen on side with SG-3 of the weld. The fatigue fracture surface of this specimen was not as smooth as in other specimens. At first it was thought that the failure might partly be related to an underbead crack, but no sign of underbead cracking* was noticed on inspection (6.7). This occurrence could be related to the size of the gap at the welded corners. Specimen BESFG-13 failed due to Type 1 and Type 2 failure. The first crack appeared at the toe of the weld on side with SG-3, then a crack of Type 2 after 776,000 cycles was seen on side with SG-3 and SG-4. The two different cracks on side with SG-3 propagated simultaneously and caused the final failure. The fatigue life of these specimens fell in the scatter band of the results. All these results were taken into account in the statistical analysis of the data.

Specimen BESFG-18 was subjected to $\sigma_R = 77.0$ N/mm^2 and zero minimum stress. It did not fail after 12.583×10^6 cycles. It was noted that the transverse locked-in stresses in this series were low so their effect on the fatigue behaviour is not great.

Fig. 6.15 shows the distribution of the fatigue life at different stress levels. The data at low stress levels fit very well to a straight line. The calculated χ^2-test for goodness-of-fit was

---

*In an underbead crack part of the surface has a fibrous texture associated with the heat affected zone of the weld and surface has a laminar type surface.

passed at 5 and 10 percent level of significance. The result of the calculation is given in Table 6.30.

The Summary of the results of the regression analysis is given in Table 6.33. The correlation coefficient for log-log function was much higher than logN - σ_R. The experimental data and the log-log regression line with its 95 percent confidence limits is plotted in Fig. 6.17. Fig. 6.16 shows the CDF of the errors. In Fig. 6.18 the mean fatigue life with different probabilities is given.

Comparison with Relevant Results: This type of welded corner joint would normally be designed as Class G of the welded details according to Merrison report [6.4]. In Fig. 6.17 the graph for Class G weld detail according to the I.D.R. is shown. As can be seen the two curves converge at a high stress level. This series of tests showed a lower fatigue life at two lower stress ranges. In the same figure the result is compared with Class G and F2 of the new bridge code [6.5]. It can be noted that the Class G detail converges to the predicted line at low stress levels but Class F2 is in the scatter band of the results.

The sample parameters of this test series were compared with test series BESFW. The results of the calculation showed that the variances of the two test series were not significantly different at different stress levels but the means were. The result is given in Table 6.31 and 6.32. In Table 6.34 it can be seen that the t-values of the comparison of the slopes of the two regression lines are in the zones of uncertainty and the two predicted lines are significantly different. The predicted line is parallel to

that of test series BEDFG. After this comparison it is clear that the existence of a gap in single welded joints subjected to bending has a significant effect on their fatigue behaviour. In Fig. 6.17 the results on specimens shown in Fig. 6.33 with single fillet weld with gap are shown [3.33]. The results show higher fatigue lives. This can be mainly related to the shape of the specimen.

6.5.4 Test Series BESFWI

In service the corner joints of a box girder or closed stiffener may be subjected to loading which would cause cyclic tensile or compressive stresses at the toe of the weld. In single fillet welds the tensile bending stresses at the toe of the weld correspond to the compressive stress at the root of the weld and vice-versa. This fact implies that the fatigue crack propagation in this type of welded joint can occur either from the toe or surface of the weld as for test series BESFW and BESFG or through the weld throat with initiation of the crack from the root of the weld. In sections 6.5.2 and 6.5.3 fatigue failures of Type 1 and Type 2 in single fillet corner welds were studied. This section is concerned with the fatigue life of single fillet corner welds in which the maximum tensile strains due to the applied load is at the root of the weld. To achieve Type 3 fatigue failures in single fillet welded joints specimens of type BESFW could have been subjected to pulling load. This would have given rise to tensile strains at the root of the weld. This method of testing was not considered to be suitable because of the special grips used. The difficulties which would have arisen were:

(a) to set and tune the vibrophore for testing would have taken longer,

(b) the possibility of obtaining a uniform strain along the specimen was less than for series BESFW, as the inner surfaces of the points of application of the load at the top and bottom of the specimen were not flat enough. The machining of the surface might have solved this problem, but this process would have been time-consuming.

Specimen BEDFW which was fixed with 12 strain gauges along the weld was subjected to pulling load. Greater variation of strains along the specimen's weld was observed. To overcome these difficulties and to subject the root of the weld to maximum tensile bending strain the position of the weld was changed. The weld was deposited inside the specimen, as shown in Fig. 4.8, and the load was applied in the usual manner. In Fig. 4.18 the measured strain distribution along the toe of the weld and on its opposite side is shown. It was noted that the strain distribution across the plate thickness for this test series was almost the same as for other types in the test series. After this experiment, the direct comparison of the static test results with test results of specimen BEDFW was made, as shown in Figs. 4.17 and 4.18, the controlling strains were those of strain gauge numbers 3 and 4 as for other types of specimens. Knowing the value of the tensile stresses at points SG-3 and SG-4 then the stresses at the root of the weld can be found theoretically by using Equation II-6, given in Appendix 4.II. It was thought that by changing the position of the weld the magnitude of the locked-in welding strains

in the specimen would have been changed. (The magnitude of the locked-in strains transverse to the weld in trapezoidal closed section of an orthotropic plate reported by Maddox [3.34] was low.) The results obtained for test series BESFW and BESFG have also shown relatively low magnitudes of locked-in strains transverse to the weld, as is given in Tables 6.9 and 6.12 to 6.14. Unexpectedly, the magnitude of the transverse locked-in strains in test series BESFWI was very high. As can be noted in Table 6.16 the transverse locked-in welding stresses are of the bending form with tensile bending stress at the toe of the weld. At this stage it was thought that the magnitude of these residual strains should be checked by another method which may give more precise measurements of the welding strains close to the weld. This objective was achieved by a destructive method. (This method of measuring and the results of the measurements are given in Chapter 7.) It was clear from the comparison of the results by the two methods that the values of the residual strains measured by Demec extensometer were of the right order. The experiments were carried out as was originally planned and all the results in this test series were analysed considering both nominal and the additional effects of locked-in residual strains.

The sizes of the welds were measured before testing. The changes of the leg and throat of the weld were in the same range as for specimen series BESFW. The angle of the weld relative to the plate surface was in the range of 32^{o} to 58^{o}. In some specimens the depth of the groove on the surface of the weld, which was formed between the boundary of the two capping runs, was over 1 mm. A feeler gauge was used to detect any gap between the two

plates at the weld joint. No gap was found. This was consistent with the high level of the transverse locked-in stresses in the specimens.

All the specimens of BESFWI which were subjected to high stress levels failed due to Type 3 fatigue failure. In Type 3 fatigue failure the fatigue fracture is developed mostly out of sight and it is not possible to observe the crack propagation process. The propagation of the crack on the side of the specimen for this test series is shown in Plate 6.23. Plate 6.24 shows one of the typical welds of this test series with the propagation of the crack through the weld throat. It can be seen that even after final failure of the specimen there is no gap visible between the two plates at the weld corner.

Two types of crack initiation from the root of the weld were involved in these failures:

(a) The crack initiated from several points of stress concentration at the root of the weld. The non-uniformity of the weld at the root is much worse than at the toe of the weld. Each of these cracks, as in Type 1 and Type 2, propagated with a semi-elliptic crack front shape. Then the joint propagation of this crack caused the final failure.

(b) The crack initiated from one point and propagated through the weld throat. This type of failure is shown in Plate 6.25.

A crack of 0.5 mm length was observed on one side of the specimen BESFWI-20 after 3.28×10^6 cycles. This crack did not propagate

further. The experiment was terminated after 12.727×10^6 cycles. The locked-in strains were measured for this test and others which did not fail after 10 million applied cycles are given in Table 6.18. After the measurement of the locked-in strains in specimen BESFWI-20 the root of the weld was inspected. There was no trace of fatigue fracture. The 0.5 mm crack may have been an accidental deep scratch on the side of the specimens. The summary of the data for test series BESFWI is given in Table 6.19.

When the specimens of this test series were subjected to high stress levels, i.e. $\sigma_{max} = 238.7$ N/mm^2 and $\sigma_{max} = 207.9$ N/mm^2 during the application of the static load, a plastic deformation was registered. The residual plastic deformation occurred at the root of the weld. As has been shown in Appendix 4-II, the maximum tensile stress due to the applied load occurs at this same location. It is obvious that the cyclic stresses at the root of the weld at high stress levels must have fluctuated from the yield tensile stress downwards and that the results given in Table 6.19 do not need to be modified for residual welding stress (see Chapter 7). In Plate 6.22 the fracture surface for this specimen series is shown. The results obtained at low stress level, i.e. $\sigma_R = 107.8$ N/mm^2 showed very optimistic fatigue lives for this test series. It seemed, at first, that the fatigue strength of this type of weld at low stress level is almost the same as for test series BEDFG. Referring to Tables 6.17 and 6.18 it can be seen that the average locked-in stress at SG-3 and SG-4 was -106.2 N/mm^2 and at SG-1 and SG-2 was +124.2 N/mm^2. These stresses should have produced compressive locked-in stresses at the root of the weld. When specimens were subjected to static

load for σ_{max} = 177.1 N/mm^2 no plastic deformation was observed. In this case the combined effect of locked-in stress and stress due to applied load is the effective cyclic stress. Therefor the effective tensile stress at SG-3 and SG-4 would have been σ_R = (177.1 - 107.2) = 69.9 N/mm^2 (see case 1 of section 7.4).

In Fig. 6.19 the CFD of logN at stress levels 138.6 N/mm^2 and 69.9 N/mm^2 are plotted. The results follow well a straight line. The CFD of errors for both uncorrected and corrected results are plotted in Fig. 6.20. As it can be seen the corrected values fit to a straight line very well. The result of the corrected regression lines with its 95 percent confidence limits is shown in Fig. 6.21. In the same graph the regression line with its 95 percent confidence limits of the original data is shown.

From the comparison of the two lines it can be stated that the higher the applied cyclic strains are the lower is the effect of residual locked-in strains. The same explanation is applicable for the specimens which were subjected to σ_R = 77.0 N/mm^2. By considering residual locked-in strains in the specimen, the actual tensile stress range at the root of the weld should have been about 106.65 N/mm^2 which corresponds to the 38.5 N/mm^2 at the tension surface of the weld. A series of specimens of this type was manufactured to study the effect of the residual stress by showing the mode failure change. All the experiments of this series were subjected to minimum zero strain. The results of this test series are represented and discussed in the next chapter. The results of the experiments which had failed at the bent corners close to the grips of the specimens were not included in the analysis

of the results. (This type of failure occurred at the grooves which were formed during manufacturing of the bent plates.)

In Fig. 6.21 the predicted line for this series is compared with the weld details W and G of (6.5), and Class G weld detail of Merrison Committee. As can be noted the Class G of [6.5] falls in the scatter band of the corrected results at high stress levels. The P-S-logN graph for different probabilities for failure is shown in Fig. 6.22.

6.5.5 Test Series BESFGI

In this test series a nominal 1 mm gap was introduced between the two plates at the joints. But the actual width of the gaps varied between .68 mm to 1.09 mm and their depths changed between 9.5 to 12.6 mm. The mean values of gaps' width and depth were 0.87 mm and 11.2 mm respectively. In Table 6.20 the measured dimensions of the weld in specimen BESFGI-10 is presented. It was found that, in general, the width of the gap in this test series was smaller than test series BESFG. This is due to the transverse locked-in strains. In Table 6.21 the results of the locked-in stresses in one of the specimens is given. As it can be noted the transverse locked-in stresses in this test series is smaller than test series BESFWI (see Tables 6.18 and 6.21).

Specimens of this test series failed due to Type 3 fatigue failure. As for test series BESFWI it was not possible to observe the propagation of the fatigue crack. When the fractured surface of the failed specimens was examined it was found that the crack propagated in an elliptical shape. Plate 6.26 shows the fracture surface of specimen BESFGI-13. The summary of all test results is given in Table 6.22.

Specimen BESFGI-4 was carried out under 138.6 N/mm^2 stress range with zero minimum stress. When the crack was propagated more than half way through the weld throat a compression crack appeared on the surface of the weld. The result of this experiment falls well within the scatter band of the results. Specimen BESFGI-19 was subjected to 77.0 N/mm^2 stress range with minimum zero stress, Type 2 fatigue failure was observed. As can be noted, the fatigue life of this specimen is rather short. After consideration of these two experiments, it was thought that the distribution of the locked-in stresses across the weld throat may not be of bending stress. There was not any available method to measure the distribution of the locked-in strains through the weld throat.

In Fig. 6.23 the P-logN curves at three stress levels are shown. The CFD of error considering only the results obtained at three stress levels and that related to whole data are shown in Figs. 6.24 and 6.25 respectively. Both results fall along a straight line. In Fig. 6.26 the experimental results and the predicted line based on all the data is shown. The results, in general, have shown a well-defined scatter band. The P-S-logN graph for different probabilities for failure is shown in Fig. 6.27.

Comparison with Relevant Results: In Fig. 6.26 the results of the experiments carried out on cantilever type specimens as shown in Fig. 6.34 subjected to bending which caused tensile stress at the root is included. As can be noted the results [6.8] fall in the scatter band of this test series at low stress levels. All the

results were compared in terms of the bending stress range at tension side of the specimen in the plate. The response for corresponding weld details in the draft code[6.5], "W", and Class G of the IDR[6.4] is shown. It can be seen that the Class weld "W" falls on the scatter band of this investigation. Finally, Fig. 6.26 includes the predicted line for test series BESFWI after the correction is made for the residual stress. It was noted that this line falls in the scatter band of this test series. In Table 6.34 the results of the statistical comparison of the regression lines is given. The results have shown that the variances and the slopes of the two predicted lines are not significantly different at 90 percent significant levels but the two predicted lines are significantly different.

6.6 SUMMARY OF THE STATISTICAL ANALYSIS OF THE TESTS ON FILLET WELDED JOINTS

The statistical analysis of the results of the fatigue tests on fillet welded corners included the following tests:

Blom's test: This test was performed to check graphically whether the observed fatigue lives, when transformed logarithmically are normally distributed. It was carried out for each sample and also for the regression residuals (distribution of errors). The results were plotted for each test series and fitted satisfactorily to straight lines, showing that the transformation of the fatigue lives into logN are normally distributed. The accuracy of the results depends on the numbers of test results, and as the results are not very large in this investigation, the next test was carried out to show the suitability of a log-normal distribution to fatigue lives.

χ^2-test for goodness-of-fit: This step in statistical analysis is very important,because before any statistical analysis of fatigue results can be performed, their frequency distribution must be known.

Examples of the χ^2-test are given in Tables 6.28 and 6.29 and the results of all χ^2-tests are summarised in Table 6.30. In all test series, the χ^2-test was passed at 5 and 10 percent levels of significance. Therefore it can be assumed that the data obtained in this investigation are log-normally distributed.

Comparison between means and variances: The equality of variances was tested by the F-test before the means were compared. The variances mut be calculated first because the calculated t-values depends not only on the difference between two means but also on their variances. The results of the comparison of variances is given in Table 6.31. They show that all variances are not significantly different at 10 percent level of significance except the results which were in the zone of uncertainty. The results of the t-tests for the comparison of means are given in Table 6.32. All the means are significantly different except for two cases. Table 6.35 gives the percentages of reduction of the means at different stress ranges due to gap, weld type and to both of them.

Regression analysis and comparison of the regression lines: A linear regression analysis was performed on the six series of tests. Two transformation equations (5.32) and (5.33) have been used to linearise the stress-fatigue life relation. Adequacy of each function was judged by the closeness of the correlation coefficient to ± 1.0. It may be seen in Table 6.33 that in general the logarithmic equations show a better correlation than

the semilogarithmic equations. The hypothesis of common variances in each test series was passed at 10 percent level of significance. The F-test was carried out to show that the predicted function did not occur by chance. The F-value for this test is the variance of the deviations of the mean about the predicted line to the average variance within samples. In most cases, the F-test was passed at the 10 percent level of significance. The summary of the statistical analysis is given in Table 6.27.

The regression lines, the 95 percent confidence limits, and some probabilities of failure were plotted for each test series. It should be noted that the confidence limits of a regression line depend on the number of observations used in the computation of the regression line. Regression lines for all test series are given in Fig. 6.28.

Fifteen comparisons of regression lines were performed - each comparison being between two lines. A typical comparison of two regression lines is given in Appendix 6-I. A summary of the results of comparisons between regression lines is given in Table 6.34. Four sets of results have shown that their predicted lines are parallel to each other at a 10 percent level of significance. Those are the lines of test series BEDFW and BEDFG, BEDFW and BBSFG, BEDFG and BESFG and finally the lines of test series BESFGI and BESFWI. After this step the statistical test was carried out to show the identity of the lines. In all cases the hypothesis that the regression lines were identical was easily rejected.

6.7 DISCUSSION OF THE RESULTS

The effect of the gap or lack of fit in welded joints subjected to bending has been shown to be a very important factor in determining their fatigue performance. In the tests with double fillet welds the mean fatigue life of test series BEDFG was, at a stress range of 169.3 N/mm^2, 39.5 percent lower than the mean fatigue life of test series BEDFW. The fatigue lives were 22.0 percent lower at the 138.6 N/mm^2 and 107.8 N/mm^2 stress ranges respectively when a gap was present. Thus the effect of the gap was more pronounced at high stress range levels. This fact can be related mainly to the stress concentration at the toe of the weld and partly may be related to the effect of residual welding stress.

The gap effect is much higher in the case of single fillet welds. In the case of a single fillet weld subjected to maximum tensile stress at the toe of the weld, the reduction of mean fatigue life was 59.5 percent for a stress range of 169.30 and about 72 percent for stress ranges of 107.8 N/mm^2 and 77.0 N/mm^2 respectively. The effect of the gap in this case was therefore more pronounced for lower stress ranges.

In test series BESFG most of the welds failed due to Type 2 failure. Thus the influence of the gap on single fillet welds not only depends on the stress concentration and residual welding stress but is also related to the type of fatigue failure which occurs. The relationship between type of fatigue failure and fatigue life was illustrated when the results of the two test series BESFW and BESFWI were compared. The reduction in mean fatigue life for 169.3 N/mm^2 stress range was 79.9 percent. The fatigue failures

for test series BESFW were of Type 1 and the crack propagated mainly through the parent material but the fatigue failure for test series BESFWI was of Type 3 and the crack propagated through the weld throat. The same comparison was made for test series BESFG and BESFGI. Although the types of failure were different (mostly Type 2 for test series BESFG and Type 3 in case of BESFGI) in both cases the fatigue crack propagated through the weld throat. The mean fatigue lives of test series BESFGI were 19.7 percent and 33.3 percent lower at stress ranges of 107.8 N/mm^2 and 77.0 N/mm^2 respectively.than the mean fatigue lives of test series BESFG.

The summary of the percentages of reduction of the means of different fillet corner welds is given in Table 6.35. The reduction of mean fatigue lives at different stress levels due to type of fillet weld (i.e. single and double fillet weld) without gap were between 76-82 percent. The mode of failure for both test series was the same. Similar calculations were made for test series BEDFG and BESFG.(Most of the specimens of these two test series failed with different types of fatigue failure.) The reduction of the mean fatigue lives at different stress levels was in the range of 87.5 - 91.7 percent. The highest reduction of mean fatigue life was observed due to both gap and fillet weld types.

6.8 FATIGUE TESTS ON BUTT WELDED CORNERS

6.8.1 General

As for fillet welded joints a considerable amount of work has been done in the past to investigate the fatigue behaviour of welded butt joints under axial loading. Most experiments have been performed on flat plate, T-type or cruciform specimens joined together by different types of butt welds. To the author's knowledge, there are no test results on corner butt-weld subjected to bending as the type carried out in this investigation for high cyclic loading. Two types of butt corner welds which are commonly used in box girder bridges are investigated. The results of these tests were compared with the test series BEDFW and with each other. The effect of a sealing run on the fatigue behaviour of butt-welded joints was investigated.

The experiments for these test series were carried out randomly, but due to the number of specimens the results were not subjected to statistical analysis. These tests therefore should be considered as pilot tests. A summary of experimental results is given in the following.

6.8.2 Test Series BEVBS

This series of tests was aimed to find whether the fatigue life of V-butt joints with sealing runs show a better or worse fatigue performance in comparison with test series BEDFW which has the highest fatigue life among the fillet welded joints studied within this thesis. The effect of sealing run to this type of weld was also studied by comparing the results of these tests with test series BEVB. The dimensions of the weld and the type of edge

preparation for this series is given in Fig. 4.10. The leg length of the sealing run in this specimen was between 4-5 mm. Specimens failed due to Type 1 fatigue failure. In specimen BEVBS-1 the fatigue crack propagated from four points along the toe of the weld through the HAZ about 1.5 mm and then through the parent material. The fractured surface of the failed specimen showed that each of these cracks propagated through the plate with semi-elliptic crack front shapes. In specimens BEVBS-2 and BEVBS-3 the crack propagated from three points along the toe of the weld and propagated in the same manner as in specimen BEVBS-1. In all specimens the crack propagated through the plate with an angle $\theta \simeq 5^{o}$ as shown in Fig. 6.35a.

A summary of the results is given in Table 6.23. In Fig. 6.29 these results are plotted together with the scatter band and the predicted line for test series BEDFW. It may be noted that the results at high stress ranges for V-butt welds are lower than the mean value of the test results for BEDFW. However, at $\sigma_R = 138.6$ N/mm^2 the results fall on the scatter band of test series BEDFW as shown in Fig. 6.29. In general after comparing these results with test series BEDFW it may be concluded that this type of corner weld, when subjected to transverse bending, responds in a similar fashion as the double fillet welds of test series BEDFW.

6.8.3 Test Series BEVB

This series of tests was carried out to investigate the effect of a sealing run on the fatigue behaviour of V-butt welds (see Fig. 4.11). As was mentioned in Section 4.3.3, to apply

the sealing run it is necessary that the root of the weld be carefully cleaned first and then filled with the filler material. However to achieve a relatively perfect condition at the root of the weld is very difficult. On examination the welded joints of series BEVBS showed that the possibility of slag or a void occurring at the root of the weld is very high. Moreover, the process of welding is very time-consuming and in general uneconomical and in some cases, e.g. in small closed sections, it is not possible to reach the root of the weld.

The specimens of this test series failed due to Type 1 fatigue failure. In specimen BEVB-1 the first cracks were visible at 4 points on the side with SG-3 and 3 points on the side with SG-4. The crack propagated much faster on the side with SG-3 and caused final failure. In specimen BEVB-3 the first crack was observed along the toe and three fatigue cracks were also observed on the surface of the weld. The specimen failed because of Type 1 fatigue failure. In specimen BEVB-4 the first crack appeared at the toe and also on the surface of the weld. The cumulative effect of these cracks caused the final failure. The gap at the part where the surface crack occurred was about 2 mm deep. (In general the irregularity at the root of the weld was between ±2 mm*.) The crack propagated through the thickness of the plate with a slope of about 15° - 20°, as shown in Fig. 6.35b. This reflects the effect that a sealing run may have on the direction of the principal stresses.

---

*These figures are given relative to the surface of the plate. The (+) sign means that the filler material was outside the root and the (-) sign means that there was a gap at the root of the weld.

The summary of the test results is given in Table 6.24. These results are plotted in Fig. 6.29, in which the results of test series BEVBS and the predicted line for test series BEDFW with its scatter band is shown. As can be noted from Fig. 6.29, for high stress ranges the results fall in the scatter of the test series BEVBS but at σ_R = 138.6 N/mm^2 all the results indicated a lower fatigue life. The $\bar{N}_{logN}$ is given in Table 6.36 and the percentage reduction of fatigue life at different stress levels is given in Table 6.37. The result of test series BEVB shows a reduction of 18 - 47 percent at both stress ranges in comparison with test series BEVBS. This fact can be related mainly to the shape of the stress concentration. In general the present results fell on the lower part of the scatter band of test series BEDFW. From these results it may be stated that the fatigue performance of test series BEVB is most probably lower than for test series BEDFW.

6.8.4 Test Series BESBS

This series of tests was carried out to investigate the fatigue performance of single bevel V-butt welds, as shown in Fig. 4.12 and compare the results with test series BEVBS and BESB. The utmost care was taken to produce the best quality of the weld under study. However, it was not easy to achieve a perfect fusion between the filler material and unprepared edge of the plate - which would seem to be one of the main disadvantages in using this type of weld.

The mode of failure for all the specimens was of Type 1a. The crack propagated through the plate with an angle $\theta \simeq 5^{o}$, as shown in Fig. 6.35c.

The summary of the results is given in Table 6.25 and they are plotted in Fig. 6.30. The mean value of the $\bar{N}_{logN}$ at each stress range is given in Table 6.36. At σ_R = 169.4 N/mm^2, the fatigue life of these specimens was 56 percent higher than that of the specimens in test series BEVBS, but at lower stress ranges the difference is small. Surprisingly the results fall very well in the scatter band of test series BEDFW and they follow the predicted line of test series BEDFW. For design purposes this type of joint could be designed as the joints in test series BEDFW.

6.8.5 Test Series BESB

This series of tests was carried out to investigate the effect of the sealing run on the fatigue behaviour of single bevel V-butt welds (see Fig. 4.13) by comparison with the result of test series BESBS.

In this type of joint, as for those in test series BESB$, premature fatigue failure occurred in some specimens along the line of fusion as shown in Fig. 6.35d. The results of these tests failing in that way were not considered in this thesis. In Table 6.26 the summary of the results of specimens which failed due to Type 1 failure is given. The pattern of the crack through the plate in this series of specimens is shown in Fig. 6.35d. As can be seen, the crack propagated with an angle of about $20^{o}.0$ as for tests series BEVB. The depth of the gap at the root of the weld for this test series at some points was about 2.5 mm.

The results are plotted in Fig. 6.30. As can be seen, the results scatter widely and show a very poor fatigue performance. This is mainly related to the existence of the gap at the root of the weld and the high irregularity of the root shape. As can be noted from Table 6.37, the sealing run has increased the fatigue life by between 52 and 92 percent at different stress ranges.

6.8.6 Comparison of the Results for Different Butt Welds

All the results of the tests on butt welds are plotted in Fig. 6.31. On the same graph the mean line and the scatter band of the test results for test BEDFW are given. It was observed that the results of the BEVBS and BESBS fell on the scatter band of the test series BEDFW at σ_R = 138.3 N/mm^2, but at high stress range two of the results fell outside the band. These experimental results suggest that at high stress levels V-butt welds with sealing runs may have lower fatigue lives than double fillet welds (BEDFW), whereas it is usually assumed that butt welds would have better fatigue lives than such fillet welds. In particular, the sealing run may have a significant effect on the fatigue life of a butt weld.

The plotted results have shown that the log-log relation remains valid for this test series.

CHAPTER SEVEN

EFFECT OF RESIDUAL STRESS ON FATIGUE

7.1 INTRODUCTION

This study was prompted by the change in mode of failure which was observed in certain test series when specimens were subjected to the same stress range but to a different minimum stress. In particular when the specimens of series BESFWI were subjected to σ_{min} = 69.8N/mm^2 (Table 6.18) they failed due to fatigue crack propagated from the root of the weld through the weld throat. When they were subjected to lower minimum stresses the fatigue cracks propagated from the toe of the weld. It was suspected that the presence of welding residual stresses might have influenced this change in mode.

In most investigations concerning the effect of residual stress on fatigue only the local system of self-equilibriating residual welding stresses,discussed in Section 3.3.5, are considered. However in most practical welded assemblages in addition to the localised residual stresses, a system of reaction stresses, caused by the restraint afforded to the component being welded to the other components of the redundant structure, also exists. The combined effect of these two systems of residual stresses may need to be considered in the design of the welded structure. In this chapter the effect of residual welding stresses on the fatigue behaviour of the welded joints in the specimens of the present test series has been studied quantitatively.

7.2 CONTROL TEST SERIES

7.2.1 General

To investigate the effect of residual welding stresses, a control series of single fillet welded specimens, BESFWIR, was designed. (The general specimen designation for this series is given in Section 4.3. The letter R is added to the designation of this series of specimens to show that they were used to study the effect of residual stress on fatigue.) The material, design, and manufacture of the specimens together with the testing procedure used are described in Chapter 4.

7.2.2 Measurement of Residual Strains

To quantitatively assess the influence of residual welding stress on fatigue it is necessary to measure accurately the residual strains. Two methods were employed in this investigation. A non-destructive method involving a mechanical extensometer of the Demec-type was used to measure strains which were not in the immediate vicinity of the welds. However, it was not possible to measure the value of the residual strains close to the welds by this method. At such locations the locked-in strains were measured using the destructive method. The procedure of the measurement was as follows. First, the specimen series BESFWIR was welded completely as described in Chapter 4. Then this specimen was sliced into four smaller specimens and finally each of the small specimens was machined to the 80 mm width as shown and designated in Fig. 7.1. Each of the specimens of the series was fitted with strain gauges at positions 1,2,3 and 4. Two nominally identical specimens

BESFWIR2 and BESFWIR4 were cut at the mid-point of the sides. The strains were measured before and after the cutting. The magnitude of the locked-in welding strains at points 1,2,3 and 4 were recorded by noting the change in strain gauge readings. The measured strains are given in Table 7.1.

After consideration of the initial results it was suspected that these measured strains might not be representative of other similar specimens in the programme. This uncertainty arose because of remedial work which had been carried out on the specimens after manufacture. The load which had been applied to bend the plates during the manufacturing process had caused grooves of about 1 mm depth to appear at the unwelded corner of the plates. These indentations were considered a fatigue risk on account of the high stress concentrations associated with them. To make use of the bent plates as fatigue specimens grooves were filled using 2.5 mm diameter welding rods, and the reinforcement was subsequently ground down and the corners polished. This procedure could have altered significantly the distribution and magnitude of the locked-in strains. To remove this source of uncertainty the next series of specimens was manufactured from plates of normal standard (i.e. without grooves at the unwelded corners). When cutting similar results to those recorded earlier were obtained, see Table 7.1. It was then clear that these stresses were caused mainly by welding of the joints.

It was noted that the magnitude of the locked-in stresses measured transversely to the direction of the weld did not reach the yield point. The remaining four specimens (two from each series), which should have contained the same magnitude of locked-in stress as those given in Table 7.1, were subjected to cyclic loading. The fatigue results of these specimens are discussed in the following sections.

7.2.3 Analysis of the Results of Test Series BESFWIR

The stress range applied to specimen BESFWIR1 was approximately 107 N/mm^2. Strain gauge locations SG-3 and SG-4 were subjected to tensile stresses ranging from σ_{max} = + 107.8 N/mm^2 (+ 7.0 $tonf/in^2$) to σ_{min} = 0. The corresponding range of applied compressive stress measured at the toes of the welds was -114.56 N/mm^2 (- 7.42 $tonf/in^2$). The first fatigue crack in this specimen was observed after 1.837 x 10^6 cycles at the toe of the weld. At 2.0475 x 10^6 cycles it had propagated through the parent material to produce failure. Thus the crack appeared to initiate from the side of the specimen where compression was produced due to the applied load.

This phenomenon can be understood, however, by considering the combined effect of the stresses caused by welding and the applied load. The distribution of the measured locked-in stresses across the plate thickness is shown in Fig. 7.2. In Fig. 7.3a the average tensile residual stress at the toe of the weld is represented as a static load on the stress-time plot. The applied sinusoidal compressive stress at this point is, also, shown on the same graph. To estimate the magnitude of the stress at the root of the weld, it was assumed that the stresses shown in Fig. 7.2 are caused by an external load. It is clear that the root of the weld must have been subjected to a compressive stress. The magnitudes of the stresses across the weld throat were calculated theoretically by the equation given in Appendix 4-II. The value of the compressive stress at the root is shown in Fig. 7.3b. In all the cases the direction in which the residual stresses are considered is the same as the direction of principal stressing caused by the applied

load. Using the principle of superposition, it is clear that the stresses at the toe of the weld for specimen BESFWIR1 varied between a tensile locked-in stress of $\sigma_{max} = \sigma_S = 137.67$ N/mm^2 and $\sigma_{min} = (\sigma_R - \sigma_{max}) = 23.11$ N/mm^2. In this way the actual mean stress $\sigma_m = -57.28$ N/mm^2, completely differed from the apparent mean stress $\bar{\sigma}_m = +80.39$/mm^2. At the root of the weld the stress fluctuated from compressive yield stress to approximately -86.24 N/mm^2 as shown in Fig. 7.3b, i.e. the root of the weld was subjected to compressive cyclic stress. The combined stresses at the root of the weld are shown in Fig. 7.3b.

The pattern of the fatigue crack propagation for this specimen series was similar to the crack pattern of specimen series BESFW. In Plate 7.1 the propagated crack at the side of specimen BESFWIR1 is shown. In Plate 7.2 the propagated fatigue crack for specimen BESFW8 which had the same applied stress range at SG-3 and SG-4 but a minimum stress of 69.3 N/mm^2, is shown. Both cases are Type 1 fatigue fractures. The fractured surface of the failed specimen BESFWIRI was examined. In this specimen also two zones, a fatigue fracture zone and the rupture zone, could be observed clearly as shown in Fig. 7.3. It can be seen that the fatigue fractured area is semi-elliptically shaped. The result of this test was compared with those of BESFW and found to fit within the same scatter band as that of test series BESFW.

The next two specimens, BESFWIR3 and BESFWIR5 were subjected to a higher stress range and a minimum stress of zero. Both of the specimens fractured with a Type 1 fatigue failure. The measured strains and corresponding stresses, together with the number of cycles causing the first 1 mm transverse crack on the side of the specimen

and the number of cycles causing final failure are given in Table 7.2. If the nominal applied stress range only was considered, the fatigue life of these two tests would not fall within the scatter band of the test series BESFW. However, when the lower value of the measured locked-in stresses is considered the actual fluctuating stress at the toe of the weld may be seen to have been of magnitude 127.67 N/mm^2 which falls within the limit of the scatter band of test series BESFW (see Fig. 6.13).

The last specimen of this series, i.e. BESFWIR7 was subjected to the same stress range as for the two previous specimens but to a different minimum stress. The σ_{min} for this test was increased to +69.3 N/mm^2 at SG-3. The specimen fractured with Type 3 fatigue failure after 0.049 x 10^6 cycles in a similar manner to the specimens of series BESFWI. During the application of the load to this specimen yielding of the welded corners at the weld roots was observed. The overall permanent plastic deflection of the specimen after the application of the maximum load was 0.55 mm. Presumably the stress at the root of the weld must have fluctuated therefore from tensile yield stress downwards, i.e. from $\sigma_{max} = + \sigma_y$ to $\sigma_{min} = (\sigma_y' - \sigma_R)$. Also, in Table 7.2, the fatigue result of the specimen BESFWI2O is given. No cracking was observed after 12.727 x 10^6 cycles. If we assume that the magnitude of the locked-in stress in this specimen is the same as those reported above, then it is not difficult to see that the stresses both at the toe and at the root of the weld were very low. Thus it is clear that consideration of the effect of residual stresses can in many cases explain results which are otherwise difficult to understand in the context of the apparent applied stresses alone.

7.3 OTHER TEST SERIES

Changes of fatigue crack propagation mode occurred in other types of welded joints of the test programme when they were subjected to zero minimum stress. In the double fillet weld test, series BEDFW, the specimen BEDFW6, and in test series BEDFG, the specimen BEDFG3, were subjected to a stress range of 169.3 N/mm^2. The fatigue crack propagation in these specimens were those found in Type 1 fatigue fractures. The difference between the fatigue fracture of these specimens and other specimens which were subjected to a higher minimum stress was, that in these specimens the crack started from the "compression side", i.e. from the side with SG-1 and SG-2. The pattern of the crack propagation through the plate was similar to the crack pattern which started from the toe of the weld on the "tension side". After the final fatigue failure of specimens BEDFW6 and BEDFG3 the fatigue fracture surfaces were examined carefully and the same failure patterns as found in others of the series were observed. In Plate 7.4 the well-defined semi-elliptical fatigue fracture zone for specimen BEDFW6 can be seen.

A change in mode of fatigue crack propagation compared to others of the same series was observed when single fillet welded specimen BESFGI19 (see Table 6.19)was subjected to a stress range of 77.0 N/mm^2 and zero minimum stress at SG-3. After the appearance of the first visual crack from the surface of the weld the experiment was terminated. The fatigue fracture surface of the weld was inspected at this stage. The fatigue crack had started from two points at the surface of the weld. No fatigue crack was

seen at the root of the weld. On the other hand, no change of fatigue mode was observed when the specimen BESFW-11 was subjected to a stress range of 107.8 N/mm^2 and zero minimum stress. The result of this test is well within the scatter-band for the series.

7.4 DISCUSSION ON INFLUENCE OF RESIDUAL STRESSES ON FATIGUE BEHAVIOUR

Careful analysis of the experimental results of the control test series BESFWIR shows that in the design of some welded joints for fatigue the combined effect of the stresses arising from welding and stresses caused by external load may have to be considered, particularly in the case where the main fluctuating stress is transverse to the direction of the weld. In general, two main cases may occur in a welded structure as described below.

Case 1: The magnitude of the total maximum locked-in stress, in the principal direction of applied fluctuating stress, is less than the tensile yield stress of the material ($\sigma_s < \sigma_y$). In this case it is not easy to give a unique prediction of the fatigue life of the welded joint. The value of the locked-in stress and hence the magnitude of combined stresses must be determined and the life of the joint estimated on the basis of this value.

When the locked-in stress is tensile and the applied stress at the point of interest varies from zero to compression, then the combined stress ranges from the tensile residual welding stress downwards. The combined effect of the stresses is shown in Fig. 7.3a and it can be seen that the new mean value of stress for this combination is

$$\bar{\sigma}_m = \sigma_s + \sigma_m \qquad (7.1)$$

where

$\bar{\sigma}_m$ - is the new mean value of stress

σ_m - is the mean of the applied stress

From equation (7.1) it can be seen that if the mean value of the applied stress is equal and of opposite sign to the residual welding stress then the combined stresses at the point of interest are symmetrical alternating stresses, i.e. $\bar{\sigma}_m = 0$, see Fig. 7.4a. When the welded joint is subjected to symmetrical alternating stress the locked-in stress for this combination will be the new mean stress:

$$\bar{\sigma}_m = \sigma_s \tag{7.2}$$

This combination is shown in Fig. 7.4b.

Whatever the combination the following expression must be fulfilled for Case 1:

$$\sigma_s + \sigma_{max} < \sigma_y \tag{7.3}$$

Case 2: This case is defined when the following expression is fulfilled:

$$\sigma_s + \sigma_{max} \geq \sigma_y \tag{7.4}$$

The effective stress varies from the yield stress of the material downwards, i.e. $\bar{\sigma}_{max} = \sigma_y$ and then the new mean stress $\bar{\sigma}_m$ will be

$$\bar{\sigma}_m = \sigma_y - \frac{\sigma_R}{2} \tag{7.5a}$$

where

σ_R - is the applied stress range

$\bar{\sigma}_{max}$ - is the new maximum strain

or

$$\bar{\sigma}_m = \sigma_y - 1/2(\sigma_{max} - \sigma_{min}) \qquad (7.5b)$$

This is illustrated in Fig. 7.4c. As was stated in Chapter 3 it has been shown that in most welded structures the magnitude of the local residual stresses in a direction parallel to the weld reaches tensile yield stress. In certain cases the residual welding stress transverse to the weld may also be as high as the tensile yield stress. If such a welded joint is subjected to partially or fully compressive cyclic stress (i.e. $-\sigma_{min}$ to $+\sigma_{max}$, or from $\sigma_{max} = 0$ to $-\sigma_{min}$) in the same direction as the residual welding stress, then the resulting effective stress cycles will vary from σ_y to $(\sigma_y - \sigma_R)$ as shown in Fig. 7.4d. It is clear that, in general, the higher the applied stresses the lower is the difference between the effective and applied stress.

7.5 SUMMARY

Residual welding stresses (including both localised self-equilibriating and overall reactive residual stresses) can have a similar effect on the fatigue behaviour of welded joints subjected to transverse bending as applied static stresses of the same magnitude. The presence of such stresses can cause the mode of failure of the joint to be different to that which would occur if they were absent. If a consideration of their effects is neglected in the interpretation of fatigue results erroneous conclusions can be drawn. The effect of

residual stresses on fatigue life at the point of interest may be advantageous if they are compressive and damaging if they are tensile. By considering the effects of residual stresses results which otherwise appear to be anomalous can be explained rationally and thus reconciled with the main body of results.

CHAPTER EIGHT

EFFECTS OF CORNER CRACKS ON BOX DISTORTIONAL BEHAVIOUR

8.1 APPLICATION OF PRESENT FATIGUE DATA TO DESIGN

8.1.1 General

In previous chapters the basic fatigue data and the derivation of the corresponding mathematical model using statistical analysis has been presented for constant amplitude transverse bending of different types of welded joint. To use these data for actual structures which are subjected to variable amplitude loading (for example, bridges subjected to a loading spectrum idealised by that given in the Road Research Laboratory report[8.1]) then it is usually necessary to have recourse to the Palmgren-Miner*linear cumulative damage rule. Such a procedure is used in BS153 part 3B[6.3] and I.D.R.[6.4].

8.1.2 Cumulative Damage

Miner's rule is based on the concept of the gradual accumulation of damage during the application of cyclic loading. Miner assumed that under cyclic stressing the phenomenon of cumulative damage is related to the total work absorbed by the specimen. This states that the damage induced by a particular number of cycles of an applied stress is linearly proportional to the damage required to cause failure at that stress and a specimen fails when the total damage reaches 100%. (He considered failure to be defined by the appearance

---

*This rule originally was proposed by Palmgren and later restated by Miner and is usually known as Miner's rule [8.2] or cumulative damage rule.

of the first crack.) In other words a number of different stress levels, σ_i, applied for a number of cycles n_i (where i = 1, 2, 3, ...) would cause failure if

$$\frac{n_1}{N_1} + \frac{n_2}{N_2} + \frac{n_3}{N_3} + \ldots\ldots + \frac{n_i}{N_i} = \sum_{i=1}^{n} \frac{n_i}{N_i} = 1.0 \qquad (8.1)$$

where N_i is the number of cycles obtained from the results of a constant amplitude test at stress σ_i. It can be seen from equation (8.1) that the total damage required to cause failure is the same regardless of whether the stress amplitude is constant or varied throughout the life of the structure. This method of calculation is simple but is generally considered to be inaccurate[8.3]. However, fatigue test results carried out on welded joints under variable amplitude loading have usually produced values of $\sum_{i=1}^{n} \frac{n_i}{N_i}$ equal or greater than unity [8.3,8.4,8.5]. This suggests that, in general, by using the Palmgren-Miner's rule the predicted life is less than the actual fatigue life. Because of this the rule is commonly assumed to produce safe results when applied to the design of welded joints, although it must be admitted that this is still the subject of considerable research and discussion among investigators active in the fatigue field.

There are several sources of inaccuracy involved in this method of calculation. One is the difference between the assumed loading spectrum and the sequence of stressing and that which occurs in actual structure[8.3,8.4,8.5]. Another is the effect of stresses which are lower than the "endurance limit" of the structural detail.

If the fatigue crack has not propagated then the ratio of $^{n}/_{N}$ is equal to zero. However, once a crack has propagated under higher stresses the low stresses which were non-damaging before may become damaging, so that ignoring them may produce errors. Another source of error in the use of this rule is a factor which is not associated with the principle of equation (8.1) but rather its application. Because of the inevitable scatter in fatigue results, if the predicted line for finding N_i is based only on the scatter limits then depending on which value of N_i is chosen, the value of $^{n}/_{N}$ can vary considerably. This source of error in the work described in this thesis has been considerably reduced by taking into account probability criteria in the design. Depending on the probabilities required appropriate values of N_i may be selected for particular stress levels.

In more recent years a new concept of fatigue design has been introduced in which fatigue damage is considered to be the growth of fatigue cracks from pre-existing flaws[8.6,8.7]. In the case of macrocrack propagation, under certain conditions, the rate of propagation of a fatigue crack may be related to the applied range of stress intensity factor " K" by the following equation

$$\frac{d(2a)}{dN} = C(\Delta K)^{m} \qquad (8.2)$$

where

2a is the crack length

N is the number of cycles

C and m are material constants which depend on the material, stress range, fracture mode and fracture mechanism

Equation (8.2) is theoretically applicable to any cracked body; effect of differences in the geometry is incorporated in the solution of ΔK. The constants C and m may be established from the results of crack propagation tests on specimens for which the solution for ΔK is known and the propagation of the crack can be observed easily. The accuracy of this method relies heavily on the accuracy of the stress intensity factor solutions[8.7,8.8].

8.1.3 Fatigue Damage to Corners of Closed Sections

In closed sections because of the complex stresses at the corner of the box the application of the fatigue crack propagation approach becomes very complicated. However, it is possible to consider what effect the presence of cracks at the box corner would have on the distortional behaviour, and by so doing gain a clearer insight into the possible significance of fatigue cracking on the life of the bridge.

When a crack starts to propagate in the welded corner of a box girder the behaviour of the closed section changes radically. In effect the section is locally no longer a closed section but is an open section along the cracked part. What significance should be attached to the occurrence of such fatigue cracks in the welded joints of closed sections such as large scale box girder bridges or the much smaller boxes which may be used in steel bridge decks? The answer to this question clearly depends on whether the local reduction in the distortional stiffness caused by the crack significantly increases the transverse bending stresses at the root of the crack. The presence of a crack in a bridge may increase the local deflections of the bridge and eventually make the bridge unserviceable[8.9] and moreover due to an increase of stress at the root of a crack, there is a

possibility of a catastrophic collapse. The rate of crack propagation is very important in determining the remaining useful life of a girder bridge subsequent to the appearance of the first crack. However, the problem of progressive cracking is a very difficult one to tackle analytically and is as yet not amenable to meaningful calculation in the context of the problem under consideration. Therefore in this study no attempt is made to study the rate of crack propagation, and only the effects of the presence of a crack on the distortional behaviour of the closed section is considered.

A limited study of this problem is investigated theoretically and is discussed within this chapter.

8.2 DESCRIPTION OF ANALYTICAL APPROACH

8.2.1 Assumptions

The following assumptions are made in this analysis:

(a) Only simply supported single cell boxes with end diaphragms are treated.

(b) The distortional component of loading alone is considered.

(c) Cracks are assumed to propagate from the points where the transverse distortional bending stresses are maximum, i.e. the mid-span of the box.

(d) Once the crack has propagated across the thickness of the joint the crack front is assumed to be perpendicular to the direction of stress.

(e) The response is assumed to be linearly elastic.

(f) Cracks occur simultaneously at diagonally opposite corners.

8.2.2 Method of Analysis

The finite element program used was that described in Chapter 2. The same elements and program were used when the linkage element was added.

8.2.3 Linkage Element

To simulate the rigid joint at the corners of the box before cracking and subsequent loss of rigidity due to cracking a special linkage element was used. This type of element has been used extensively in the past to study the bond stress transfer between concrete and reinforcement, cracking in concrete[8.10,8.11, 8.12,8.13] and in composite box girders[8.14].

The linkage element has two nodal points and can be conceptually thought of as springs in the structure. The three-dimensional representation of the linkage element as used at the corners of the boxes is shown in Fig. 8.1. Such linkage elements have no physical dimensions at all, and only their mechanical properties are of importance. Since they have no actual dimensions, they can be placed anywhere in the structure without disturbing the structure's geometry.

To include the linkage element into the finite element program the stiffness matrix of the element needs to be developed. The stiffness matrix $[K]$ for a linkage element having nodal degrees of freedom u,v,w, θ_x, θ_y and θ_z would take the following form.

$$
\begin{bmatrix}
K_x & 0 & 0 & 0 & 0 & 0 & -K_x & 0 & 0 & 0 & 0 & 0 \\
 & K_y & 0 & 0 & 0 & 0 & 0 & -K_y & 0 & 0 & 0 & 0 \\
 & & K_z & 0 & 0 & 0 & 0 & 0 & -K_z & 0 & 0 & 0 \\
 & & & K_{\theta x} & 0 & 0 & 0 & 0 & 0 & -K_{\theta x} & 0 & 0 \\
 & & & & K_{\theta y} & 0 & 0 & 0 & 0 & 0 & -K_{\theta y} & 0 \\
 & & & & & K_{\theta z} & 0 & 0 & 0 & 0 & 0 & -K_{\theta z} \\
 & & & & & & K_x & 0 & 0 & 0 & 0 & 0 \\
 & & & & & & & K_y & 0 & 0 & 0 & 0 \\
 & & \text{Symmetric} & & & & & & K_z & 0 & 0 & 0 \\
 & & & & & & & & & K_{\theta x} & 0 & 0 \\
 & & & & & & & & & & K_{\theta y} & 0 \\
 & & & & & & & & & & & K_{\theta z}
\end{bmatrix}
$$

where K_x, K_y, K_z, $K_{\theta x}$, $K_{\theta y}$ and $K_{\theta z}$ are the spring stiffness associated with the appropriate degrees of freedom[8.12,8.13,8.14].

8.3 EXAMPLE BOXES

8.3.1 General

The dimensions of the boxes which were chosen for the present investigation are shown in Fig. 8.2. The same boxes together with the finite element meshes without linkage elements and with the introduction of the linkage elements at the corners of the boxes are shown in Figs. 8.3 and 8.4 respectively.

The distortional stiffness* for Box A which represents a single cell box girder bridge was K = 0.433 N/mm^2 per unit length. The

---

*The distortional stiffness of Boxes K were calculated using equation 2.12 in Chapter 2.

dimensions of Boxes B, C, D and E are of the same order as those of closed section stiffeners used in steel deck bridges. The distortional stiffness of Boxes B and C was K = 58.42 N/mm^2 per unit length while that of Boxes D and E was K = 24.65 N/mm^2 per unit length. The thickness of plate used for Boxes B and C was 8.0 mm - the boxes differed only in their span lengths. The spans of Boxes D and E were the same as those of Boxes B and C respectively. However the plate thickness used for Boxes D and E was 6.0 mm. (The plates' Young's Modulus was the same for all boxes, i.e. E = 205277.0 N/mm^2.) These combinations were chosen to find how the cross-sectional stiffness of the boxes and their span lengths may affect the transverse distortional bending stresses at a joint adjacent to a crack along the corners of the box. In all boxes analysed the value of $B_{T/C}$, i.e. the ratio of top width of the boxes to their depth, was chosen to be the same. (For Box A, $B_{T/C} = \frac{2000}{1600} = 1.25$ and for other boxes; $B_{T/C} = \frac{260}{208} = 1.25$) to exclude extra variables in the analysis of the results.

The elements used in the FE analysis were high order quadrilateral elements. The effect of the element's aspect ratio on the accuracy of the FE analysis was examined by Moffatt[8.14] on simply supported box girders having the same cross-sectional dimensions and material properties but of varying spans. The girders were considered to be loaded by a point load over each web at the mid-span. The results obtained have shown that the accuracy of the analysis was almost in dependent of the aspect ratio of the elements.

The number of elements in all the examples analysed in this investigation was kept the same. At the middle of the boxes the size of the mesh was made as small as possible to obtain

accurately the stresses associated with small crack lengths.

8.3.2 Details of Loading and Cases Analysed

All the boxes were analysed for the distortional component of the loads. Two load cases were considered in the analysis of Box A. These were distortional components of an eccentrically placed point load at the mid-span, and uniformly distributed line load (U.D.L.) along one web of the box. Boxes B, C, D and E were analysed for the distortional component of a point load at mid-span only.

Because of symmetry only a quarter of each box was analysed. Appropriate boundary conditions were applied along the longitudinal centre line and at the mid-span to obtain the correct antisymmetrical behaviour.

In each case boxes were first analysed without the introduction of the linkage elements, i.e. assuming the corners were rigid and retained the corner angle at 90 degrees. The distribution of the transverse bending stresses "σ_{DB}" and deflections in the horizontal and vertical directions, (i.e. x and z directions) were found. Then linkage elements with various assumed rigidities were introduced at the corners where the crack was to occur. The boxes were analysed for the same loading conditions as used in the previous cases. The results were then compared with those obtained without linkage elements. When both results were identical then the rigidity of the linkage element was accepted to be representative of the box corner stiffness. After several trials a value of $k = 1.5 \times 10^{10}$ N/mm^2 was found to give satisfactory results. A crack with a pre-assigned length was then introduced at the corners by reducing the stiffness of the linkage

element along that length to zero. The box was then reanalysed for the same loading condition. The changes in deflections and stresses were noted in each case. To check that the stiffnesses of the linkage elements were truly representative of the rigid corners, the relative movement of the flange and web at the tip of the crack was observed after each computation. When there was no such movements the value of the rigidity was considered to be satisfactory for the loading conditions considered.

In the present study, the cracking was arbitarily divided into six or seven stages. Each new stage represented a deeper crack penetration. A computer analysis was performed for the box at each stage of cracking. This can be regarded for purposes of analysis as six or seven different box types.

8.4 PRESENTATION AND DISCUSSION OF RESULTS

The value of transverse distortional bending stresses in the joint adjacent to the end of crack "σ_{DBC}" were non-dimensionalised against the maximum transverse distortional bending stresses for the uncracked box "σ_{DB}" for the same loading condition (the maximum "σ_{DB}" is at the mid-span of the box). The deflections in the horizontal and vertical directions are greatest at the mid-span of the boxes in all cases as may be expected. The results for the cracked boxes are given in relation to the deflections of the uncracked box as δ_{xc}/δ_{x} and δ_{zc}/δ_{z} :

where

δ_x is the deflection of the box corner at the mid-span for the uncracked box in the horizontal direction (i.e. x-direction)

δ_{xc} is the deflection of the top flange or the web* at the corner of the cracked box at the mid-span in the horizontal direction

δ_z is the vertical deflection of the uncracked box at the mid-span (i.e. z-direction)

δ_{zc} is the vertical deflection of the top flange or web at the corner of the cracked box.

The values of δ_{xc}/δ_x and δ_{zc}/δ_z are given for both nodes at the corner, i.e. nodes 113 and 114 at the mid-span. The differences between the values at the two nodes give the width of the crack in the x and z-directions.

In addition the transverse distortional bending stresses and the deflections in x and z-directions in the joints adjacent to the end of crack are presented in relation to uncracked values at the corresponding locations as $\sigma_{DBC}/_{DBL}$, δ_{xcL}/δ_{xL} and δ_{zcL}/δ_{zL}

---

*Points at the top flange or web are defined by their node numbers in the analysis (see Fig. 8.4). In the tables, odd numbers, i.e. 113, 103, 93,.... are on the top flange and even numbers, i.e. 114, 104, 94,... are on the web.

where

σ_{DBL} is the local transverse distortional bending stress for the uncracked box corresponding to the end of the crack

δ_{xL} is the local deflection for the uncracked box corresponding to the position of the end of the crack in the x-direction

δ_{xcL} is the deflection at the end of the crack in the x-direction

δ_{zL} is the local deflection for the uncracked box corresponding to the end of the crack in the z-direction

δ_{zcL} is the deflection at the end of the crack in the z-direction.

These values show the local increase of the transverse bending stresses and deflections in the x and z directions due to the crack.

The results for all boxes are given in Tables 8.1 to 8.6 inclusive and are discussed in the following.

Box A: The first series of boxes analysed were designated as Box A. These boxes were representative of a full scale rectangular box girder. The uncracked box schematically is shown in Fig. 8.2. The summary of the results for seven stages of analysis for both point load and U.D.L. is given in Tables 8.1 and 8.2.

Referring to Tables 8.1 and 8.2 it was noted that for both point load and U.D.L., when a crack of up to 150 mm length (which is about 0.5 per cent of the span) occurred along the corners of the box, the increase in deflection at the mid-span was negligible and the increase of σ_{DBC}/σ_{DB} and $\sigma_{DBC}/\sigma_{DBL}$ was less than 3.0 per cent. The width of the crack at the mid-span (i.e. the differences between deflections at nodes 113 and 114) theoretically was zero. This percentage of crack length for the box considered may be regarded as being insignificant. However when this crack was 300 mm, i.e. about 1.0 per cent of the box span length, the ratios σ_{DBC}/σ_{DB} and $\sigma_{DBC}/\sigma_{DBL}$ were increased by about 10.0 - 12.0 per cent for point load and U.D.L. At this stage the increase in overall deflections and local deflections was still negligible. Beyond this point the growth of σ_{DBC}/σ_{DB} and $\sigma_{DBC}/\sigma_{DBL}$ increased significantly with growth of crack length and the width of the crack was also significant. When the crack length was more than 1100.0 mm there was no significant increase in σ_{DBC}/σ_{DB} and $\sigma_{DBC}/\sigma_{DBL}$.

Boxes B and C: To examine the effect of a crack in small boxes, a second series of boxes was analysed. This series includes Boxes B and C which have higher distortional rigidities than Box A. These two boxes had the same distortional rigidities, i.e. $K = 58.42\ N/mm^2$ per unit length, only their span lengths were different. The span length for Box B was 3.3 m and for Box C was 2.5 m. The thickness of plates was 8.0 mm in both cases. These boxes are shown schematically in Fig. 8.2. A summary of the results

for Box B for point load is given in Table 8.3 and in Table 8.4 a summary of the results is given for Box C. For a length of crack equal to 50.0 mm the increase of transverse distortional bending stress at the end of the crack in relation to the maximum σ_{DB} for the uncracked case in both cases was about 10 per cent, and that corresponding to the σ_{DBL} was between 14.4 - 16.4 per cent. (Although the values of $\sigma_{DBC}/\sigma_{DBL}$ are higher than the values of σ_{DBC}/σ_{DB}, as may be expected, the latter are more important in practical design than the former.) The ratio of $a/_L$ was 1.52 and 2.0 per cent for Boxes B and C respectively. The growth of deflections at this stage is not significant. In Fig. 8.5 plots of crack length against σ_{DBC}/σ_{DB} are presented for Boxes A, B and C. For the same crack length the increase in the maximum distortional bending stress was much higher for a short box than for a long box. Although the distortional stiffnesses of Boxes B and C were the same the increase of σ_{DBC}/σ_{DB} for Box C (which was shorter than Box B) was higher. When the ratio of the crack length to span length, i.e. $a/_L$ was plotted against σ_{DBC}/σ_{DB} as shown in Fig. 8.10, the picture changed. It can be seen from Fig. 8.10 that an increase of σ_{DBC}/σ_{DB} for Box A in the early stages of crack propagation was much higher than for Boxes B and C. It was observed that the relationship between $a/_L$ and σ_{DBC}/σ_{DB} was not following the same pattern as compared with the relationship between crack length and σ_{DBC}/σ_{DB}. For Box A when the crack length is higher than about 4 per cent of the span the increase in σ_{DBC}/σ_{DB} is not significant at all. After this stage a large increase in crack length had little effect on σ_{DBC}/σ_{DB}.

The same pattern was observed for Boxes B and C when $a/_L$ was higher than about 10 per cent.

Boxes D and E: To investigate the effect of distortional stiffness on σ_{DBC} in small boxes, another series of boxes was analysed. This series is called Boxes D and E. These boxes were identical to Boxes B and C respectively except for differences in their distortional stiffnesses. The distortional stiffness for both boxes was K = 24.65 N/mm^2 per unit length and the thickness of plate used was 6.0 mm as shown in Fig. 8.2.

Results of the analysis for Box D are summarized in Table 8.5 and that for Box E are given in Table 8.6. It was noted from the results that for both boxes when a crack of up to 50.0 mm length occurred along the corners of the box, the increase in deflections, in general, was negligible but the growth of σ_{DBC}/σ_{DB} and $\sigma_{DBC}/\sigma_{DBL}$ was about 11.0 and 14.0 per cent respectively. After this stage up to $a/_L \simeq$ 10.0 per cent both deflections and σ_{DBC}/σ_{DB} increased rapidly. Beyond that the spread of cracks had a diminishing effect on σ_{DBC}/σ_{DB} but still significantly affected the maximum deflections. The increase of σ_{DBC}/σ_{DB} for the same crack length in the shorter Box E was higher than in Box D. This can be seen in Fig. 8.6 where the results for both boxes are plotted on a - σ_{DBC}/σ_{DB} axis. In Fig. 8.11 the results are presented on $a/_L$ - a σ_{DBC}/σ_{DB} axis. It can be seen that when the results are represented in this manner a simple relationship does not exist. The curves cross each other when $a/_L$ reaches about 6.0 per cent. However in this case when

the value of $a/_L$ is about 10.0 per cent a large increase in crack makes little difference to the ratio σ_{DBC}/σ_{DB}.

Comparison of Results for All Boxes: In Figs. 8.7 and 8.8 the results of each pair of boxes which had the same span lengths but different distortional stiffneses (except Box A) are shown. It was observed that in general the effect of distortional stiffness on σ_{DBC}/σ_{DB} was not very high. This fact could be seen clearly when all results are plotted as in Fig. 8.9. The curves indicated that the dominant factor on the determination of σ_{DBC} is the span length of the box. The shorter the box, the higher is σ_{DBC}/σ_{DB}.

It can be seen also that at the early stages of cracking up to about 150 mm crack, the relationship between a - σ_{DBC}/σ_{DB} is approximately linear. The gradient of the lines are very high for small boxes in contrast to a full scale box. After this stage and up to a crack length of 600 mm the gradient of the curves for small boxes becomes smaller but for Box A increases.

In Fig. 8.12 all values of σ_{DBC}/σ_{DB} are plotted against $a/_L$. It can be seen that when $a/_L$ in Box A exceeds 4 per cent and in Boxes B, C, D and E exceeds 10 per cent, large increases in crack length make little difference to the maximum transverse distortional bending stresses. The curves as plotted appear to be asymptotic to a value of $\sigma_{DBC}/\sigma_{DB} \simeq 1.5 - 1.6$ for the cases consider in this investigation.

8.6 SUMMARY

This exploratory investigation, even though confined to linear elastic models of simply supported boxes subjected to transverse distortional component of loading with cracks occurring simultaneously at diagonally opposite corners, has demonstrated several points of importance.

(a) When cracking is at the early stages the relationships between crack length and σ_{DBC}/σ_{DB} is approximately linear.

(b) The gradient of lines on a - σ_{DBC}/σ_{DB} axes for short boxes are much higher than for longer boxes at early stages of crack propagation. This pattern changes when $a/_L$ against σ_{DBC}/σ_{DB} is considered, i.e. the gradient of lines on $a/_L$ - σ_{DBC}/σ_{DB} for long boxes are higher than for short boxes at the early stages of crack propagation.

(c) The increase of deflections at the early stages of crack propagation are almost negligible but with the development of cracks beyond 250 mm the deflections increase significantly.

(d) Most increases in maximum transverse distortional bending stress at the crack end occur while the crack length is less than 10 per cent of the span for small boxes and 4 per cent for large boxes. After this stage the increase in maximum transverse distortional stress rarely exceeds 1.6 times the maximum distortional stress in the equivalent uncracked box.

(e) The dominant factor in the increase of σ_{DBC}/σ_{DB} in relation to crack length is the span length of the box.

CHAPTER NINE

CONCLUSIONS AND RECOMMENDATIONS FOR FURTHER RESEARCH

9.1 CONCLUSIONS RELATING TO ESTIMATION OF DISTORTIONAL STRESSES

A comparison of several analytical methods has shown that the BEF analogy is the most economical method to be used for the calculations of distortional stresses in box girder bridges. A parametric study of a wide range of practical box girder bridges has resulted in a simple method for estimating distortional stresses which has been incorporated in the Interim Design Rules for Box Girder Bridges[2.12].

A simple method has also been developed to estimate the distribution of torsional moments in multibox bridges. This method can be combined with the BEF method to estimate distortional stresses in the most critically loaded box without the need to resort to laborious and costly load redistribution techniques at the initial stages of design.

It has been shown that the magnitude of transverse distortional bending stresses in box girders, particularly in the absence of intermediate diaphragms, may be large and they must therefore be considered in design. The maximum transverse bending stresses occur at the box corners, where the welded joints are located. As these stresses may fluctuate, and indeed reverse due to the passage of live loading, it is necessary to consider carefully their fatigue behaviour in design.

9.2 MAIN CONCLUSIONS RELATING TO FATIGUE INVESTIGATION

1. The P-S-N curves for different fillet corner weld details subjected to fluctuating transverse bending stresses have been presented. Types investigated include single fillet and double fillet welded joints. The effects of poor fit-up have also been investigated. In each case the fatigue lives have been found to be log-normally distributed.

2. The best mathematical function to represent the experimental results was a logarithmic equation in each case.

3. The best fatigue performance was that of a double fillet weld with good fit-up between plates. For a 50 per cent probability its performance corresponded closely to a Class D detail as given in Ref. (6.4). The worst fatigue performance was observed for a single fillet weld with poor fit-up between plates. For a similar probability this performance corresponded to Class W detail in Ref. (6.5).

4. In general,it was established that poor fit-up between plates at a box corner weld had a significant deleterious effect on the fatigue behaviour of a joint. Gaps reduced the fatigue lives, and had their worst effect on single fillet corner welds in which the maximum stresses occurred at the toe of the weld. The reduction in life for such welds with gaps compared to those with good fit-up was as much as 74 per cent in some instances. Furthermore the introduction of a gap frequently led to a change in failure mode.

5. Butt welded joints with sealing runs had almost the same fatigue life as double fillet welded joints with good fit-up between plates.

6. The effect of sealing runs on butt welded joints was to increase the fatigue life. In the best case presented, an increase of 92 per cent was observed between comparable joints.

7. It was found that locked-in transverse bending stresses such as those caused by welding closed sections can have a similar effect on the fatigue behaviour of welded joints subjected to fluctuating transverse bending as applied static stresses of the same magnitude. In the fatigue design of such cases the combined effect of the stresses arising from welding and stresses caused by external load must be considered.

8. Fatigue cracks in all cases propagated across the weld through the plate thickness with an almost semi-elliptical crack front shape.

9.3 CONCLUSIONS RELATING TO EFFECT OF CRACKS ON DISTORTIONAL BEHAVIOUR

1. Although no attempt was made to investigate the rate of crack propagation along the weld length, theoretical studies were carried out to investigate the effect of the presence of cracks on the distortional behaviour of a box. Quantitative information has been presented for two types of boxes, one representing approximately a full-scale single cell box girder bridge, and the other idealising a closed box stiffener of relatively small dimensions. This investigation is by no means an exhaustive study and is more in the nature of a pilot study.

2. It was found that the presence of small cracks ($a < 150$ mm) at diagonally opposite corners increased the transverse distortional bending stress in the uncracked weld immediately adjacent to the ends of the cracks, but had negligible effect on overal deflections.

3. An increase in length of the cracks increased the maximum transverse distortional bending stress, although the rate of increase rapidly reduced when the crack length exceeded 4 per cent and 10 per cent of the span between diaphragms in full scale and small boxes respectively. At this stage the increase in overall deflections in the vertical direction was between 8-21 per cent. However these results relate only to cases where the load is kept mid-way between diaphragms. If it also holds true for moving loads then it is possible that sufficient warning of the presence of fatigue cracks would be given by the increased flexibility of the structures before catastrophic collapse occurred.

4. The size of the crack opening for different crack lengths was also quantified. Such cracks would lead to a tearing action between plates at their ends aggravated by repeated loading, which would almost certainly influence the rate of crack propagation in real structures.

9.4 RECOMMENDATIONS FOR FURTHER RESEARCH

1. More tests are needed on butt welded corner joints to supplement those presented, so that appropriate design curves can be developed.

2. The fatigue life of corner joints stiffened by ring stiffeners needs investigation.

3. The scale effect should be checked by conducting a series of tests to a larger scale to confirm application of results presented.

4. The problem of the rate of crack propagation in corner welds and the significance of such cracks on box behaviour needs to be studied.

5. Modification of the BEF approach to deal with the box with cracked corner seems possible by simply reducing the support stiffness in the equivalent BEF over a length corresponding to the crack length in the real box. Such a method could be used to study the effects of different variables and crack lengths on distortional behaviour.

6. Experimental work on boxes with cracked corners would also be useful to verify the results of whatever theoretical approach is used.

REFERENCES

1.1 Chapman, J.C. and Dowling, J.C. Proposed research on steel elevated highways. Engineering Structures Laboratories. Imperial College, June 1969.

1.2 Frieze, P.A. and Dowling, P.J. Steel box girders, Model 7 - progress report 2. Engineering Structures Laboratories, Imperial College, February 1975.

1.3 Chapman, J.C., Dowling, P.J., Lim, P.T.K. and Billington, C.J. The structural behaviour of steel and concrete box girder bridges. Structural Engineer, vol. 49, March 1971, pp. 111-120.

1.4 Billington, C.J., Ghavami, K. and Dowling, P.J. Steel box girders, parametric study of cross-sectional distortion due to eccentric loading. Engineering Structures Laboratories, Imperial College, London. CESLIC Report BG16, September 1971.

2.1 Moffat, K.R. and Dowling, P.J. Shear lag in steel box girder bridges. The Structural Engineer, Vol. 53, No. 10, Oct. 1975, pp. 439.

2.2 Reissner, H. Neuere, Probleme der Flugzeugstatik. Zeitschrift für Flugtechnik und Motorluftschiffahrt, No. 18, 1926, pp. 384-393 (in German).

2.3 Ebner, Z.H. Die Beanspruchung dünnwandiger Kastenträger auf Drillung bei behinderter Querschnittswolbung. Zeitschrift für Flugtechnik und Motorluftschiffahrt No. 24, 1933, pp. 684-692 (in German).

2.4 Dalton, D.C. and Richmond, B. Twisting of thin walled box girders of trapezoidal cross-section. Proc. of the Inst. of Civil Eng., Vol. 39, Jan. 1968, pp. 61-73.

2.5 Richmond, B. Twisting of thin walled box girders. Proc. of the Inst. of Civil Eng., Vol. 33, April 1966, pp. 659-675.

2.6 Timoshenko, S.P. Strength of materials, Part 2. D. Van Nostrand Co. Inc., Princeton, N.J., 1956.

2.7 Vlasov, V.Z. Thin walled elastic beams. U.S. Department of Commerce, PST Catalogue No. 428, 1959.

2.8 Wright, R.N., Abdel-Samad, S.R. and Robinson, A.R. BEF analogy for analysis of box girders. Journal of the Structural Division, Proc. of the American Society of Civil Eng., Vol. 94, ST7, July 1968, pp. 1719-1943.

2.9 Wright, R.N. Design of box girders of deformable cross-section. Highway Research Record, No. 295, Washington, 1969.

2.10 Billington, C.J. The theoretical and experimental elastic behaviour of box girder bridges. Ph.D. Thesis, Civil Eng. Dept., Imperial College, University of London, March 1974.

2.11 Lim, P.T.K., Kilford, J.T. and Moffatt, K.R. Finite element analysis of curved box girder bridges. Proc. Development in Bridge Design and Construction, Conference, Cardiff, March 1971.

2.12 Inquiry into the basis of design and method of erection of steel box girder bridges. Interim design and workmanship rules. Part II: Design Rules. HMS, London 1973.

3.1 Gurney, T.R. Fatigue of welded military structures. British Welding Journal, vol. 15, June 1968.

3.2 Munse, W.H. and Grover, L.M. Fatigue of welded steel structures. Welding Research Council, New York, 1964.

3.3 Nunn, D.E. and Morris, S.A.H. Trials of experimental orthotropic bridge deck panels under traffic loading. TRRL Report 627, 1974.

3.4 Lomas, T.W., Ward, J.O., Rait, J.R. and Colbeck, E.W. The influence of frequency of vibration on the endurance limit of ferrous alloys at speeds up to 150,000 c/m using a pneumatic resonant system. International Conference on Fatigue. Institute of Mechanical Engineers, 1956.

3.5 Forrest, P.G. and Tapsell, M.J. Some experiments on alternating stress fatigue of a mild steel specimen and aluminium alloy. Proc. Instn. Mech. Engineers, September 1954.

3.6 Moore, H.F., Wilson, B.L., Howell, F.M. and Gohn, G.R. Report of task group on effect of speed of testing on fatigue. Test Results. ASTM Proc. vol. 50, 1950.

3.7 Gurney, T.R. Some tests to examine the influence of elapsed time after welding on the fatigue strength of welded joints. Welding Institute Research Report E23/12/68, December 1968.

3.8 Fisher, J.W. Fatigue strength of welded A514 steel beams. Proc. Conf. on Fatigue of Welded Structures, Brighton 1970, The Welding Institute, 1971.

3.9 Fisher, J.W., Frank, K.H., Hirt, M.A. and McNamee, B.M. Effect of weldments on the fatigue strength of steel beams. Final report, National Co-operative Highway research programme, Project 12-7. Fritz Engineering Laboratory Report No. 334.2. Lehigh University Institute of Research, September 1969.

3.10 Cazaud, R. Fatigue of metals. English translation by Fenner, A.J., Chapman and Hall Ltd., London 1953.

3.11 Signes, E.G., Baker, R.G., Harrison, J.D. and Burdekin, F.M. Factors affecting the fatigue strength of welded high strength steels. British Welding Journal , vol. 14, No. 3, 1967, pp.108-116.

3.12 Watkinson, F., Bodger, P.H. and Harrison, J.D. The fatigue strength of welded joints in high strength steels and methods for its improvement. Proc. Conf. on Fatigue of Welded Structures, Brighton, 1970, The Welding Institute, 1971.

3.13 Hempel, M. and Möller, H. The effect of weld defects in specimens of steel ST37 on their tensile fatigue strength. Archiv. für das Eisenhüttenwesen, vol. 20, No. 11/12, 1949, pp. 375-383.

3.14 Munse, W.H. Comments on fatigue properties of materials by E.G. Eeles and R.C.A. Thurston. Ocean Engineering, vol. 1, No. 2, 1968, pp.189-195.

3.15 Matting, A. and Neitzel, M. The influence of weld defects on the fatigue behaviour of welded constructions. B.W.J., vol. 14, January 1967, pp. 3-12.

3.16 Dwight, J.B. and Young, J.G. Residual stresses due to welding. Conference on Joints in Structures, Sheffield University, 1971.

3.17 Dwight, J.B. Effect of welding on compression elements. Conference on Improving Welded Product Design, The Welding Institute, November, 1971.

3.18 Kudryavtsev, L.V. The influence of internal stresses on the fatigue endurance of steel, International Conference on Fatigue, Instn. Mech. Eng., 1956.

3.19 Gurney, T.R. The influence of residual stresses on the fatigue strength of plates with fillet welded attachments. British Welding Journal , vol. 7, No. 6, 1960, pp. 415-431.

3.20 Gurney, T.R. Fatigue of welded structures. Cambridge University Press, 1968.

3.21 Blatherwick, A.A. and Lazan, B.J. The effect of changing cyclic modulus on bending fatigue strength. A paper presented at the 59th Annual Meeting of A.S.T.M., June 17-22, 1956.

3.22 Massonnet, Ch. The effect of size, shape and grain size on the fatigue strength of medium carbon steel. Proc. A.S.T.M., vol. 56, 1956, pp. 954-978.

3.23 Christopher, P.R. and Grabe, D.R. A discourse of factors which control fatigue behaviour in high yield alloy steel structures. Ocean Engineering, vol. 1, Pergamon Press, July 1969, pp. 497-520.

3.24 Neuber, H. Theory of notch stress: Principles for exact stress calculation. A.W. Edwards, Ann Arbor, Michigan, 1946.

3.25 Forrest, P.G. Fatigue of metals. Pergammon Press, 1962.

3.26 Thielsch, H. Weld surface contour variations. Welding Engineers, vol. 51, No. 11, 1966, pp. 60-67.

3.27 Ros, M. Experiments for the determination of the influence of residual stresses on the fatigue strength of structures. Welding Research BWRA, vol. 4, No. 5, 83s-93s (October, 1950).

3.28 Hebrant, F., Louis, H., Soete, W. and Vinckier, A. The relaxation of residual welding stresses by static and fatigue loading. Welding Research abroad. 58s-63s (September 1957).

3.29 Dugdale, D.S. Effect of residual stress on fatigue strength. Welding Journal, vol. 38, No. 1, Research suppl., 45s-48s (1958).

3.30 Sanders, W.W., Derecho, A.T. and Munse, W.H. Effect of external geometry on fatigue behaviour of welded joints. Welding Research Suppl., vol. 30, No. 2, 49s-55s (Feb. 1965).

3.31 Davis, H.L. and Toprac, A.A. Fatigue testing of ribbed orthotropic plate bridge elements. Research report 77-1, Center for Highway Research, the University of Texas, May 1965.

3.32 Seim, C. and Ferwerda, R. Fatigue study of orthotropic bridge deck welds. Research report M & R No. 666473 Department of Public Works, Division of Highways, State of California, April 1972.

3.33 Maddox, S.J. Fatigue of welded joints loaded in bending. Department of the Environment, TRRL Suppl. Report 84UC, 1974.

3.34 Maddox, S.J. The fatigue behaviour of trapezoidal stiffener to deck plate welds in orthotropic bridge decks. Department of the Environment, TRRL Suppl. Report 96UC, 1974.

5.1 Freudenthal, A.M. The statistical aspect of fatigue of materials. Proceedings of the Royal Society of London, Series A, vol. 187, Dec. 1946.

5.2 Guide for fatigue testing and statistical analysis. American Society for Testing Materials, STP 91.A, 1963.

5.3 Stulen, F.R. On the statistical nature of fatigue. Symposium on statistical aspects of fatigue. A.S.T.M. Atlantic City, 19 June, 1951, pp. 23-40.

5.4 Owens, L.D. and Goldsmith, P.L. Statistical methods in research and production. Oliver and Boyd 1972 (4th edition).

5.5 Hald, A. Statistical theory with engineering application. John Wiley and Sons Inc., New York, 1952.

5.6 Abramowitz, M. and I.A. Slegan (Editors). Handbook of mathematical functions with formulas, graphs and mathematical tables. Dover Publications Inc., New York, 1964.

5.7 Neville, A.M. and Kennedy, J.B. Basic statistical methods for engineers and scientists. International Textbook Company, Feb. 1966.

5.8 Weibull, W. Fatigue testing and analysis of results. Pergammon Press, 1961.

5.9 Freudenthal, A.M. Planning and interpretation of fatigue tests. Symposium on statistical aspects of fatigue. Atlantic City, 19 June, 1951 A.S.T.M., STP 121.

5.10 Blom, G. Statistical estimates and transformed Beta-variables. John Wiley and Sons Inc., New York, 1952.

5.11 Draper, N.R. and Smith, H. Applied regression analysis. John Wiley and Sons, 1966.

6.1 British standard 3518. Part 5. Guide to the application of statistics. British Standards Institution, 1962.

6.2 Committee E-9 on Fatigue. A guide for fatigue testing and statistical analysis of fatigue data. ASTM, STP 9HA, Philadelphia, 1963.

6.3 British standard 153. Part 3B,specification for steel girder bridges. British Standard Institution, 1972.

6.4 Inquiry into the basis of design and method of erection of steel box girder bridges. Report of the committee, Appendix I. Interim design and workmanship rules. PartIII and IV. HMSO, London, 1973.

6.5 Halse, W.I. and Smith, D.W. New code of practice for bridges fatigue specifications. Department of the Environment Report BE/22/2/029, Sept. 1974

6.6 Evans, R.B. and Jones, A.W. The fatigue behaviour of fillet welded mild steel under sinusoidal loading at room temperature and 350^{o}C. Proc. conf. on fatigue of welded structures; Brighton, 1970, the Welding Institute 1971. pp. 350-357.

6.7 Baillie, J.G. Underbead and toe cracks. British Welding Journal, Vol. 14, Feb. 1967, pp.51-61.

6.8 Maddox, S.J. Fracture mechanics applied to fatigue of welded structures. Fatigue of welded structures conference. The Welding Institute. Brighton 6-9 July, 1970, pp.73-96.

8.1 Leonard, D.R. A traffic loading and its use in the fatigue life assessment of highway bridges. Department of the Environment, TRRL Report LR252, 1972.

8.2 Miner, M.A. Cumulative damage in fatigue. Journal of Applied Mechanics, Vol. 12, No. 3, Sept. 1945, pp.159-164.

8.3 Harrison, J.D., Gurney, T.R. and Smith, B. Cumulative damage of fillet welded joints in Aℓ: zn: Mg alloy. Proc. Conf. on Fatigue of Welded Structures, Brighton, 6-9 July 1970. The Welding Institute.

8.4 Whitman, J.G. and Webber, D. The problem of cumulative damage in welded structures. Proc. Conf. on Fatigue of Welded Structures, Brighton 6-9 July 1970. The Welding Institute.

8.5 Alder, J.F. Cumulative damage in fatigue of welded structures. British Welding Journal, Vol. 11, No. 10, Oct. 1964, pp.501-506.

8.6 Paris, P.C. The fracture mechanics approach to fatigue. Proc. 10th Sagamore Conf. Syracuse Univ. Press, 1965.

8.7 Maddox, S.J. Assessing the significance of flaws in welds subjected to fatigue. Welding Journal, Welding research supplement, Vol. 53, 1974, pp. 401s-409s.

8.8 Sih, G. Handbook of stress-intensity factors; stress-intensity factor solutions and formulas for reference. Lehigh University, 1973.

8.9 Cullimore, M.S.G. and Horsington, R.W. The extension of a fatigue crack in a model steel plate under cyclic loading. Developments in Bridge Design and Construction. Edited by Rockey, K.C., Bannister, J.L. and Evans, H.R. Crosby Lockwood & Son Ltd., London, 1971, pp.577-587.

8.10 Ngo, D. and Scordelis, A.C. Finite element analysis of reinforced concrete beams. American Concrete Institute Journal, Proc., Vol. 64, No. 3, March, 1967, pp.152-163.

8.11 Nilson, A.H. Non-linear analysis of reinforced concrete by finite element method. American Concrete Institute Journal, Proc,,Vol. 65, No. 9, Sept. 1968, pp.757-766.

8.12 Nilson, A.H. Finite element analysis of reinforced concrete. Ph.D. thesis, Civil Eng. Dept., University of California, Berkeley, 1967.

8.13 Ngo, D., Franklin, H.A. and Scordelis, A.C. Finite element study of reinforced concrete beams with diagonal tension cracks. Report No. UC-SESM 70-19, Dept. Civ. Eng., University of California, Berkeley, Dec. 1970.

8.14 Moffatt, K.R. Finite element analysis of box girders. Ph.D. thesis. Civ. Eng. Dept., Imperial College, University of London, Jan. 1974.

APPENDIX 2-I

PARAMETRIC STUDY OF CROSS-SECTIONAL DISTORTION OF SINGLE CELL BOX GIRDER

2.1.1 Cross-sectional Properties of Practical Steel Box Girder

Details of approximately 26 recent practical steel box girder bridge designs were studied in order to investigate possible simplifications to the BEF method. The bridges are listed in Table I.1. Most of the bridges are of multibox construction. The method of analysis given in Chapter 2 makes use of the BEF method for single cell boxes to be determined separately. The BEF properties for each bridge listed in Table I.1, are given in Table I.2. The following observations can be made:

(a) βL (span) the dimensionless panel length of the span of the box. If this is greater than approximately 2.5, the support diaphragms have small influence on the stresses at midspan and the box may be analysed as an infinite BEF for which there is a simple solution. As can be seen in all cases studied βL (span) is bigger than 2.5.

(b) βL_D (panels) is the dimensionless panel length between diaphragms or cross-bracing. If βL_D is smaller than 2.0 then diaphragms control the stresses at midpanel under both point load and uniformly distributed load. If βL_D is smaller than 0.2 diaphragm stiffness alone is the controlling factor. Therefore as a general rule

diaphragms are most effective if spaced in the range $0.2 < \beta L_D < 2.0$. From thirteen bridges with internal diaphragm studied only one had $\beta L_D > 2.0$ (Bridge No. 22 and also only one had $\beta L_D < 0.2$ (Bridge No. 6).

(c) $Ic/4I_b$, r_β, r_s. The expressions leading to the warping stiffness of the box "I_b" are complicated and therefore as an approximation the use of $Ic/4$ has been suggested [2.7]. This is used in the BEF analysis at two stages. First in the calculation of the β parameter

$$\beta = \sqrt[4]{\frac{K}{4EI_b}} \qquad \text{(I-1)}$$

and secondly in the calculation of warping stresses from the BEF moment. A further approximation may be introduced into the warping stress calculation by using the analogy to bending about the horizontal axis as

$$\sigma_{DW} = E\bar{Y}W'' \qquad \text{(I-2)}$$

where $\bar{Y}$ is the distance from the neutral axis to the extreme fibres

and W is the BEF deflection.

The values of $Ic/4I_b$ given in Table I-2 compare the exact and approximate warping stiffnesses and r_β is a measure of the error in β resulting from use of the approximation $I_b/4$. r_s is a measure of the error resulting from the use of equation (I-2) rather than the exact expression for σ_{DW}. Table I-2 shows that the maximum value of r_β is 1.19 - an error of 19 percent - but in only two cases r_β shows errors greater than 10 percent. When r_β is greater than 1.0 this leads to conservative values of σ_{DW} and values of r_β less than 1.0 do not exceed 6 percent error. The approximation of equation (I-2) measured by r_s leads to slightly larger errors, the maximum being 46 percent. However where values of r_s are small (representing larger errors in σ_{DW}) values of r_β are generally greater than one and discrepancies tend to compensate. The maximum error in using equation (I-2) together with $I_b/4$ is 19 percent. Since the warping stresses have generally less importance than distortional bending stresses, the above figures suggest that the use of these approximations leads to sufficient accuracy for design.

(d) V is the redundant shear at a cut on the centre line of the bottom flange of unit length of the box subjected to unit antisymmetrical load. The expression for V is complicated (see equation (2.10)) and is used in the calculations of the frame stiffness K. As can be noted from Table I-2, the value of V is almost always between 0.2 and 0.25 and if an approximate value of say 0.225 could be used the

calculation of K would be greatly simplified. However the value of V is outside the normal range for two bridges. For bridge 1 the use of a value of 0.225 would lead to a large error. Construction of bridge 1 is peculiar in that there are no transverse stiffeners on the bottom flange, although a substantial transverse web stiffening is used (12" bulb flat). Such detail may lead to high stress concentration in the bottom flange plate adjacent to the web stiffeners and is, therefore, in general, to be avoided.

(e) γ and λ. These are geometrical properties of the boxes and may be used to define the practical ranges of box girders. For rectangular boxes $\gamma = 1$ and trapezoidal boxes obviously have $\gamma < 1$. λ - the ratio of slant height to top flange width - varies between 4 and 0.24.

(f) α and ν. These are ratios of the transverse flexural rigidities of bottom to top flanges and web to top flanges respectively. These ratios have a large influence in the calculation of the frame stiffness of the box and they reflect the levels of σ_{DB} in the various plates of the box.

Where there is a large difference in the flexural rigidities of adjacent box walls, transverse stresses may often be high in the wall with the smaller flexural rigidity especially where the section modulus of the stiffener-plate combination is low. Transverse stiffeners are usually proportioned for considerations other than that of distortional stresses and this often leads to large differences in flexural rigidity and hence high stress levels. Table I-2 shows that in almost half the bridges investigated the ratio ν has a value less than .002.

1.2 Simplification of Design Formula

The simplified design approach for the design of distortion using BEF analogy was possible after having studied the above-mentioned parameters which influence the distortional behaviour of steel box girders. Ratios γ, λ, α and ν may be used to simplify the calculation of K. If the dimensionless groups

$$\gamma = B_B/B_T$$

$$\lambda = C/B_T$$

$$\alpha = D_B/D_T$$

$$\nu = D_C/D_T$$

are substituted into equation (2.12). This equation reduces to

$$K = \frac{1}{\delta_1} = \frac{24 \cdot D_T \cdot R}{B_T^3} \qquad \text{(I-3)}$$

where

$$R = \frac{1 + \alpha}{\gamma\{\frac{\lambda}{\gamma}\left[\frac{2\gamma}{1+\gamma} - (2+\gamma)\ S\right] + \frac{\gamma}{1+\gamma} - S\}}$$

and (I-4)

$$S = \frac{(\gamma\lambda/\nu) \cdot (2+\gamma) + \gamma}{1 + \gamma + \frac{2\lambda}{\nu}(1+\gamma)(1+\gamma+\gamma^2) + \frac{\gamma^3(1+\gamma)}{\alpha}}$$

then

$$\beta = \frac{24 . D_T . R}{EI_b . B_T^3} \qquad \text{(I-5)}$$

For rectangular boxes, $\gamma = 1$ and the equation for R reduces to

$$R = \frac{2}{\frac{\lambda}{\nu}\left[1 - \frac{3(3\lambda/\nu + 1)}{(2 + 12\ \lambda/\nu + 2/\alpha)}\right] + \frac{1}{2} - \frac{3(\lambda/\nu + 1)}{(2 + 12\ \lambda/\nu + 2/\alpha)}} \qquad \text{(I-6)}$$

This expression for R is in terms of two variables only (λ/ν and α) and therefore families of curves can be plotted of R against α for different values of λ/ν. Values of λ/ν and α in Table I-2 suggest that the practical range of α is from 0.005 to 1.0 and the practical range of λ/ν is from 1 to 2500 and values of R are plotted for these ranges in Fig. I-1.

The general expression for R for trapezoidal boxes has the additional variable γ, it may be related to λ by the expression

$$\lambda = (1 - \gamma)/2 \cos\theta$$

where θ is the side slope of the box.

Curves similar to those for the rectangular box may be plotted for particular values of θ and λ. A common side slope is 60° and it was decided that a series of curves for evaluation of R for this slope would be useful. Curves were plotted for values of λ of 0.8, 0.5 and 0.3 and are shown in Figs. I-2 to I-4 for the practical range of parameters. Values of R for other values of α may be found by logarithmic interpolation between the curves for particular values of α and λ/γ.

APPENDIX 4.I

CALCULATION OF BENDING STRESSES FOR SPECIMEN TYPE B

In this section both theoretical and experimental static stresses as well as overall deflections of some specimens are calculated. Stresses are calculated at two main points of interest, i.e. points B and C and the deflection is calculated and measured at the loading point A.

4.1 Theoretical and Experimental Analysis of Specimen BESBS

The measured dimensions of the specimen were:

W = 80.0 mm (3.15 in)

d = 30.0 mm (1.18 in)

l_1 = 60.0 mm (2.36 in)

l_2 = 240.0 mm (9.45 in)

$a = b$ = 170.0 mm (6.69 in)

t = 12.7 mm (0.50 in)

E = 205.436 x 10^3 N/mm^2 (13340.0 tonf/in^2)

where W = width of the specimen

t = thickness of the plate

E = modulus of elasticity

for the rest of the notation see Fig. 4.21.

It is assumed that the second moment of inertia of the specimen where it is gripped by the Vibrophore is equal to infinity (i.e. $I_1 = \infty$) and

$$I = I_2 = I_3 = 13655.9 \text{ mm}^4 \ (0.033 \text{ in}^4)$$

$$Z = Z_2 = Z_3 = 2150.5 \text{ mm}^3 \ (0.131 \text{ in}^3)$$

The vertical deflection of the specimen at the point of the load application is calculated using equation (4.3) for p = 1 tonne (0.984 tonf)

$$\Delta_{AP} = 2\{[(\ell^2_1 - d^2) + 4\ell_2 (\ell_1 + b)] \frac{P}{16EI}\}$$

$$\Delta_{AP} = -2.471 \text{ mm } (- 0.0971 \text{ in})$$

The measured deflection for specimen BESBS was 2.4 mm (.094 in). As can be seen the theoretical analysis agrees with the experiment to within 3.0 per cent of the experimental results. The calculated bending moments in the specimen are:

$$\delta_{11} = \frac{1}{2EI}[(\ell_1 - d) + 2\ell_2] = \frac{10.0395}{EI}$$

$$\delta_{11} = -0.0229$$

$$M_A = 2.1566p \text{ tonf.in}$$

$$M_B = 1.5661p \text{ tonf.in}$$

$$M_C = 1.7804p \text{ tonf.in}$$

The bending moment at point C is 13.7 per cent higher than at point B indicating that the objective of achieving the maximum stresses at the welded joint in the specimen is fulfilled.

As far as $I_1 = \infty$ then $\sigma_A = 0.0$

hence $M_B = 390.0$ kN mm (1.541 tonf.in)

$\sigma_B = 181.349$ N/mm^2 (11.745 tonf/in^2)

and $M_C = -443.384$ kN/mm (-1.752 tonf in)

hence $\sigma_C = -206.169$ N/mm^2 (-13.353 tonf/in^2)

The maximum shear force at point C is

$$Q = \frac{M_B - M_C}{\ell_2} = 3.472 \text{ kN } (0.348 \text{ tonf})$$

from which

$$\tau = \frac{6Q}{w.t^3} \left(\frac{t^2}{4} - y^2 \right)$$

Normal force in the specimen's element is

$$N = 6.931 \text{ kN } (0.69 \text{ tonf})$$

hence the normal stress is as follows:

$\sigma_N = 6.802$ N/mm^2 (0.4417 tonf/in^2)

and

$$\sigma_{B\ comp} = -188.151\ N/mm^2 \quad (12.217\ tonf/in^2)$$

$$\sigma_{B\ Ten} = 174.418\ N/mm^2 \quad (11.326\ tonf/in^2)$$

and

$$\sigma_{C\ comp} = -213.1\ N/mm^2 \quad (13.837\ tonf/in^2)$$

$$\sigma_{C\ Ten} = 199.367\ N/mm^2 \quad (12.946\ tonf/in^2)$$

The theoretical stress-distribution along one specimen's element is given in Fig. 4.23 and 4.24.

The value of the normal stress in the specimen's element as calculated from the experimental data at point $\bar{B}'$ is $\sigma_T = 144.37\ N/mm^2$ ($9.375\ tonf/in^2$), $\sigma_C = 159.91\ N/mm^2$ ($10.319\ tonf/in^2$).

Hence bending

$$\sigma_{Bend} = \frac{\sigma_{comp} + \sigma_{Ten}}{2} = \frac{10.319 + 9.375}{2} = 9.847\ tonf/in^2$$

$$\sigma_{Bend} = 151.64\ N/mm^2$$

and

$$\sigma_N = \frac{\sigma_{comp} - \sigma_{Ten}}{2} = \frac{10.319 - 9.375}{2} = 0.474\ tonf/in^2$$

$$\sigma_N = 7.3\ N/mm^2$$

The theoretical and experimental stress distribution in the specimen is given in Fig. 4.23. The difference between the experimental and the theoretical values of the normal stress is 6.9 per cent and that of bending at point B' is 6.7 per cent. The experimental result at point B' is much smaller than the theoretical, i.e. about 15 per cent. The somewhat large difference may be due to the curvature of the bent part.

4.2 Theoretical and Experimental Analysis of Specimen BESFW

The measured dimensions of the specimen (along the centre-line) are:

$W = 80.0$ mm (3.15 in)

$d = 30.0$ mm (1.18 in)

$l_1 = 60.0$ mm (2.36 in)

$a=b = 173.0$ mm (6.81 in)

$t = 12.0$ mm (0.47 in)

$l_2 = 244.5$ mm (9.63 in)

$E = 208.24 \times 10^3$ N/mm^2 (13560 tonf/in^2)

The assumptions in calculating the stresses in this specimen are exactly the same as for BESBS

$I_1 = \infty$

$I_2 = I_3 = I = 11520.0$ mm^4 (0.0276 in^4)

$Z_2 = Z_3 = Z = 1920.0$ mm^3 (0.1171 in^3)

P = 1 tonne (= .984 tonf) applied load

The vertical deflection of the specimen at point A is

$\Delta_{AP} = -2.933$ mm (0.1155 in)

This value is very close to the result obtained from the test which was equal to 3.157 mm (.1243 in), i.e. the experimental value is 7.6 per cent higher than the theoretical.

The calculated bending moment of the specimen is as follows:

$$\delta_{11} = \frac{1}{2EI} \left[(\ell_1 - d) + 2\ell_2 \right]$$

$$\delta_{11} = 0.0273$$

hence the bending moment and bending stress at point A are

$$M_A = X_1 = \frac{-\Delta_{1P}}{2\delta_{11}} = 535.276 \text{ kN mm } (2.115 \text{ tonf. in})$$

$$I_1 = \infty ; \sigma_1 = 0.0$$

The bending moment and bending stress at point B are

$$M_B = (M_A - \frac{P\ell_1}{4}) = 388.233 \text{ kN mm } (1.534 \text{ tonf.in})$$

$$\sigma_B = 201.738 \text{ N/mm}^2 \ (13.099 \text{ tonf/in}^2)$$

and the bending moment and its corresponding stress at point C are

$$M_C = -459.872 \text{ kN mm } (-1.817 \text{ tonf.in})$$

$$\sigma_C = -239.577 \text{ N/mm}^2 \ (-15.516 \text{ tonf/in}^2)$$

and the shear force in the specimen at point C is

$$Q = \frac{M_B - M_C}{\ell_2} = 3.467 \text{ kN } (0.348 \text{ tonf.})$$

the axial force in the specimen's element is calculated by using equation (4.7)

$$N = 6.932 \text{ kN } (0.6957 \text{ tonf.})$$

hence the axial stress is

$$\sigma_N = 7.212 \text{ N/mm}^2 \ (0.468 \text{ tonf/in}^2)$$

the final comparison of the results for this type of specimen is given in Fig. 4.26 and 4.27.

APPENDIX 4.II

CALCULATION OF BENDING STRESS IN FILLET WELDED THROAT FOR SPECIMEN SERIES BESFWI AND BESFGI

Referring to Plates 6.23, 6.24 and Fig. 4.28, it can be seen that the root of the weld for the Series BESFWI and BESFGI is subjected to tensile bending stress. The plane of fatigue fracture does not pass through the theoretical throat of the fillet weld, but it propagates through the narrowest section of the weld. In the derivation of the equation for the calculation of the stress in the weld the theoretical dimension of the weld joint as shown in Fig. 4.28 was considered. The actual stress at the root of the weld could not be measured. For this reason the discrepancy of the theoretical and experimental result cannot be ascertained.

Using the notations shown in Fig. 4.28 the bending moment at the cross-section b-b for the applied load P is

$$M_{b-b} = P\left[L - \left(\frac{t}{2} + \ell\right)\right] \qquad \text{(II-1)}$$

and the section modulus at b-b is

$$Z_{b-b} = \frac{w.t^2}{6}$$

corresponding bending moment and the section modulus of the weld throat with the consideration of a gap between the two plates at the weld

corner is given by the following equation:

$$M_E = P\left[L - (t + \delta)\right] \qquad \text{(II.2)}$$

$$Z_{E-E'} = \frac{W.EE'^2}{6} = \frac{W.(\ell - \delta)^2}{12} \qquad \text{(II.3)}$$

when $\delta = 0$

$$M_E = M_{A'} = P\left[L - t\right] \qquad \text{(II.4)}$$

$$Z_{A'-D} = \frac{W.S^2}{6} = \frac{W\ell^2}{12} \qquad \text{(II.5)}$$

where W is the specimen's width.

The stress at the root of the weld is

$$\sigma_E = \frac{12P\left[L - (t + \delta)\right]}{W\left[\ell - \delta\right]^2} \qquad \text{(II.6)}$$

and at the section b-b is

$$\sigma_{B'} = \sigma_{B''} - \sigma_N = \frac{3P}{Wt^2}\left[2(L - \ell) - t\right] - \frac{P}{Wt} \qquad \text{(II.7)}$$

where σ_N is the stress due to normal force P

or $\sigma_{B'}$ in the other form is

$$\sigma_{B'} = \frac{P}{Wt^2}\left\{3\left[2(L - \ell) - t\right] - t\right\}$$

hence the ratio of the stresses at the root of the weld upon the stress at the toe of the weld at point B' is

$$\frac{\sigma_E}{\sigma_{B'}} = \frac{6t^2}{(\ell - \delta)^2} \quad \frac{[L - (t + \delta)]}{[3(L - \ell) - 2t]} \qquad \text{(II.8)}$$

In the following the ratio of stresses, i.e. $\frac{\sigma_E}{\sigma_{B'}}$ is calculated, by equation (II.8) for the weld joint given in Plate 6.24. The width and thickness of the specimen is the same as in other specimens (i.e. w = 80, t = 12.7 mm).

δ = 0 and the measured l = 11.2 mm,

L = 128

hence

$$\frac{\sigma_E}{\sigma_{B'}} = \frac{6 \times 12.7^2 [128-12.7]}{11.2^2 [3(128-12.7) - 2 \times 12.7]} = 2.77$$

APPENDIX 6-I

A TYPICAL CALCULATION OF THE COMPARISON OF TWO REGRESSION LINES

In the following the regression lines of two test series BEDFW and BEDFG are compared. The values used in the calculations are those given in Table 6.33.

1. The equality of the two variances about the regression lines is verified by the F-test.

$$F = \frac{s_1^2}{s_2^2} = \frac{0.0161}{0.0146} = 1.103$$

2. The number of degrees of freedom for s_1^2 and s_2^2 is

$$\gamma_1 = N_1 - 1 = 24$$

$$\gamma_2 = N_2 - 2 = 21$$

3. The theoretical value of F is found in the table of statistics for

$$F_\beta , \ (\gamma_1 , \gamma_2)$$

$$F.975 \ (24,21) = 2.37$$

$$F.950 \ (24,21) = 2.05$$

Hence the following expression holds:

$$F < F.95 < F.975$$

It can be concluded that the two variances are not significantly different. Thus the pooled variance about the regression line is calculated by Equation (5.42):

$$S^2_{RP} = \frac{(N_1 - 2)\, S_1^2 + (N_2 - 2)\, S_2^2}{N_1 + N_2 - 4}$$

$$S^2_{RP} = \frac{23(.0161) + 20(.0146)}{43} = .0154$$

and the standard deviation is

$$S_{RP} = 0.124$$

4. The slopes of the two regression lines are compared by using Equation (5.43)

$$h_1 = \sum_{i=1}^{K} n_1 (X_i - \bar{X}_1)^2 = \frac{S_1^2}{S^2_{b_1}} = \frac{.0161}{.0988} = 0.163$$

$$h_2 = \sum_{i=1}^{K} n_i (X_i - \bar{X}_2)^2 = \frac{S_2^2}{S^2_{b_2}} = \frac{.0146}{.1069} = 0.137$$

hence

$$t = \frac{b_1 - b_2}{S_{RP}\sqrt{\frac{1}{h_1} + \frac{1}{h_2}}} = \frac{-2.1786 + 2.6783}{0.124\sqrt{\frac{1}{0.163} + \frac{1}{0.137}}}$$

$$t = 1.0995 \approx 1.1$$

The number of degrees of freedom is:

$$N_1 + N_2 - 4 = 43$$

$$\therefore t._{9,43} = 1.3 \quad \text{and} \quad t._{95,43} = 1.68$$

Since $1.1 < 1.3 < 1.68$

Then the slopes of the two regression lines are not significantly different.

5. The identity of the two regression lines is tested by using Equation (5.41)

$$D = \frac{a_1 - a_2}{\bar{X}_1 - \bar{X}_2} = \frac{10.996 - 11.915}{2.138 - 2.143} = 183.8$$

$$E = \frac{\sum_{i=1}^{2} b_i h_i}{\Sigma h_i} = \frac{(-2.179)(0.163) + (-2.678)(0.137)}{0.163 + 0.137} = -2.41$$

$$H = \frac{(b_1 - b_2)^2}{\frac{1}{h_1} + \frac{1}{h_2}} = \frac{(2.179 - 2.678)^2}{\frac{1}{.163} + \frac{1}{.137}} = .0186$$

and the S^2 is calculated by Equation (5.44)

$$S^2 = \frac{\left[23(.0161) + 20(.0145) + .0186 \right]}{44} = .015$$

$$S = 0.124$$

$$t = \frac{183.8 + 2.41}{0.124 \left[\frac{1}{(.005)^2} \left(\frac{47}{(25)(22)} \right) + \frac{.3}{(.163)(.137)} \right]^{\frac{1}{2}}}$$

$$t = 25.635$$

Number of degrees of freedom $= N_1 + N_2 - 3 = 44$

$$t._{9,44} = 1.3 \quad ; \quad t._{95,44} = 1.675$$

Since

$$t < t._{9,44} < t._{95,44}$$

Then the two regression lines are significantly different.

NOTATION

CHAPTER 2

B	Width of the flange in rectangular box
B_B	Width of the bottom flange
B_T	Width of the top flange
C	Slant height of the box web between flange centre lines
d_i	Distortional stiffness of the diaphragm
D_B	Transverse flexural rigidity of the bottom flange
D_C	Transverse flexural rigidity of the web
D_T	Transverse flexural rigidity of the top of flange
h	Depth of the box
E	Young's modulus
G	Shear modulus
I_b	Second moment of area of beam on elastic foundations
I_c	Second moment of area of box cell
K	Distortional stiffness of box cell per unit length
k	Foundation modulus of BEF
L	Span of the box girder
M	Bending moment in BEF
N_B	Number of boxes
N_L	Number of lanes

P_A	Antisymmetrical component of vertical loading
P_B	Symmetrical component of vertical loading
P_T	Torsional component of the load
P_D	Distortional component of the load
$\{P\}_i$	Column matrix of the applied load in Richmond's method
$P(x)$	Applied distributed distortional load
Q	Diaphragm stiffness in BEF method
r_s	Error in σ_{DW} resulting from use of equation I-2
r_β	Error in β resulting from use of approximate warping property $I_c/4$
$\{S\}$	Column matrix of end forces
t_B	Thickness of bottom flange
t_T	Thickness of top flange
t_C	Thickness of web plate
V	Redundant shear force at centre of bottom flange
$\bar{V}$	Distortional forces in the diaphragm
W	Distortional deflection of the box
$[y]$	Stiffness matrix in Richmond's displacement solution
Z	Section modulus of the plate
$\bar{y}$	Perpendicular distance from neutral axis to centroid of top flange
δ_1	Vertical distortional deflection at the top corner of the box for unit antisymmetrical loading

γ	Poisson's ratio
σ_{DB}	Transverse distortional bending stress
σ_{DW}	Distortional warping stress
$\{\Delta\}$	Column matrix of displacements
β	Distortional parameter

CHAPTER 3

K_t	Stress concentration factor
L	Leg length of the weld
r,R	Toe radius of the weld

CHAPTER 4

a	Height of the specimen from horizontal axis of symmetry
b,d	Dimensions of the specimen shown in Fig. 4.2.1
ℓ_1, ℓ_2	Length of the specimen's elements
ℓ	Leg length of the weld
I, I_1, I_2, I_3	Second moment of inertia of the specimen's element
M_A, M_B, M_C	Bending moments at points A,B and C as shown in Fig. 4.22
M_A', M_B', M_{b-b}, M_E	Bending moment at points A', B' and E as shown in Fig. 4.28
N	Normal force
P	Applied load
Q	Shear stress
$R_{A'}$	Ratio of the nominal stress at the root of the weld to the nominal stress at the toe of the weld

R_M	Ratio of the bending moment at the root of the weld to the bending moment at the toe
s	Size of the weld throat
t	Plate thickness
w	Width of the specimen
I_{b-b}	Section modulus at b-b in Fig. 4.28
σ_N	Normal stress
σ_B, σ_{Bend}	Bending stress
σ_t	Tensile bending stress
σ_c	Compression bending stress
σ_B, σ_C	Stresses at points B and C as shown in Fig. 4.22
δ	Gap between two plates

CHAPTERS 5, 6 and 7

K_v	Coefficient of variation
n	Sample size (Number of results at each stress level)
N	Number of cycles to fatigue failure
logN	Transformation of N (Dependent variable)
P	Probability of failure
R	Correlation coefficient
S	Estimated standard deviation
S^2	Estimated variance
S_i^2	Estimated variance at each stress level
S_w^2	Combined (or pooled) variance within samples
t	t-distribution

F	F-distribution
χ^2	χ^2-distribution
x, X	Independent variable
σ_R, $\log\sigma_R$	Stress range (independent variable)
y, Y	Dependent variable
$\bar{y}$, $\overline{\log N}$	Estimate of population mean or sample mean
x_i, y_i	Each individual result
y_{ij}	jth value of the dependent variable in the ith sample
μ	True population mean
σ	True standard deviation
σ^2	True variance
γ	Number of degrees of freedom
σ_{max}, $\bar{\sigma}_{max}$	Maximum stress. (The highest algebraic value of the stress in the stress cycle*.)
σ_{min}, $\bar{\sigma}_{min}$	Minimum stress. (The lowest algebraic value of the stress in the stress cycle.)
σ_m, $\bar{\sigma}_m$	Mean stress. (The algebraic mean of the maximum and the minimum stress in one cycle: $\sigma_m = \frac{1}{2}(\sigma_{max} + \sigma_{min})$)
σ_s	Residual (or locked-in) welding stress
σ_y	Tensile yield stress

CHAPTER 8

a	Crack length
B_T, B_B, C	As defined in Chapter 2
L	Span length of the box girder
t	Thickness of the plate
δ_x	Deflection of the box corner in the x-direction

*Tensile stress being considered positive and compressive stress negative.

δ_{xc} Deflection of the box corner for the cracked box at the mid-span

δ_{xL} Local deflection for the uncracked box corresponding to the position of the crack end in the x-direction

δ_{xcL} Deflection of the box corner at the end of the crack in the x-direction

δ_{z} Vertical deflection of the uncracked box at the mid-span (in z-direction)

δ_{zc} Vertical deflection of the cracked box (in z direction) at the mid-span

δ_{zL} Local deflection for the uncracked box corresponding to the position of the crack end in the z-direction

δ_{zcL} Vertical deflection of the box corner at the end of the crack

σ_{DB} Transverse distortional bending stress at the mid-span of the uncracked box

σ_{DBC} Transverse distortional bending stresses at the end of the crack

σ_{DBL} Local transverse distortional bending stress for the uncracked box corresponding to the end of the crack

Analysis Method	Program Name	Computer time (seconds)	Computer Storage
FE	ICSAS	400	60K
BEF	BEF4 and ELASBM1	0.9	6K
Richmond	RD1SP	9	16K

TABLE 2.1: Comparison of computer time and storage for analysis of box shown in Fig. 2.7

N_B \ N_L	2	3	4	6	8
2	1.919	2.765	3.925	5.144	9.033
3	-	3.292	3.661	-	-
4	-	-	4.563	5.012	8.179
6	-	-	-	5.781	8.522
8	-	-	-	-	8.226

TABLE 2.2: Antisymmetrical loading (kN/m) on most critically loaded box for HA uniformly distributed loading

N_B \ N_L	2	3	4	6	8
2	234.629	370.05	481.777	691.782	1108.125
3	-	444.671	450.849	-	-
4	-	-	561.152	675.333	1006.705
6	-	-	-	780.671	1046.95
8	-	-	-	-	1011.882

TABLE 2.3: Antisymmetrical loading (kN) on most critically loaded box for HB loading

where N_L = number of lanes

N_B = number of boxes.

Box No.	Name	DoE ref.	Type
1	Fylde Bridge	4/1	3 cell rectangular multi cell
2	Irwell Valley Bridge	4/2	Trapezoidal multibox
3	Samlesbury Bridge	4/3	Rectangul ar multibox
4	Rosebank Bridge	4/7	Rectangular
5	Bidston Moss Viaduct	4/11a	Twin rectangular box
6	Porton Road Bridge	6/5	Rectangular
7	Red Lane Dyke	9/10	Single rectangular box
8	Lofthouse Interchange	9/11a	Trapezoidal multibox
9	Neath Bridge 15	10/3a	Rectangular
10	Taff River Bridge	10/4	Rectangular
11	Neath Bridge 4	10/7a	Trapezoidal
12	Coombe Lane Flyover	11/1	Rectangular multibox
13	Watford By-Pass	11/9	Rectangular multibox
14	Elstree Road Bridge	11/10	Rectangular
15	Kirkless Viaduct	14/1	Rectangular multibox
16	Blakelow Lane Bridge	14/3	Rectangular
17	Foxcover Lane Overbridge	14/11	Twin rectangular boxes
18	South Moor Accommodation Bridge	14/15	Trapezoidal
19	Hylton Bridge	14/23	Twin rectangular boxes
20	Wrey Bridge	15/1	Trapezoidal multibox
21	Monks Lane Bridge	15/2	Trapezoidal
22	Thomham East Bridge	15/4	Rectangular
23	Wardley Moss Bridge	15/6	Trapezoidal multibox
24	Station Road Bridge	16/15	Trapezoidal multibox
25	Roughetts Road Bridge	16/16	Trapezoidal multibox
26	Huntworth Viaduct	17/2	Twin rectangular boxes

TABLE I.1: List of practical box girder bridges used in parametric study

Bridge No.	βL span	βL_D panel	$I_c/4I_b$	r_β	r_s	ν	$\gamma = \frac{B_B}{B_T}$	$\lambda = \frac{C}{B_T}$	$\alpha = \frac{D_B}{D_T}$	$\nu = \frac{D_C}{D_T}$	λ/ν
1	8.55	0.95	1.00	1.00	0.98	0.060	1	1.71	.00940	.327	5.23
2	6.70	1.67	0.82	1.06	0.77	0.247	.667	.917	.248	.159	5.77
3	12.36	-	0.64	1.12	0.91	0.241	1	4.00	.203	.237	16.9
4	9.67	-	0.88	1.03	1.09	0.255	1	3.53	1.50	1.29	2.74
5	3.33	-	1.01	1.00	0.84	0.243	1	.566	.0105	.00101	560.
6	3.54	0.19	1.24	0.95	0.93	0.248	1	.755	.0232	.000670	1120.
7	8.26	0.25	1.10	0.98	0.85	0.251	1	.750	54.1	.0153	49.0
8	10.79	0.69	0.88	0.97	0.98	0.243	.545	1.09	.0509	.0285	38.2
9	6.48	-	1.13	0.97	0.94	0.250	1	1.25	.878	.000520	2385.
10	6.75	-	1.19	0.96	1.01	0.229	1	.824	.0506	.0242	34.0
11	7.47	-	1.12	0.97	0.92	0.238	.862	.552	.388	.269	2.05
12	4.85	0.56	0.75	1.08	0.79	0.230	1	1.61	.418	.0156	103.2
13	12.21	0.92	1.27	0.95	0.99	0.249	1	1.52	0.179	.00127	1197.
14	2.72	1.12	1.13	0.97	0.87	0.249	1	1.61	.0460	.00191	843.
15	8.12	-	0.91	1.03	0.83	0.202	1	1.33	.0410	.0284	46.8
17	5.78	1.35	0.80	1.06	0.81	0.156	1	1.29	.0401	.207	5.23
18	3.74	0.93	1.23	0.95	1.00	0.241	.924	.453	.0120	.00181	250.
19	8.26	-	0.88	1.03	0.79	0.230	1	.956	.179	.114	8.38
20	6.02	0.41	0.51	1.19	0.54	0.210	.364	.538	.0106	.000550	971.
21	8.12	0.24	0.91	1.03	0.83	0.202	.333	.528	.134	.0869	6.07
22	7.99	2.50	1.26	0.94	1.01	0.242	1	.650	.00360	.000450	1438.
23	3.27	-	1.25	0.94	0.91	0.213	.843	.243	.0523	.0233	10.4
26	7.02	-	0.77	1.07	0.75	0.225	1	.783	.0114	.00620	126.

TABLE I-2: Table of parameters for practical boxes (see Table I-1 for list of bridge numbers)

Investigator	$t/_r$	$L/_t$	K_t	
			At the toe	At weld root
Solakian	0.50	1.0	3.5	6.7
Solakian	0.50	1.0	4.7	6.9
Ros	0.67	0.75	3.1	5.3
Norris	1.0	0.75	3.6	7.6
Norris	1.0	1.0	2.5	6.1
Kenyon	1.0	1.0	3.5	3.5
Coker	1.0	1.0	2.2	2.0

Table 3.1: Stress concentration factors obtained in photoelastic studies of fillet-welded lap joints (3.20)

Plate thickness mm	(in)	Mean yield stress N/mm^2	($tonf/in^2$)	Mean UTS N/mm^2	($tonf/in^2$)	Elongation %	Reduction of area after fracture %	Note
12.00	(.472)	282.66	(18.355)	461.488	(29.772)	24.53	57.32	Used in specimens BEDFW, BESFW
12.70	(.50)	254.17	(16.504)	432.09	(28.057)	25.24	55.92	
12.70	(.50)	352.00	(22.857)	508.00	(32.90)	23.00	-	As supplied by steel manufacturer
12.70	(.50)	316.50	(20.552)	487.577	(31.656)	22.77	57.329	Tensile specimen at Imperial College

(a) Mechanical properties of the parent material

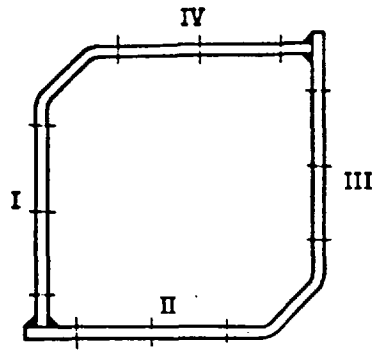
Yield stress N/mm^2	($tonf/in^2$)	UTS N/mm^2	($tonf/in^2$)	Elongation %	Reduction of area after fracture %	Note
414.66	(26.926)	503.315	(32.685)	26.664	48.730	

(b) Mechanical properties of the weld metal

TABLE 6.1 Mechanical properties of the parent material and weld metal

Plate Thickness		Elements' Composition (%)						Note
mm	(in)	C	Mn	Si	S	P	Cu	
12.00	(.472)	0.195	0.81	0.07	0.03	0.008	0.2	As supplied by steel manufacturer
12.70	(.50)	0.21 0.23	0.79 0.79	- 0.01	0.024 0.022	0.011 .008	- .035	

TABLE 6.2 Chemical analysis of the parent material



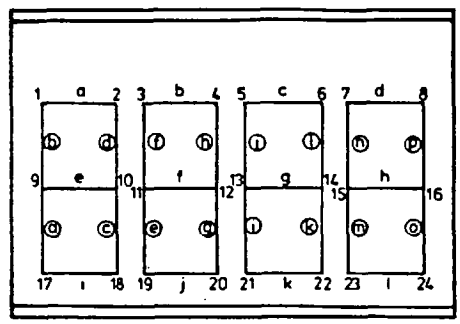


Table 6·3 Residual welding stress in N/mm² for specimen series BEDFW after completion of the welding.

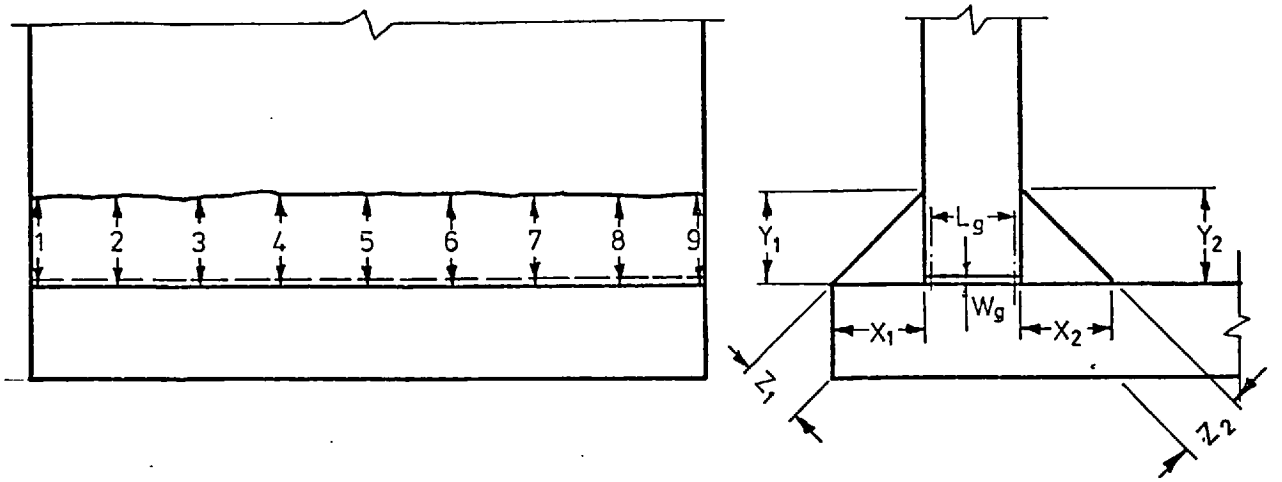
	PART I		PART II		PART III		PART IV	
	outside	inside	outside	inside	outside	inside	outside	inside
a	0	5·219	-134·503	-62·532	0	- 31·266	-145·908	- 112·093
b	-20·844	7·813	-184·987	-158·955	-52·11	- 23·453	- 161·549	- 153·535
c	- 13·027	10·422	-179·783	-153·721	- 23·453	10·422	-195·409	-119·861
d	0	2·609	- 96·407	- 119·861	10·422	0	-125·064	- 114·642
e	-33·86	5·219	- 33·875	- 5·219	- 31·266	- 36·469	- 20·844	- 31·266
f	- 80·767	44·282	- 85·985	- 41·688	- 93·798	- 62·532	- 78·173	-54·719
g	- 72·954	46·907	- 78·173	-65·126	- 99·001	- 41·688	- 88·58	-36·469
h	-20·844	10·422	- 2·609	-33·875	- 26·047	-20·844	- 18·235	-33·875
i	- 134·487	- 16·469	- 5·219	-2·609	-179·783	-132·877	- 80·767	-26·047
j	- 151·111	- 122·455	-20·844	-15·641	-153·721	-132·877	- 46·907	-33·875
k	- 171·955	-117·236	- 10·422	- 18·235	-213·659	-145·908	- 33·875	0
l	- 184·99	- 99·001	- 10·422	- 7·813	-164·143	-106·814	0	- 7·813
ⓐ	- 39·079	44·297	- 18·235	135·486	15·641	75·548	- 79·783	114·642
ⓑ	- 10·422	91·189	-17·813	78·173	-26·047	104·22	- 15·641	78·173
ⓒ	- 28·564	46·907	- 75·548	65·126	-52·11	78·173	- 72·954	75·548
ⓓ	-62·532	52·11	- 47·447	62·532	- 80·767	62·532	-70·345	67·751
ⓔ	-62·532	78·173	- 91·189	78·173	- 88·579	101·611	- 57·406	57·406
ⓕ	-72·954	83·374	- 75·548	85·985	- 93·798	75·548	- 75·548	114·642
ⓖ	-65·125	127·673	- 88·579	91·189	- 80·767	130·267	-101·626	80·767
ⓗ	-83·376	96·392	- 83·376	145·908	-104·22	91·189	- 91·189	122·455
ⓘ	- 72·954	140·689	- 93·798	93·798	- 83·376	140·689	- 93·798	91·189
ⓙ	- 75·548	88·579	- 83·376	99·017	-106·814	106·814	- 65·126	130·267
ⓚ	- 91·189	114·642	-106·814	91·189	-140·504	140·689	- 76·814	101·626
ⓛ	-106·814	80·767	- 119·861	122·455	-117·236	65·126	-101·626	122·455
ⓜ	- 85·97	104·22	- 114·642	88·579	- 112·033	106·814	-104·22	96·39
ⓝ	-122·455	93·798	-114·642	106·814	- 114·642	93·798	-106·814	88·579
ⓞ	- 70·345	135·486	- 44·282	182·346	- 36·469	156·33	- 59·923	112·033
ⓟ	- 59·923	153·721	- 83·376	175·565	- 62·532	148·517	- 72·954	161·549
*Mean	- 64·47	99·02	- 79 123	103·235	76·185	116 265	- 80 81	91 2

* The calculated mean is based on the values of stresses near weld which are given in the shaded rows

Specimen Number	Corner Nos	σ_{range} N/mm^2	σ_{range} (tonf/in^2)	σ_{mean} N/mm^2	σ_{mean} (tonf/in^2)	N_1 1st Visual Crack $\times 10^6$	N_2 Failure $\times 10^6$	Notes
BEDFW-1	3 4	169.30 169.30	(11.00) (11.00)	154.00 154.00	(10.00) (10.00)	- 0.897	- 1.235	
BEDFW-2	3 4	169.30 169.30	(11.00) (11.00)	154.00 156.46	(10.00) (10.16)	- 1.065	- 1.139	
BEDFW-3	3 4	174.50 169.00	(11.30) (10.95)	156.50 154.50	(10.15) (10.02)	1.2375 1.313	1.313 -	crack along the toe
BEDFW-4	3 4	169.30 169.30	(11.00) (11.00)	154.00 154.00	(10.00) (10.00)	1.486 1.767	1.767 -	crack* = 0.5 mm
BEDFW-5	3 4	169.40 169.50	(11.04) (11.05)	154.00 154.00	(10.00) (10.00)	1.650 1.890	1.890 -	crack* = 2 mm
BEDFW-6	3 4	169.30 169.30	(11.00) (11.00)	84.65 85.65	(5.50) (5.56)	2.179 -	2.7505 -	
BEDFW-7	3 4	145.00 138.15	(9.41) (8.96)	139.88 138.02	(9.00) (8.96)	1.1895 -	1.300 -	corner sides are not polished
BEDFW-8	3 4	138.60 138.60	(9.00) (9.00)	140.14 138.60	(9.10) (9.00)	1.554 -	1.631 -	corner sides are not polished
BEDFW-9	3 4	138.60 137.67	(9.00) (8.94)	138.6 138.6	(9.00) (9.00)	1.682 1.805	1.805 -	57 mm crack along the toe
BEDFW-10	3 4	140.14 138.60	(9.10) (9.00)	139.38 138.60	(9.05) (9.00)	1.695 -	1.765 -	
BEDFW-11	3 4	141.37 138.60	(9.18) (9.00)	138.60 138.60	(9.00) (9.00)	2.546 2.509	- 2.546	crack* = 0.5 mm
BEDFW-12	3 4	138.60 138.60	(9.00) (9.00)	138.60 138.60	(9.00) (9.00)	3.467 -	4.058 -	
BEDFW-13	3 4	107.00 107.80	(6.91) (7.01)	120.74 123.12	(7.74) (7.99)	3.067 2.967	3.164 -	crack along the toe 50 mm
BEDFW-14	3 4	106.26 107.00	(6.98) (7.00)	117.19 117.19	(8.00) (8.00)	3.038 3.648	4.278 -	crack along the toe + 1 mm side
BEDFW-15	3 4	107.00 109.95	(7.00) (7.14)	123.20 123.20	(8.00) (8.00)	- 3.872	- 3.995	
BEDFW-16	3 4	103.33 107.00	(6.71) (7.00)	117.19 123.20	(7.61) (8.00)	4.923 4.453	- 6.718	
BEDFW-17	3 4	107.00 107.00	(7.00) (7.00)	117.19 117.19	(8.00) (8.00)	5.624 -	6.912 -	
BEDFW-18	3 4	78.00 77.00	(5.05) (5.00)	104.01 107.75	(6.75) (6.99)	16.180↗ 16.180↗	- -	no visual crack
BEDFW-19	3 4	78.00 78.50	(5.05) (5.10)	104.33 104.72	(6.77) (6.80)	14.527↗ 14.527↗	- -	no visual crack

*Final depth of the crack as seen at the side of the specimen

TABLE 6.4 Summary of Data for Test Series BEDFW

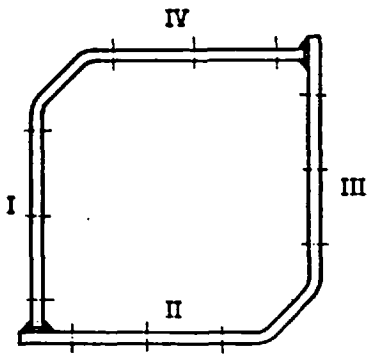


No.	X_1	Y_1	Z_1	W_g	L_g	X_2	Y_2	Z_2	Note
1	11.5	9.5	8.3	1.1	10.0	11.5	9.0	7.9	Values of Z, L_g and W_g at these points were not possible to be measured
2	11.5	9.6	-	-	-	11.5	9.5	-	
3	11.5	9.75	-	-	-	11.5	9.0	-	
4	11.5	9.75	-	-	-	11.5	10.0	-	
5	11.3	10.0	-	-	-	12.0	10.0	-	
6	11.3	9.5	-	-	-	12.0	10.0	-	
7	12.0	9.5	-	-	-	11.5	10.0	-	
8	12.0	10.5	-	-	-	11.5	10.0	-	
9	11.5	10.25	8.6	0.9	10.5	11.75	10.0	8.5	

TABLE 6.5a: Measured dimensions of the specimen BEDFG-9 at the points shown on the diagram (side with strain gauge No. 3)

No.	X_1	Y_1	Z_1	W_g	L_g	X_2	Y_2	Z_2	Note
1	12.0	11.0	7.0	0.84	10.0	9.7	12.0	9.0	Values of
2	12.0	11.0	-	-	-	9.5	12.0	-	Z, L_g and
3	12.0	12.2	-	-	-	9.2	12.0	-	W_g at these
4	12.0	12.2	-	-	-	9.5	11.4	-	points
5	12.0	12.2	-	-	-	10.0	11.0	-	were not
6	12.2	11.0	-	-	-	10.0	11.0	-	possible
7	12.2	12.8	-	-	-	10.0	11.5	-	to be measured
8	12.2	12.5	-	-	-	10.0	11.5	-	
9	12.2	12.0	7.5	1.1	11.0	10.0	11.0	8.5	

TABLE 6.5b: Measured dimension of the weld in specimen BEDFG-9 at the points shown on the diagram (side with strain gauge No. 4)



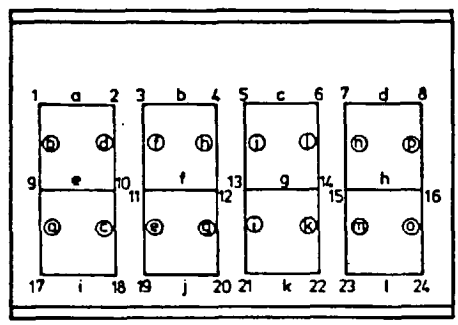
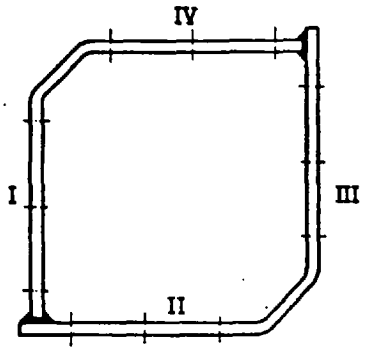


Table 6·6 Residual welding stress in N/mm² for specimen series BEDFG after completion of the welding.

	PART I		PART II		PART III		PART IV	
	outside	inside	outside	inside	outside	inside	outside	inside
a	-15·641	0	-177·174	-62·532	10·422	-15·641	-208·44	-114·642
b	-10·422	-5·219	-182·346	-145·908	-15·641	20·998	-104·22	-187·565
c	-10·422	-5·219	-156·33	-62·532	-25·219	-26·047	-192·799	-125·064
d	-26·047	-46·907	-151·111	-52·11	-41·688	-15·219	901·279	-15·641
e	-67·751	-26·047	-20·844	-15·641	-26·047	-5·219	-46·907	20·844
f	-93·789	-62·532	-62·532	-31·266	-78·173	-52·11	-151·111	-62·532
g	-99·017	-83·376	-57·406	-46·907	-72·954	-93·798	-62·532	-46·907
h	-15·641	-36·469	-10·422	-36·469	41·688	-46·907	10·422	-10·422
i	118·877	99·001	5·219	26·047	145·908	130·267	15·641	41·688
j	124·081	192·799	0	0	151·111	99·017	78·173	-15·641
k	198·003	145·908	5·219	0	161·549	145·908	46·907	-10·422
l	130·267	36·469	0	0	130·267	99·017	26·047	5·219
ⓐ	-52·11	156·33	-62·532	156·33	-72·954	114·642	-46·907	166·752
ⓑ	-57·406	151·111	-62·532	166·752	-52·11	135·486	-20·844	135·486
ⓒ	-88·579	99·001	-83·376	114·642	-109·423	36·469	-93·798	67·751
ⓓ	-187·565	93·798	-99·017	119·861	-83·376	41·688	-99·017	-130·267
ⓔ	-93·798	67·751	-104·22	83·375	-38·175	136·469	-109·423	72·954
ⓕ	-165·752	78·173	-109·423	114·642	-93·798	141·688	-88·579	125·064
ⓖ	-140·689	156·33	-109·423	83·375	62·532	78·173	-88·579	114·642
ⓗ	-130·267	104·22	67·751	109·423	88·579	62·532	-99·017	125·064
ⓘ	-135·486	156·33	-83·376	78·173	-26·047	62·532	-83·376	57·406
ⓙ	-135·486	104·22	-88·579	119·861	-83·376	78·173	-109·423	104·22
ⓚ	-88·579	145·908	93·798	62·532	67·751	26·047	-74·22	-83·376
ⓛ	-114·642	78·173	72·954	78·173	88·579	52·11	-114·642	-46·907
ⓜ	-109·439	99·001	-52·11	78·173	-57·406	5·219	-99·016	88·579
ⓝ	-99·001	99·001	-57·406	36·469	-62·532	46·907	-78·173	78·173
ⓞ	-31·266	171·955	-20·844	119·861	10·422	88·579	-31·266	161·549
ⓟ	62·532	182 346	-36·469	83·375	26·047	119·861	57·406	166·752
Mean*	-92·49	131·59	-76·21	97 06	55·588	56·01	-82·07	102·3

* see Table 6·3



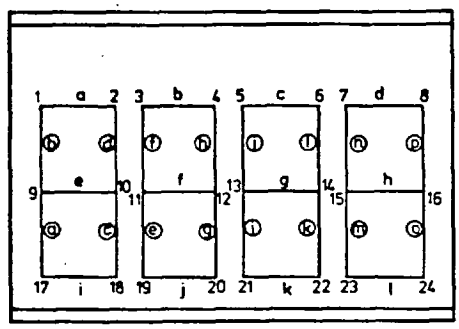


Table 6·7 Residual welding stress in N/mm² of specimen series BEDFG before testing.

	PART I		PART II		PART III		PART IV	
	outside	inside	outside	inside	outside	inside	outside	inside
a	-26·047	- 5·219	-93·798	-26·047	-5·219	41·688	-62·532	-41·688
b	-41·688	- 5·219	-109·439	-114·642	-46·907	15·641	57·406	-99·017
c	- 5·219	-36·469	-46·876	- 10·422	-57· 406	31·266	41·688	-41· 688
d	26·047	- 5·219	- 67·751	- 67·751	- 5·219	36·469	31·266	-31·266
e	-171·955	- 57· 406	-119·861	- 26·047	- 52·11	26·047	88·579	-20·844
f	- 26·047	-15·641	36·469	-41·688	-99·001	26·047	5·219	- 20·844
g	- 52·11	-20·844	- 57·406	- 41·688	- 10·422	-15·641	119·861	-41·688
h	10·422	-41·688	0	- 41·688	62·532	-36·469	-10·422	- 20·844
i	25·064	67·751	- 31·266	15·641	88·579	72·954	36·469	140·689
j	93·798	67·751	- 67·751	-41·688	104·22	67·751	52·11	- 26·047
k	57·406	20·844	- 5·219	- 5·219	119·861	57·406	-15·641	- 52·11
l	41·688	31·266	- 26·047	-15·641	88·579	31·266	5·219	-10·422
ⓐ	-88·579	135·486	-104·22	41·688	-114·642	57·406	- 129·284	140·689
ⓑ	- 80·267	93·798	- 88·579	70·422	-156·33	140·689	0	70·422
ⓒ	- 70·422	10·422	- 67·751	46·907	- 20·844	15·219	- 52·11	83·376
ⓓ	109·439	85·219	- 62·532	67·751	- 72·954	67·751	130·267	15·641
ⓔ	-67·751	155· 331	-78·173	130·267	-52·11	62·532	-114·642	161·549
ⓕ	- 77·174	78·173	-119·861	176·175	- 31·266	76·75	- 72·954	166·752
ⓖ	- 57·406	192·799	20·844	15·641	- 41·688	15·641	- 31· 266	31·266
ⓗ	- 41·688	151· 111	15·641	- 151·111	- 36·469	154·348	-10·422	36·469
ⓘ	- 99·001	46·907	-93·798	151·111	-125·064	67·751	- 62·532	134·487
ⓙ	- 56·33	51·111	- 125·064	- 67·751	- 26·047	130·267	125·064	41·688
ⓚ	- 45·219	130· 267	- 20·844	- 72·954	0	151·111	- 20·844	140·689
ⓛ	- 31·266	187·565	- 31·266	55· 331	- 36·469	78·173	5·991	166·752
ⓜ	- 79·861	134·487	- 78·173	109·423	- 46·907	186·597	- 104·22	114·642
ⓝ	-104·22	139·706	-52·11	46·907	- 57·406	227·302	- 88·579	125·064
ⓞ	- 56·469	135·486	20·844	26·047	- 62·532	78·173	-104·22	62·532
ⓟ	- 20·844	117·879	- 46·907	83·376	- 57·406	171·955	- 93·798	78·173
▪ Mean	- 70·58	115·36	- 63·08	74·25	- 57·19	79·903	- 77·39	121·125

▪ see Table 6·3

Specimen Number	Corner Nos	σ_{range} N/mm^2	σ_{range} (tonf/in^2)	σ_{mean} N/mm^2	σ_{mean} (tonf/in^2)	N_1 1st Visual Crack $\times 10^6$	N_2 Failure $\times 10^6$	Notes
BEDFG-1	3 4	171.71 169.40	(11.15) (11.00)	155.54 154.00	(10.01) (10.00)	0.535 -	0.609 -	
BEDFG-2	3 4	169.30 170.94	(11.00) (11.10)	154.00 155.54	(10.00) (10.10)	- 0.685	- 0.795	
BEDFG-3	3 4	169.30 169.30	(11.00) (11.00)	84.65 84.65	(5.50) (5.50)	0.764 0.942	1.211	compression crack
BEDFG-4	3 4	169.30 169.30	(11.00) (11.00)	154.00 154.00	(10.00) (10.00)	0.940 0.884	- -	crack along the toe = .5 mm side crack
BEDFG-5	3 4	166.17 169.30	(10.79) (11.00)	151.38 154.00	(9.83) (10.00)	1.195 1.320	1.462 -	crack along the toe
BEDFG-6	3 4	138.60 138.60	(9.00) (9.00)	138.60 138.60)	(9.00) (9.00)	- 0.881	- 1.052	
BEDFG-7	3 4	137.67 138.60	(8.94) (9.00)	135.67 138.6	(8.81) (9.00)	- 1.250	- 1.347	width of the specimen = 73 mm
BEDFG-8	3 4	138.60 138.60	(9.00) (9.00)	138.60 138.6	(9.00) (9.00)	1.463 -	1.663 -	
BEDFG-9	3 4	138.60 138.60	(9.00) (9.00)	138.60 138.60	(9.00) (9.00)	1.484 1.884	1.978	crack along the toe
BEDFG-10	3 4	138.60 138.60	(9.00) (9.00)	138.60 138.60	(9.00) (9.00)	1.754 1.690	- 1.906	45 mm crack along the toe
BEDFG-11	3 4	138.60 138.60	(9.00) (9.00)	138.60 138.6	(9.00) (9.00)	2.213 -	- -	
BEDFG-12	3 4	111.04 107.80	(7.21) (7.00)	125.97 123.2	(8.18) (8.00)	- 1.85	- 2.135	
BEDFG-13	3 4	107.00 107.00	(7.00) (7.00)	123.20 123.20	(8.00) (8.00)	2.65 -	3.102 -	
BEDFG-14	3 4	107.00 107.00	(7.00) (7.00)	123.20 123.20	(8.00) (8.00)	3.662 3.001	3.853	= 0.5 mm crack on the side
BEDFG-15	3 4	107.80 111.65	(7.00) (7.25)	123.20 125.51	(8.00) (8.15)	4.0725 -	4.8485 -	
BEDFG-16	3 4	107.00 107.00	(7.00) (7.00)	123.20 123.20	(8.00) (8.00)	3.301 -	4.553	crack along the toe = .5 mm side
BEDFG-17	3 4	86.24 77.00	(5.60) (5.00)	115.00 107.00	(7.50) (7.00)	10.19 ↙ 10.19 ↗	- -	no visual crack

TABLE 6.8 Summary of Data for Test Series BEDFG

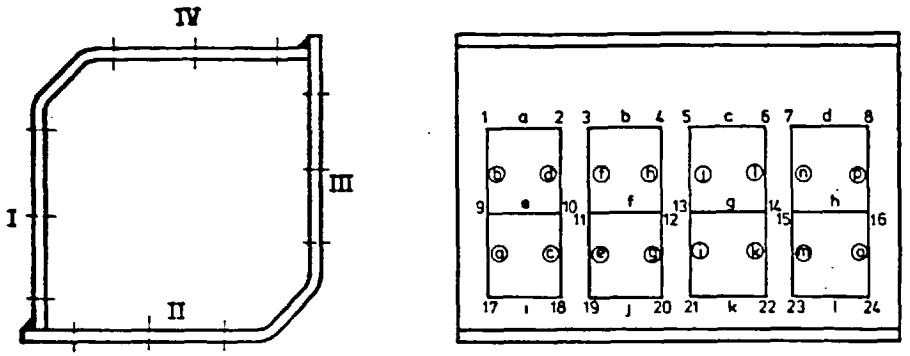


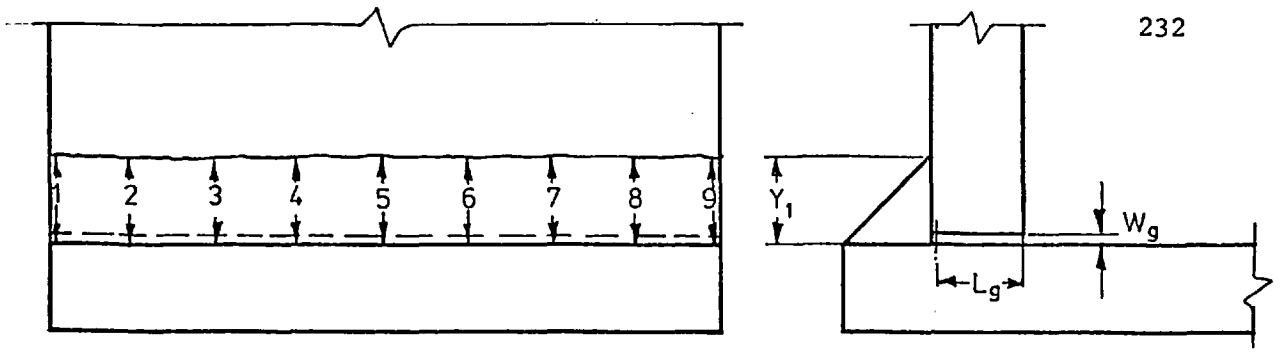
Table 6·9 Measured residual welding stress in N/mm² for specimen series BESFW after completion of the welding.

	PART I		PART II		PART III		PART IV	
	outside	inside	outside	inside	outside	inside	outside	inside
a	-22·453	-5·431	-53·48	-11·525	-28·657	2·609	-73·529	-9·117
b	-28·657	-18·944	-70·622	-60·934	-24·312	0	-68·293	-60·934
c	-19·325	-9·117	-88·951	-70·622	-28·657	9·117	-53·596	-58·042
d	-23·031	-18·944	-28·657	-66·844	-19·468	11·525	-88·951	-38·611
e	-72·954	-24·312	-45·434	-15·38	-38·611	30·488	-53·48	-28·657
f	-56·604	-14·151	-60·934	-30·488	-60·934	28·657	-48·134	-19·325
g	-62·173	-7·848	-48·438	-28·657	-43·021	15·38	-60·934	-31·092
h	-39·079	-19·325	-28·657	-11·525	-29·314	28·657	-43·021	-22·059
i	-66·844	-34·673	-12·307	-6·283	-88·951	45·828	-22·059	-5·431
j	-83·672	-45·828	-15·38	-15·38	-62·173	15·38	-24·312	-15·38
k	-98·293	-38·611	-9·117	-2·609	-70·379	83·672	-38·783	-11·525
l	-61·982	-19·468	-11·525	-11·525	-78·58	0	-19·325	-7·97
ⓐ	64·917	-67·372	70·379	-30·488	92·524	-45·828	68·293	-48·657
ⓑ	53·246	-28·657	88·951	-45·434	67·372	-30·488	73·672	-52·059
ⓒ	45·828	-80·767	40·15	-45·434	53·48	-38·763	67·372	-39·325
ⓓ	29·314	-59·053	62·173	-53·48	37·891	-19·325	40·15	-41·525
ⓔ	48·434	-45·937	31·092	-29·314	43·021	-5·431	45·434	-38·763
ⓕ	28·657	-69·386	31·092	-40·15	34·673	-11·525	50·98	-37·891
●	40·15	-83·173	24·312	-31·092	38·783	-15·38	38·783	-41·238
ⓗ	28·657	-38·763	22·059	-22·059	24·312	-5·431	15·38	-50·203
ⓘ	38·763	-45·828	15·38	-19·468	22·059	-15·38	29·314	-19·117
ⓙ	23·14	-38·611	56·604	-48·438	24·312	-28·657	15·38	-28·657
ⓚ	30·488	-53·48	41·572	-38·611	31·092	-19·468	0	-28·657
ⓛ	24·312	-60·934	28·657	-19·468	15·38	-38·763	15·38	50·203
ⓜ	19·468	-49·537	15·38	-18·944	48·438	-45·937	28·657	-45·937
ⓝ	15·38	-29·314	38·763	-45·828	22·059	-38·763	45·937	-38·763
●	35·032	-67·372	45·937	-40·15	38·783	-19·468	60·934	-19·325
ⓟ	37·479	-19·117	29·314	-4·349	53·48	-15·38	58·293	-50·203
Mean*	45·385	-61·68	35·52	-31·68	46·022	-25·71	42·35	-34·95

* see Table 6·3

Specimen Number	Corner Nos	σ_{range} N/mm²	σ_{range} (tonf/in²)	σ_{mean} N/mm²	σ_{mean} (tonf/in²)	N_1 1st Visual Crack $\times 10^6$	N_2 Failure $\times 10^6$	Notes
BESFW-1	3 4	169.5 169.0	(11.01) (11.0)	154.0 154.0	(10.0) (10.0)	0.161 0.19	0.21 -	
BESFW-2	3 4	169.3 169.3	(11.00) (11.00)	154.00 154.00	(10.00) (10.00)	0.205 0.230	.256 -	= 3 mm crack
BESFW-3	3 4	169.3 170.9	(11.0) (11.11)	154.0 155.5	(10.0) (10.1)	0.241 0.261	0.299	
BESFW-4	3 4	169.3 169.3	(11.00) (11.00)	154.00 154.00	(10.00) (10.00)	0.286 0.321	0.341 -	= 2 mm crack
BESFW-5	3 4	169.3 169.3	(11.0) (11.0)	154.0 154.0	(10.0) (10.0)	0.4315 0.3525	- 0.446	crack along the toe
BESFW-6	3 4	107.8 107.8	(7.0) (7.0)	123.2 123.2	(8.0) (8.0)	0.668 0.566	- 0.679	1 mm crack
BESFW-7	3 4	107.8 106.26	(7.0) (6.9)	123.2 126.28	(8.0) (8.2)	0.7115 0.795	0.883 -	= 2 mm crack
BESFW-8	3 4	107.8 107.8	(7.0) (7.0)	123.2 123.2	(8.0) (8.0)	0.729 0.7891	0.919 -	complete failure = 8 mm crack depth
BESFW-9	3 4	110.11 107.8	(7.15) (7.0)	125.05 123.2	(8.12) (8.0)	0.916 1.078	1.158	
BESFW-10	3 4	107.8 107.8	(7.0) (7.0)	123.2 123.2	(8.0) (8.0)	1.045 0.989	1.269	
BESFW-11	3 4	107.8 107.8	(7.0) (7.0)	53.9 53.9	(3.5) (3.5)	- 1.228	- 1.411	σ_{min} = 0.0
BESFW-12	3 4	107.8 107.8	(7.0) (7.0)	123.2 123.2	(8.0) (8.0)	1.749 -	2.1625 -	1st. visual crack = 6 mm crack
BESFW-13	3 4	77.0 77.0	(5.0) (5.0)	110.8 107.8	(7.2) (7.0)	- 1.494	- 1.639	
BESFW-14	3 4	79.156 77.0	(5.14) (5.00)	110.88 107.80	(7.20) (7.0)	1.674 -	2.164 -	
BESFW-15	3 4	77.0 77.0	(5.0) (5.0)	107.8 107.8	(7.0) (7.0)	- 1.994	- 2.633	crack along the toe
BESFW-16	3 4	77.0 77.0	(5.00) (5.00)	107.80 107.80	(7.00) (7.00)	- 2.35	- 2.91	crack along the toe
BESFW-17	3 4	78.6 77.0	(5.13) (5.0)	107.8 107.8	(7.0) (7.0)	2.943 2.432	- -	crack at toe = 2 mm side crack
BESFW-18	3 4	77.0 77.0	(5.00) (5.00)	107.80 107.80	(7.00) (7.00)	3.41 3.92	4.131 -	= 4 mm crack
BESFW-19	3 4	77.0 77.0	(5.0) (5.0)	107.8 107.8	(7.0) (7.0)	- 4.659	- 5.395	

TABLE 6.10 Summary of Data for Test Series BESFW



No.	$\bar{y}$ mm	$\bar{W}_g$ mm	$\bar{L}_g$ mm	Note
1	11.5	1.09	10.3	
2	12.0	.97	10.25	
3	10.25	.88	9.27	
4	11.00	.92	10.75	
5	10.5	1.35	8.25	
6	11.75	1.22	10.50	
7	11.15	1.21	11.25	BESFG-5
8	11.50	1.29	12.60	BESFG-12
9	12.00	1.50	10.50	
10	10.5	1.07	10.65	
11	9.85	1.18	9.75	
12	12.25	1.12	10.00	
13	12.50	1.16	10.13	
14	11.1	1.05	11.20	BESFG-5
15	10.75	1.40	10.25	
16	11.25	1.08	10.00	
17	10.75	1.11	11.30	
18	11.50	1.50	12.50	
19	10.75	0.99	11.00	
20	10.25	1.12	10.75	
21	11.00	0.70	8.92	
22	10.75	0.58	9.5	
23	11.50	0.57	10.00	
24	11.50	0.49	10.00	
25	12.50	0.60	11.00	
26	11.00	0.60	-	
27	11.00	0.46	-	
28	11.50	1.06	-	
Σ	313.85	28.35	265.52	

$\bar{\bar{y}}_1 = 11.21$ mm

$s^2_{y_1} = .45$

$s_{y_1} = .67$ mm

$C_{vy_1} = .06$

$\bar{\bar{W}}_g = 1.01$ mm

$s^2_{wg} = .093$

$s_{wg} = .305$

$C_{vwg} = .302$

$\bar{\bar{L}}_g = 10.5$ mm

$s^2_{Lg} = .268$

$s_{Lg} = .517$

$C_v = .049$

$$\bar{y}_1 = \frac{\sum_{i=1}^{9} y_i}{9} \quad ; \quad \bar{W}_g = \frac{\sum_{i=1}^{9} W_{g_i}}{9} \quad ; \quad \bar{L}_g = \frac{\sum_{i=1}^{9} L_{g_i}}{9}$$

TABLE 6.11: Summary of the measured dimensions of the test series BESFG

Specimen No.	SG No. 1	SG No. 2	SG No. 3	SG No. 4
BESFG-18	-8.78 (-0.57*)	-9.69 (-0.63)	+11.63 (+0.75)	+14.53 (+0.943)
BESFG-19	-13.95 (-0.91)	-13.39 (-0.87)	+20.32 (+1.32)	+24.64 (+1.6)
Mean	-11.36 (-0.74)	-11.54 (-0.75)	+15.98 (+1.04)	+19.58 (+1.27)

TABLE 6.12: Results of the measured locked-in stresses in N/mm^2 for specimen series BESFG

*Numbers in $tonf/in^2$

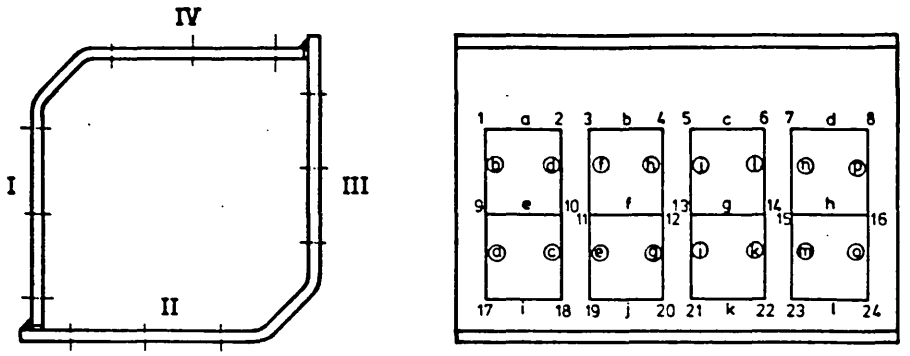
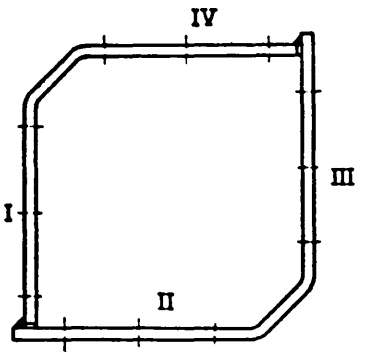


Table 6·13 Residual welding stress in N/mm² for specimen series BESFG after completion of the welding.

	PART I		PART II		PART III		PART IV	
	outside	inside	outside	inside	outside	inside	outside	inside
a	-18·235	- 2·609	-75·548	-15·641	-26·047	-5·219	-109·439	18·235
b	-23·453	-13·031	-85·97	-72·954	-18·235	7·828	-125·064	-85·97
c	-15·641	-2·609	-106·814	-65·126	-20·844	5·219	-104·22	-70·345
d	-10·422	13·031	-62·532	-70·345	-15·641	7·828	-88·579	39·079
e	-65·126	-18·235	-31·266	0	-36·469	23·453	-46·907	20·844
f	-49·516	-13·031	-52·11	-26·047	-57·406	-33·875	-46·907	-18·235
g	-57·406	-2·609	-41·688	-20·844	-57·11	-18·234	-46·907	-13·031
h	-31·266	-26·047	-18·235	-7·828	-31·266	7·828	-36·469	-23·453
i	-88·579	-44·282	-15·219	-2·609	-40·689	-18·235	-28·657	15·641
j	-109·439	-67·751	-17·828	-2·609	-104·22	-13·031	0	-2·609
k	-114·642	-52·11	-15·641	0	-122·455	-83·376	-15·641	-26·047
l	-78·173	-20·844	-13·031	-7·828	-106·814	-13·031	-13·031	-7·828
ⓐ	70·345	-46·907	46·907	0	72·954	-31·266	27·751	-15·641
ⓑ	46·907	-13·031	59·923	-15·641	59·923	-5·219	46·392	-26·047
ⓒ	15·641	-62·56	23·453	-23·453	41·688	-36·469	26·047	-36·469
ⓓ	23·453	-46·907	36·469	-20·844	10·422	-15·641	25·641	-57·406
ⓔ	2·609	-18·235	5·219	-13·031	31·266	-12·609	10·422	-52·11
ⓕ	5·219	-57·719	15·641	-15·641	18·235	-7·828	15·641	-41·688
ⓖ	26·047	-54·719	10·422	-15·641	18·235	7·828	18·235	-46·907
ⓗ	18·235	-28·826	10·422	-20·844	10·422	-7·828	26·047	-10·422
ⓘ	13·031	-23·453	7·828	-15·641	13·031	-2·609	15·641	-41·688
ⓙ	10·422	-39·079	20·844	-23·453	2·609	-13·031	28·657	-7·828
ⓚ	10·422	-39·079	13·031	-7·828	15·641	-10·422	18·235	-36·469
ⓛ	0	-46·907	18·235	-7·828	10·422	-26·047	13·031	-28·657
ⓜ	15·641	-46·907	10·422	-13·031	26·047	-20·844	26·047	-41·688
ⓝ	18·235	-33·875	36·469	0	15·641	-23·453	23·453	-46·907
ⓞ	80·767	-7·813	44·282	-31·266	36·469	0	85·985	20·844
ⓟ	44·282	-13·031	31·266	-7·828	41·688	-10·422	93·798	31·266
▪ Mean	29·312	-37 46	20·195	-14·98	31·916	-15·28	28 55	-36·47

▪ see Table 6·3



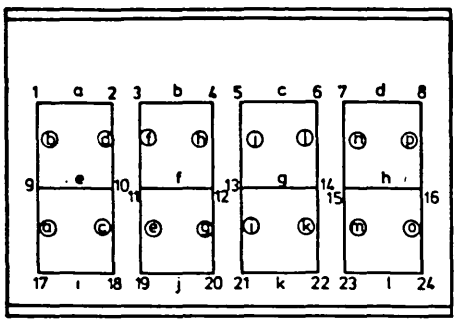


Table 6·14 Residual welding stress in N/mm^2 for specimen series BESFG before testing.

	PART I		PART II		PART III		PART IV	
	outside	inside	outside	inside	outside	inside	outside	inside
a	- 49·516	54·719	- 44·282	- 2·609	-26·047	13·031	20·844	41·688
b	- 23·453	-23·453	2·609	- 41·688	- 54·719	59·923	57·406	- 5·219
c	- 33·875	- 5·219	- 13·031	- 55·755	- 41·688	2·609	67·751	2·609
d	- 15·641	- 7·828	- 5·219	- 23·453	231·893	33·875	15·641	49·516
e	- 7·828	- 7·828	57·406	- 44·282	46·907	39·079	- 26·047	2·609
f	- 36·469	-23·453	- 15·641	0	5·219	18·235	0	- 31·266
g	- 36·469	- 10·422	- 41·688	-53·409	- 31·266	23·453	10·422	234·534
h	- 26·047	- 7·828	- 18·235	44·282	0	23·453	10·422	10·422
i	- 62·532	- 28·657	- 16·482	28·657	- 52·11	23·453	- 52·11	234·534
j	- 70·345	- 46·907	- 2·609	33·875	- 36·469	- 13·031	- 41·688	36·469
k	- 140·689	23·453	- 26·047	- 48·704	- 18·23	- 39·079	135·486	57·406
l	- 41·688	23·453	23·453	23·453	35·234	7·828	26·047	41·688
ⓐ	23·393	10·395	26·047	15·641	36·469	- 13·031	0	- 41·688
ⓑ	25·979	46·77	23·452	5·219	39·079	- 41·688	- 33·875	- 26·047
ⓒ	10·395	15·58	70·345	44·282	33·875	- 85·346	- 5·219	- 10·422
ⓓ	44·182	12·99	- 36·469	- 31·266	57·406	- 2·609	- 20·844	10·422
ⓔ	18·203	7·793	20·844	- 10·422	15·641	10·422	- 67·751	- 32·238
ⓕ	36·39	31·185	39·079	0	18·235	13·031	- 15·641	70·956
ⓖ	36·375	12·99	31·266	- 10·422	23·453	15·641	33·875	- 66·752
ⓗ	59·783	18·25	13·031	15·641	15·641	26·047	- 26·047	25·064
ⓘ	12·709	2·609	13·031	- 31·266	- 23·453	- 13·031	- 57·406	10·422
ⓙ	62·37	7·81	31·266	75·548	20·844	- 2·609	- 5·219	7·828
ⓚ	0	36·344	- 23·453	2·609	- 2·609	5·219	- 15·641	10·422
ⓛ	46·785	10·395	2·609	- 18·23	20·844	- 15·641	- 2·609	13·031
ⓜ	0	20·79	- 46·907	13·031	- 5·219	15·641	49·516	- 44·282
ⓝ	20·79	80·55	39·079	10·422	83·376	7·828	- 7·828	- 13·031
ⓞ	12·99	2·609	48·517	13·031	- 18·235	0	13·031	- 18·235
ⓟ	2·609	64·97	15·641	13·031	- 5·219	- 10·422	20·844	- 36·469
▪ Mean	14·24	13 64	35·05	17·59	19·87	19·79	- 30·30	25·56

▪ see Table 6·3

Specimen Number	Corner Nos	σ_{range} N/mm²	σ_{range} (tonf/in²)	σ_{mean} N/mm²	σ_{mean} (tonf/in²)	N_1 1st Visual Crack ×10⁶	N_2 Failure ×10⁶	Notes
BESFG-1	3 4	169.40 172.30	(11.00) (11.18)	154.00 157.08	(10.00) (10.20)	0.0725 -	.0805 -	(2)*
BESFG-2	3 4	169.40 169.40	(11.00) (11.00)	154.00 154.0	(10.00) (10.00)	0.0987 0.0895	- 0.125	(2)
BESFG-3	3 4	169.40 169.40	(11.00) (11.00)	154.00 154.00	(10.00) (10.00)	0.105 -	- -	test stopped at 1st. visual crack(2)
BESFG-4	3 4	169.40 172.30	(11.00) (11.18)	154.00 157.10	(10.00) (10.20)	0.182 -	0.201 -	(2)
BESFG-5	3 4	112.42 107.00	(7.30) (7.00)	125.97 123.20	(8.12) (8.00)	0.148 0.158	- 0.162	= 37 mm crack along the toe (1) & (2)
BESFG-6	3 4	108.26 107.80	(7.03) (7.00)	127.2 123.20	(8.26) (8.00)	0.218 -	- -	test stopped at 1st. visual crack(2)
BESFG-7	3 4	107.80 107.80	(7.00) (7.00)	123.20 123.20	(8.00) (8.00)	0.237 0.223	0.262 -	= 1.5 mm crack (2)
BESFG-8	3 4	107.80 107.80	(7.00) (7.00)	127.51 123.20	(8.27) (8.00)	0.278 -	0.298 -	(2)
BESFG-9	3 4	108.42 107.80	(7.04) (7.00)	126.89 123.20	(8.24) (8.00)	0.478 0.432	- 0.48	(2)
BESFG-10	3 4	83.30 77.00	(5.41) (5.00)	114.35 107.80	(7.43) (7.00)	0.472 0.562	0.586 -	(2) 18 mm crack length
BESFG-11	3 4	83.16 77.00	(5.40) (5.00)	120.12 107.80	(7.80) (7.00)	0.501 0.475	- 0.578	(2)
BESFG-12	3 4	77.60 77.00	(5.04) (5.00)	111.49 107.80	(7.24) (7.00)	0.6625 0.732	0.793 -	(1)
BESFG-13	3 4	77.00 77.15	(5.00) (5.01)	107.80 115.20	(7.00) (7.475)	0.776 0.803	0.814	(1) (2)
BESFG-14	3 4	77.47 77.00	(5.03) (5.00)	103.90 107.80	(6.74) (7.00)	0.7825 0.906	0.93 -	(2)
BESFG-15	3 4	77.00 77.00	(5.00) (5.00)	107.80 107.80	(7.00) (7.00)	- 0.841	- 0.874	(1) & (2)
BESFG-16	3 4	77.00 77.00	(5.00) (5.00)	107.8 107.8	(7.00) (7.00)	- 1.08	- 1.21	(2)
BESFG-17	3 4	77.00 79.30	(5.00) (5.15)	107.8 110.88	(7.00) (7.20)	- 1.125	- -	(2)
BESFG-18	3 4	77.00 77.00	(5.00) (5.00)	38.50 38.50	(2.5) (2.5)	12.5835 -	- -	no visual crack
BESFG-19	3 4	61.60 61.60	(4.00) (4.00)	100.10 100.10	(6.50) (6.50)	10.787 -	- -	no visual crack
BESFG-20	3 4	57.29 61.60	(3.72) (4.0)	96.40 100.10	(6.26) (6.50)	10.311 -	- -	no visual crack

*Type of fatigue failure

TABLE 6.15 Summary of Data for Test Series BESFG

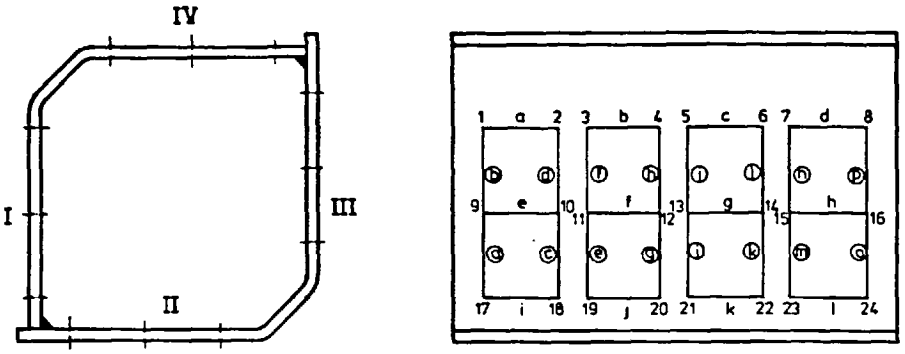
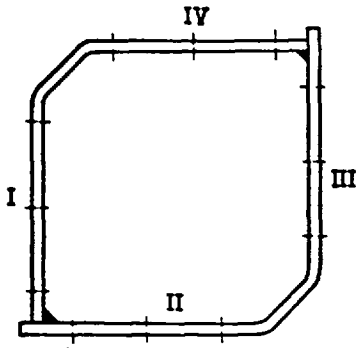


Table 6·16 Measured residual welding stress in N/mm² for specimen series BESFWI after completion of the welding.

	PART I		PART II		PART III		PART IV	
	outside	inside	outside	inside	outside	inside	outside	inside
a	0	-10·422	-119·861	-15·641	26·047	0	-78·173	-20·844
b	-15·641	-187·565	-140·689	41·688	-5·219	-119·861	-114·642	10·422
c	-15·641	-125·064	-114·642	-46·907	-31·266	-109·438	-130·267	15·641
d	20·844	-46·907	-104·22	-15·641	26·047	-15·641	-83·376	-5·219
e	15·641	-26·047	-10·422	10·422	10·422	-10·422	-5·219	-15·641
f	-62·532	-31·266	-52·11	-26·047	-15·641	-57·406	-41·688	-36·469
g	-62·532	-36·469	-57·406	-52·11	-67·751	-5·219	-46·907	-46·907
h	-26·047	-26·047	-10·422	-5·219	10·422	-62·532	-5·219	-36·469
i	-99·001	20·844	10·422	5·219	-67·751	-36·469	41·688	-10·422
j	-109·439	-20·844	-15·641	5·219	-109·438	15·641	-78·173	-119·861
k	-166·752	-15·641	-10·422	-130·267	-156·33	26·047	-20·844	-135·486
l	-125·064	-57·406	10·422	-10·422	-72·954	-5·219	41·688	-114·642
ⓐ	-52·11	109·439	-125·064	166·752	-114·642	192·799	-46·907	99·001
ⓑ	-83·376	78·173	-130·267	182·346	-140·689	192·799	-46·907	151·111
ⓒ	-83·376	145·908	-151·111	177·158	-114·565	145·908	-83·376	114·642
ⓓ	-109·439	62·532	-166·752	151·111	-140·689	192·799	-78·173	125·064
ⓔ	-109·439	88·579	-161·549	166·752	-177·158	151·111	-99·017	99·001
ⓕ	-114·642	104·22	-166·752	109·439	-145·908	156·33	-62·532	119·861
ⓖ	-114·642	83·376	-171·955	135·486	-135·177	135·485	-104·22	140·689
ⓗ	-125·064	130·267	-171·955	177·158	-135·177	182·346	-99·017	109·439
ⓘ	-119·861	119·861	-156·33	192·799	-151·111	119·861	-114·642	151·111
ⓙ	-135·486	140·689	-151·111	119·861	-119·861	177·158	-99·017	99·017
ⓚ	-109·439	114·642	-156·33	161·549	-145·908	125·064	-104·22	114·642
ⓛ	-135·486	109·439	-198·003	156·33	-145·908	161·549	-109·439	99·017
ⓜ	-114·642	119·861	-140·689	135·486	-130·267	130·267	-104·22	229·284
ⓝ	-125·064	99·001	-140·689	156·33	-135·177	203·221	-104·22	114·641
ⓞ	-88·579	156·33	-119·861	151·11	-104·22	166·752	-83·376	151·111
ⓟ	-109·439	99·001	-109·439	166·752	-130·267	151·111	-99·017	166·752
▪ Mean	-99·011	117·25	-147·63	163·12	-152·38	145·9	-92·49	137·44

▪ see Table 6·3



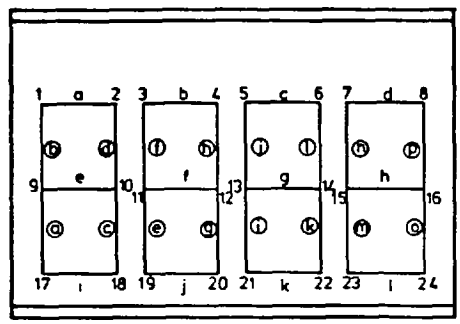


Table 6·17 Measured residual welding stress in N/mm² for specimen series BESFWI before testing.

	PART I		PART II		PART III		PART IV	
	outside	inside	outside	inside	outside	inside	outside	inside
a	15·641	-20·844	- 46·907	- 5·219	57·406	0	-10·422	36·469
b	-26·047	-93·798	- 52·11	20·844	31·266	-151·111	-46·907	72·954
c	- 46·907	- 78·173	- 31·266	5·219	5·219	- 62·532	-62·532	57·406
d	5·219	- 41·688	-10·422	-26·047	41·688	- 46·907	- 5·219	36·469
e	5·219	- 5·219	26·047	- 15·641	62·532	- 46·907	-10·422	31·266
f	-26·047	15·641	36·469	-26·047	104·22	- 78·173	15·641	36·469
g	31·266	67·751	20·844	-26·047	46·907	5·219	41·688	-57·406
h	15·641	10·422	36·469	-10·422	62·532	-36·469	52·11	- 5·219
i	- 20·844	109·438	36·469	- 35·486	31·266	- 20·844	-36·469	- 41·688
j	- 26·047	26·047	- 5·219	- 67·751	10·422	-20·844	-103·525	-104·22
k	- 93·798	36·469	-15·641	- 36·469	-20·844	-20·844	-36·469	-109·438
l	- 67·751	- 36·469	-20·844	-10·422	- 20·844	- 5·219	- 36·469	- 66·978
ⓐ	- 88·579	119·861	-145·908	171·955	-161·549	166·752	-62·532	104·22
ⓑ	- 135·486	99·001	-161·549	177·159	-109·439	187·565	- 72·954	93·798
ⓒ	- 99·001	83·376	-135·177	171·955	- 156·33	166·752	- 62·532	119·861
ⓓ	- 62·532	88·579	-182·346	156·361	-125·064	203·221	- 83·376	119·861
ⓔ	- 114·642	119·861	-161·549	224·081	-208·44	187·565	-104·22	125·064
ⓕ	-109·439	140·689	-161·549	130·267	-161·549	177·159	- 78·173	119·861
ⓖ	- 119·861	104·22	-156·33	171·955	-166·906	140·689	-109·439	145·908
ⓗ	- 114·642	119·861	-161·549	145·908	-156·33	205·939	-104·22	109·439
ⓘ	-161·549	93·798	-151·549	156·33	- 166·906	114·642	-104·22	140·699
ⓙ	- 99·001	109·439	-171·955	177·159	- 156·33	182·346	-125·064	104·22
ⓚ	- 114·642	88·579	- 161·549	177·159	- 161·549	151·111	-109·439	145·908
ⓛ	- 125·064	140·689	- 208·44	130·267	- 145·908	187·565	- 93·798	99·017
ⓜ	- 109·439	187·565	- 130·267	130·267	- 140·689	145·908	- 99·017	145·908
ⓝ	- 114·642	135·486	- 156·33	171·955	-130·267	205·939	-125·064	130·267
ⓞ	-125·064	156·33	- 166·752	125·064	- 78·173	125·064	-114·642	151·111
ⓟ	- 135·486	140·689	-135·177	177·159	- 93·798	151·111	- 99·017	171·955
* Mean	-116·6	120·00	-152·39	166·10	-155·06	149·75	- 96·98	134·60

* see Table 6·3

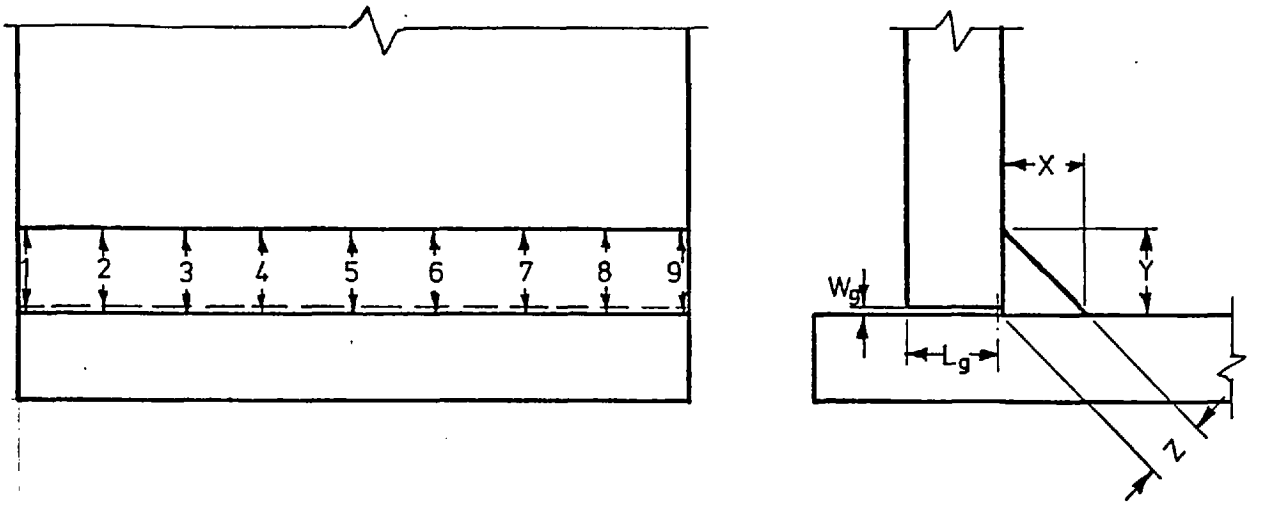
Specimen No.	SG No. 1	SG No. 2	SG No. 3	SG No. 4
BESFWI-18	109.49 (7.11*)	134.69 8.74	-83.37 (-5.41)	-118.96 (-7.72)
BESFWI-19	129.27 (8.39)	114.74 (7.45)	-114.35 (-7.43)	-98.87 (-6.42)
BESFWI-20	132.75 (8.62)	105.63 (6.85)	-120.16 (-7.80)	-109.50 (-7.11)
Mean	123.84 (8.04)	118.35 (7.68)	-105.96 (-6.88)	-109.06 (-7.08)

TABLE 6.18: Results of the measured locked-in stresses in N/mm^2 for test series BESFWI after fatigue testing. (For their fatigue behaviour see Table 6.19.)

*Numbers in $tonf/in^2$

Specimen Number	Corner Nos	σ_{range} N/mm^2	σ_{range} (tonf/in^2)	σ_{mean} N/mm^2	σ_{mean} (tonf/in^2)	N_1 1st Visual Crack $\times 10^6$	N_2 Failure $\times 10^6$	Notes
BESFWI-1	3	169.40	(11.00)	154.00	(10.00)	.041	0.05	
	4	169.40	(11.00)	154.00	(10.00)	.034	-	
BESFWI-2	3	169.40	(11.00)	154.00	(10.00)	-	-	
	4	169.40	(11.00)	154.00	(10.00)	.0985	0.115	
BESFWI-3	3	130.75	(8.49)	135.45	(8.795)	.043	.047	
	4	138.00	(9.00)	138.00	(9.00)	-	-	
BESFWI-4	3	138.00	(9.00)	138.00	(9.00)	.059	-	
	4	138.00	(9.00)	138.00	(9.00)	.049	.079	
BESFWI-5	3	138.00	(9.00)	141.68	(9.20)	-	-	
	4	138.00	(9.00)	138.00	(9.00)	.076	.096	
BESFWI-6	3	138.00	(9.00)	138.60	(9.00)	-	-	
	4	138.00	(9.00)	138.60	(9.00)	.095	0.159	
BESFWI-7	3	138.00	(9.00)	138.60	(9.00)	0.116	.179	
	4	138.00	(9.00)	138.60	(9.00)	-	-	
BESFWI-8	3	107.80	(7.00)	123.20	(8.00)	0.608	0.723	
	4	107.80	(7.00)	123.20	(8.00)	-	-	
BESFWI-9	3	107.80	(7.00)	123.20	(8.00)	-	-	
	4	106.57	(6.92)	121.66	(7.90)	0.81	1.01	
BESFWI-10	3	107.80	(7.00)	123.00	(8.00)	-	-	
	4	107.80	(7.00)	123.00	(8.00)	0.841	0.952	
BESFWI-11	3	97.95	(6.36)	115.80	(7.52)	1.067	1.521	
	4	107.80	(7.00)	123.20	(8.00)	-	-	
BESFWI-12	3	107.00	(7.00)	123.20	(8.00)	1.14	1.45	
	4	107.00	(7.00)	123.20	(8.00)	-	-	
BESFWI-13	3	107.80	(7.00)	123.20	(8.00)	1.266	2.032	
	4	107.80	(7.00)	123.20	(8.00)	-	-	
BESFWI-14	3	107.80	(7.00)	125.51	(8.15)	1.312	1.346	
	4	107.80	(7.00)	123.20	(8.00)	-	-	
BESFWI-15	3	107.80	(7.00)	123.00	(8.00)	1.47	1.617	
	4	107.80	(7.00)	123.00	(8.00)	-	-	
BESFWI-16	3	103.03	(6.69)	113.49	(7.37)	2.308	2.365	
	4	107.80	(7.00)	123.00	(8.00)	1.934	2.365	
BESFWI-17	3	107.80	(7.00)	123.20	(8.00)	-	-	
	4	107.80	(7.00)	123.20	(8.00)	2.051	2.282	
BESFWI-18	3	77.00	(5.00)	107.80	(7.00)	10.207 ↙	-	no crack visible
	4	77.00	(5.00)	107.80	(7.00)		-	
BESFWI-19	3	77.00	(5.00)	107.80	(7.00)	10.115 ↙	-	no crack visible
	4	77.00	(5.00)	107.80	(7.00)	-	-	
BESFWI-20	3	77.00	(5.00)	107.80	(7.00)	12.727	-	no crack visible
	4	77.00	(5.00)	107.80	(7.00)	-	-	
BESFWI-21	3	77.00	(5.00)	107.80	(7.00)	13.649 ↙	-	no crack visible
	4	77.00	(5.00)	107.80	(7.00)	-	-	

TABLE 6.19 Summary of Data for Test Series BESFWI



Side 1						Side 2				
No.	X_1	y_1	Z_1	L_{g_1}	W_g	X_2	Y_2	Z_2	L_{g_2}	W_{g_2}
1	10.0	10.0	7.5	12.0	0.76	10.0	12.5	7.0	12.0	.76
2	11.0	10.0	-	12.0	0.78	10.0	12.5	-	12.0	.66
3	10.0	11.0	-	11.5	0.84	10.0	12.5	-	11.5	.69
4	10.0	11.0	-	11.5	0.87	10.5	11.0	-	11.5	.69
5	10.5	10.5	-	11.5	0.89	10.0	11.5	-	11.0	.69
6	11.0	11.0	-	11.5	0.96	10.0	11.5	-	11.0	.76
7	11.0	11.0	-	11.0	0.94	10.5	12.0	-	11.0	.76
8	11.0	11.5	-	11.5	0.97	10.0	12.5	-	12.0	.76
9	11.5	11.0	8.0	12.0	0.97	10.5	12.0	8.0	12.5	.79
Ave	10.67	10.78	7.75	11.61	.89	10.17	12.22	7.5	11.61	.72

TABLE 6.20: Measured dimensions of the specimen BESFGI-10 at points shown on the diagram. (All dimensions are in mm.)

Specimen No.	SG No.1	SG No. 2	SG No. 3	SG No. 4
BESFGI	+112.73 (+7.32*)	121.51 (7.89)	-82.24 (-5.34)	-91.78 (-5.96)

TABLE 6.21: Results of the measured locked-in stresses in N/mm^2 for specimen series BESFGI

*Numbers in $tonf/in^2$

Specimen Number	Corner Nos	σ_{range} N/mm²	σ_{range} (tonf/in²)	σ_{mean} N/mm²	σ_{mean} (tonf/in²)	N_1 1st Visual Crack ×10⁶	N_2 Failure ×10⁶	Notes
BESFGI-1	3	169.40	(11.00)	154.00	(10.00)	0.052	0.071	
	4	169.40	(11.00)	154.00	(10.00)	0.059	-	= .5 mm crack
BESFGI-2	3	138.60	(9.00)	141.83	(9.21)	0.041	-	= 1 mm crack
	4	138.60	(9.00)	138.60	(9.00)	0.031	0.062	
BESFGI-3	3	138.60	(9.00)	138.60	(9.00)	-	-	
	4	138.60	(9.00)	138.60	(9.00)	0.039	0.045	
BESFGI-4	3	138.60	(9.00)	69.30	(4.50)	0.058	0.11	
	4	138.60	(9.00)	69.30	(4.50)	0.072	-	= .7 mm crack
BESFGI-5	3	138.60	(9.00)	138.60	(9.00)	0.068	-	
	4	138.60	(9.00)	138.60	(9.00)	0.057	.076	
BESFGI-6	3	107.80	(7.00)	123.00	(8.00)	-	-	
	4	107.80	(7.00)	123.00	(8.00)	0.107	0.150	
BESFGI-7	3	98.40	(6.39)	111.50	(7.23)	0.189	-	= 3 mm crack
	4	107.80	(7.00)	123.20	(8.00)	0.169	0.239	
BESFGI-8	3	107.80	(7.00)	123.00	(8.00)	0.215	0.302	
	4	107.80	(7.00)	123.00	(8.00)	-	-	
BESFGI-9	3	107.80	(7.00)	123.00	(8.00)	0.264	-	= 1 mm crack
	4	107.80	(7.00)	123.00	(8.00)	0.229	0.294	
BESFGI-10	3	107.80	(7.00)	123.00	(8.00)	-	-	
	4	107.80	(7.00)	123.00	(8.00)	0.299	0.305	
BESFGI-11	3	77.00	(5.00)	104.79	(6.80)	0.462	-	= 1.5 mm crack
	4	77.00	(5.00)	107.80	(7.00)	0.386	0.5205	
BESFGI-12	3	77.00	(5.00)	107.80	(7.00)	0.5035	-	= 3 mm crack
	4	77.00	(5.00)	107.80	(7.00)	0.4165	0.5625	
BESFGI-13	3	77.00	(5.00)	107.80	(7.00)	0.615	0.769	
	4	77.00	(5.00)	107.80	(7.00)	-	-	
BESFGI-14	3	77.00	(5.00)	107.80	(7.00)	1.321	2.490	
	4	77.00	(5.00)	107.80	(7.00)	-	-	
BESFGI-15	3	72.38	(4.70)	110.11	(7.15)	1.228	3.403	
	4	72.38	(4.70)	110.11	(7.15)	1.128	3.403	1.5 mm crack
BESFGI-16	3	61.60	(4.00)	100.10	(6.50)	1.433	-	= 4 mm crack
	4	61.60	(4.00)	100.10	(6.50)	1.031	1.930	
BESFGI-17	3	60.05	(4.1)	116.27	(7.55)	1.824	-	
	4	61.40	(4.00)	123.20	(8.00)		2.025	
BESFGI-18	3	60.05	(3.9)	116.27	(7.58)	2.62	3.124	
	4	61.40	(4.0)	123.20	(8.0)	-	-	
BESFGI-19	3	77.00	(5.00)	38.50	(2.50)	0.252	-	= 0.5 mm crack
	4	77.00	(5.00)	38.50	(2.50)	0.364	-	

TABLE 6.22 Summary of Data for Test Series BESFGI

Specimen Number	Corner Nos	σ_{range} N/mm^2	σ_{range} (tonf/in^2)	σ_{mean} N/mm^2	σ_{mean} (tonf/in^2)	N_1 1st Visual Crack $\times 10^6$	N_2 Failure $\times 10^6$	Notes
BEVBS-1	3	169.40	(11.00)	154.00	(10.00)	-	-	
	4	169.40	(11.00)	154.00	(10.00)	.705	.761	
BEVBS-2	3	169.40	(11.00)	154.00	(10.00)	1.653	2.03	2 mm crack
	4	169.40	(11.00)	154.00	(10.00)	-	-	
BEVBS-3	3	138.60	(9.00)	138.60	(9.00)	-	-	
	4	138.60	(9.00)	138.60	(9.00)	3.2165	3.291	
BEVBS-4	3	77.00	(5.00)	107.80	(7.00)	11.535	-	no crack visible
	4	77.00	(5.00)	107.80	(7.00)		-	
BEVBS-5	3	77.00	(5.00)	107.80	(7.00)	14.235	-	no crack visible
	4	77.00	(5.00)	107.80	(7.00)		-	

TABLE 6.23 Summary of Data for Test Series BEVBS

Specimen Number	Corner Nos	σ_{range} N/mm^2	σ_{range} (tonf/in^2)	σ_{mean} N/mm^2	σ_{mean} (tonf/in^2)	N_1 1st Visual Crack $\times 10^6$	N_2 Failure $\times 10^6$	Notes
BEVB-1	3	175.25	(11.64)	163.24	(10.60)	0.837	.837	crack along weld root
	4	169.40	(11.00)	154.00	(10.00)	0.748		
BEVB-2	3	83.16	(5.40)	113.96	(7.4)	12.508	-	no visual crack
	4	77.00	(5.00)	107.00	(7.0)	-	-	
BEVB-3	3	138.60	(9.00)	138.60	(9.00)	3.078	3.156	
	4	138.60	(9.00)	138.60	(9.00)	-	-	
BEVB-4	3	138.60	(9.00)	138.60	(9.00)	0.877	-	
	4	138.60	(9.00)	138.60	(9.00)	1.853	2.046	
BEVB-5	3	104.72	(6.80)	117.19	(7.61)	-	-	
	4	107.80	(7.00)	123.20	(8.00)	4.84	5.01	
BEVB-6	3	169.40	(11.00)	163.24	(10.00)	-	-	
	4	169.40	(11.00)	163.24	(10.00)	.999	1.044	

TABLE 6.24 Summary of Data for Test Series BEVB

Specimen Number	Corner Nos	σ_{range} N/mm²	σ_{range} (tonf/in²)	σ_{mean} N/mm²	σ_{mean} (tonf/in²)	N_1 1st Visual Crack ×10⁶	N_2 Failure ×10⁶	Notes
BESBS-1	3	166.62	(10.82)	149.22	(9.69)	-	-	
	4	169.24	(10.99)	151.92	(9.865)	1.6335	-	crack along the toe
BESBS-2	3	169.40	(11.00)	154.00	(10.00)	1.74	2.0225	
	4	169.40	(11.00)	154.00	(10.00)	-	-	
BESBS-3	3	140.91	(9.15)	140.125	(9.12)	2.173	2.802	
	4	138.60	(9.00)	138.60	(9.00)	-	-	
BESBS-4	3	141.68	(9.20)	143.22	(9.30)	2.743	-	
	4	138.60	(9.00)	138.60	(9.00)	-	-	
BESBS-5	3	138.60	(9.00)	138.60	(9.00)	3.085	3.17	
	4	132.44	(8.60)	130.90	(8.50)	3.105	-	crack along the toe
BESBS-6	3	107.8	(7.0)	123.20	(8.00)	-	-	
	4	107.8	(7.0)	123.20	(8.00)	4.634	4.763	
BESBS-7	3	77.00	(5.00)	107.80	(7.00)	10.231 ↗	-	
	4	77.00	(5.00)	107.80	(7.00)	-	-	no crack visible
BESBS-8	3	77.00	(5.00)	107.80	(7.00)	12.135 ↗	-	
	4	77.00	(5.00)	107.80	(7.00)	-	-	

TABLE 6.25 Summary of Data for Test Series BESBS

Specimen Number	Corner Nos	σ_{range} N/mm²	σ_{range} (tonf/in²)	σ_{mean} N/mm²	σ_{mean} (tonf/in²)	N_1 1st Visual Crack ×10⁶	N_2 Failure ×10⁶	Notes
BESB-1	3	167.86	(10.90)	148.61	(9.65)	0.8	0.91	
	4	169.40	(11.00)	154.00	(10.00)	-	-	
BESB-2	3	138.60	(9.00)	138.60	(9.00)	-	-	
	4	141.52	(9.19)	146.22	(9.495)	.213	.242	
BESB-3	3	107.80	(7.00)	107.80	(7.00)	.585	.594	
	4	107.80	(7.00)	121.35	(7.88)	-	-	
BESB-4	3	77.00	(5.00)	107.80	(7.00)	2.884	2.924	
	4	77.00	(5.00)	107.80	(7.00)		-	

TABLE 6.26 Summary of Data for Test Series BESB

Test Series	Stress Range N/mm^2	Sample Size n	Standard Deviation $S_{\overline{logN}}$	Sample Mean $\overline{logN}$	K_v
BEDFW	169.30	9.0	0.124	6.160	.0204
	138.60	8.0	0.148	6.2904	.0234
	107.80	8.0	0.104	6.5853	.0158
BEDFG	169.30	8.0	0.127	5.9423	.0213
	138.60	8.0	0.122	6.1838	.0198
	107.80	6.0	0.122	6.4766	.0187
BESFW	169.30	10.0	0.130	5.4102	.0240
	107.80	12.0	0.133	5.9525	.0224
	77.0	9.0	0.167	6.4131	.0260
BESFG	169.30	5.0	0.149	5.0175	.0296
	107.80	8.0	0.184	5.3986	.0340
	77.00	13.0	0.126	5.8569	.0216
BESFGI	138.60	7.0	0.137	4.701	.029
	107.80	7.0	0.147	5.303	.027
	77.0	8.0	0.211	5.681	.037
BESFWI	169.30	3.0	0.247	4.713	.0523
	138.60	6.0	0.168	4.836	.0347
	107.8	11.0	0.181	6.096	.0297
	69.0*				

TABLE 6.27: Summary of the statistical results for the fillet corner joints

*The value of the stress with the allowance of residual locked-in stress

No.	Groups	Observed Frequency "O_i"	Expected Frequency "E_i"	$\frac{(O_i - E_i)^2}{E_i}$
1	$-\infty<u<-.842$	6.0	5.0	0.20
2	$-.842\leqslant u<-.253$	5.0	5.0	0.00
3	$-.253\leqslant u<+.253$	4.0	5.0	0.20
4	$+.253\leqslant u<-.842$	5.0	5.0	0.00
5	$-.842\leqslant u<+\infty$	5.0	5.0	0.00
6	Σ	25.0	25.0	0.40

TABLE 6.28: χ^2-test "for goodness-of-fit" for test series"BEDFW"

Total number of data : $n = 25.0$

Number of groups : $K = \frac{25}{5} = 5.0$

Theoretical relative frequency : $\frac{1}{K} = 0.2$

Theoretical frequency : $E_i = \frac{25}{5} = 5.0$

Summation of the theoretical relative frequency is always equal to 1

d.f. = 2.0

$\chi^2_{.90,(2)} = 4.61$

$\chi^2_{.95,(2)} = 5.99$

; $0.4 \leqslant \chi^2_{.90,(2)} \leqslant \chi^2_{.95,(2)}$

No.	Groups	Observed Frequency "O_i"	Expected Frequency "E_i"	$\frac{(O_i - E_i)^2}{E_i}$
1	$-\infty < u < -.842$	4.0	5.80	.55862
2	$-.842 \leqslant u < -.253$	8.0	5.8	.83448
3	$-.253 \leqslant u < +.253$	5.0	5.8	.11034
4	$+.253 \leqslant u < .842$	7.0	5.8	.28800
5	$+.842 \leqslant u < +\infty$	5.0	5.8	.11034
6	Σ	29.0	29.0	1.9018

TABLE 6.29: χ^2-test "for goodness-of-fit" for test series "BESFGI"

Total number of data: $n = 25.0$

Number of groups: $K \leqslant \frac{29}{5} = 5.8$, say $K = 5.0$

Theoretical relative frequency: $= \frac{1}{5} = .20$

$E_i = \frac{29}{5} = 5.8$

d.f. = 2.0

$\chi^2_{.90,(2)} = 4.61$

$\chi^2_{.95,(2)} = 5.99$

$1.9018 \leqslant \chi^2_{.90,(2)} \leqslant \chi^2_{.95,(2)}$

No.	Test Series	Series Size	d.f.	Calculated χ^2	$\chi^2_{.90}$	$\chi^2_{.95}$
1	BEDFW	25.0	2.0	.40	4.61	5.99
2	BEDFG	22.0	1.0	.909	2.71	3.84
3	BESFW	31.0	3.0	.419	6.25	7.89
4	BESFG	26.0	2.0	.923	4.61	5.99
5	BESFGI	29.0	2.0	1.902	4.61	5.99
6	BESFWI	20.0	1.0	2.000	2.71	3.84

TABLE 6.30: Summary of χ^2-test for "goodness-of-fit" for all fillet welded test results

Stress Range N/mm^2	$BEDFW_{Vs}$ BEDFG		$BEDFW_{Vs}$ BESFW		$BESFW_{Vs}$ BESFG		$BESFG_{Vs}$ BESFGI		$BEDFG_{Vs}$ BESFGI		$BEDFG_{Vs}$ BESFG		$BESFW_{Vs}$ BESFWI		$BEDFW_{Vs}$ BESFG	
	F	$F_{.95}$	F	$F_{.95}$	F	$F_{.95}$	F	$F_{.95}$	F	$F_{.95}$	F	$F_{.95}$	F	$F_{.95}$	F	$F_{.95}$
169.3	1.045**	3.23	1.098**	3.14	1.307**	3.330	-	-	-	-	1.373**	3.69	-	-	1.435**	3.48
138.6	1.454**	3.44	-	-	-	-	-	-	1.25**	3.50	-	-	1.503**	3.87	-	-
107.8	1.357**	3.58	1.636**	3.39	1.893**	2.850	1.565**	3.73	1.458**	4.21	2.282**	4.15	-	-	3.097***	3.44
77.0	-	-	-	-	1.747**	2.710	2.782***	2.77	-	-	-	-	-	-	-	-

TABLE 6.31: Comparison of two variances of different test series

** Variances not significantly different

*** F-values in the zone of uncertainty

Stress range N/mm^2	BEDFW Vs BEDFG		BEDFW Vs BEDSFW		BESFW Vs BESFG		BESFG Vs BESFGI		BESFW Vs BESFGI		BESFW Vs BESFWI	
	t	$t_{\cdot 95,\gamma}$	t	$t_{\cdot 95,\gamma}$	t	$t_{\cdot 95,\gamma}$	t	$t_{\cdot 95,\gamma}$	t	$t_{\cdot 95,\gamma}$	t	$t_{\cdot 95,\gamma}$
169.3	3.358*	1.753	12.126*	1.740	4.8036*	1.771	-	-	-	-	5.656*	1.796
138.6	1.471**	1.761	-	-	-	-	-	-	-	-	-	-
107.8	1.660**	1.782	10.648*	1.740	7.3976*	1.734	5.939*	1.771	7.381*	1.771	-	-
77.0	-	-	-	-	8.454*	1.725	2.28*	1.729	7.583*	1.753	-	-

TABLE 6.32: Comparison of two means for different test series

* Means significantly different

** t-value in the zone of uncertainty

Equation	Test Series	Regression Coefficient		Correlation Coefficient	Residual	Test of common variances		
		A	B	R	S_R	χ^2	$\chi^2_{.9}$	$\chi^2_{.95}$
(5.32)	BEDFW	10.996	-2.1786	-0.822	0.1269	1.099	4.61	5.89
(5.33)		7.297	-0.0068	-0.813	0.1299	1.099	4.61	5.89
(5.32)	BEDFG	11.915	-2.678	-0.878	0.1207	0.0137	4.61	5.99
(5.33)		7.379	-0.0086	-0.877	0.1212	0.0137	4.61	5.99
(5.32)	BESFW	11.9002	-2.916	-0.945	0.1413	0.684	4.61	5.99
(5.33)		7.155	-0.0105	-0.934	0.1533	0.684	4.61	5.99
(5.32)	BESFG	10.579	-2.517	-0.909	0.1553	1.287	4.61	5.99
(5.33)		6.514	-0.0092	-0.888	0.1726	1.287	4.61	5.99
(5.32)	BESFGI	12.653	-3.654	-0.936	0.1920	1.095	4.61	5.99
(5.33)		6.923	-0.015	-0.921	0.2130	1.095	4.61	5.99
(5.32)	BESFWI	13.211	-3.871	0.976	0.1950	0.504	4.61	5.99

TABLE 6.33: Results of linear regression analysis for all fillet welded joints

No.	Test Series Compared	Test of Common Variances of Regression Lines			Test of Common Slopes of Regression Lines			Test of Identity of Regression Lines		
		F	$F_{.95}$	$F_{.975}$	t	$t_{.90}$	$t_{.95}$	t	$t_{.90}$	$t_{.95}$
1	BEDFW and BEDFG	** 1.103	2.05	2.37	++ 1.099	1.3	1.65	25.63	1.3	1.675
2	BEDFW and BESFW	** 1.236	1.94	2.21	+ 1.94	1.3	1.66	X	-	-
3	BEDFW and BESFWI	* 2.363	2.04	2.33	+ 2.1	1.25	1.67	X	-	-
4	BEDFW and BESFG	*** 1.497	1.97	2.26	++ .821	1.3	1.6	X	-	-
5	BEDFW and BESFGI	* 2.279	1.94	2.24	+++ 1.772	1.706	2.056	X	-	-
6	BEDFG and BESFW	** 1.363	2.01	2.3	+ 2.1	1.25	1.67	X	-	-
7	BEDFG and BESFG	** 1.651	2.04	2.37	++ .367	1.3	1.68	X	-	-
8	BEDFG and BESFGI	* 2.513	2.03	2.32	+			X	-	-
9	BEDFG and BESFWI	* 2.603	1.79	2.12	+			X		

Continued on the following page

No.	Test Series Compared	Test of Common Variances of Regression Lines			Test of Common Slopes of Regression Lines			Test of Identity of Regression Lines		
		F	$F_{.95}$	$F_{.975}$	t	$t_{.90}$	$t_{.95}$	t	$t_{.90}$	$t_{.95}$
10	BESFW and BESFG	** 1.211	1.89	2.14	+++ 1.337	1.3	1.68	X	-	-
11	BESFW and BESFGI	** 1.844	1.86	2.09	+ 2.31	1.3	1.68	X	-	-
12	BESFW and BESFWI	*** 1.92	1.92	2.23	+ 2.867	1.3	1.68	X	-	-
13	BESFG and BESFGI	** 1.523	1.93	2.21	+ 4.032	1.3	1.68	X	-	-
14	BESFG and BESFWI	** 1.577	2.03	2.33	+ 3.879	1.299	1.679	X	-	-
15	BESFGI and BESFWI	** 1.035	1.97	2.25	++ 0.586	1.3	1.68	10.183	-	-

TABLE 6.34: Summary of results of comparison of the Regression Lines

* Variances significantly different
** Variances not significantly different
*** Variances in the zone of uncertainty
\+ Slopes of the Regression Lines significantly different
++ Slopes of the Regression Lines not significantly different
+++ Slopes of the Regression Lines in the zone of uncertainty
X Regression Lines significantly different

Stress range N/mm^2	Due to gap		Due to weld type		Due to stress type		Due to gap and weld type	
	$\frac{(DFW-DFG)}{DFW}$	$\frac{(SFW-SFG)}{SFW}$	$\frac{(DFW-SEW)}{DFW}$	$\frac{(DFG-SFG)}{DFG}$	$\frac{(SFW-SFWI)}{SFW}$	$\frac{(SFG-SFGI)}{SFG}$	$\frac{(DFW-SFG)}{DFW}$	$\frac{(DFG-SFW)}{DFG}$
169.30	39.458	59.517	82.217	87.538	79.92	-	92.801	88.109
138.60	22.011	-	-	-	-	-	-	-
107.80	22.136	72.067	76.706	91.64	-	19.772	93.493	75.994
77.06	-	72.212	-	-	-	33.313	-	-

TABLE 6.35: Percentages of reduction of the means of different fillet corner welds

No.	Type of weld / σ_R N/mm^2	BEVBS	BEVB	BESBS	BESB	Note
1	169.4	1.0795	0.8852	1.6859	0.80	—
2	138.6	3.216	1.7102	2.7488	.213	—
3	107.8	-	4.840	4.634	.585	—
4	77.0	-	-	-	2.884	—

TABLE 6.36: Mean fatigue life ($\bar{N}$logN) in million cycles at different stress levels for butt corner welds

σ_R N/mm^2	Due to sealing		Due to type		Due to sealing and type		Note
	VBS-VB / VBS	SBS-SB / SBS	VBS-SBS / VBS	VB-SB / VB	VBS-SB / VBS	SBS-VB / SBS	
169.4	18.00	52.55	56.17	9.62	26.89	47.49	—
138.6	46.82	92.25	14.53	87.55	93.38	37.78	—
107.8	-	87.38	-	87.91	-	-4.45	—

TABLE 6.37: Percentages of reduction of the means of different butt corner welds

Specimen No.	SG No. 1	SG No. 2	SG No. 3	SG No. 4	Note
BESFWIR2	+140.71 (+9.135*)	+155.104 (+10.07)	-102.72 (-6.67)	-114.02 (-7.40)	First series
BESFWIR4	127.70 (8.27)	+143.14 (+9.27)	-108.90 (-7.07)	-112.98 (-7.33)	
BESFWIR6	139.87 (9.08)	+124.43 (+8.06)	-122.14 (-7.93)	-98.39 (-6.39)	Second series
BESFWIR8	102.4 (6.65)	+128.00 (+8.31)	-90.6 (-5.88)	-86.90 (-5.62)	
AVERAGE	+127.67 (+8.29)	137.67 (+8.93)	-106.09 (-6.88)	-103.07 (-6.69)	

*Values in tonf/in^2

TABLE 7.1: Measured locked-in stresses transverse to direction of weld in N/mm^2 for specimen series BESFWIR

Specimen No.	SG Nos	Range N/mm^2	Range tonf/in^2	N_1 1st visual crack x 10^6	N_2 Failure x 10^6	Note
BESFWIR1	1	-114.56	(-7.42)	1.837	2.0475	toe crack
	2	-114.56	(-7.42)			
	3	+104.77	(+6.98)			
	4	+107.8	(+7.00)			
BESFWIR3	1	-149.61	(-9.69)	1.048	1.113	toe crack
	2	-149.61	(-9.69)			
	3	+131.37	(+8.53)			
	4	+138.96	(9.00)			
BESFWIR5	1	-148.98	(-9.61)	1.3755	1.445	toe crack
	2	-147.68	(-9.59)			
	3	+138.45	(+8.99)			
	4	+139.52	(+9.06)			
BESFWIR7 (BESFWIR4)	1	-151.38	(-9.83)	.049	.079	root crack *σ_{min} = 69.3 N/mm^2
	2	-150.76	(-9.79)			
	3	+146.15	(+9.49)			
	4	+138.60	(+9.00)			
(BESFWI20)	1	- 79.46	(-5.16)	12.727		no crack σ_{min} = 69.3 N/mm^2
	2	- 81.46	(-5.29)			
	3	+ 71.76	(+4.66)			
	4	+ 77.0	(+5.00)			

TABLE 7.2: Summary of fatigue data for test series BESFWIR

No.	Crack Length a mm	a/L%	At the midspan δ_{xc}/δ_x	At the midspan δ_{zc}/δ_z	$\frac{\sigma_{DBC}}{\sigma_{DB}}$	Node No.	At the crack tip δ_{xcL}/δ_{xL}	At the crack tip δ_{zcL}/δ_{zL}	$\frac{\sigma_{DBC}}{\sigma_{DBL}}$
1	0.0	0.0	1.0	1.0	1.0	113 114	1.0	1.0	1.0
2	50.0	0.17	1.0 1.0	1.0001 1.0001	1.001	103 104	1.0001	1.0001	1.0026
3	150.0	0.5	1.0006 1.0006	1.0005 1.0005	1.013	93 94	1.0012	1.0012	1.028
4	300.0	1.0	1.0018 1.0041	1.0028 1.0014	1.101	83 84	1.0012	1.0051	1.119
5	600.0	2.0	1.0053 1.0219	1.0171 1.0057	1.266	73 74	1.0051	1.0051	1.288
6	1100.0	3.65	1.0153 1.0580	1.0617 1.0157	1.395	63 64	1.0152	1.0153	1.425
7	2100.0	6.98	1.0420 0.9621	1.1556 1.0417	1.391	53 54	1.0414	1.0414	1.433

TABLE 8.1: Effect of longitudinal crack along the corners of the Box A on maximum deflections in x and z directions at the midspan and at the end of the crack, and on the transverse distortional bending stress at the tip of the crack for point load

No.	Crack Length a mm	a/L%	At the midspan		$\frac{\sigma_{DBC}}{\sigma_{DB}}$	Node No.	At the crack tip		$\frac{\sigma_{DBC}}{\sigma_{DBL}}$
			δ_{xc}/δ_x	δ_{zc}/δ_z			δ_{xcL}/δ_{xL}	δ_{zcL}/δ_{zL}	
1	0.0	0.0	1.0	1.0	1.0	113 114	1.0	1.0	1.0
2	50.0	0.17	1.0000 1.0000	1.0005 1.0005	1.002	103 104	1.000	1.0001	1.0026
3	150.0	0.5	1.0001 1.0001	1.0005 1.0005	1.029	93 94	1.0002	1.0002	1.0287
4	300.0	1.0	1.0040 1.0037	1.0030 1.0015	1.118	83 84	1.0012	1.0012	1.118
5	600.0	2.0	1.0054 1.0224	1.0175 1.0054	1.286	73 74	1.0051	1.0051	1.287
6	1100.0	3.65	1.0156 1.0584	1.0619 1.0155	1.419	63 64	1.0152	1.015	1.422
7	2100.0	6.98	1.0418 0.9655	1.1582 1.0418	1.423	53 54	1.0412	1.0412	1.431

TABLE 8.2: Effect of longitudinal crack along the corners of the Box A on maximum deflections in x and z directions at the midspan, at the end of the crack and on the transverse distortional bending stress at the tip of the crack for U.D.L.

No.	Crack Length a mm	$a/L\%$	At the midspan		$\frac{\sigma_{DBC}}{\sigma_{DB}}$	Node No.	At the crack tip		$\frac{\sigma_{DB}}{\sigma_{DBL}}$
			δ_{xc}/δ_x	δ_{zc}/δ_z			δ_{xcL}/δ_{xL}	δ_{zcL}/δ_{zL}	
1	0.0	0.0	1.0	1.0	1.0	113 114	1.0	1.0	1.0
2	50.0	1.52	1.0084 1.0093	1.0075 1.0075	1.096	103 104	1.0042	1.0042	1.144
3	150.0	4.54	1.0372 1.0791	1.0865 1.0376	1.3201	93 94	1.0356	1.0356	1.43
4	300.0	9.09	1.1116 1.372	1.2143 1.1128	1.403	83 84	1.111	1.111	1.573
5	750.0	22.73	1.535 -2.267	1.4925 1.5376	1.498	73 74	1.5575	1.56	2.076
6	1050.0	31.82	2.009 -4.772	1.7069 2.0226	1.613	63 64	2.1286	2.1304	2.735

TABLE 8.3: Effect of longitudinal crack along the corners of the Box B on maximum deflections in x and z directions at the midspan, at the end of the crack and on the transverse distortional bending stress at the tip of the crack for point load

No.	Crack Length a mm	$a/L\%$	At the midspan		$\frac{\sigma_{DBC}}{\sigma_{DB}}$	Node No.	At the crack tip		$\frac{\sigma_{DBC}}{\sigma_{DBL}}$
			δ_{xc}/δ_x	δ_{zc}/δ_z			δ_{xcL}/δ_{zL}	δ_{zcL}/δ_{zL}	
1	0.0	0.0	1.0	1.0	1.0	113 114	1.0	1.0	1.0
2	50.0	2.0	1.0044 1.0088	1.0036 1.0036	1.098	103 104	1.0044	1.0043	1.144
3	150.0	6.0	1.0398 1.0796	1.0893 1.0393	1.346	93 94	1.038	1.0379	1.436
4	250.0	10.0	1.0903 1.0221	1.1750 1.0929	1.466	83 84	1.0909	1.0918	1.604
5	400.0	16.0	1.1903 0.4602	1.2821 1.1929	1.516	73 74	1.1929	1.1945	1.747
6	550.0	22.0	1.3363 -0.6106	1.3786 1.3357	1.598	63 64	1.3407	1.3428	1.969
7	1000.0	40.0	2.0310 -4.6062	1.7571 2.029	1.758	53 54	2.1296	2.1306	2.857

TABLE 8.4: Effect of longitudinal crack along the corners of the Box C on maximum deflections in x and z directions at the midspan, at the end of the crack and on the transverse distortional bending stress at the tip of the crack for point load

No.	Crack Length a mm	a/L%	At the midspan		$\frac{\sigma_{DBC}}{\sigma_{DB}}$	Node No.	At the crack tip		$\frac{\sigma_{DBC}}{\sigma_{DBL}}$
			δ_{xc}/δ_{x}	δ_{zc}/δ_{z}			δ_{xcL}/δ_{zL}	δ_{zcL}/δ_{zL}	
1	0.0	0.0	1.0	1.0	1.0	113 114	1.0	1.0	1.0
2	50.0	1.52	1.0036 1.0078	1.0059 1.0037	1.109	103 104	1.0036	1.0034	1.142
3	150.0	4.54	1.0319 1.0789	1.0847 1.0315	1.346	93 94	1.0312	1.0313	1.41
4	300.0	9.09	1.0978 0.909	1.2095 1.1092	1.424	83 84	1.097	1.0975	1.538
5	500.0	15.15	1.224 -0.158	1.3317 1.224	1.462	73 74	1.2251	1.2262	1.677
6	750.0	22.73	1.459 -2.137	1.488 1.461	1.5306	63 64	1.4735	1.7206	1.942

TABLE 8.5: Effect of longitudinal crack along the corners of the Box D on maximum deflections in x and z directions at the midspan, at the end of the crack and on the transverse distortional bending stress at the tip of the crack for point load

No.	Crack Length a mm	$a/L\%$	At the midspan		$\frac{\sigma_{DBC}}{\sigma_{DB}}$	Node No.	At the crack tip		$\frac{\sigma_{DBC}}{\sigma_{DBL}}$
			δ_{xc}/δ_x	δ_{zc}/δ_z			δ_{xcL}/δ_{xL}	δ_{zcL}/δ_{zL}	
1	0.0	1.0	1.0	1.0	1.0	113 114	1.0	1.0	1.0
2	50.0	2.0	1.004 1.008	1.006 1.004	1.110	103 104	1.0043	1.0036	1.142
3	150.0	6.0	1.033 1.079	1.086 1.033	1.365	93 94	1.0328	1.033	1.427
4	250.0	10.0	1.080 1.016	1.167 1.079	1.484	83 84	1.0793	1.0800	1.582
5	400.0	16.0	1.167 0.469	1.274 1.167	1.532	73 74	1.1668	1.1673	1.699
6	550.0	22.0	1.288 -0.565	1.363 1.288	1.606	63 64	1.291	1.2923	1.882
7	750.0	30.0	1.500 -2.202	1.503 1.502	1.644	53 54	1.5143	1.5157	1.924

TABLE 8.6: Effect of longitudinal crack along the corners of the Box E on maximum deflections in x and z directions at the midspan, at the end of the crack and on the transverse distortional bending stress at the tip of the crack for point load

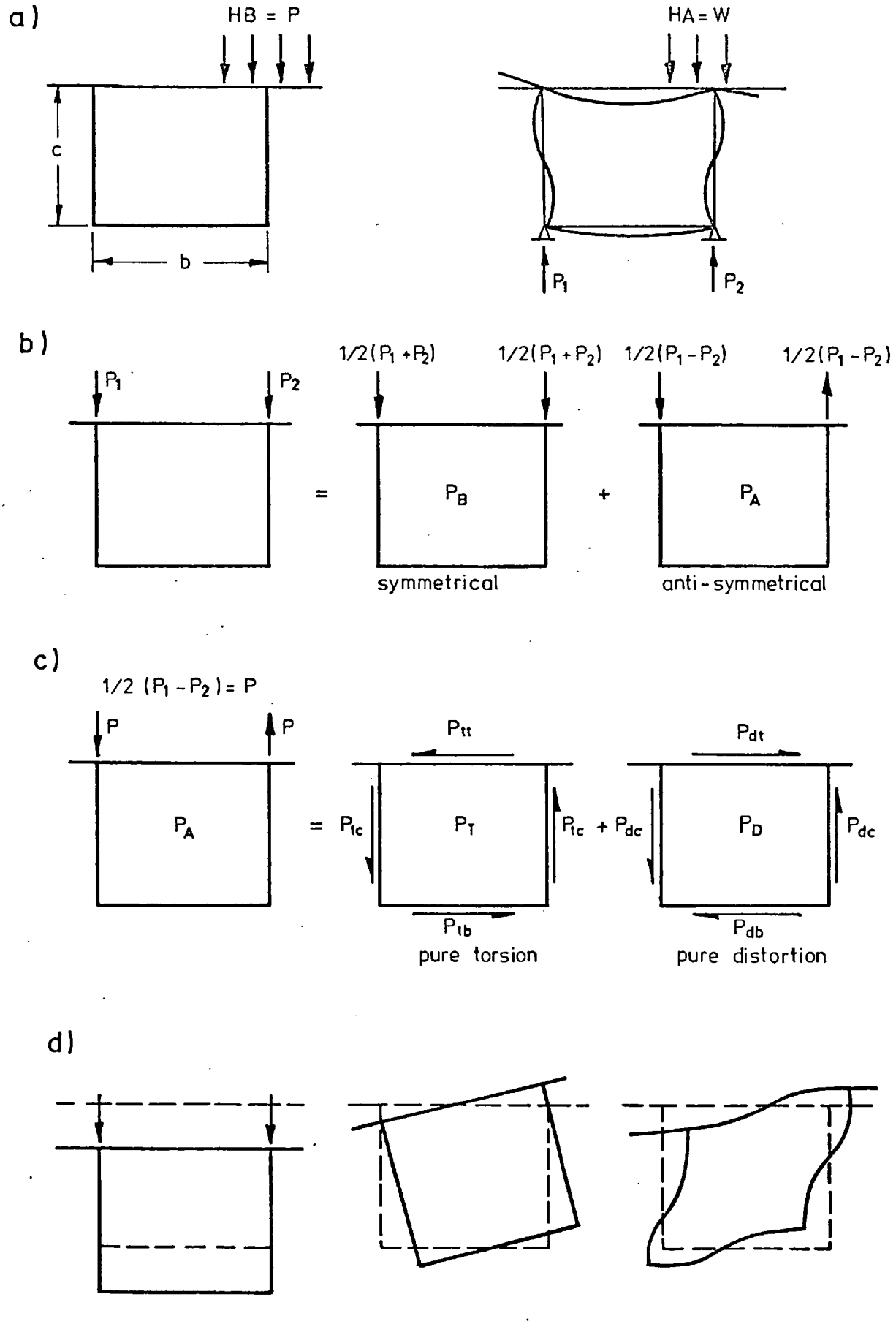


Fig. 2·1 Behaviour of box girder under eccentric loading

a) External load and cross-section of a box girder
b) Symmetrical and anti-symmetrical components of load
c) Pure torsion and pure distortional components of load
d) Displacement of cross-section due to different components of load

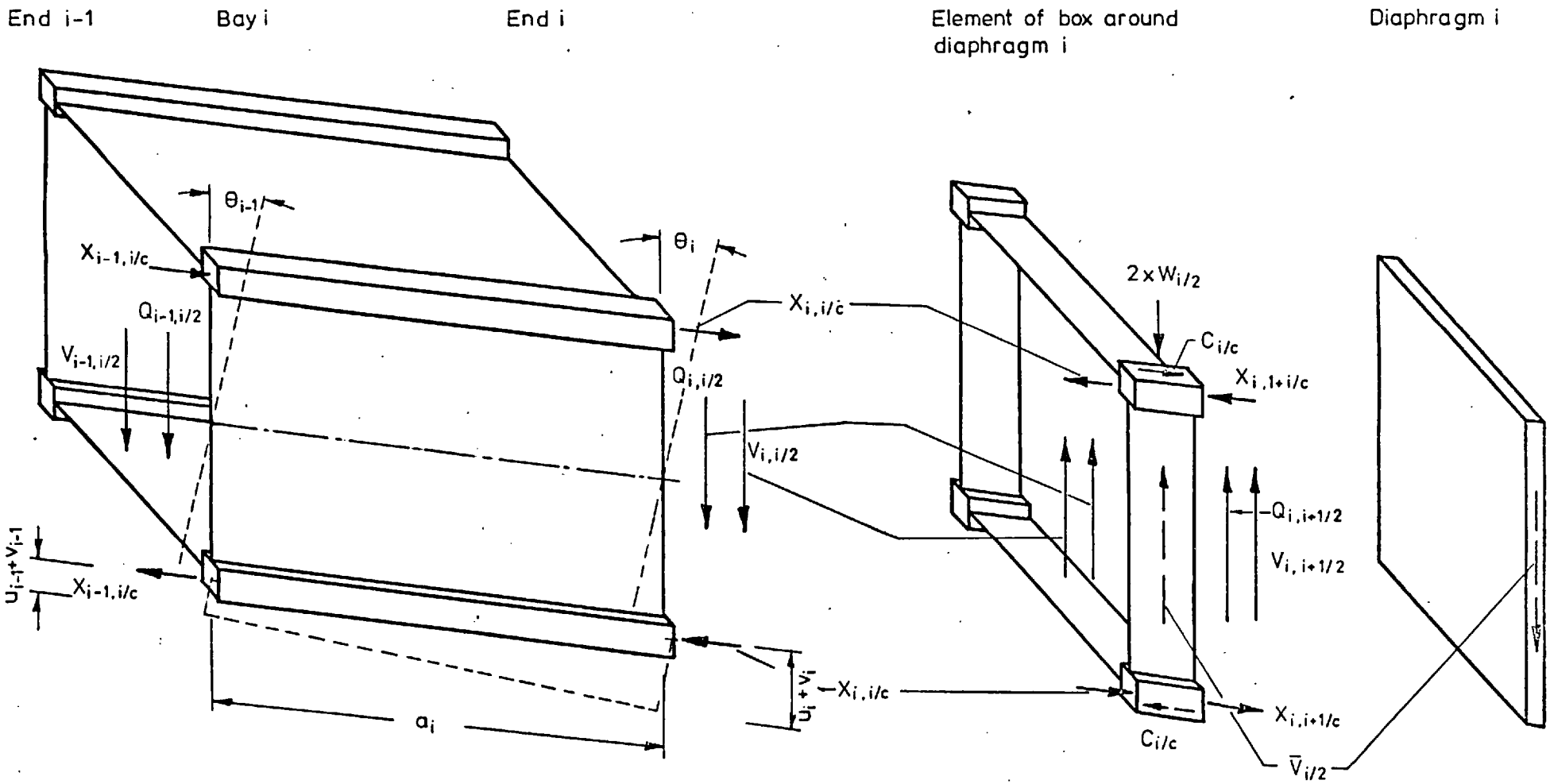


Fig. 2·2 Idealization of the box by Richmond's displacement method

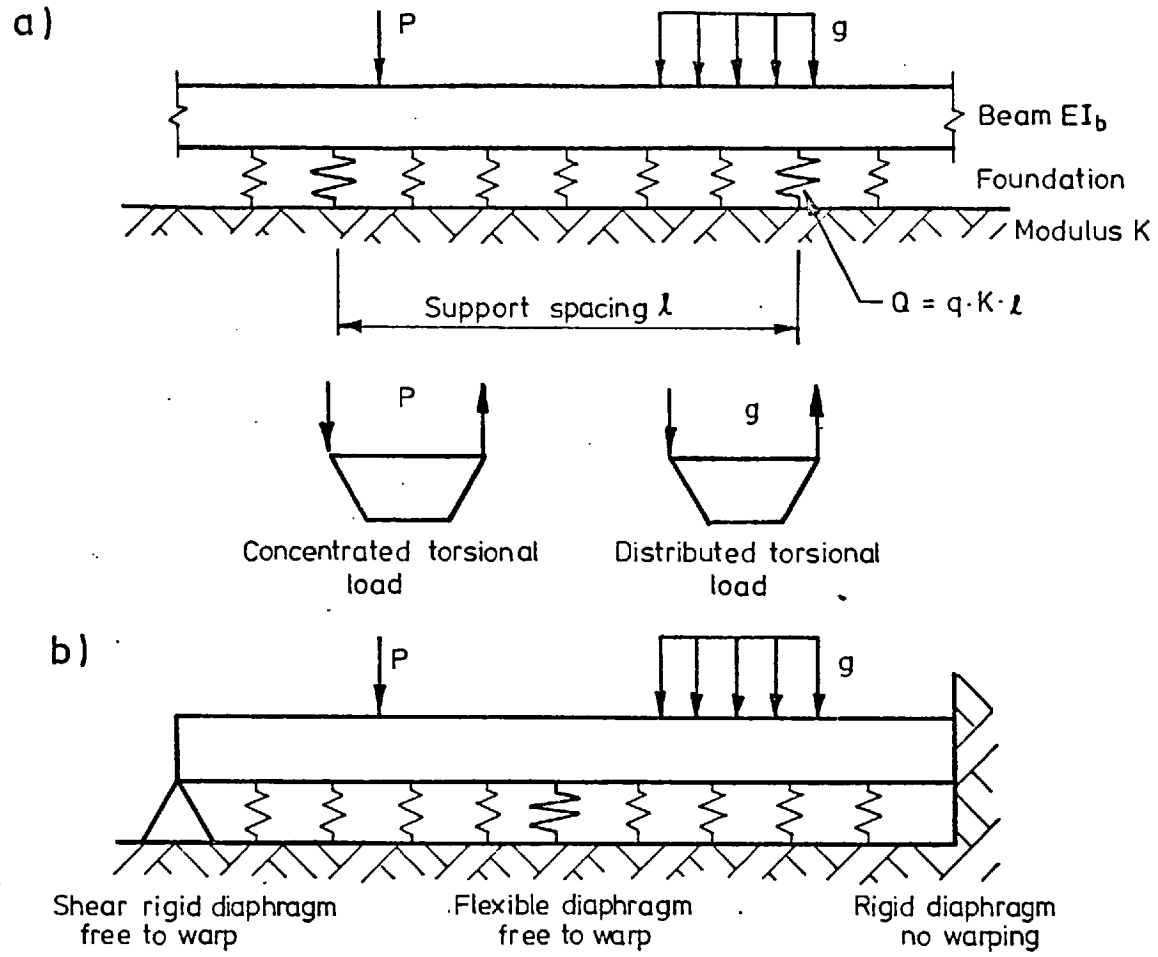
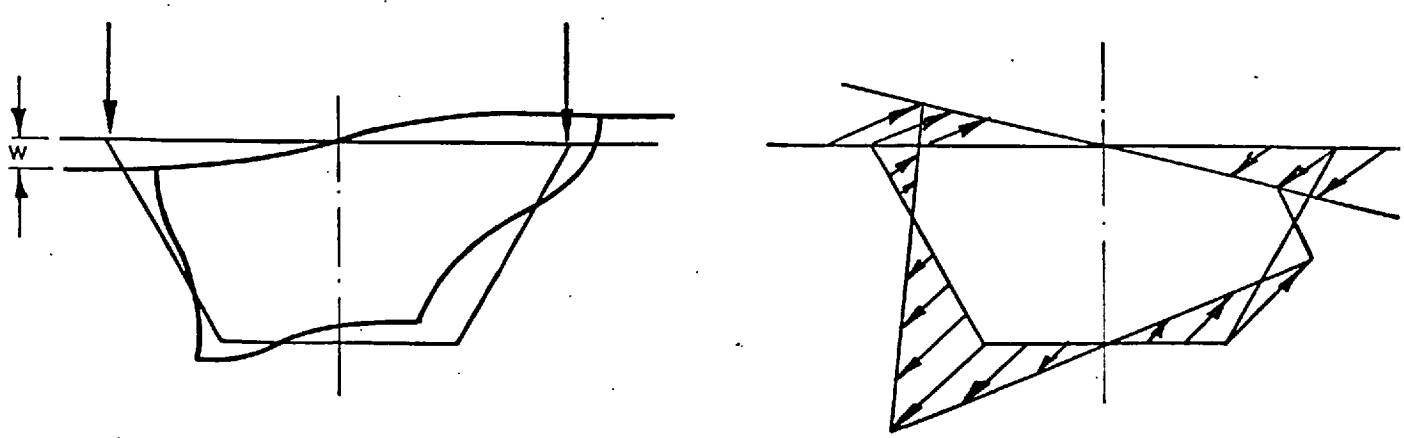


Fig. 2·3 Analogy between box girder and B.E.F.

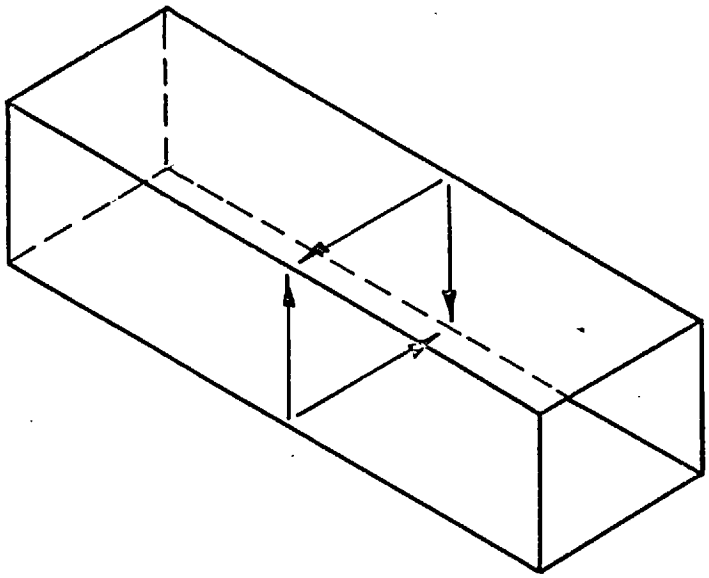


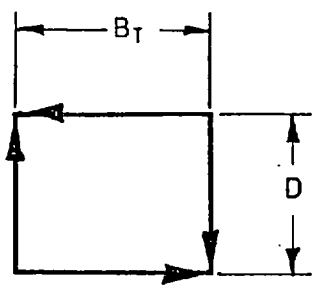
a) Deformation of cross-section

b) Warping stress pattern

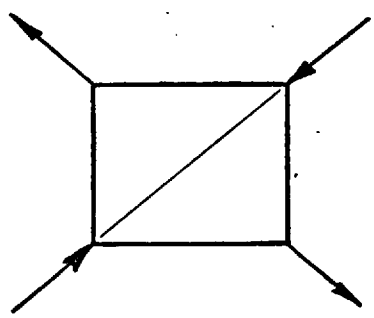
Fig. 2·4 Deformation of cross-section under anti-symmetrical load

a)



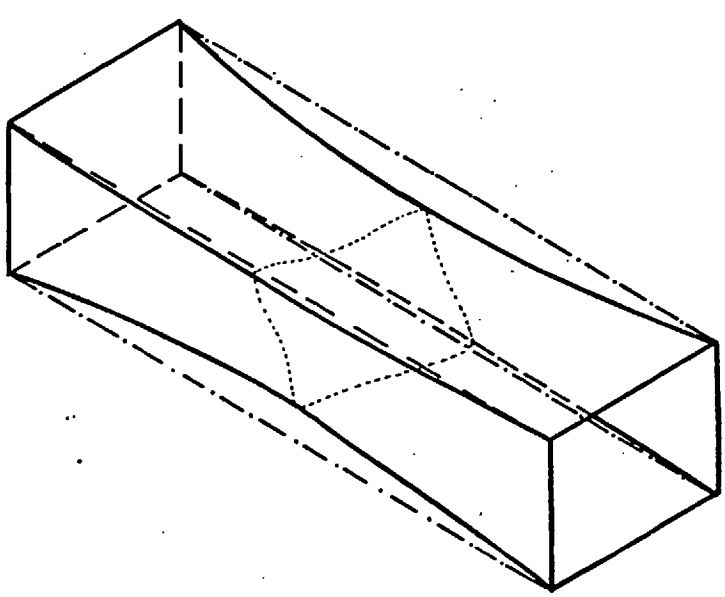


Distortional component of loading from Fig. 2·1c

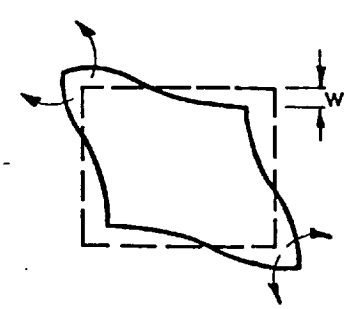


Distortional forces resolved at the corners of box girder

b)



Lozenging of box girder under distortional component of loading



Transverse distortional bending which causes transverse distortion stresse

Fig. 2·5 Distortion of box girder

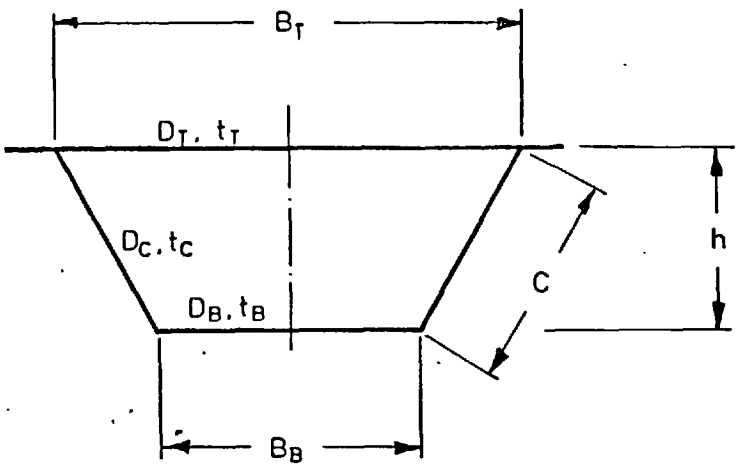
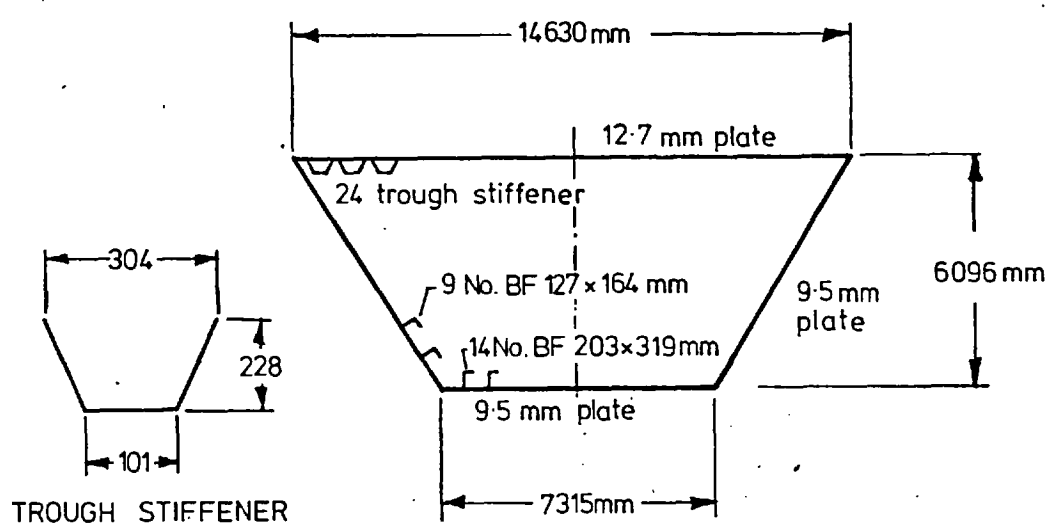


Fig. 2·6 Parameter of box girder cell



Span 64M Support Diaphragms 31·75 mm plate
No Intermediate Diaphragms

Cross frame at 4·572 M c/c	Top flange	381×9·5 mm
	Web	330×7·9 mm
	Bottom flange	330×7·9 mm

Fig. 2·7 Dimensions of analysed box

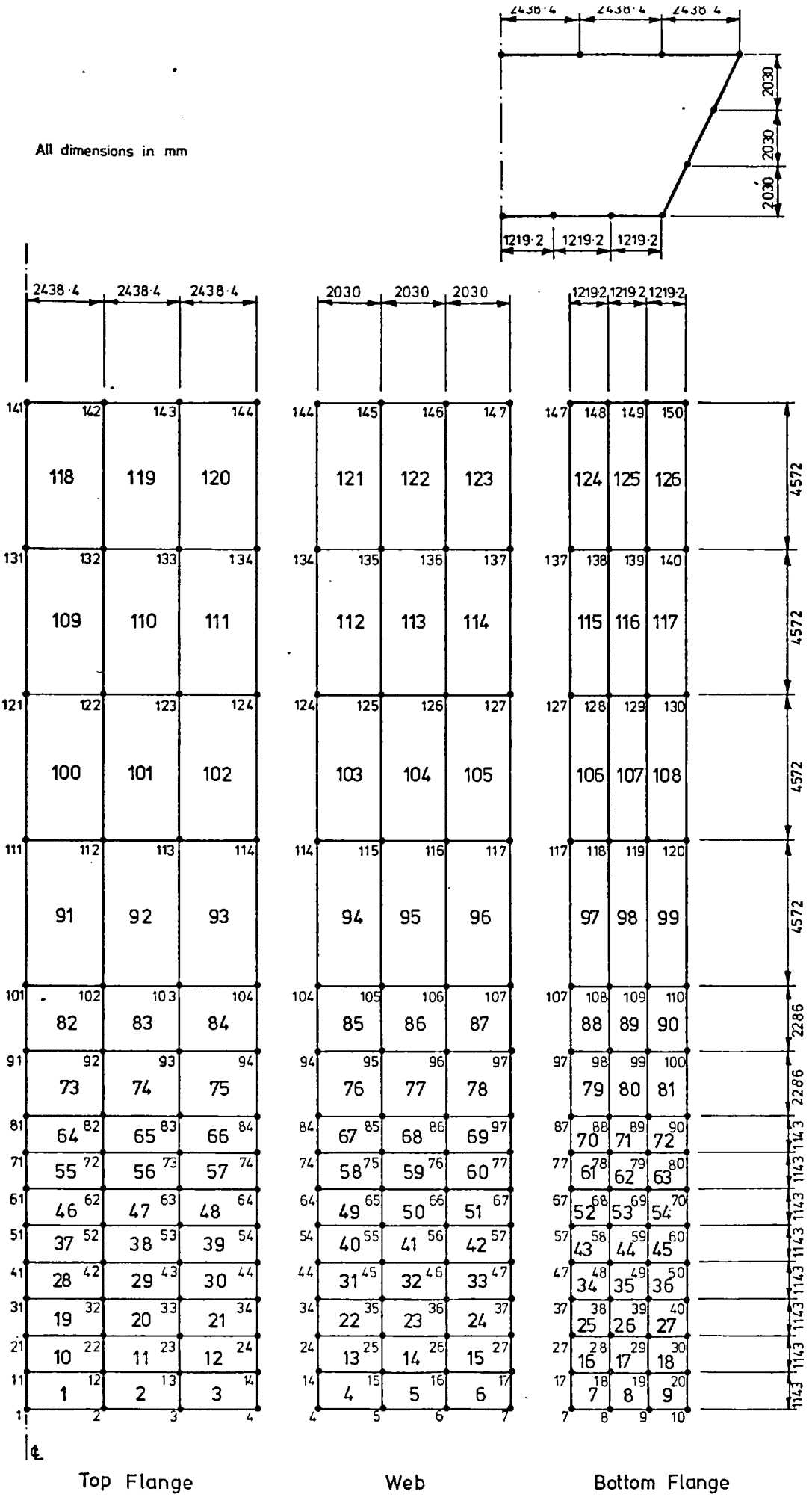
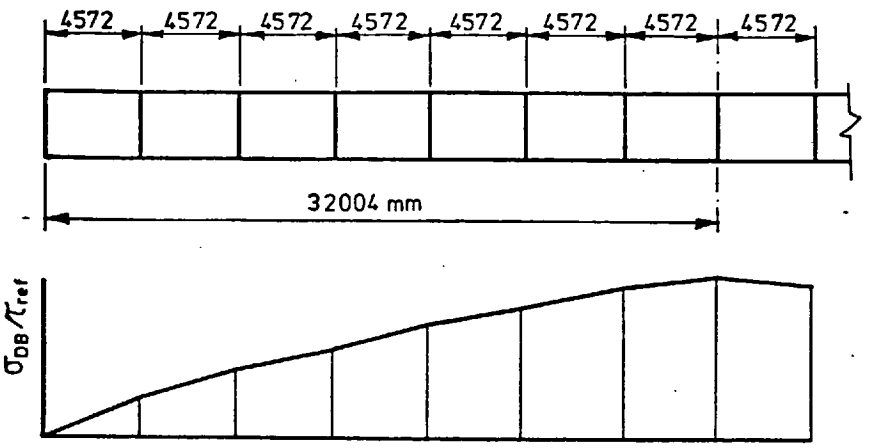
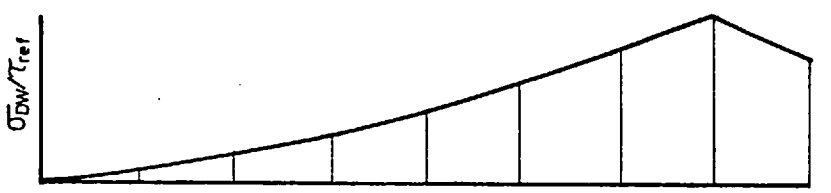


Fig. 2·8 Finite element mesh



0·0	7·776	16·838	25·089	32·409	38·634	42·023	45·212	42·023	F.E. Method
0·0	9·092	17·913	26·163	33·487	39·454	43·526	45·051	43·526	B.E.F. Method

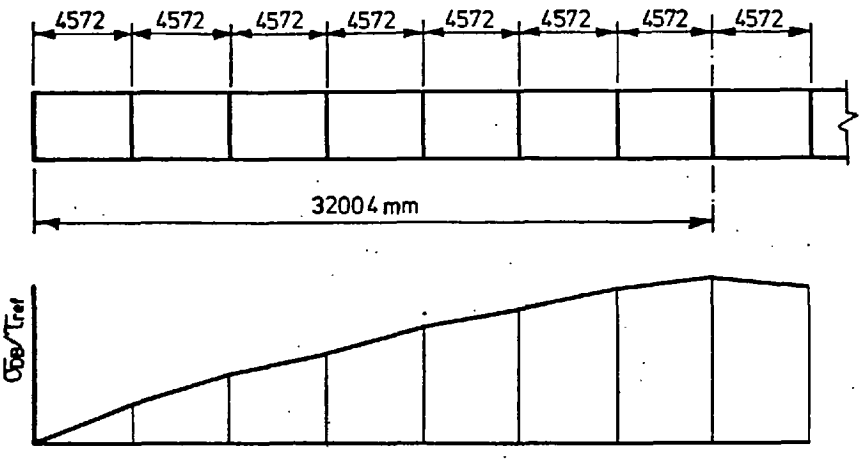
a) Comparison of σ_{DB} of F.E. and B.E.F. methods



0·0	0·523	1·140	1·800	2·618	3·627	5·158	6·587	5·158	F.E. Method
0·0	0·553	1·163	1·880	2·771	3·867	5·208	6·820	5·208	B.E.F. Method
0·0	0·377	0·811	1·359	2·076	3·011	4·204	5·686	4·204	Richmond's Displacement Method

b) Comparison of σ_{DW} of F.E. B.E.F. and Richmond's Displacement

Fig. 2·9 Longitudinal distribution of transverse distortional bending σ_{DB} and distortional warping σ_{DW} stresses for central concentrated load



0·0	5·687	11·994	17·247	21·392	24·455	25·612	26·285	25·612	F.E. Method
0·0	6·361	12·315	17·544	21·815	24·975	26·907	27·560	26·907	B.E.F. Method

a) Comparison of σ_{DB} of F.E. and B.E.F. methods



0·0	0·822	1·507	1·927	2·226	2·433	2·545	2·580	2·545	F.E. Method
0·0	0·855	1·500	1·972	2·302	2·518	2·640	2·679	2·640	B.E.F. Method
0·0	0·725	1·238	1·599	1·842	1·995	2·079	2·105	2·079	Richmond's Displacement Method

b) Comparison of σ_{DW} of F.E., B.E.F. and Richmond's Displacement methods.

Fig. 2·10 Longitudinal distribution of transverse distortional bending σ_{DB} and distortional warping σ_{DW} stresses for U.D.L.

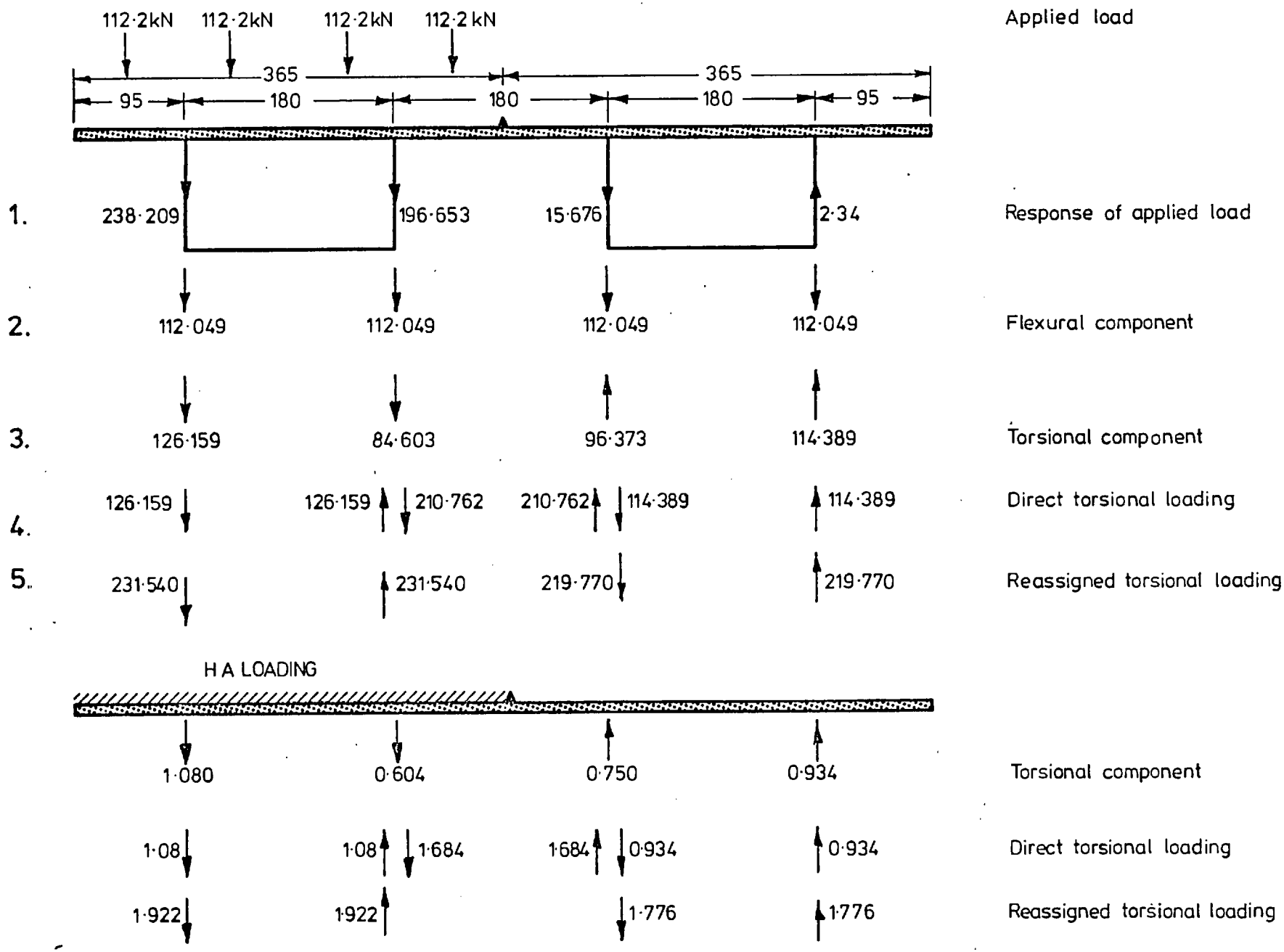


Fig. 2·11 Example of load distribution method for multibox structures

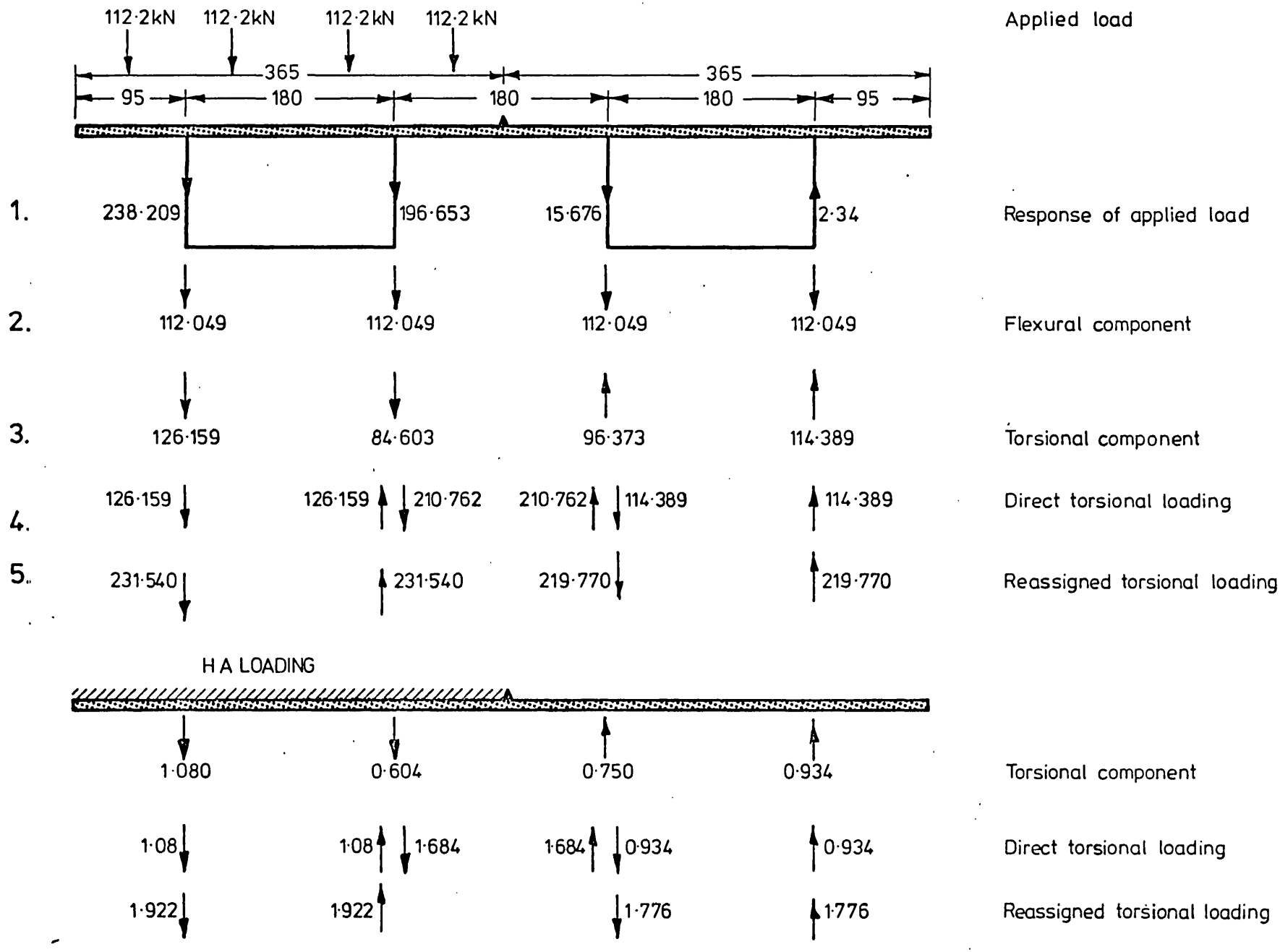


Fig. 2·11 Example of load distribution method for multibox structures

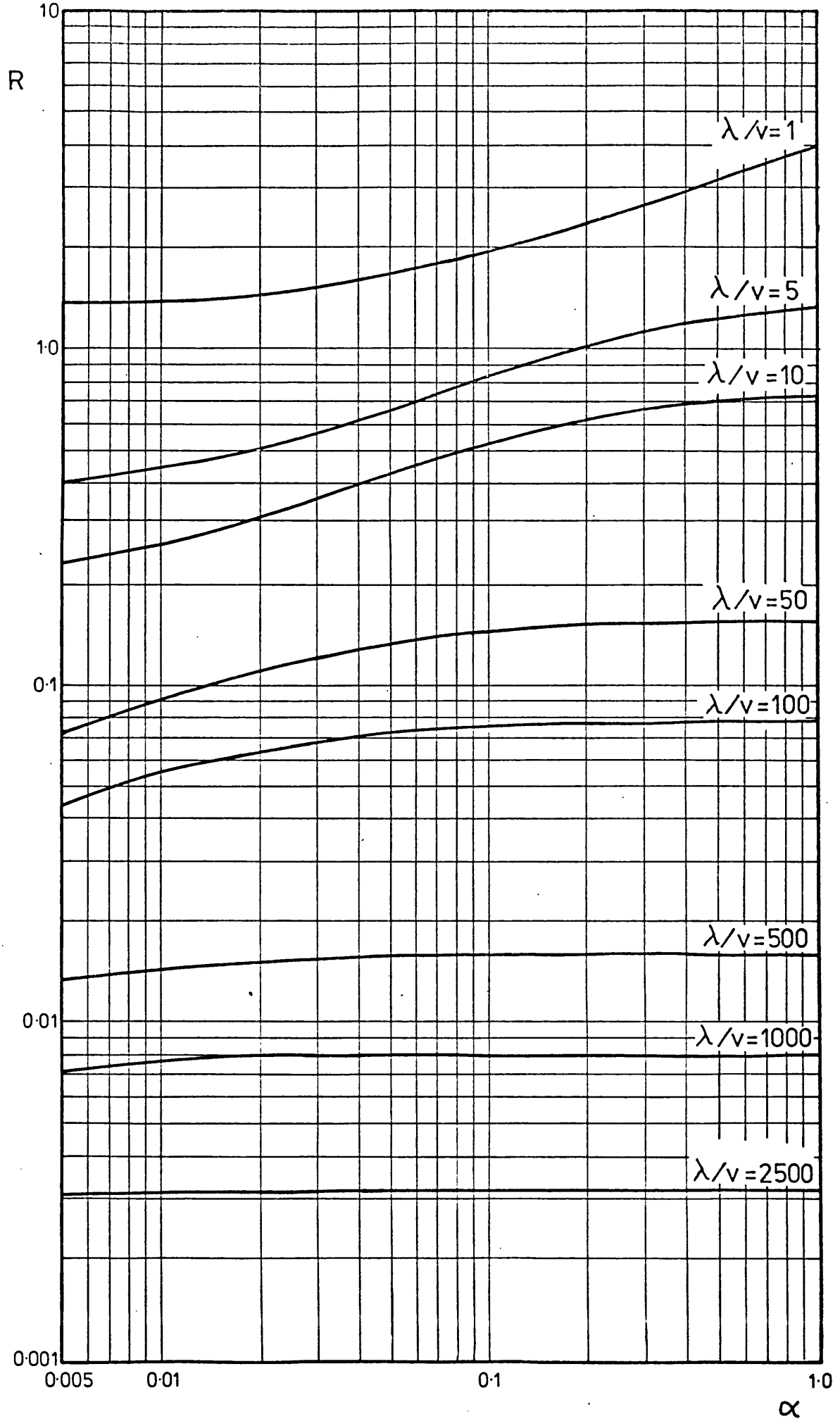


Fig. I-1 Simplification of β calculations for rectangular box i.e. $\alpha = 1$

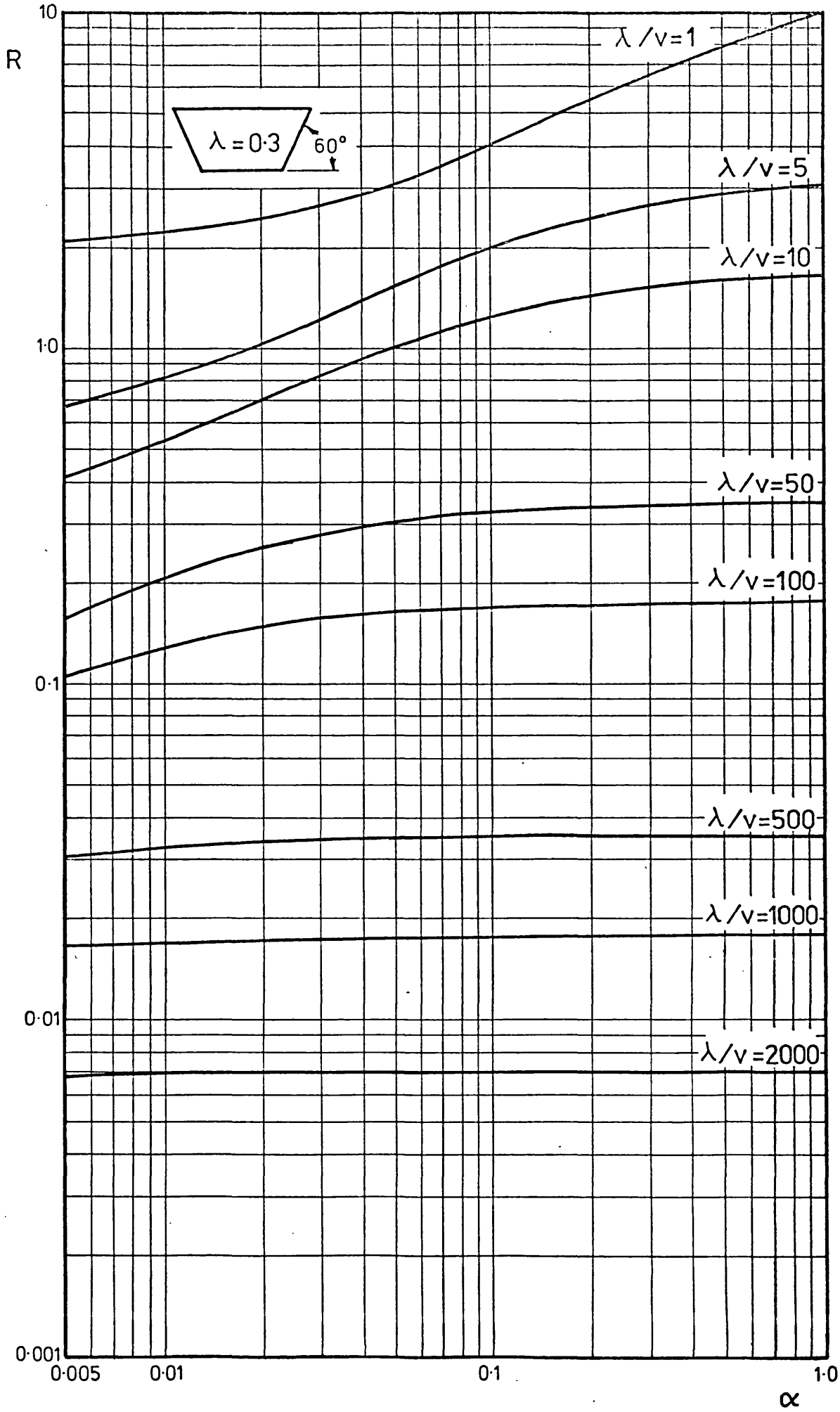


Fig. I-2 Simplification of β calculations for 60° trapezoidal box when λ = 0·3

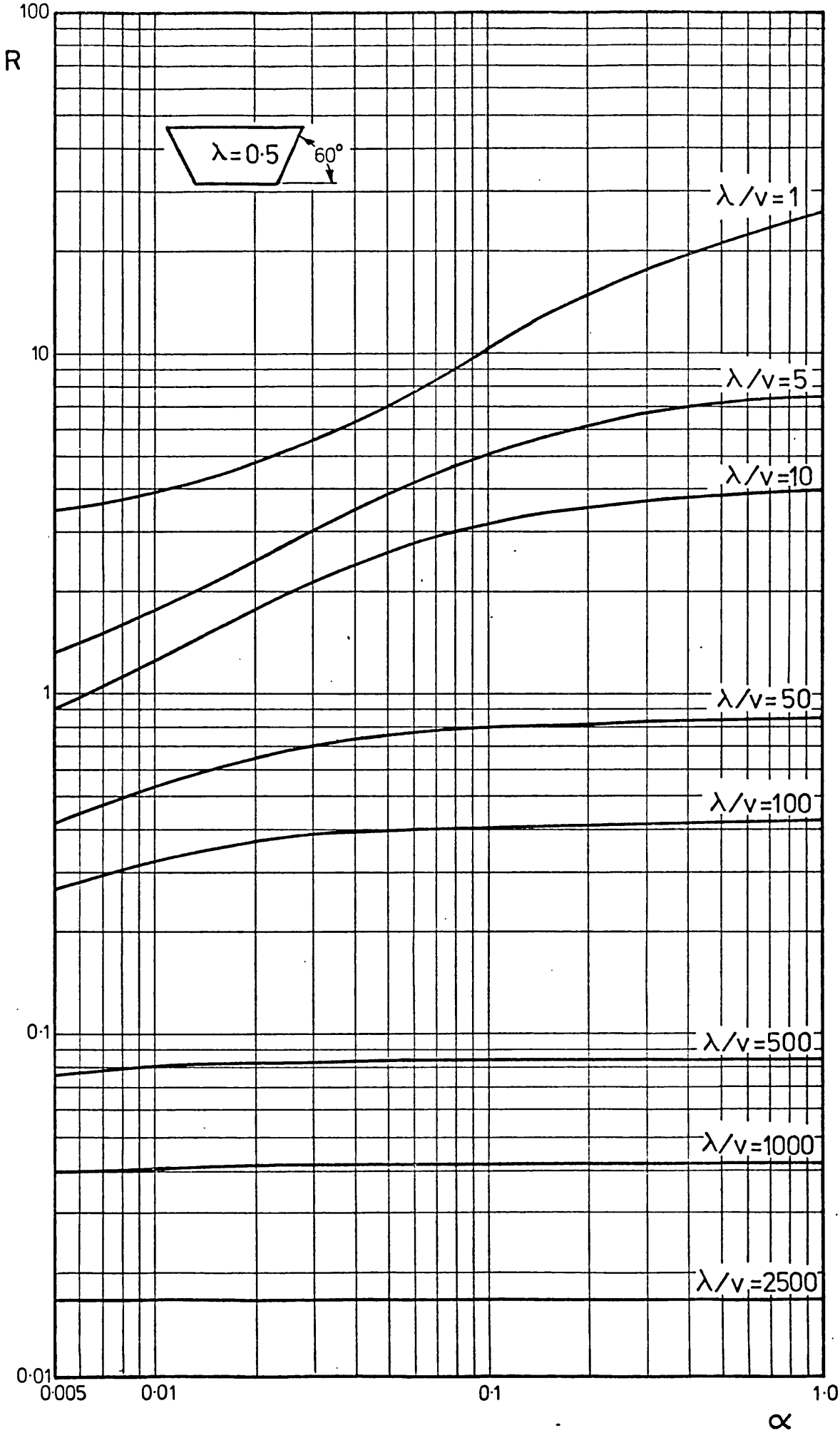


Fig. I-3 Simplification of β calculations for 60° trapezoidal box when $\lambda = 0{\cdot}5$

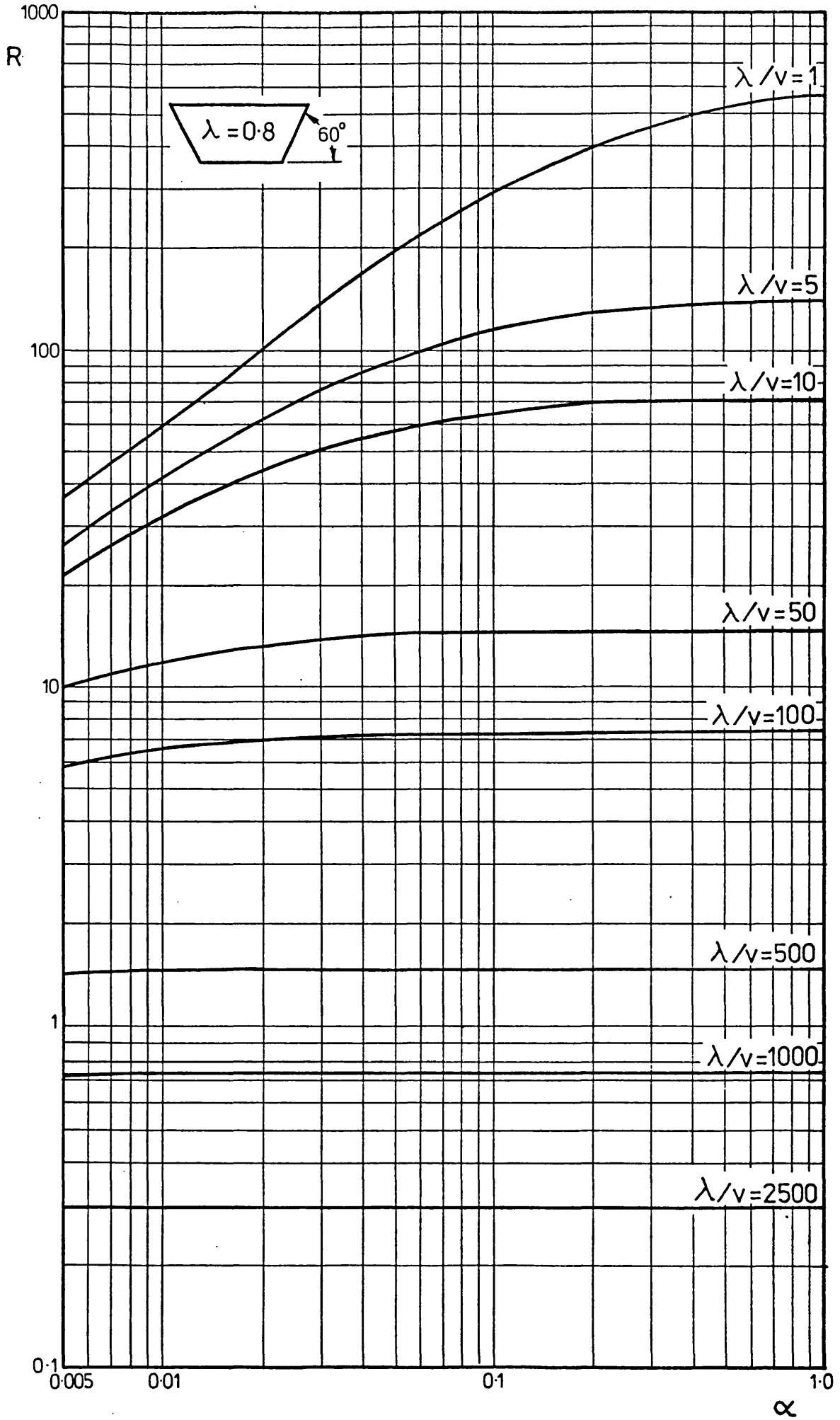


Fig. I-4 Simplification of β calculations for 60° trapezoidal box when λ = 0·8

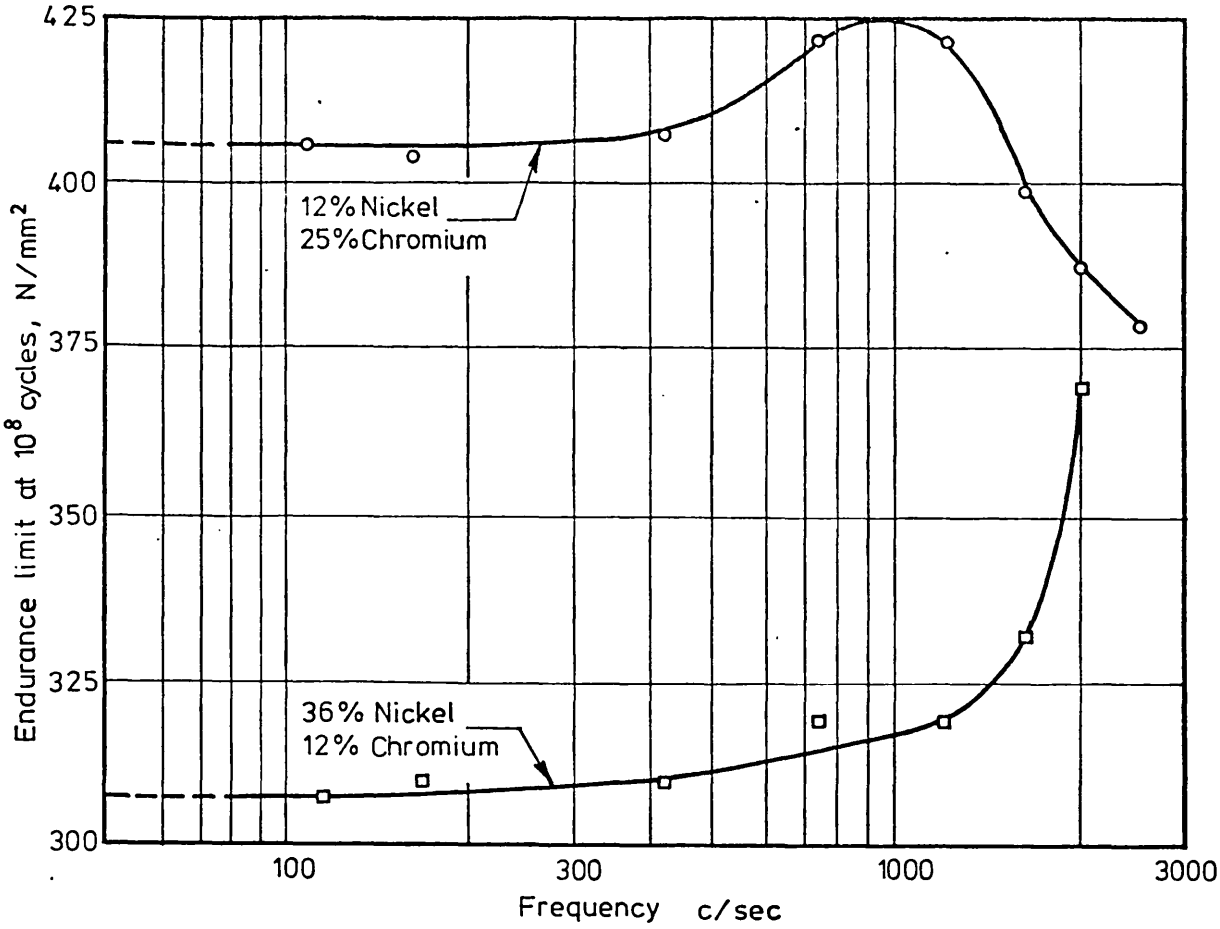


Fig. 3·1 The effect of frequency on endurance limits for alloy steels. (3·4)

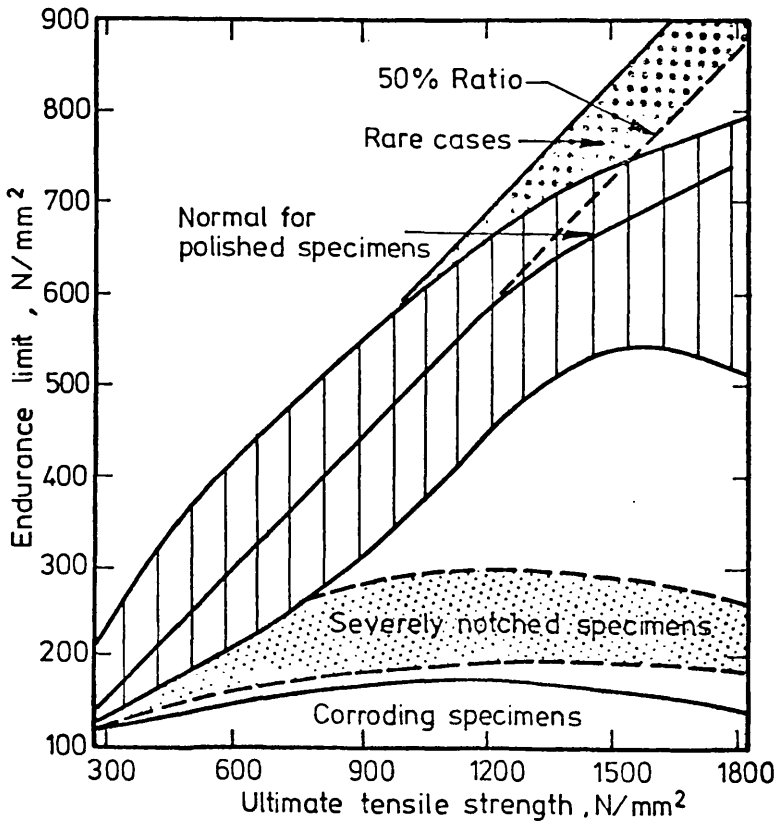


Fig. 3·2 Relationship between the endurance limit and ultimate tensile strength of various steels. (3·25)

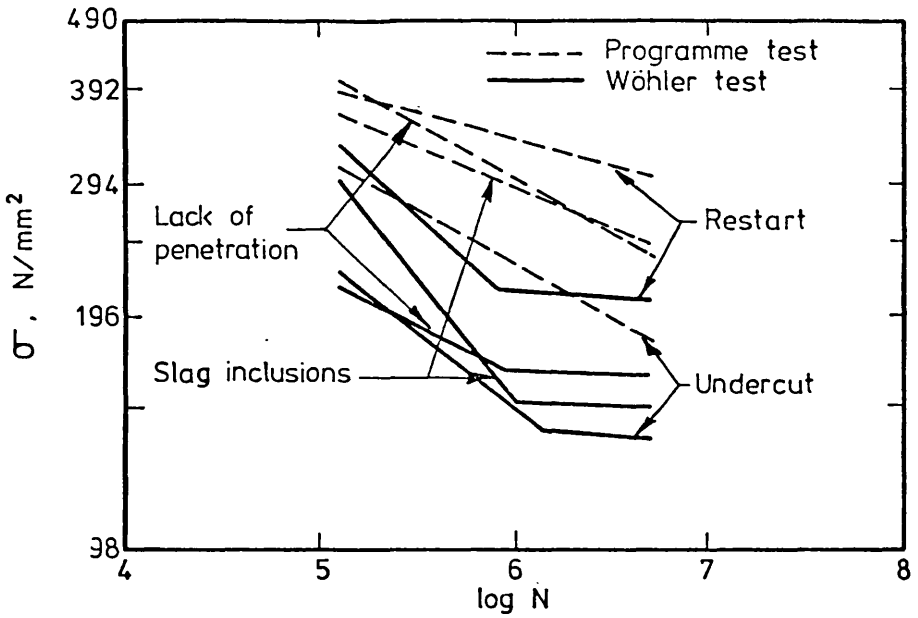


Fig. 3·3 Results of Wöhler and programme tests with specimens containing different defects. (3·15)

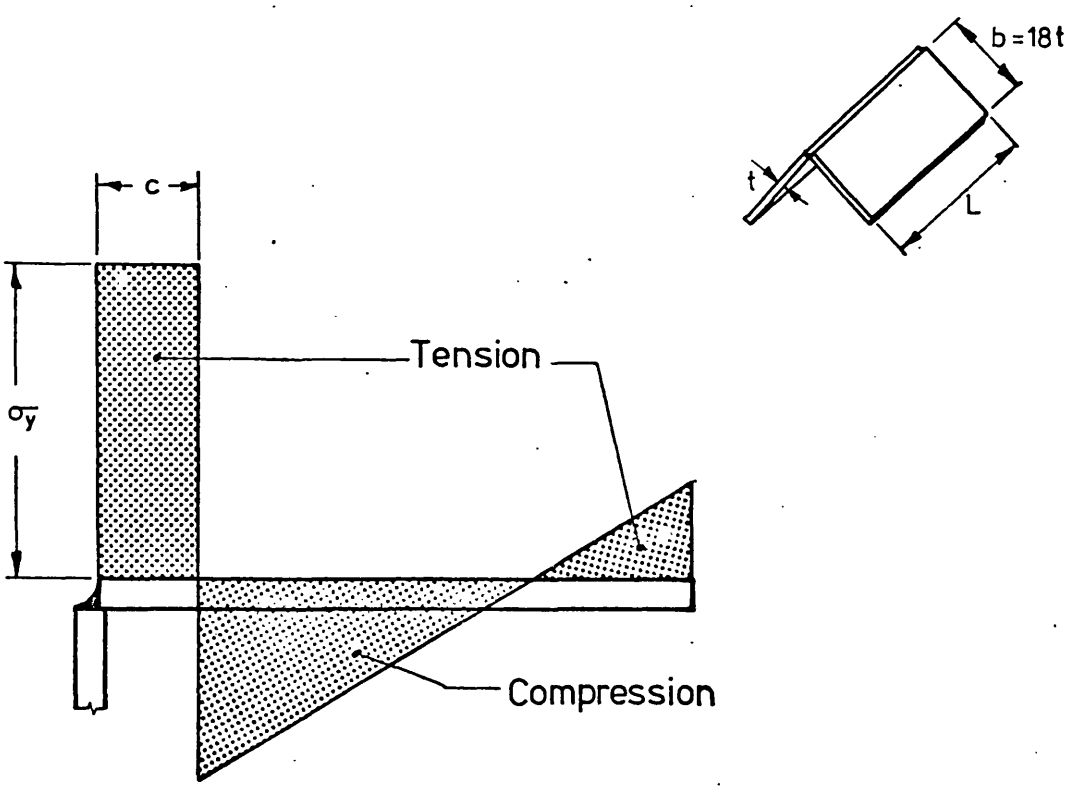


Fig. 3·4 Typical residual stress pattern in welded plates (3·16, 3·17)

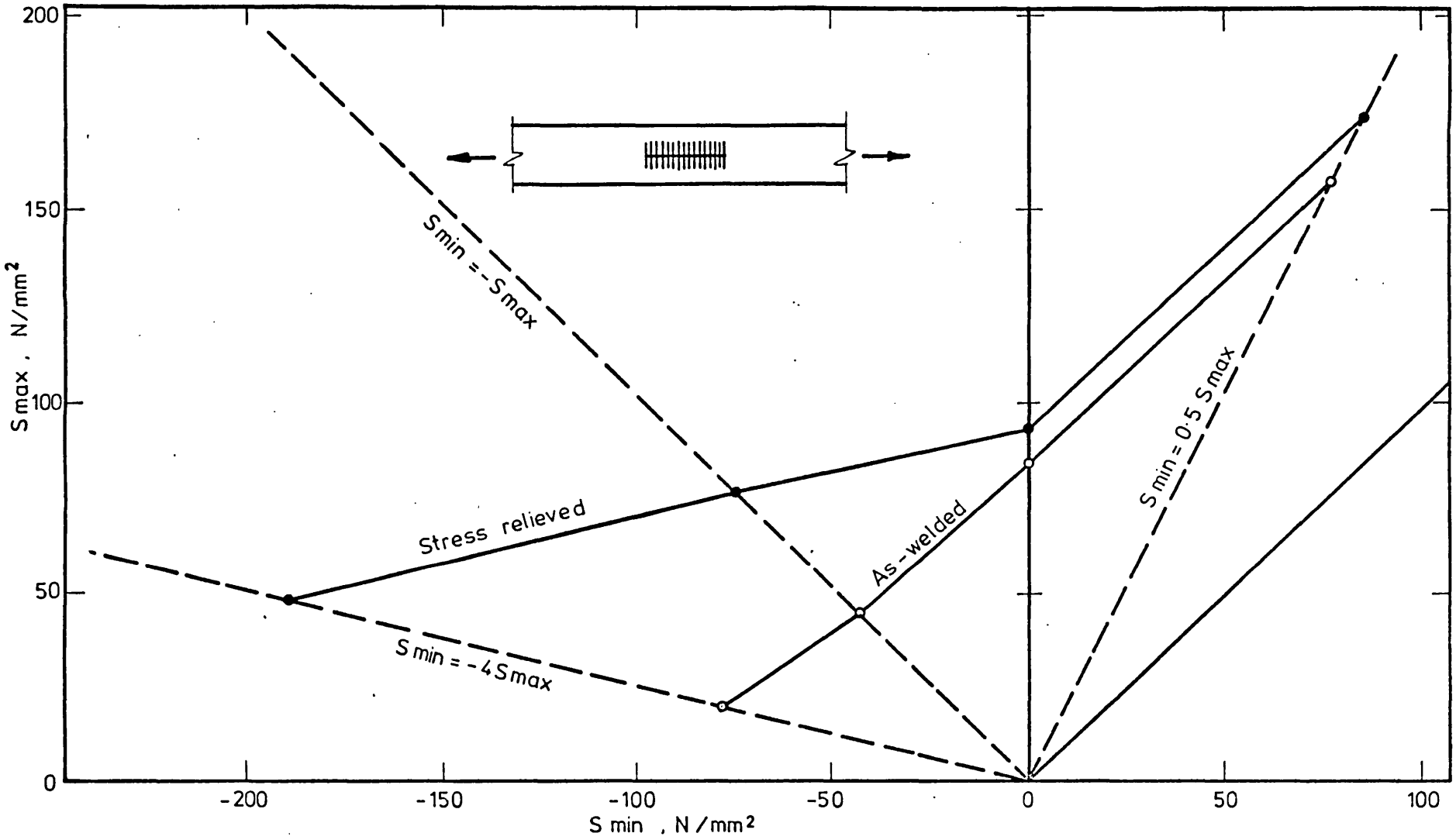
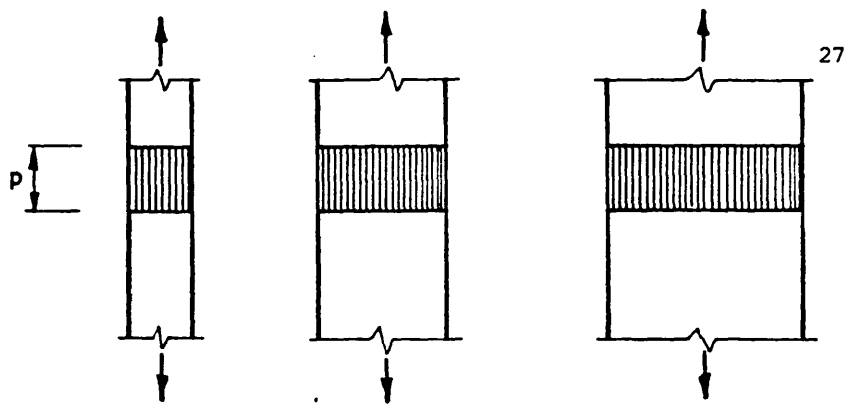


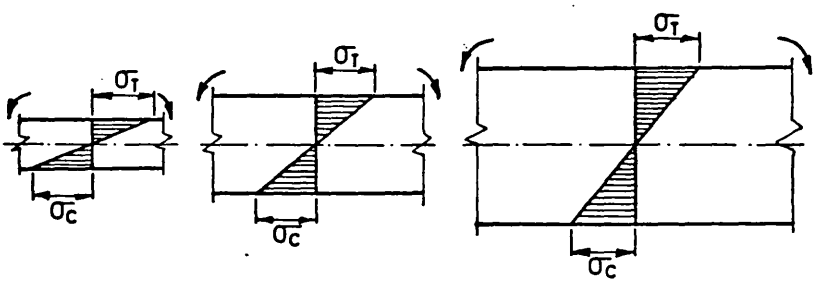
Fig. 3·5 Effect of stress relief on the fatigue strength at 2×10^6 cycles of fillet welded mild steel specimens. (3·1)



Stress to cause failure for a given life $(\sigma_A)_1$ $(\sigma_A)_2$ $(\sigma_A)_3$

No size effect $(\sigma_A)_1 = (\sigma_A)_2 = (\sigma_A)_3$

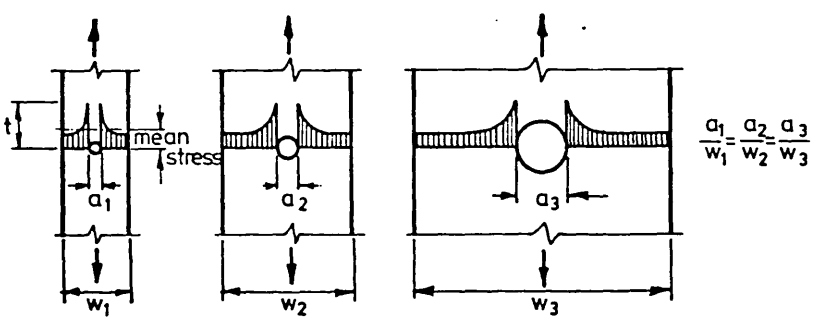
Case 1 - Axially loaded specimens



Stress to cause failure for a given life $(\sigma_B)_1$ $(\sigma_B)_2$ $(\sigma_B)_3$

Size effect present $(\sigma_B)_1 > (\sigma_B)_2 > (\sigma_B)_3$

Case 2 - Specimens in bending

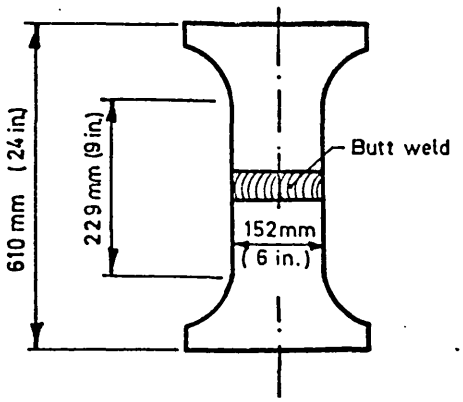


Nominal stress on net. section to cause failure for a given life $(\sigma_N)_1$ $(\sigma_N)_2$ $(\sigma_N)_3$

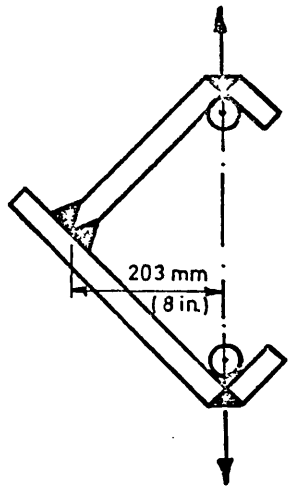
Size effect present $(\sigma_N)_1 > (\sigma_N)_2 > (\sigma_N)_3$

Case 3 - Notched specimens

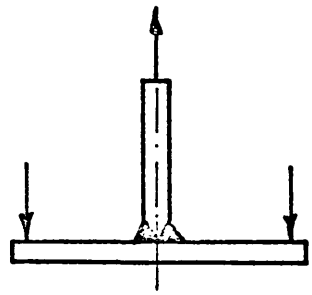
Fig. 3·6 Size effect on fatigue behaviour related to the stress gradient



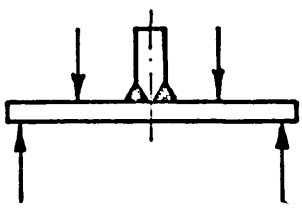
a) Axial full thickness butt weld



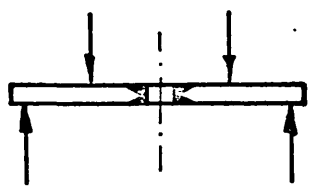
b) Knee bend full thickness tee butt welded



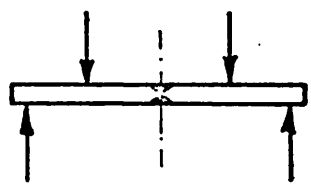
c) Three point bend full thickness tee butt weld



d) Four point bend through thickness tee butt weld



e) Four point bend through thickness



f) Four point bend butt weld

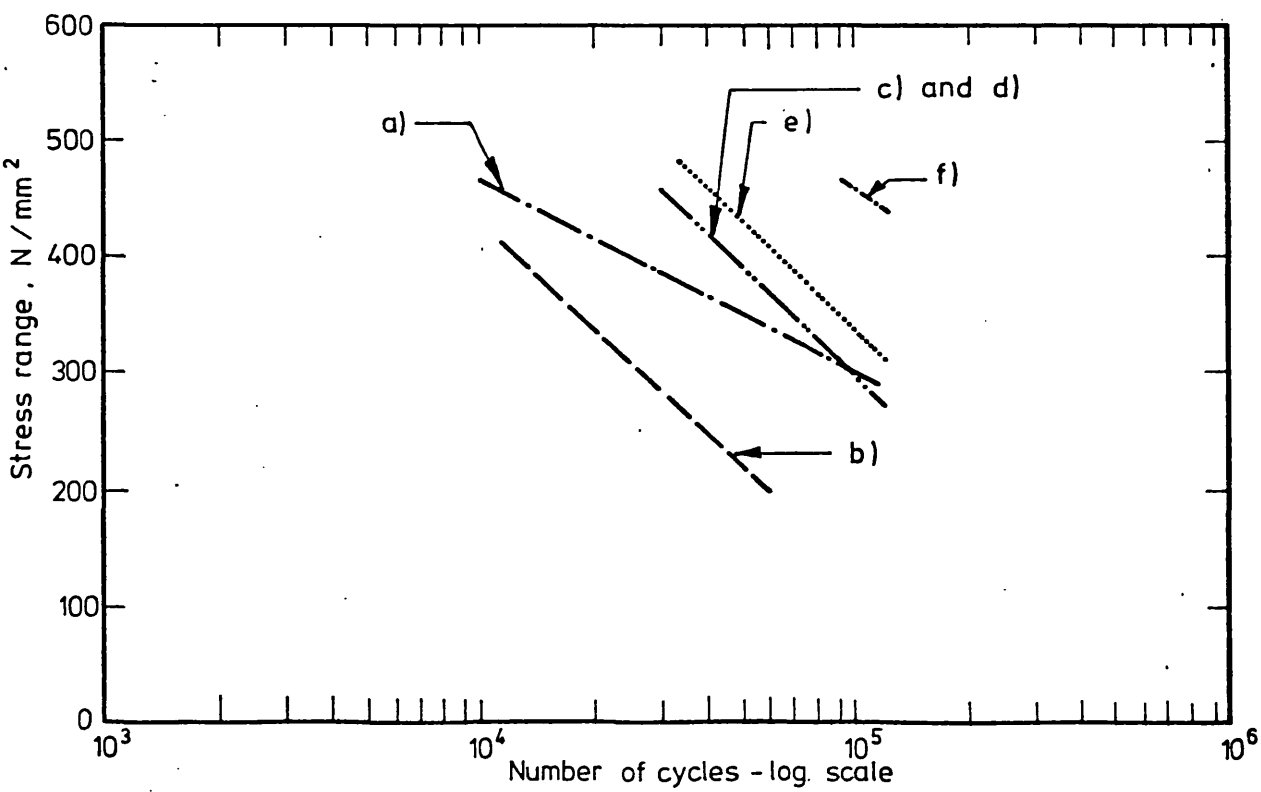


Fig. 3·7 Generalized results from Q.T. 35 type tests (zero-tension stress cycles) showing the shape effect on fatigue (3·23)

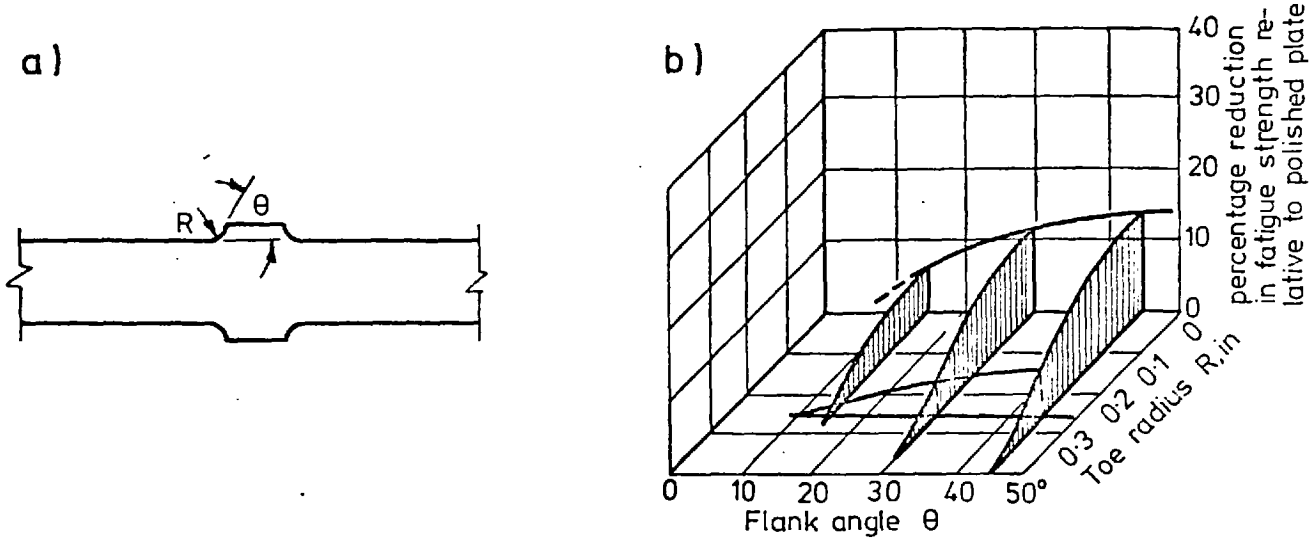


Fig. 3·8 The effect of reinforcement shape in tests on parent metal specimens, type shown in Fig. a, subjected to alternating loading ±25 KSI (3·30)

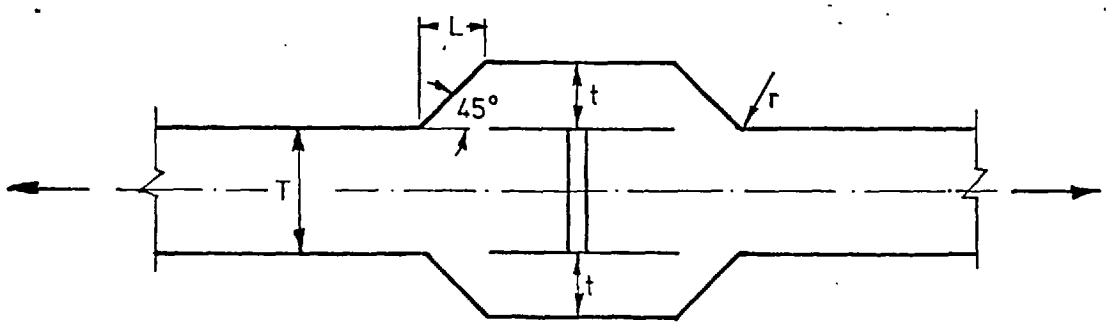
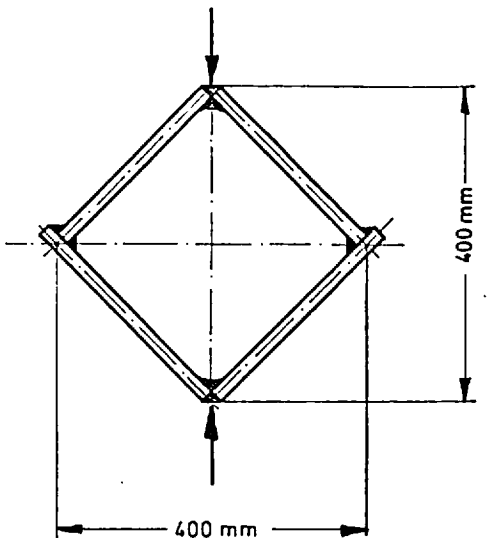
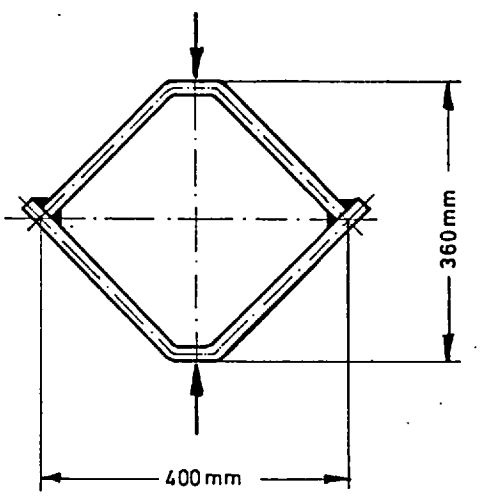


Fig. 3·9 Details of photoelastic model used to study transverse load-carrying fillet welds. (3·20)



A) Four corner welded specimen



B) Two corner welded specimen (two bent plates). For details see drawing No. 4-1

Fig. 4-1 Typical test specimens.

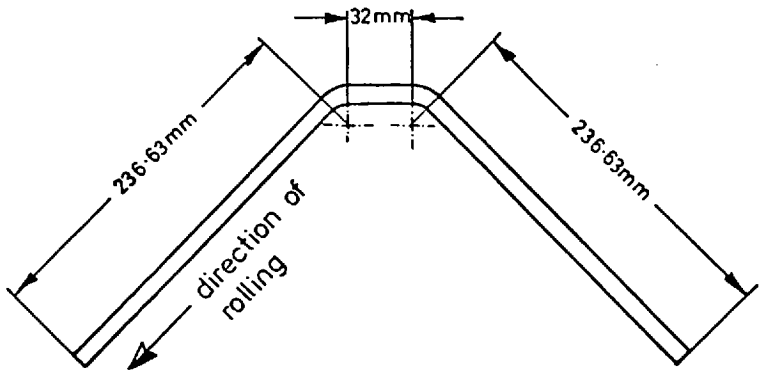


Fig. 4·2 Bent plate used in the specimen
For detail see Drawing No. 4·1

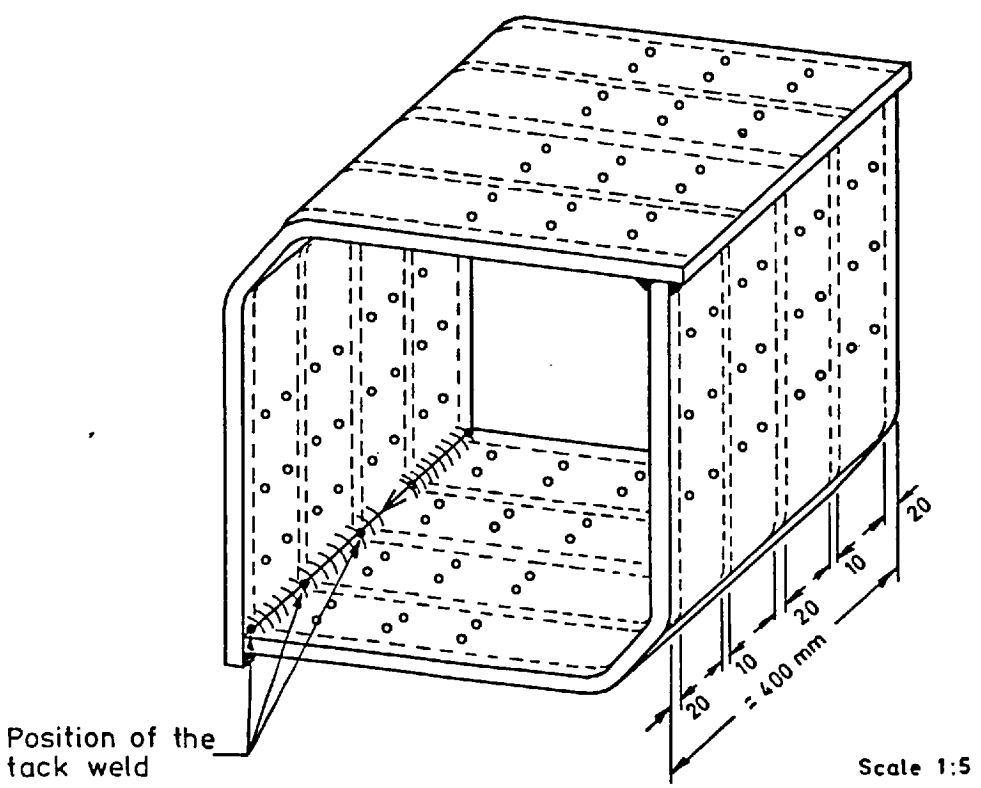


Fig. 4·3 General view and dimensions of the welded specimen before cutting to final size

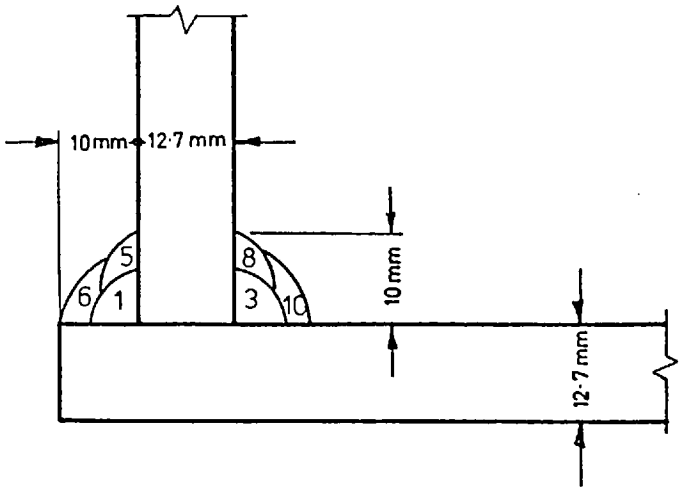


Fig. 4·4 Typical weld detail of the double fillet weld and its sequence of welding runs (Series BEDFW).

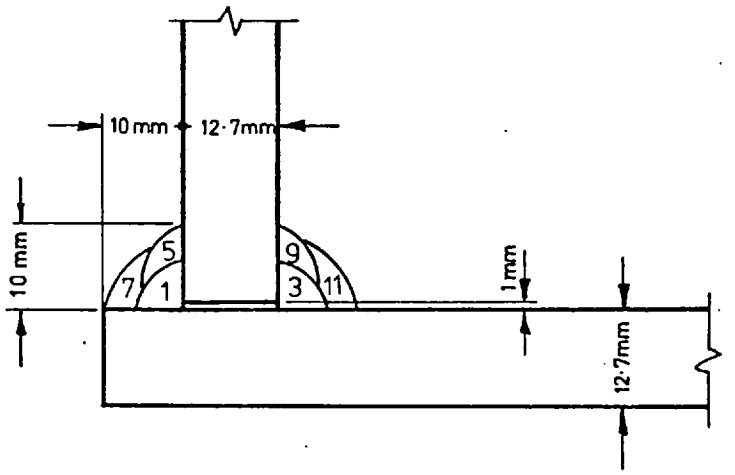


Fig. 4·5 Typical weld detail and sequence of welding runs for series BEDFG

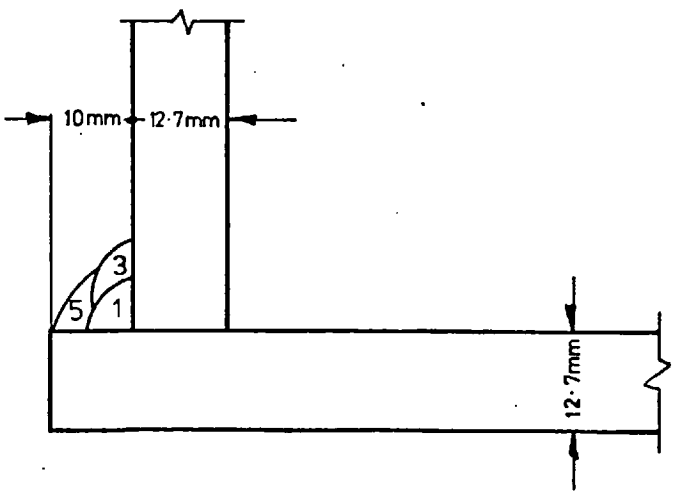


Fig. 4·6 Typical detail of the single fillet weld and its sequence of welding runs (Series BESFW).

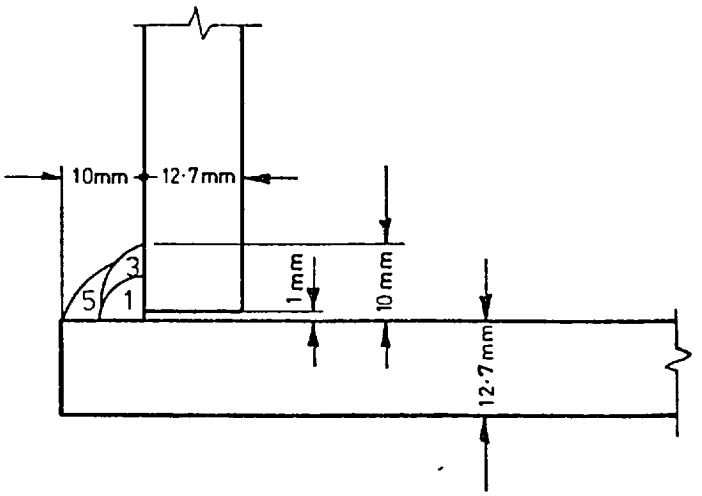


Fig. 4·7 Typical detail and welding sequence of series BESFG.

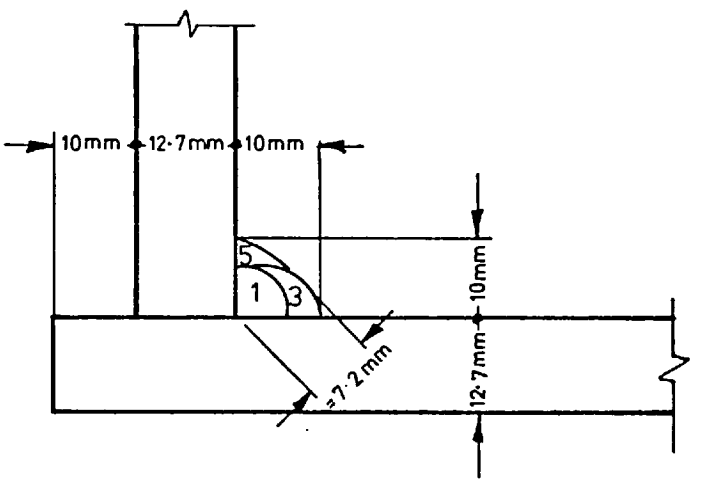


Fig. 4·8 Typical detail of the single fillet weld without gap between plates and its sequence of welding runs (Series BESFW I)

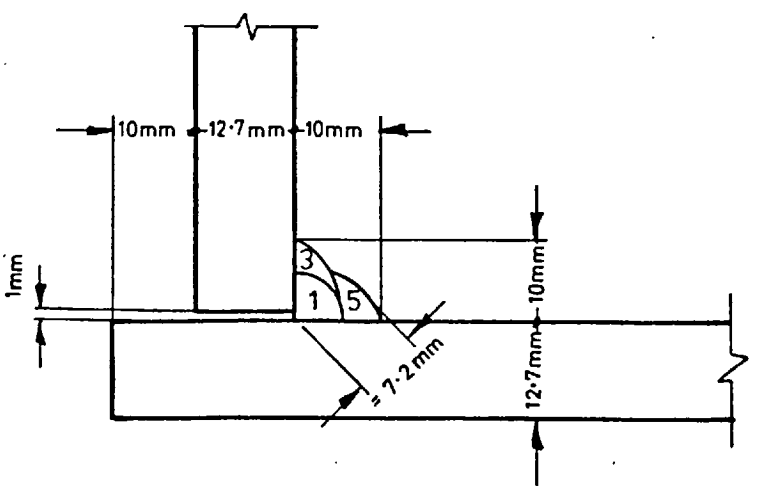


Fig. 4·9 Typical detail of the single fillet weld with gap between plates and its sequence of welding runs (Series BESFG I)

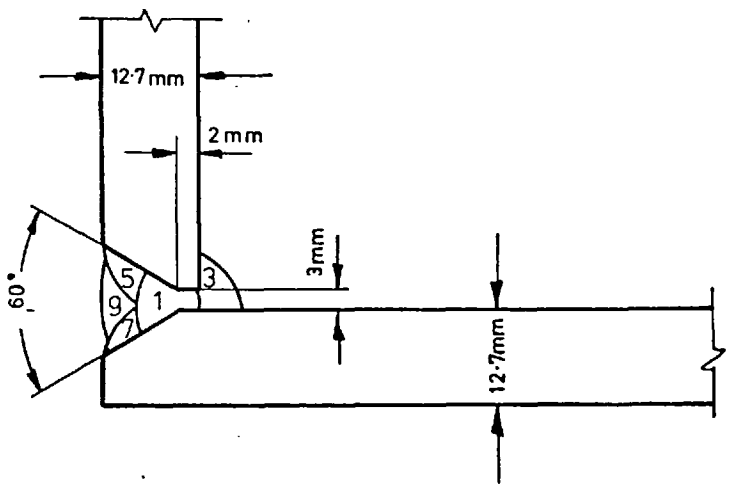


Fig. 4·10 Typical detail of the V- butt weld with its sequence of welding runs (Series BEVBS)

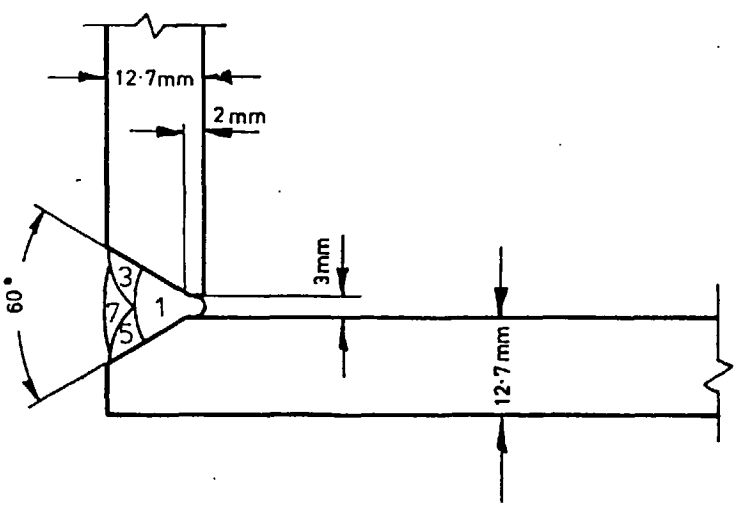


Fig. 4·11 Typical detail of V- butt weld without sealing run with its sequence of welding (Series BEVB)

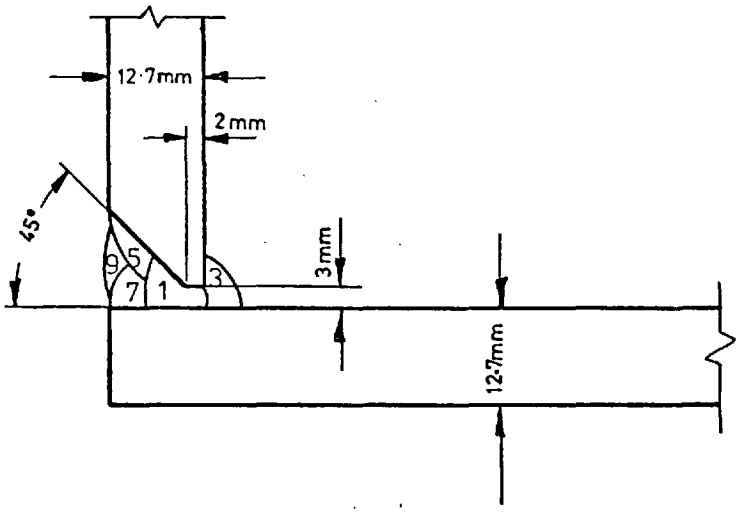


Fig. 4·12 Typical detail of the single bevel V-butt weld with its sequence of welding runs (Series BESBS)

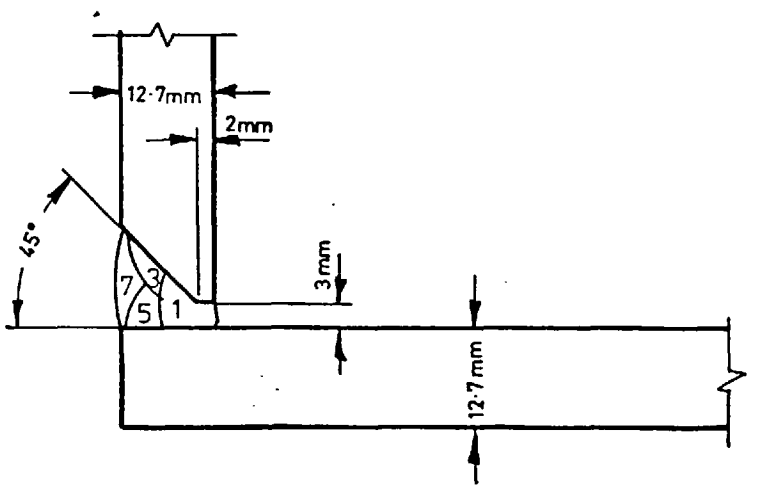


Fig. 4·13 Typical detail of single V-butt weld without sealing run with its sequence of welding runs (Series BESB)

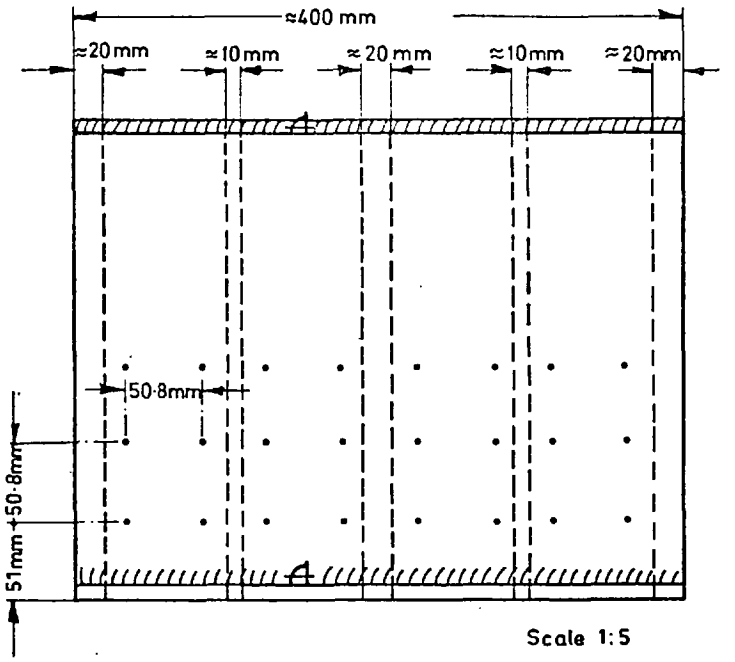


Fig.4·14 Location of the Demec Extensometer.

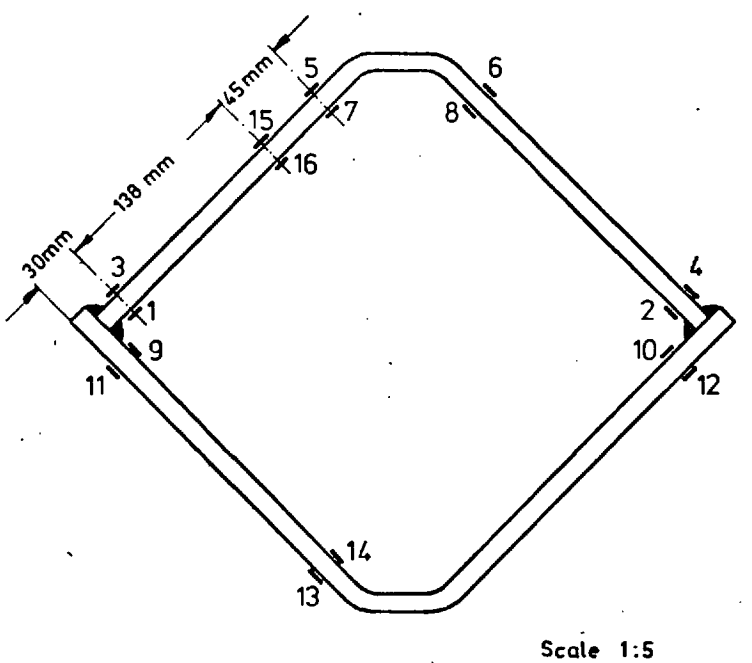


Fig.4·15 Positions of the strain gauges for static test.

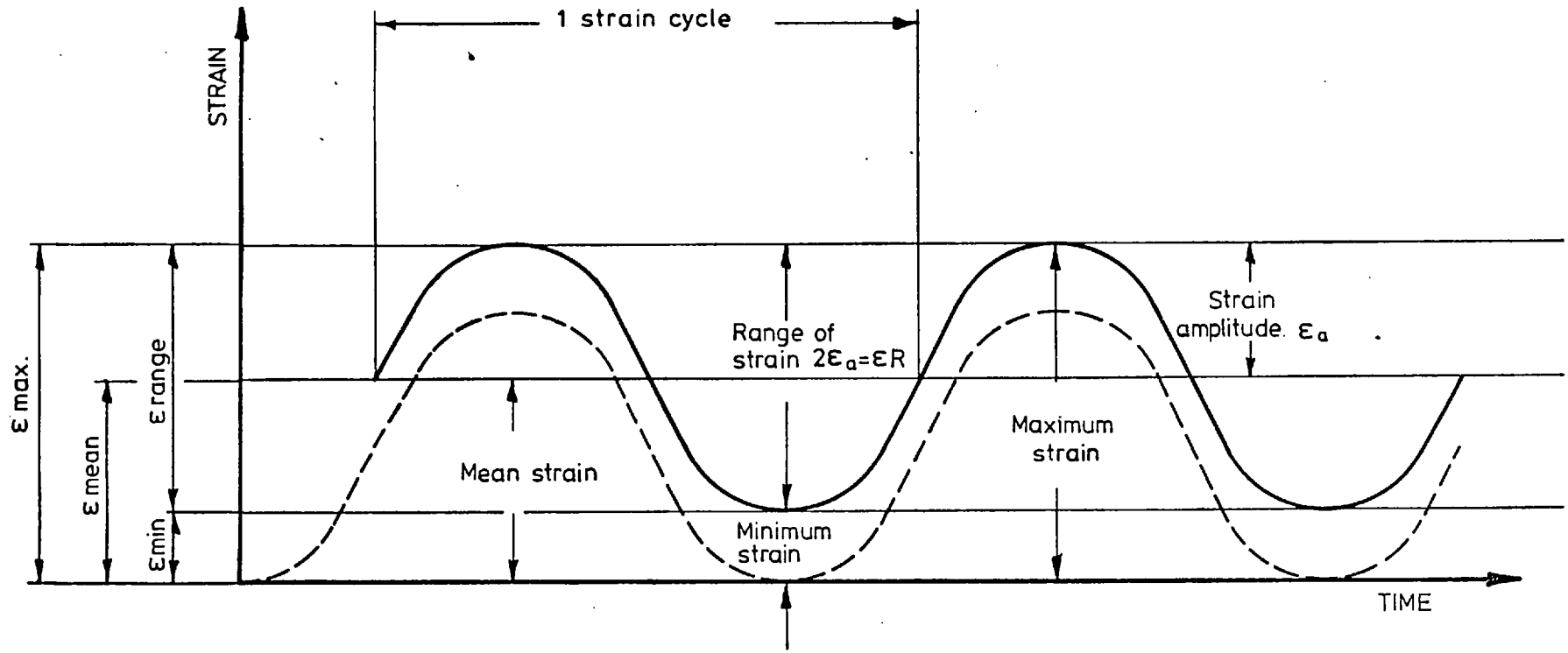


Fig. 4·16 Fatigue stress cycle

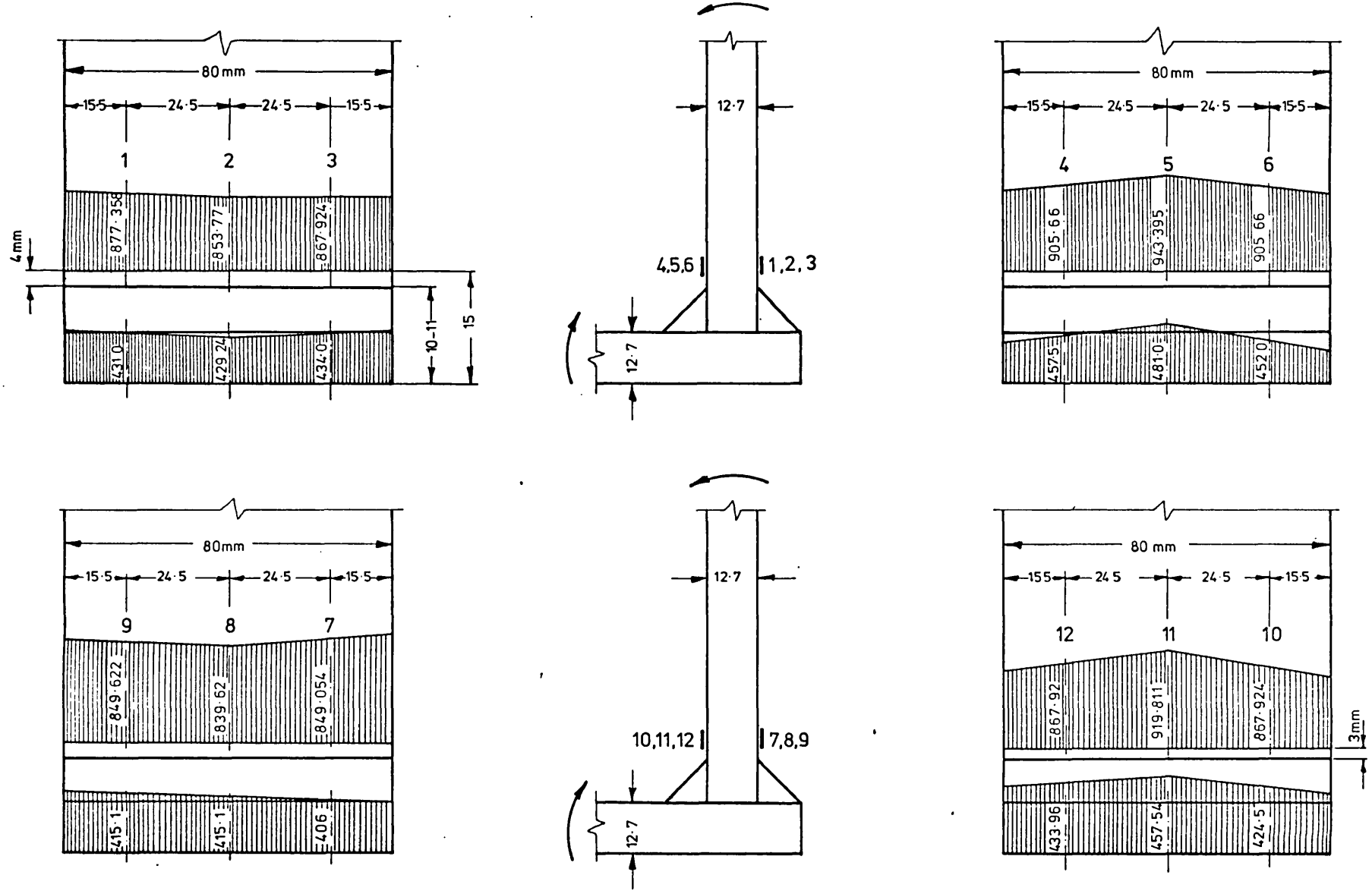


Fig. 4·17 Strain distribution along the toe of the weld for series BEDFW (the values are in micro-strain)

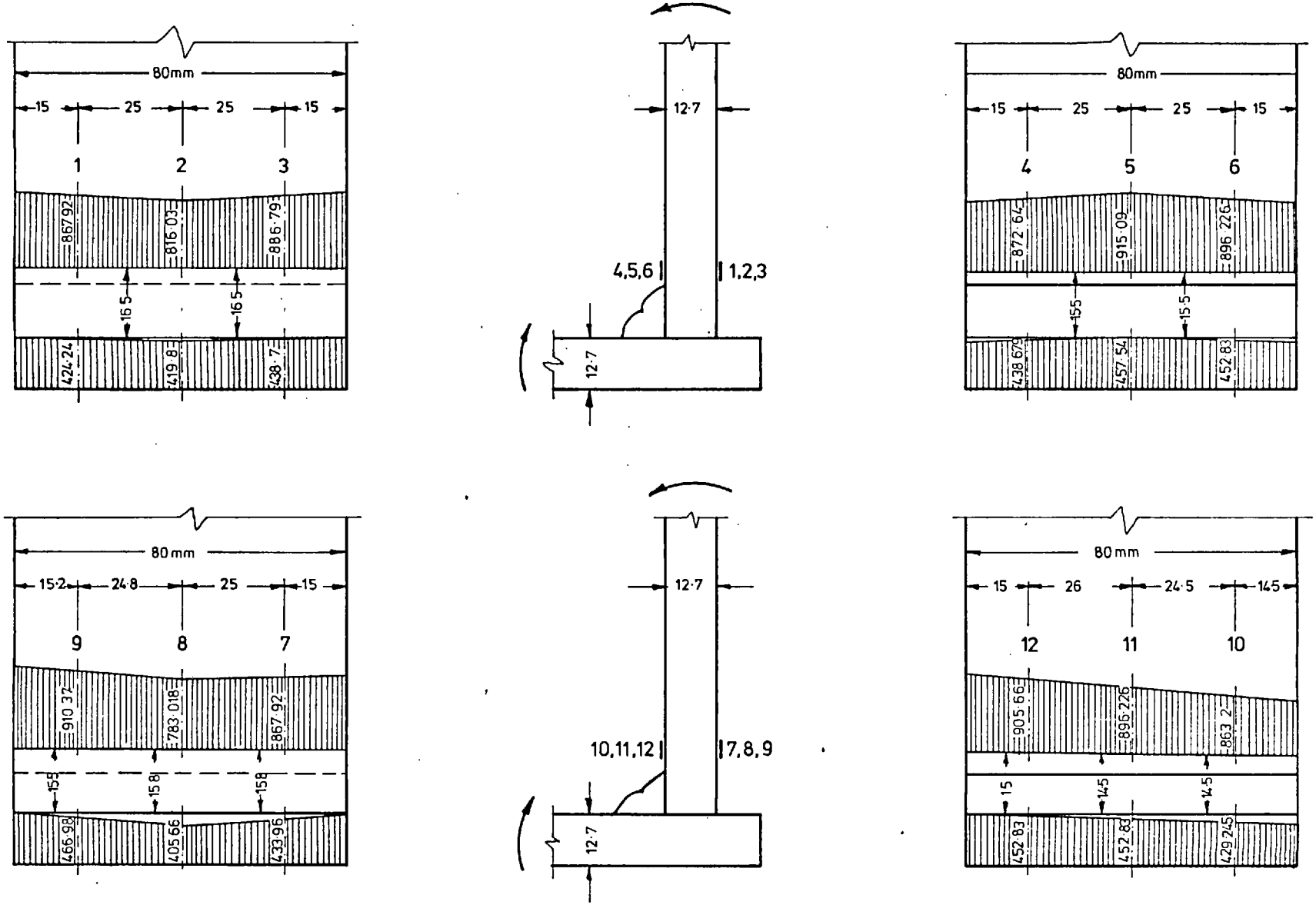


Fig.4·18 Strain distribution along the toe of the weld for series BESFW I. (the values are in micro-strain)

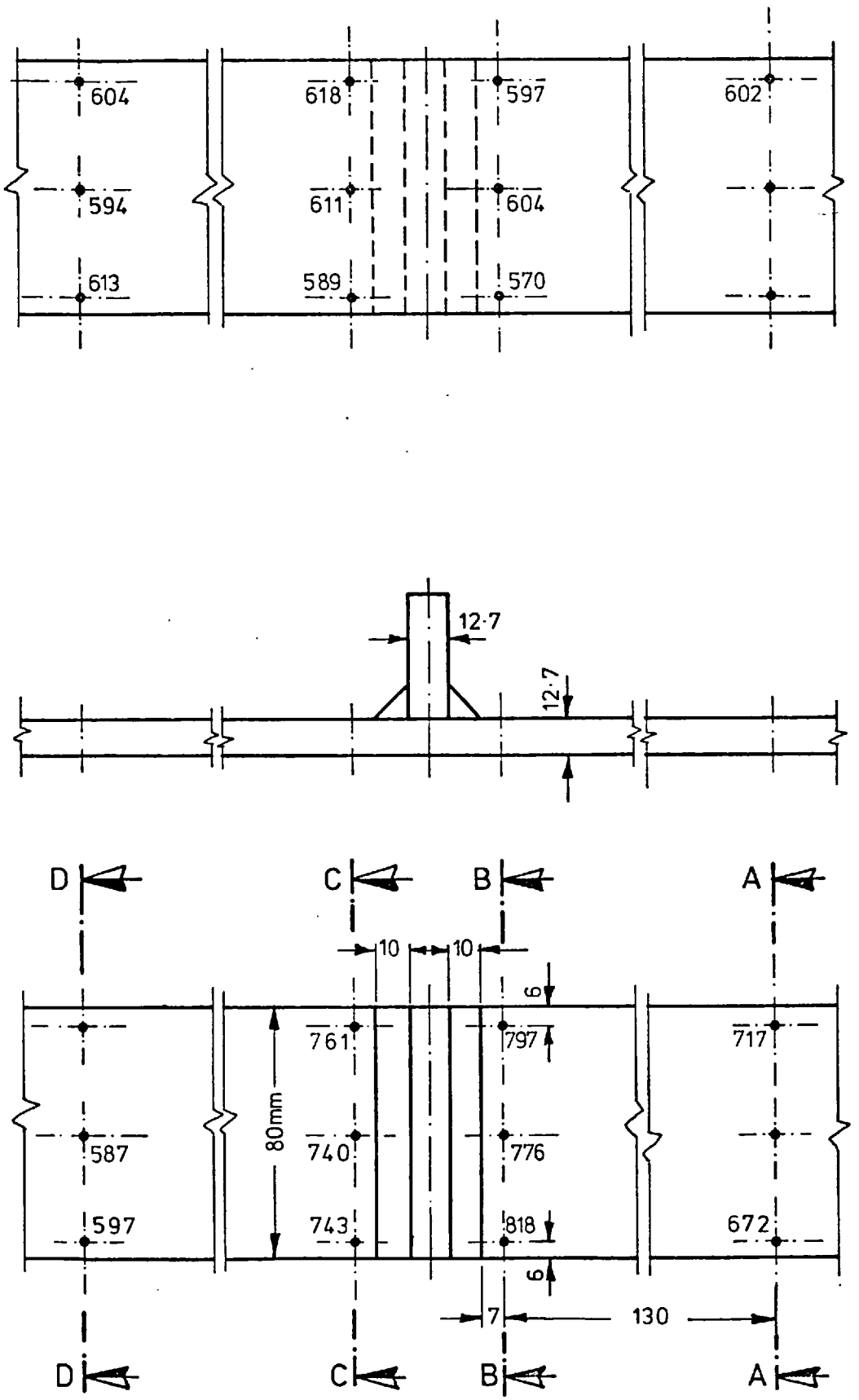


Fig. 4·19 Strain distribution along the toe of the weld for simple T-specimen subjected to tension.

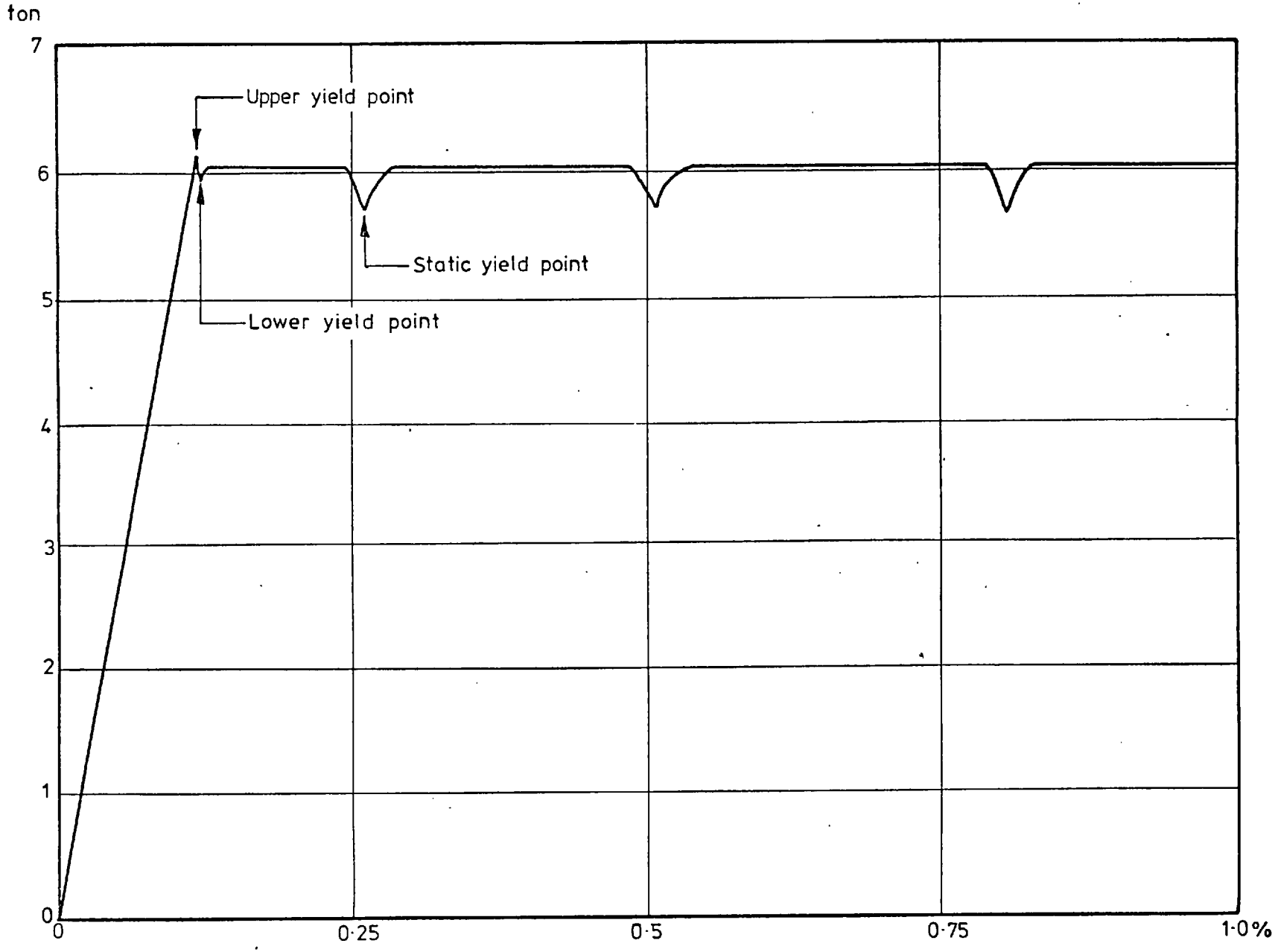


Fig. 4·20 Tensile load stress-strain curve for the parent material (mild steel)

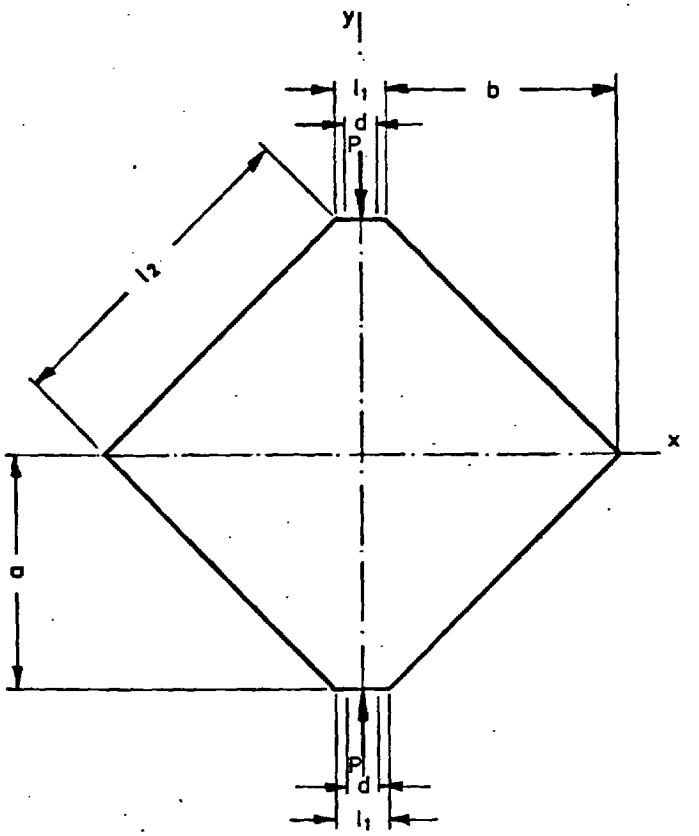


Fig. 4·21 Theoretical dimensions of the specimen

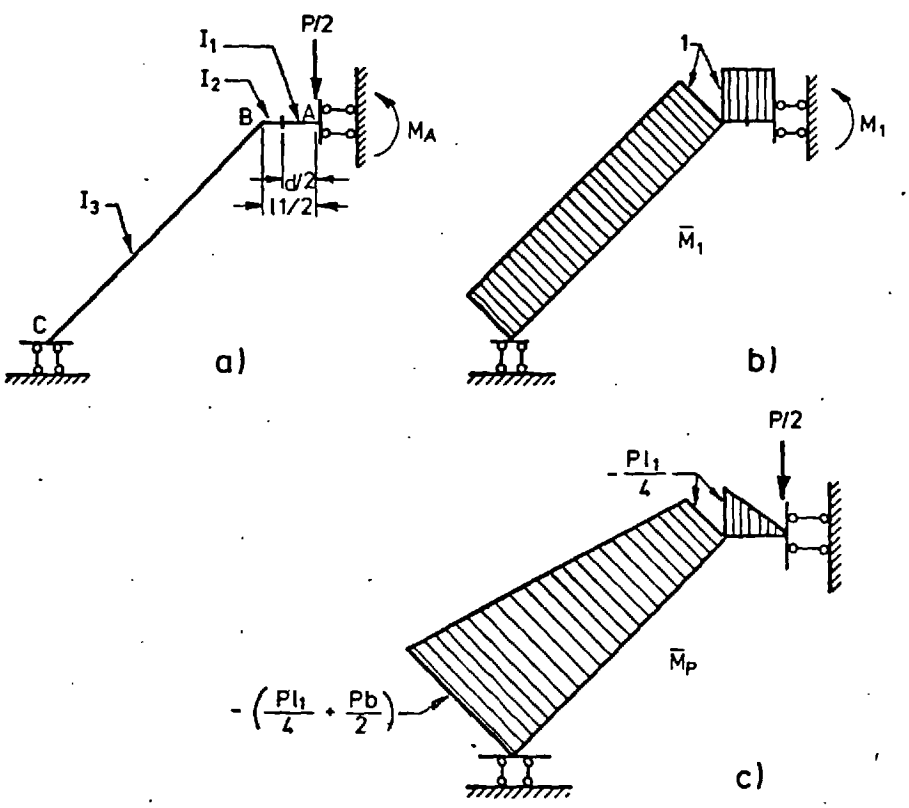


Fig.4·22 a) Basic system. b) Bending moment diagram due to unit bending moment $M_1=1$. c) Bending moment diagram due to applied load in the basic system.

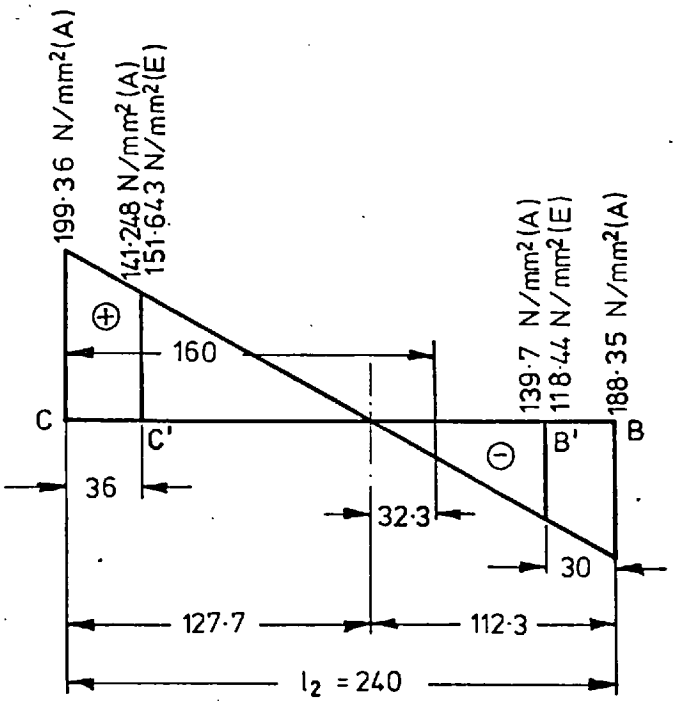


Fig. 4·23 Comparison of analytical and experimental results of the bending stresses in the frame element. (For series BESBS)

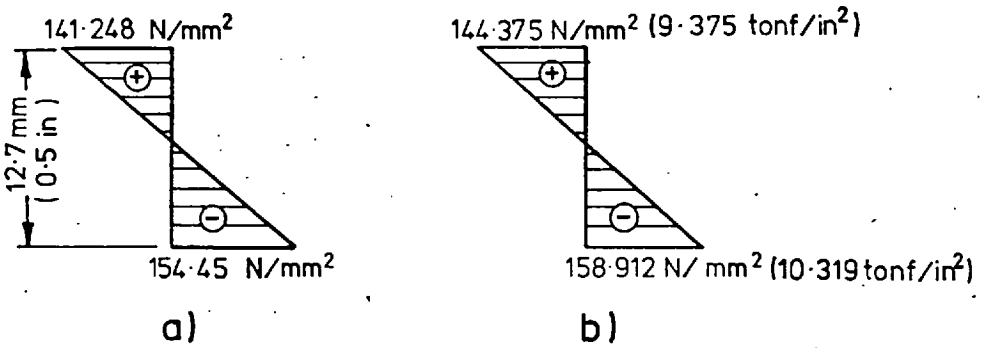


Fig. 4·24 Stress distribution across the plate thickness at toe of the weld a) analytical result b) experimental result. (Series BESBS)

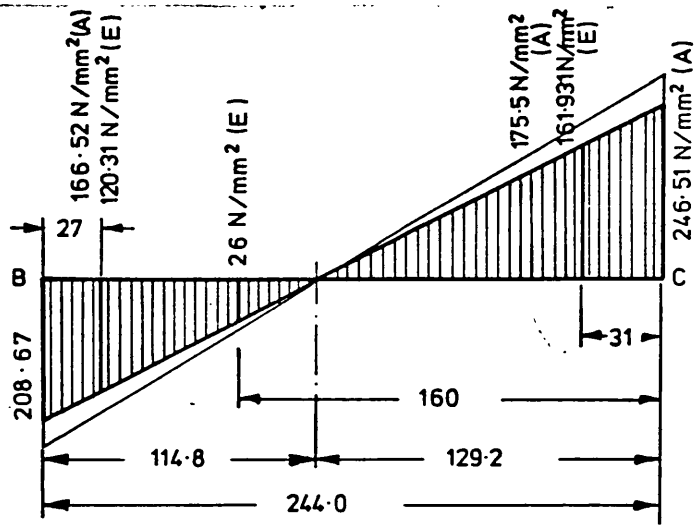


Fig. 4·25 Theoretical and experimental stress distribution along the specimen's element for series BESFW.

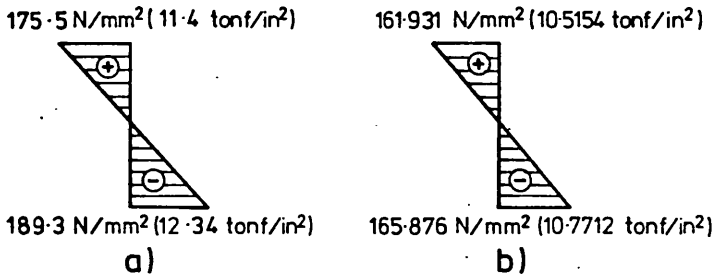


Fig. 4·26 Stress distribution across the plate thickness at the toe of the weld a) analytical result b) experimental result (Series BESFW)

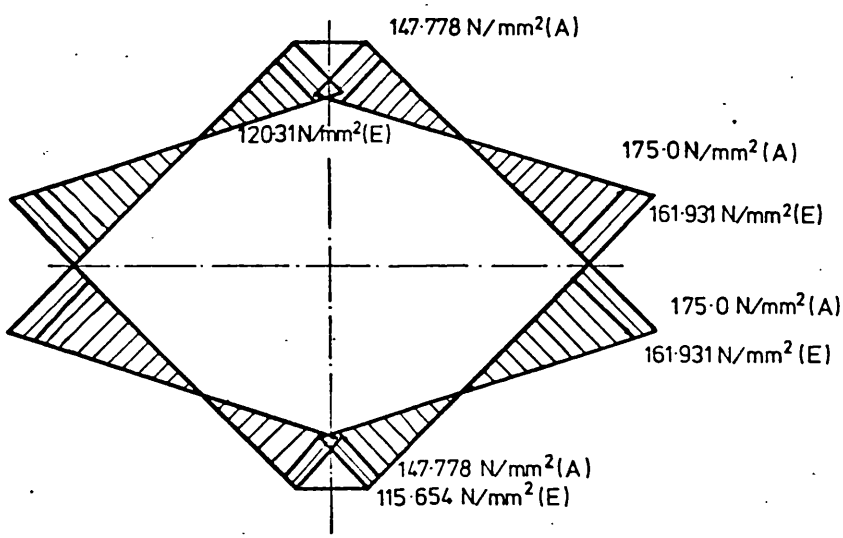
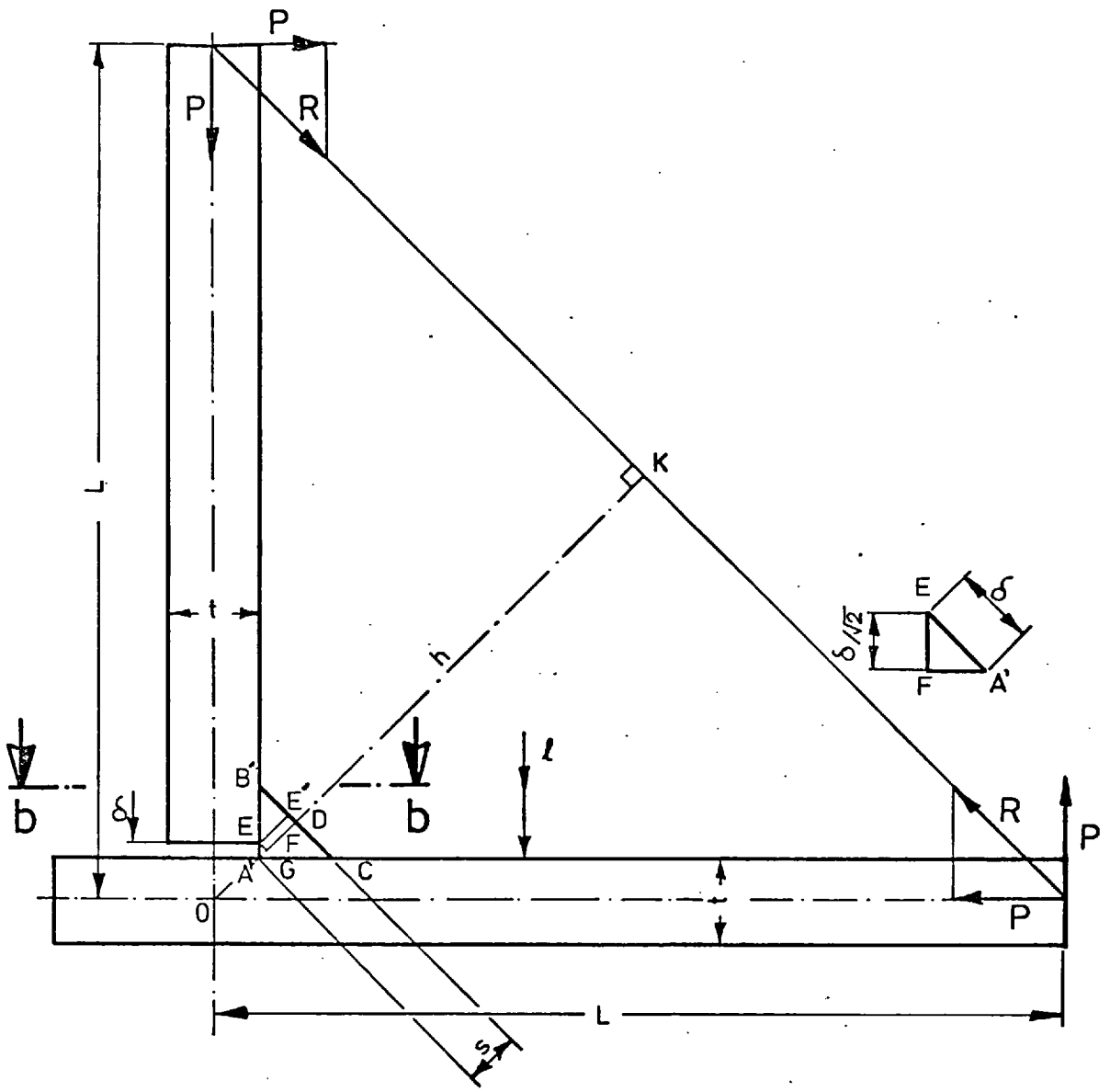


Fig. 4·27 Stress diagram in the specimen type BESFW (E shows the experimental result and A the analytical result.)



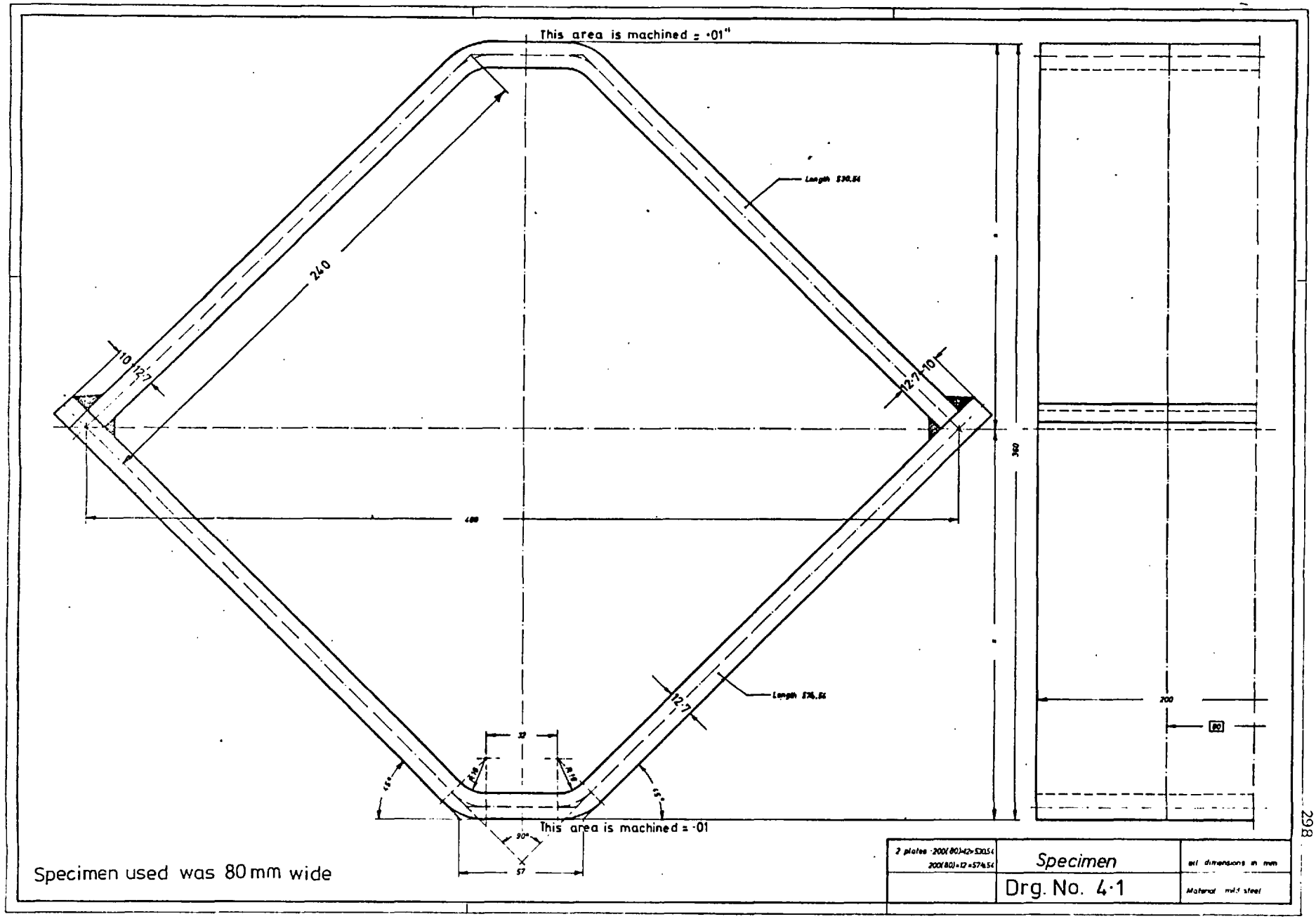
$R = \sqrt{2}\,P$; $s = \frac{\sqrt{2}}{2} \cdot l$; $OK = h = \frac{\sqrt{2}}{2} \cdot L$; $OA = \frac{\sqrt{2}}{2} \cdot t$; $A'F = \frac{\sqrt{2}}{2}\,\delta$

Bending Moment at point A $M_{A'} = R\,[OK - OA]$ $M_A = P\,[L - t]$

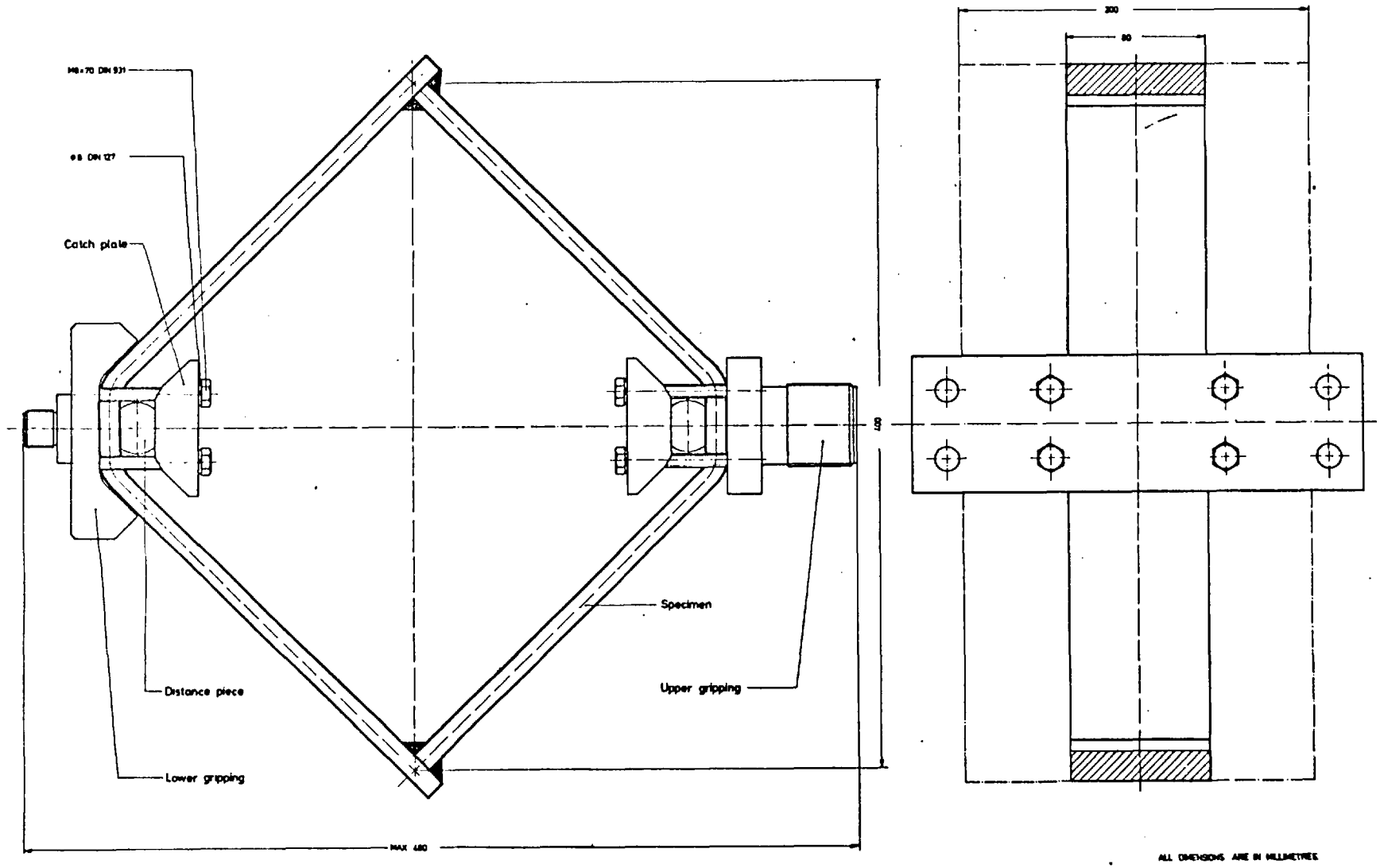
This relation could be achieved $M_{A'} = P\,[L - t/2] - P \cdot t/2 = P\,[L - t]$

and at point E $M_E = P\,[L - (t + \delta)]$

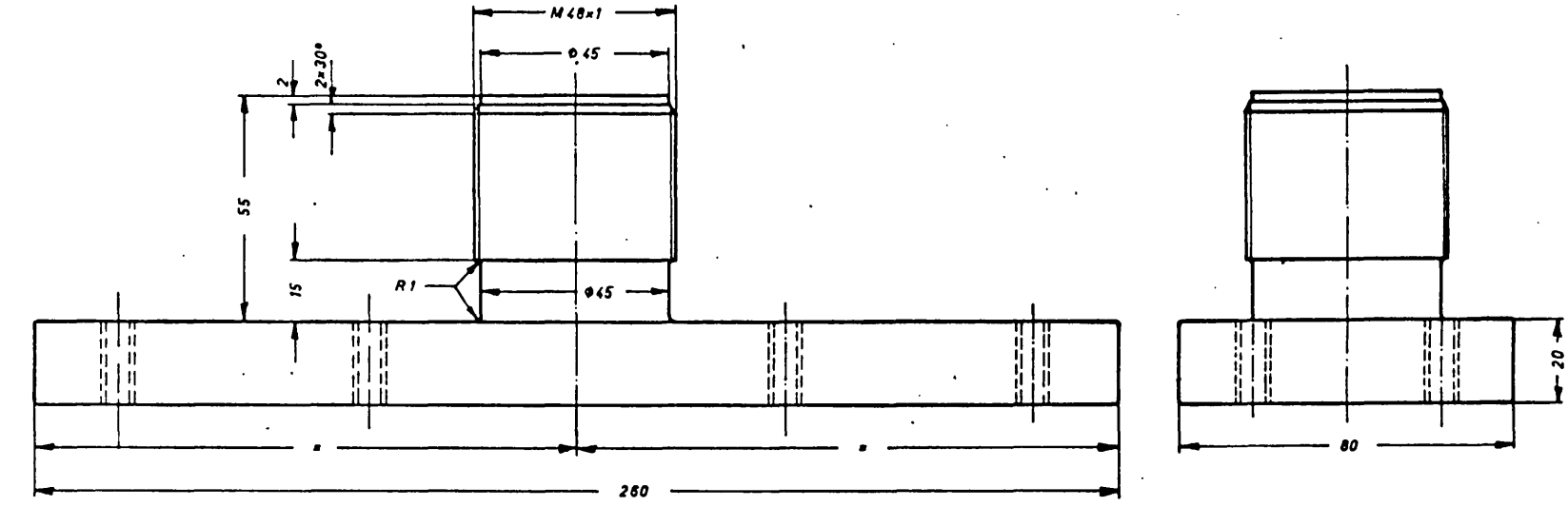
Fig. 4·28 Theoretical dimensions of the welded joint considered in the calculation of the nominal stress in the weld throat for series BESFW I and BESFG I.

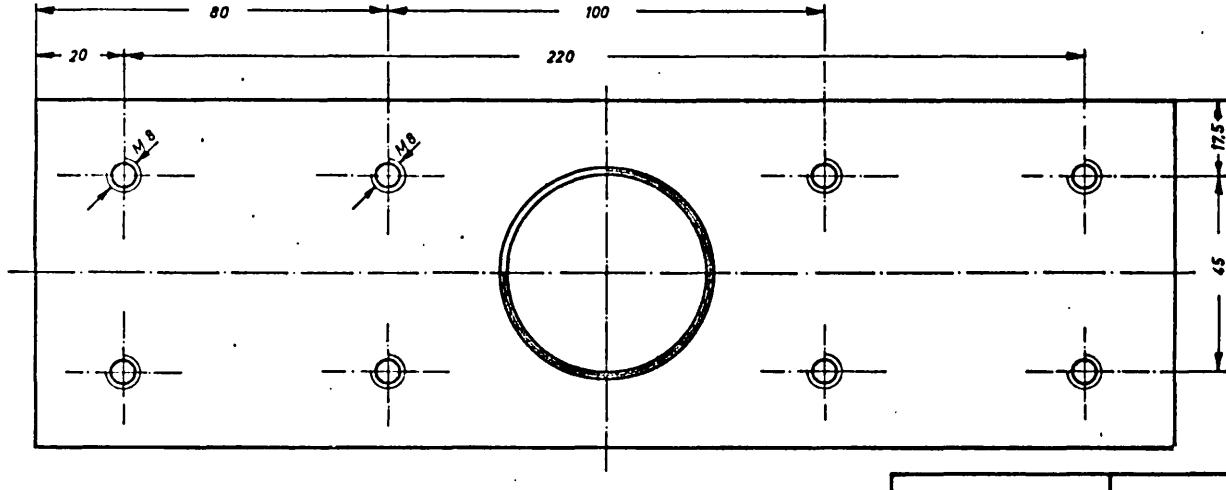


Specimen used was 80 mm wide

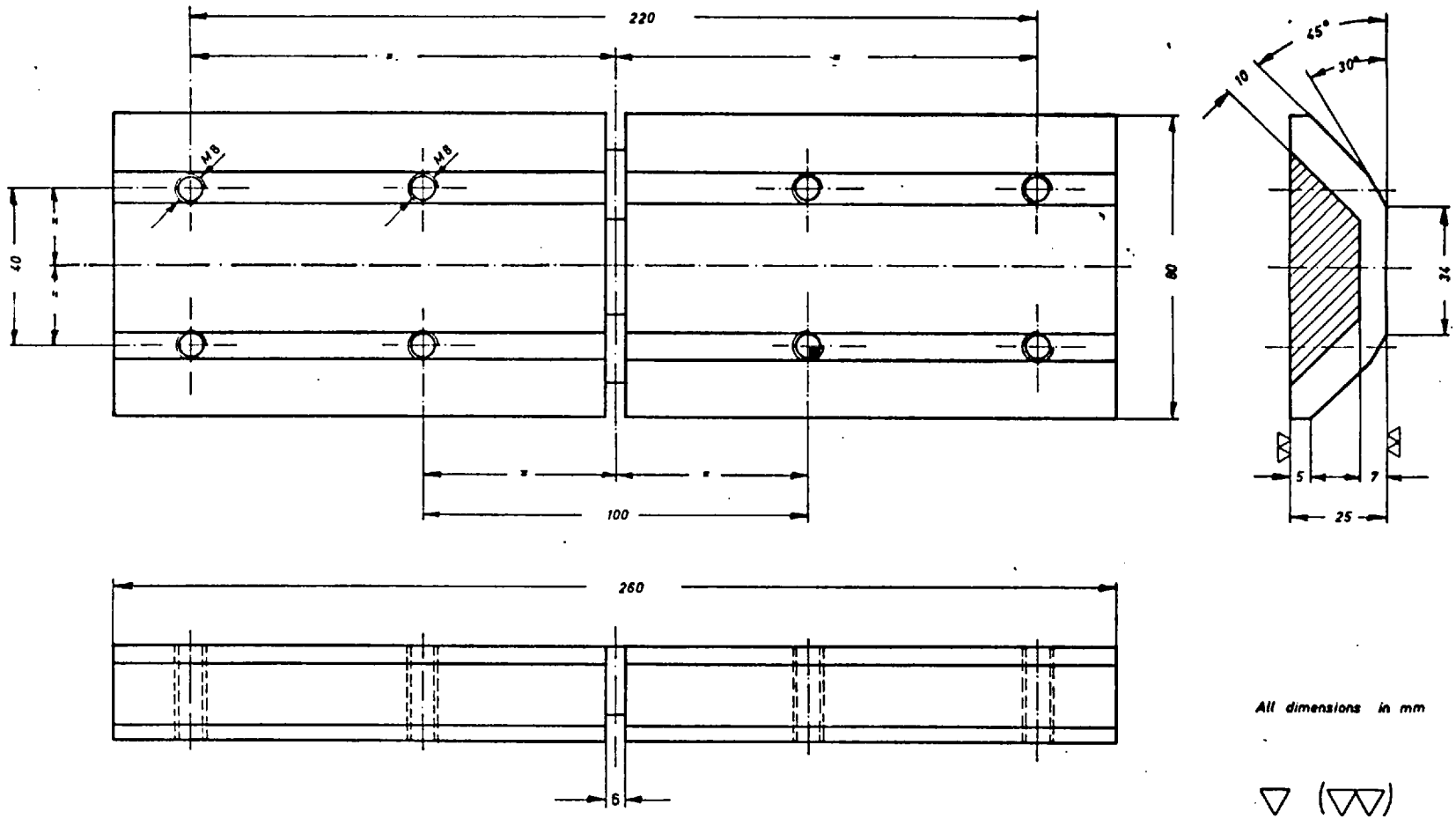


	Specimen with Gripping	
	Drg. No. 4·2	





Drg. No. 4·3	*Holder*	*all dimensions in mm*
		Material: mild steel



All dimensions in mm

Drg. No. 4·4

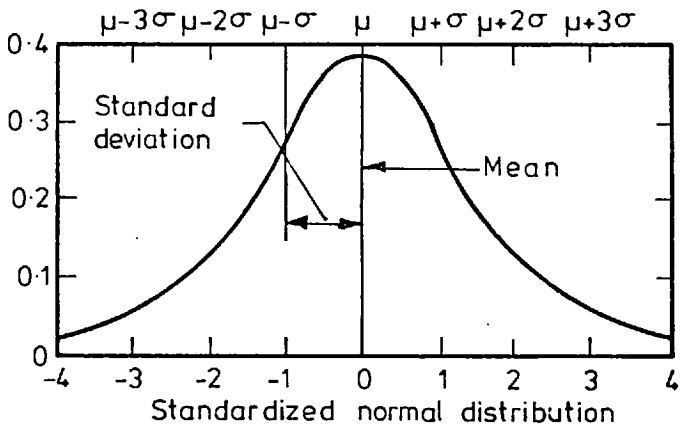


Fig. 5·1 Normal Gaussian distribution curve

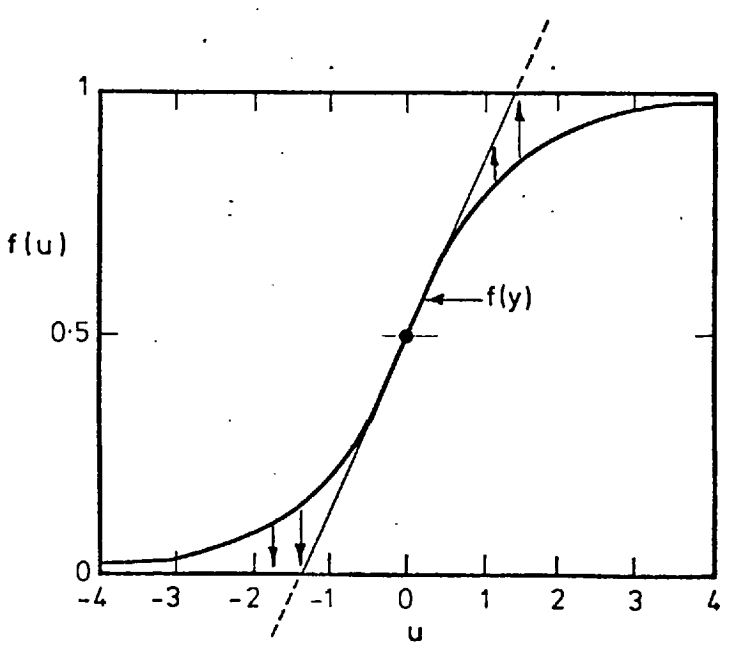


Fig. 5·2 Cumulative frequency distribution curve

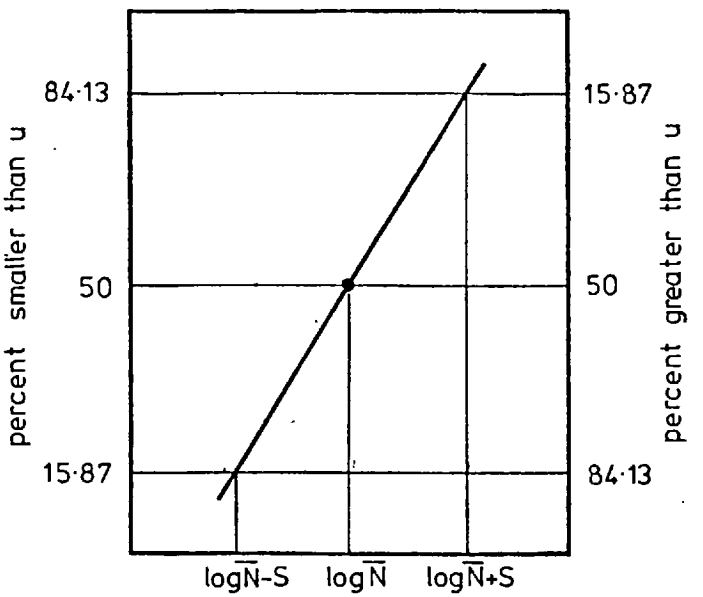


Fig.5·3 Construction of cumulative frequency distribution

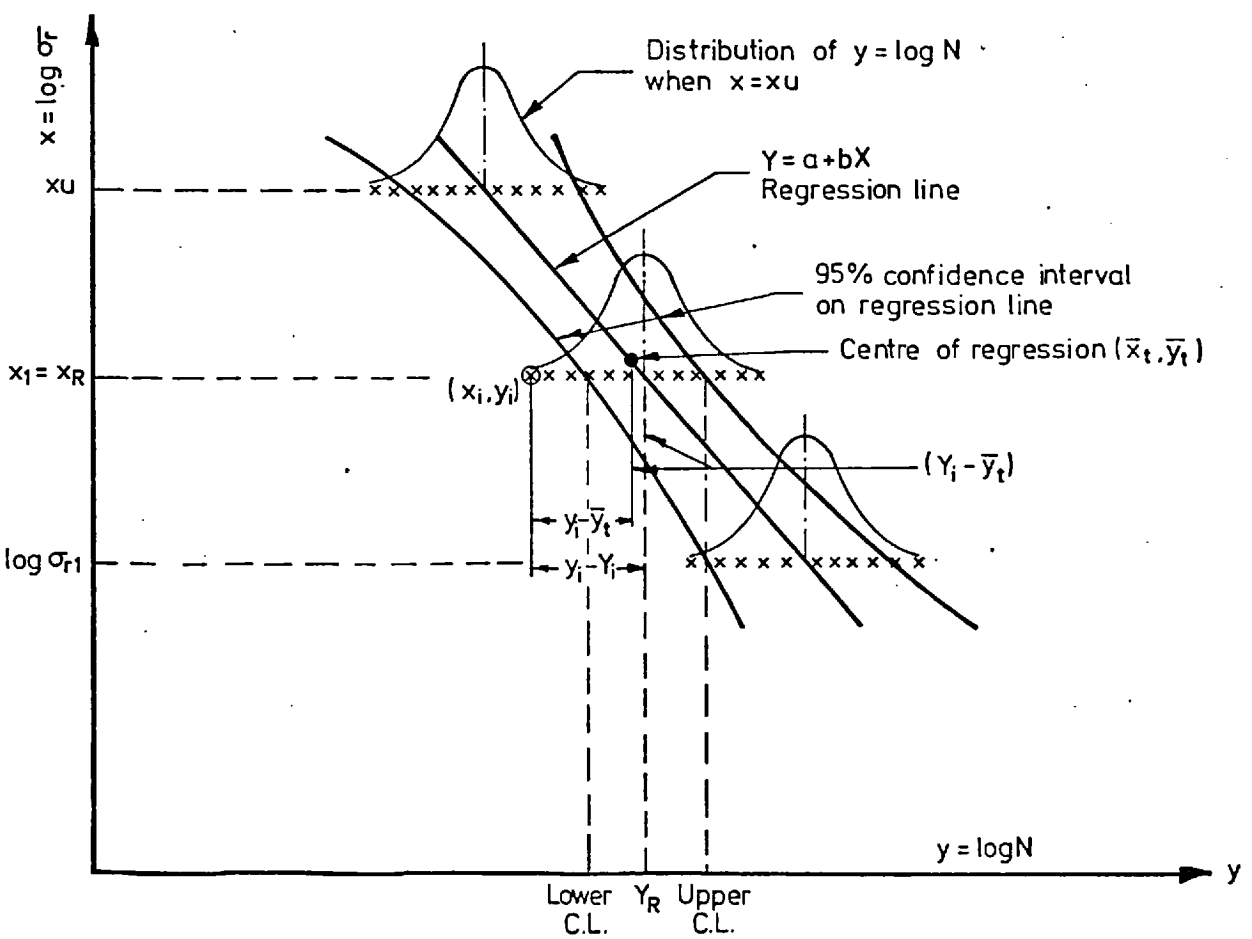


Fig.5·4 S-N curve fitted by method of least squares with their 95% confidence interval.

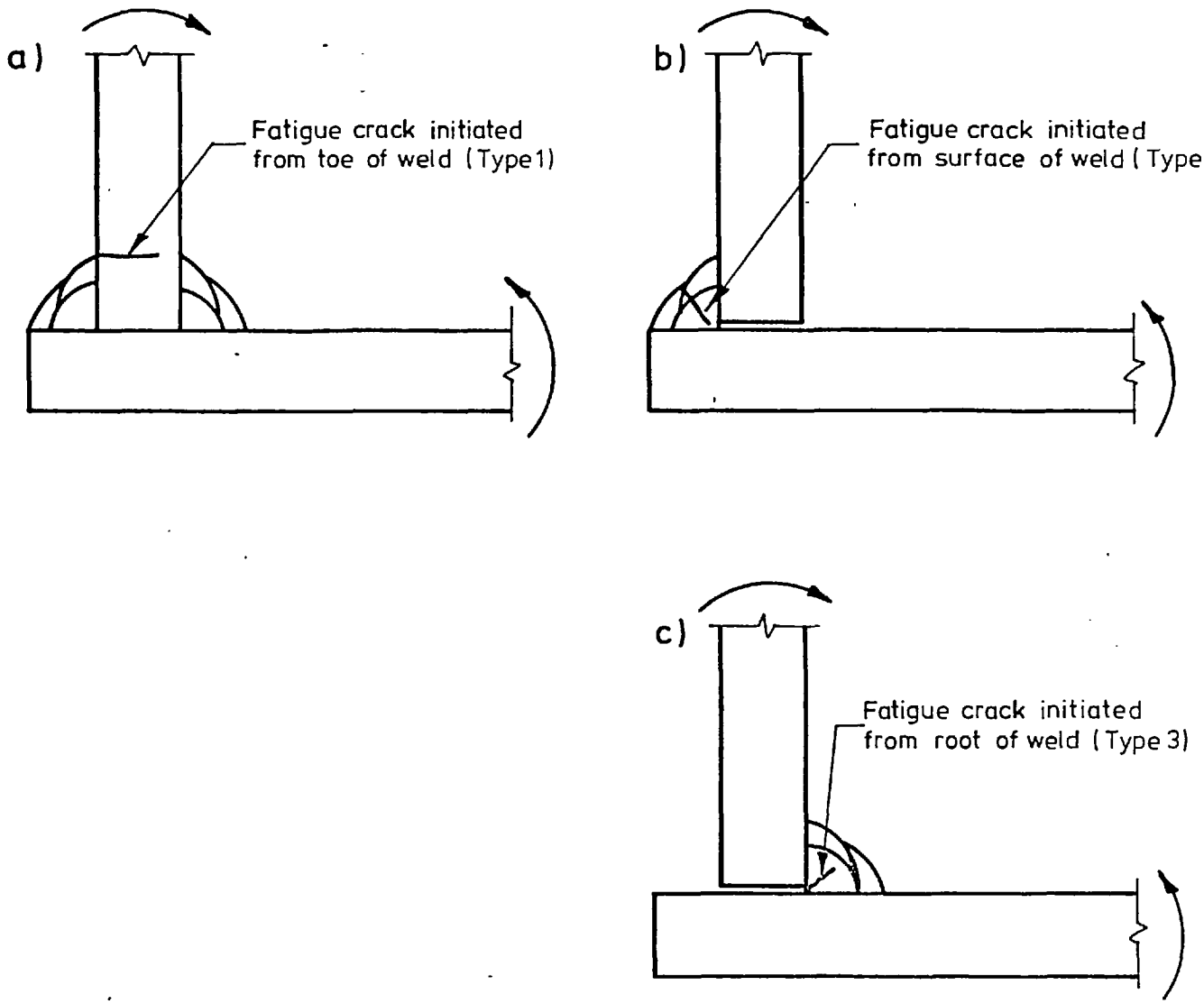


Fig. 6·1 Main types of fatigue crack initiation

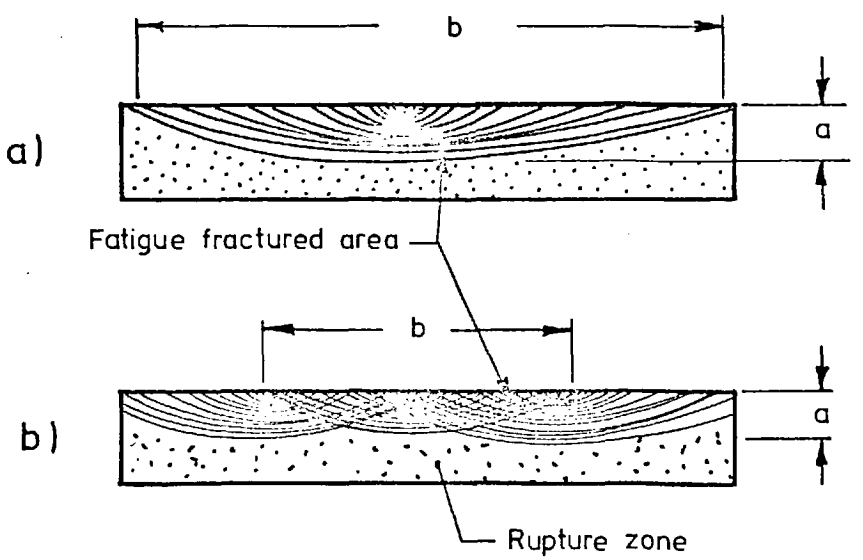


Fig. 6·2 Fatigue fracture surface
a) fatigue crack initiated from one point
b) fatigue crack initiated from several points

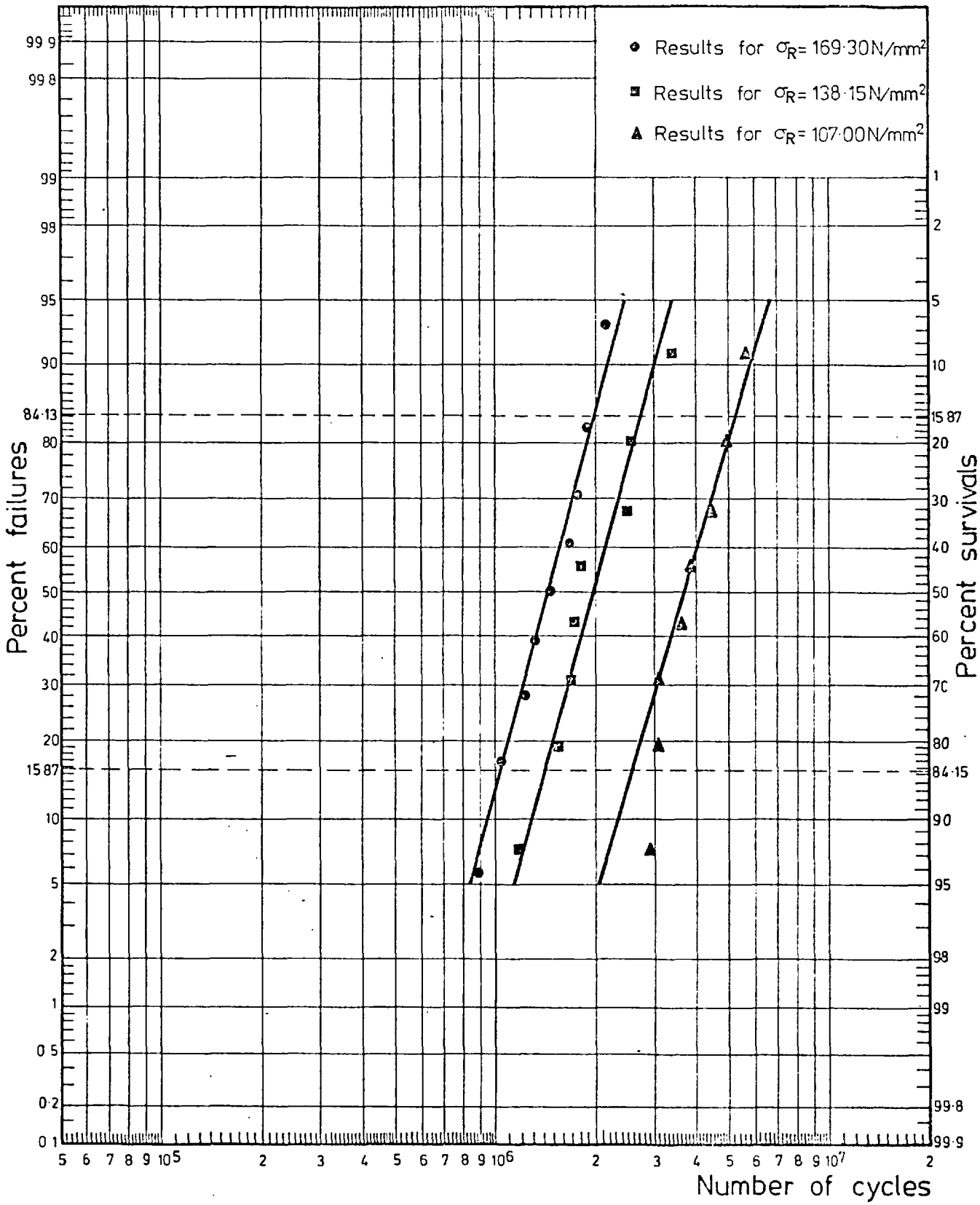


Fig.6·3 Cumulative frequency distribution of logN for series BEDFW (P - log N)

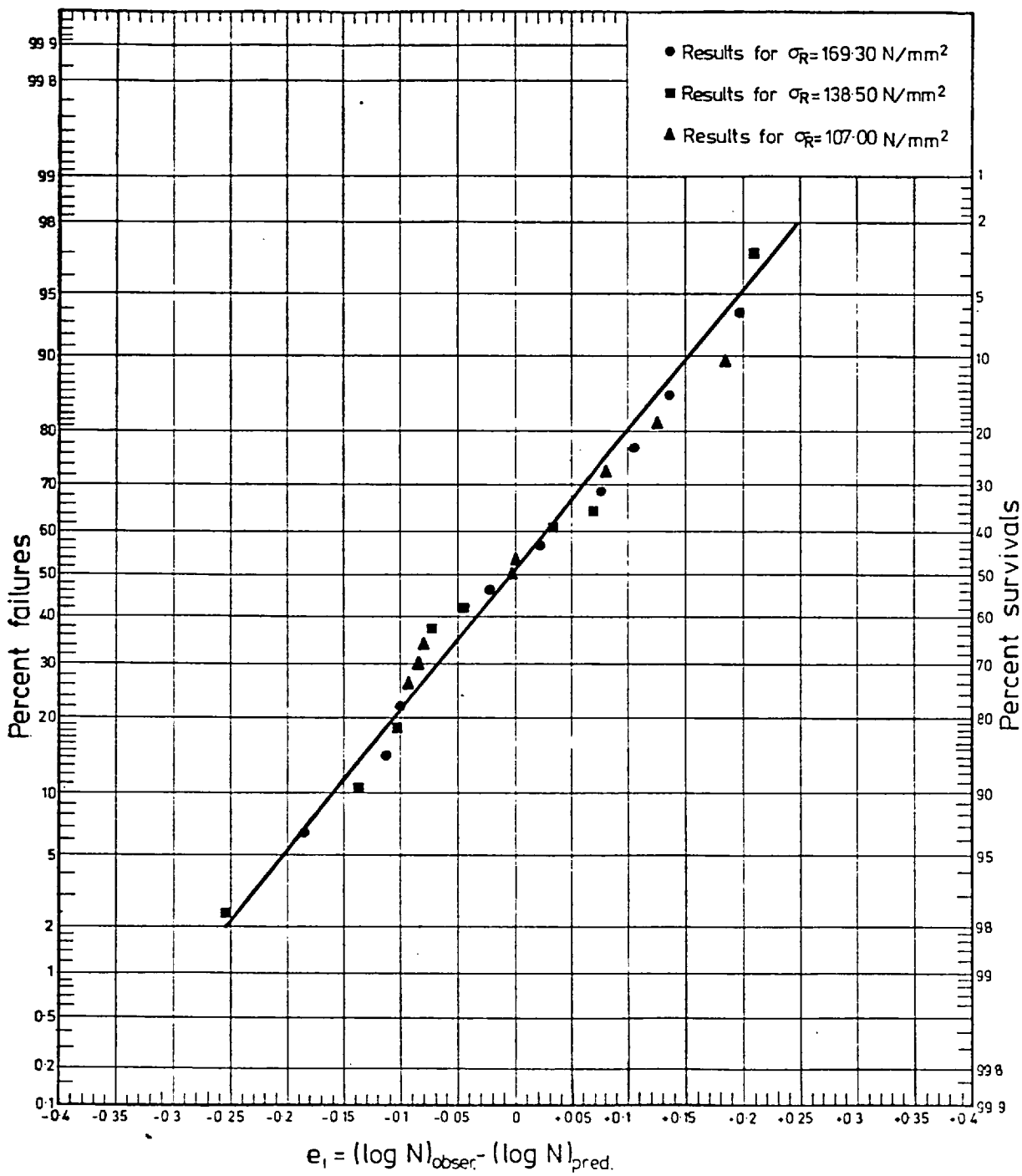


Fig. 6·4 Cumulative frequency distribution of error for series BEDFW

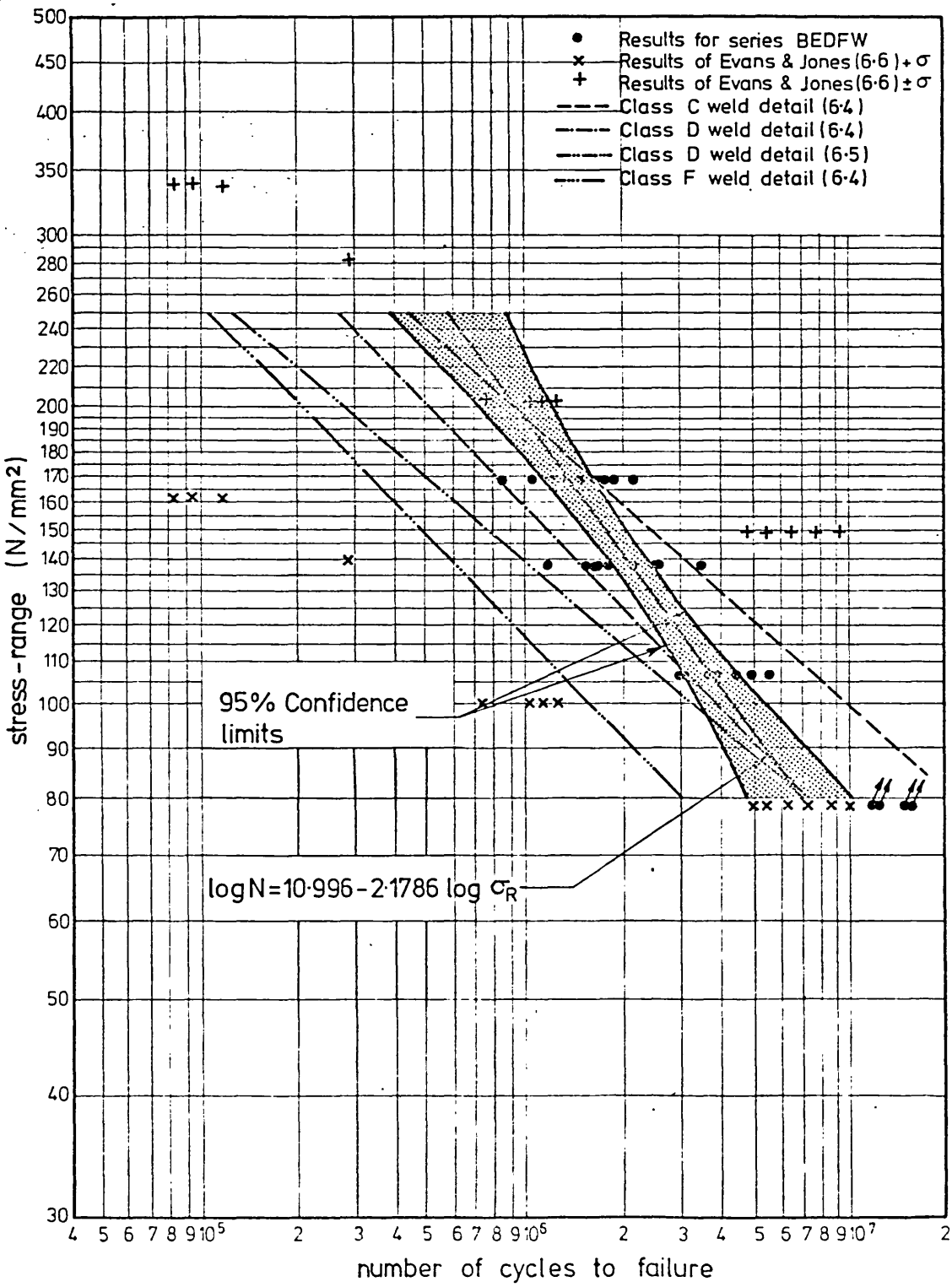


Fig. 6·5 Experimental data, mean fatigue life, and 95 % confidence limits for series BEDFW.

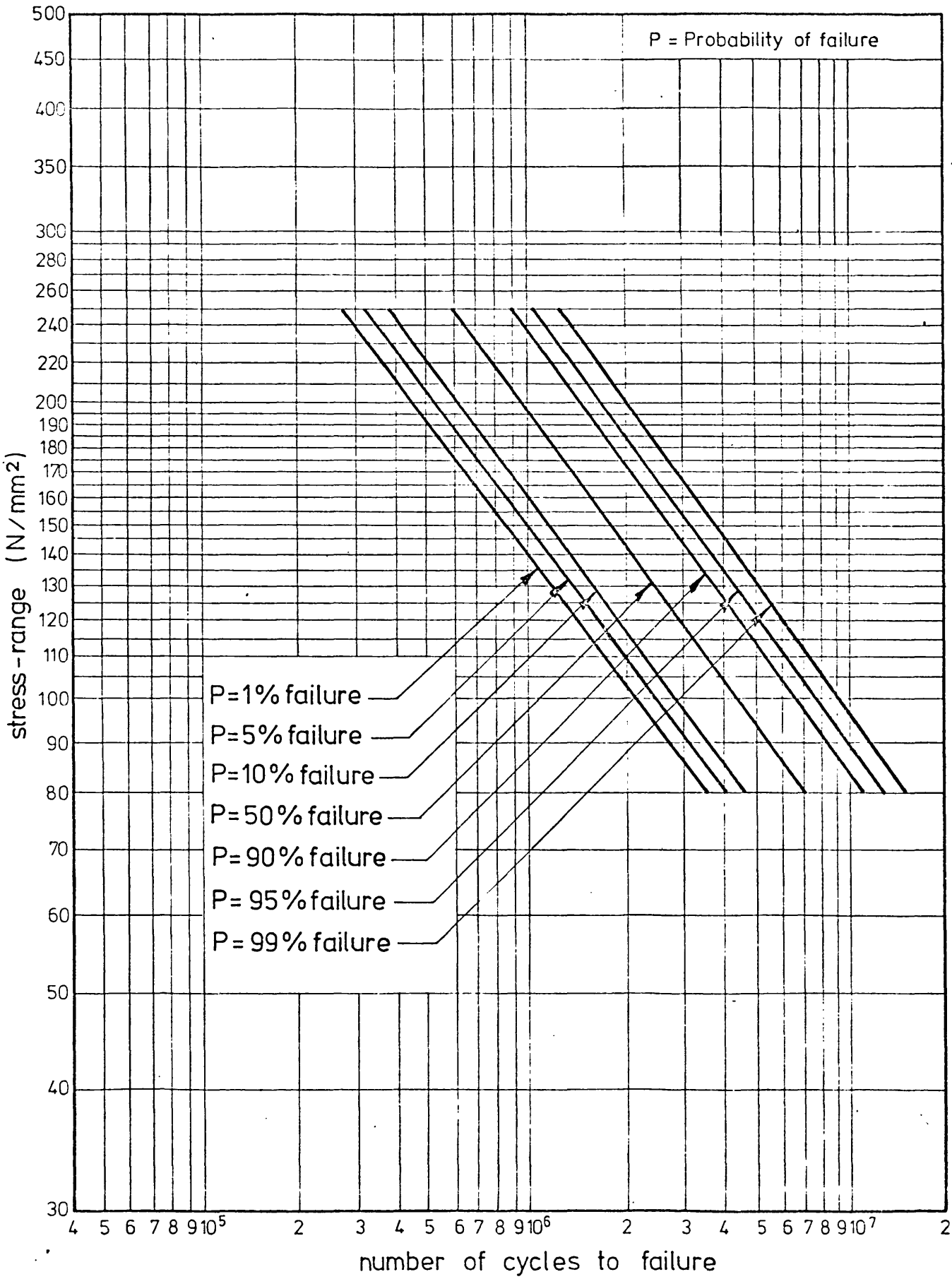


Fig. 6·6 P - S - N Diagram for series BEDFW

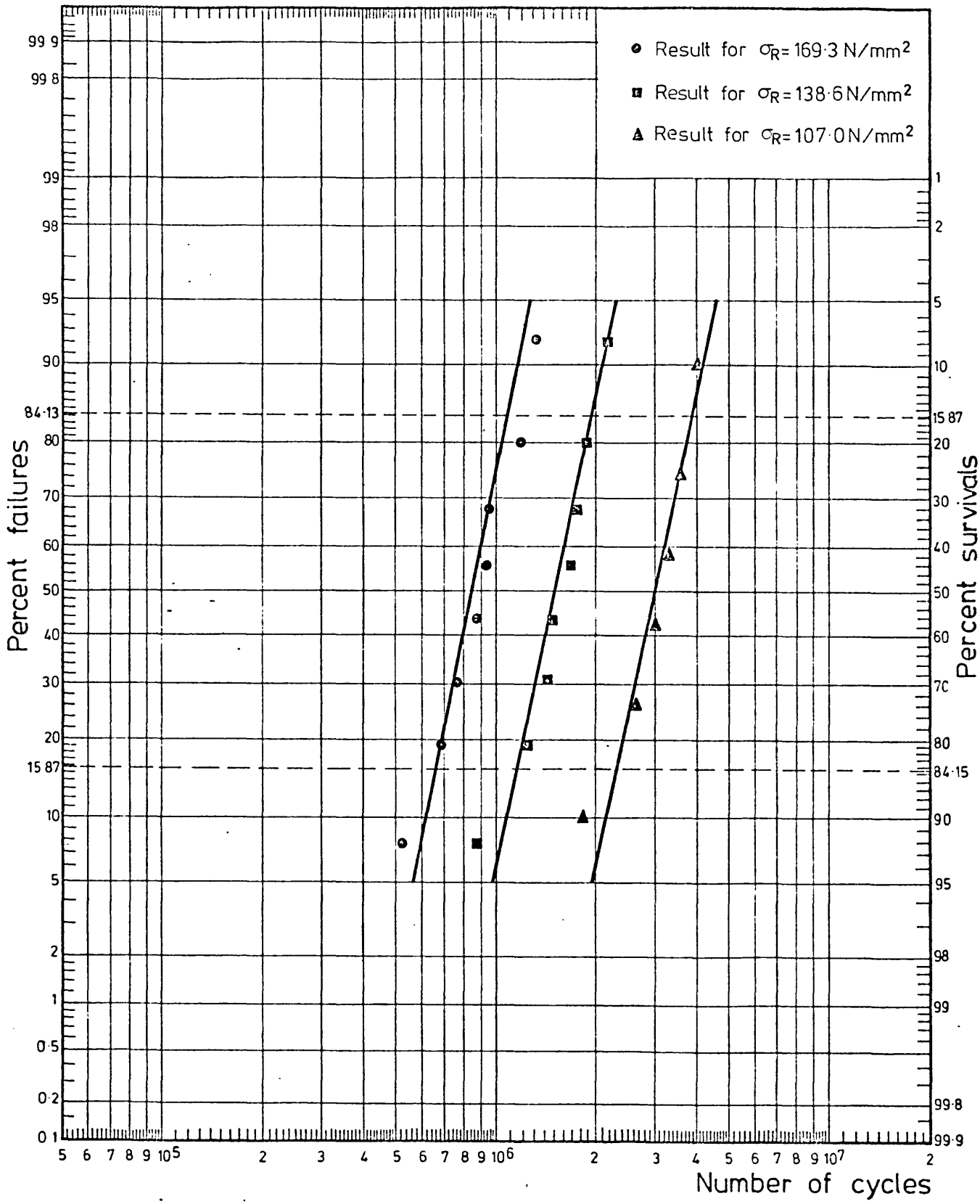


Fig. 6·7 Cumulative frequency distribution of logN for series BEDFG (P - logN)

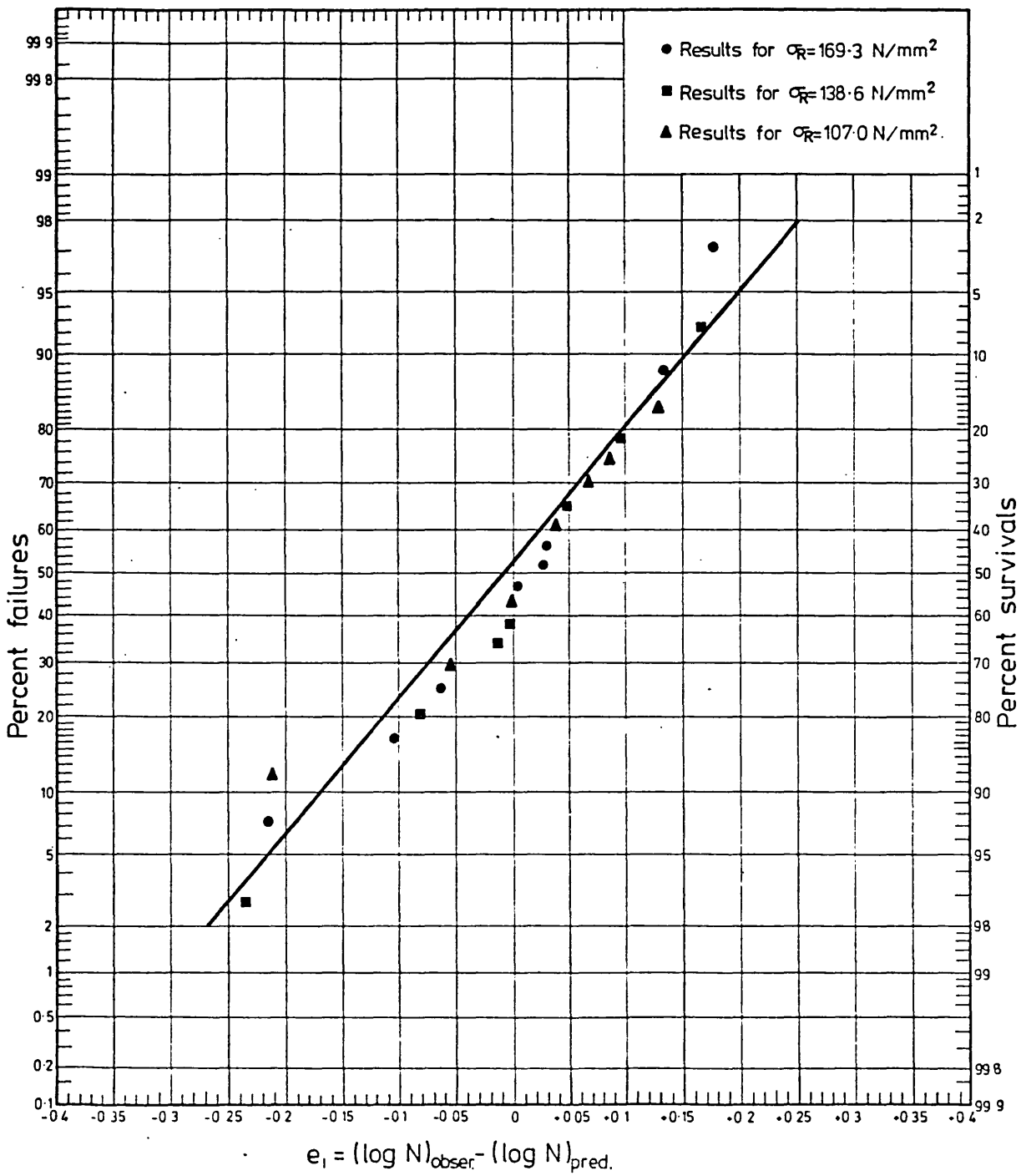


Fig. 6·8 Cumulative frequency distribution of error for series BEDFG

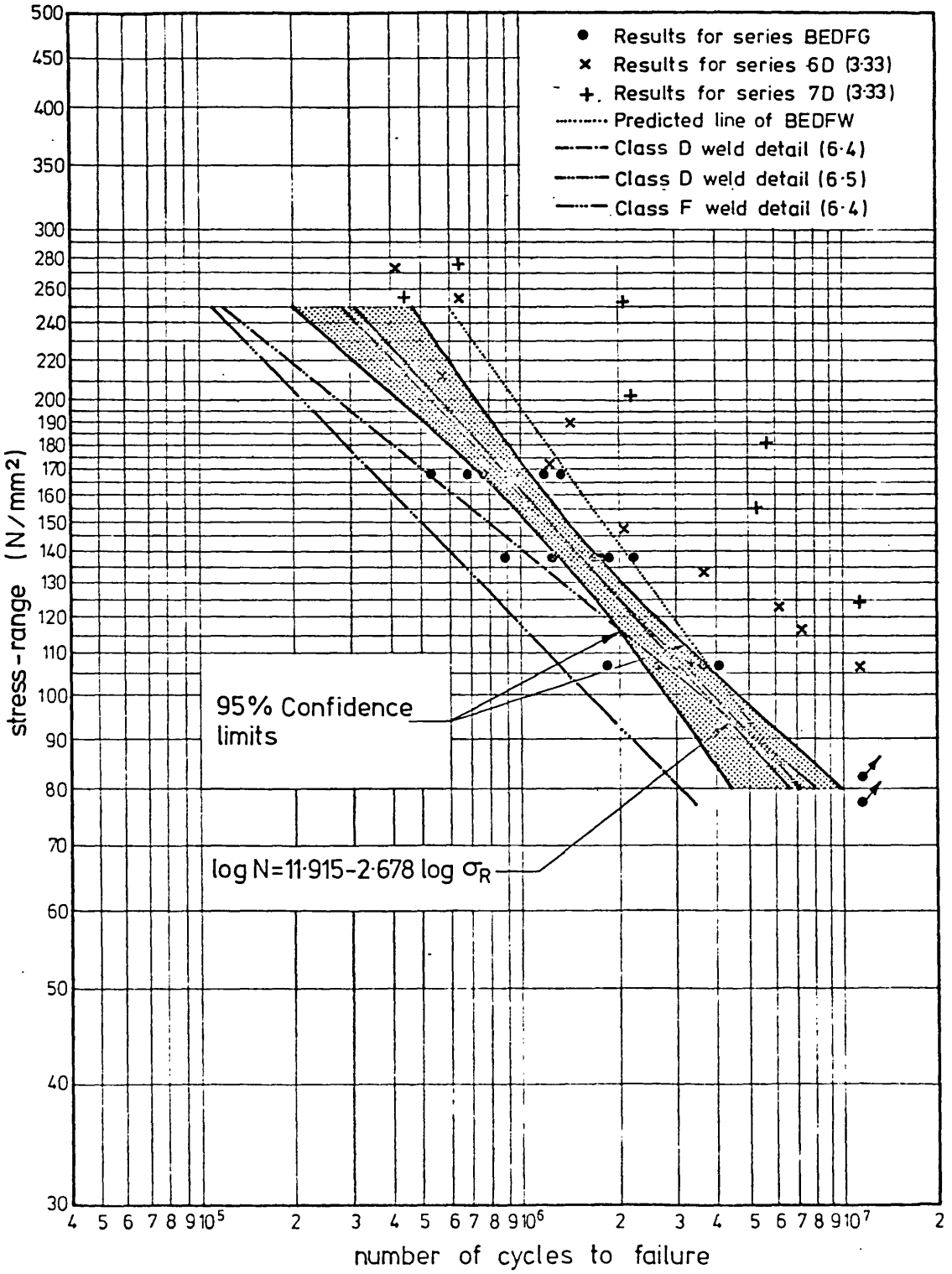


Fig. 6·9 Experimental data, mean fatigue life and 95% confidence limits for series BEDFG.

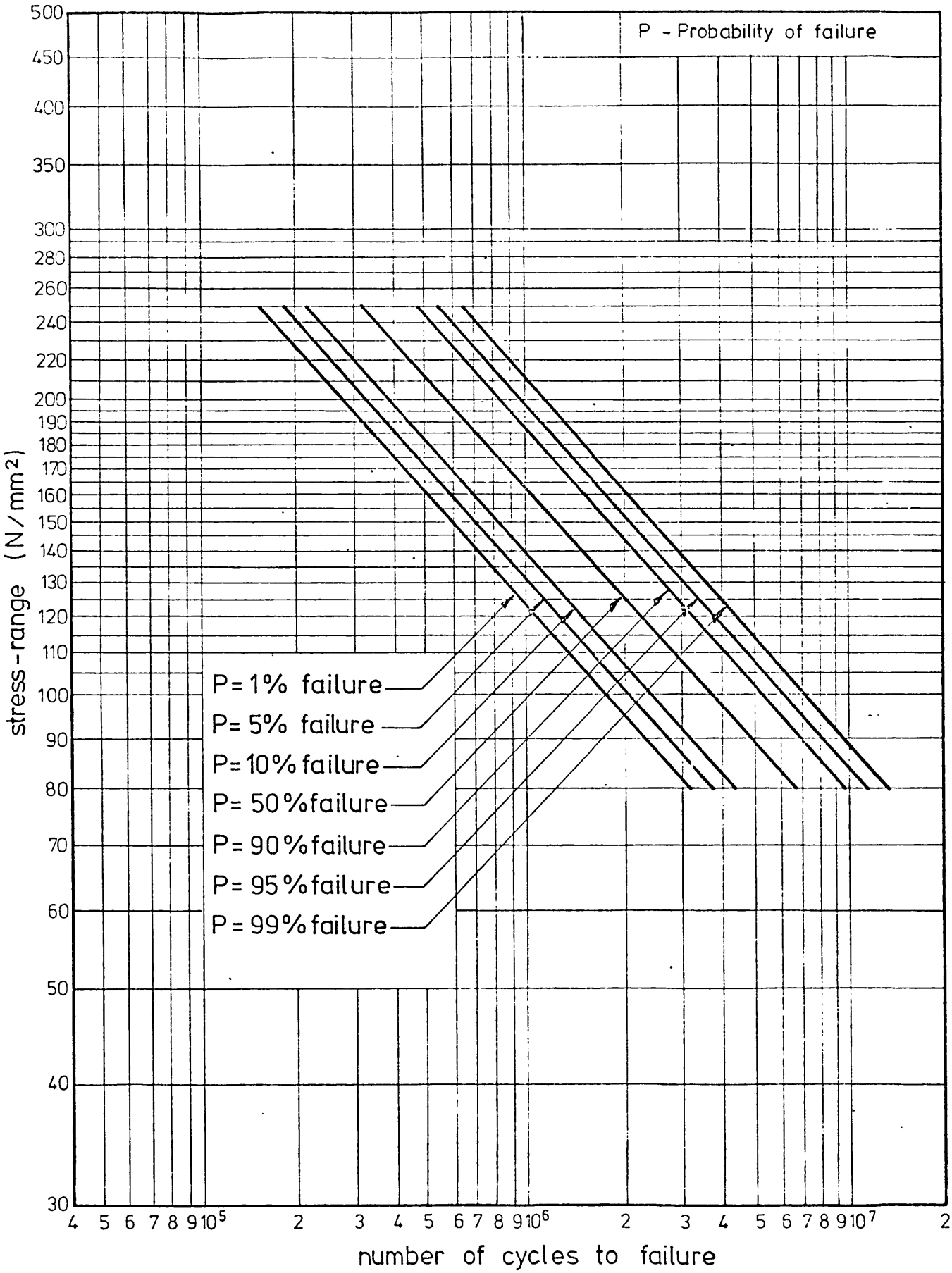


Fig. 6-10 P - S - N Diagram for Series BEDFG

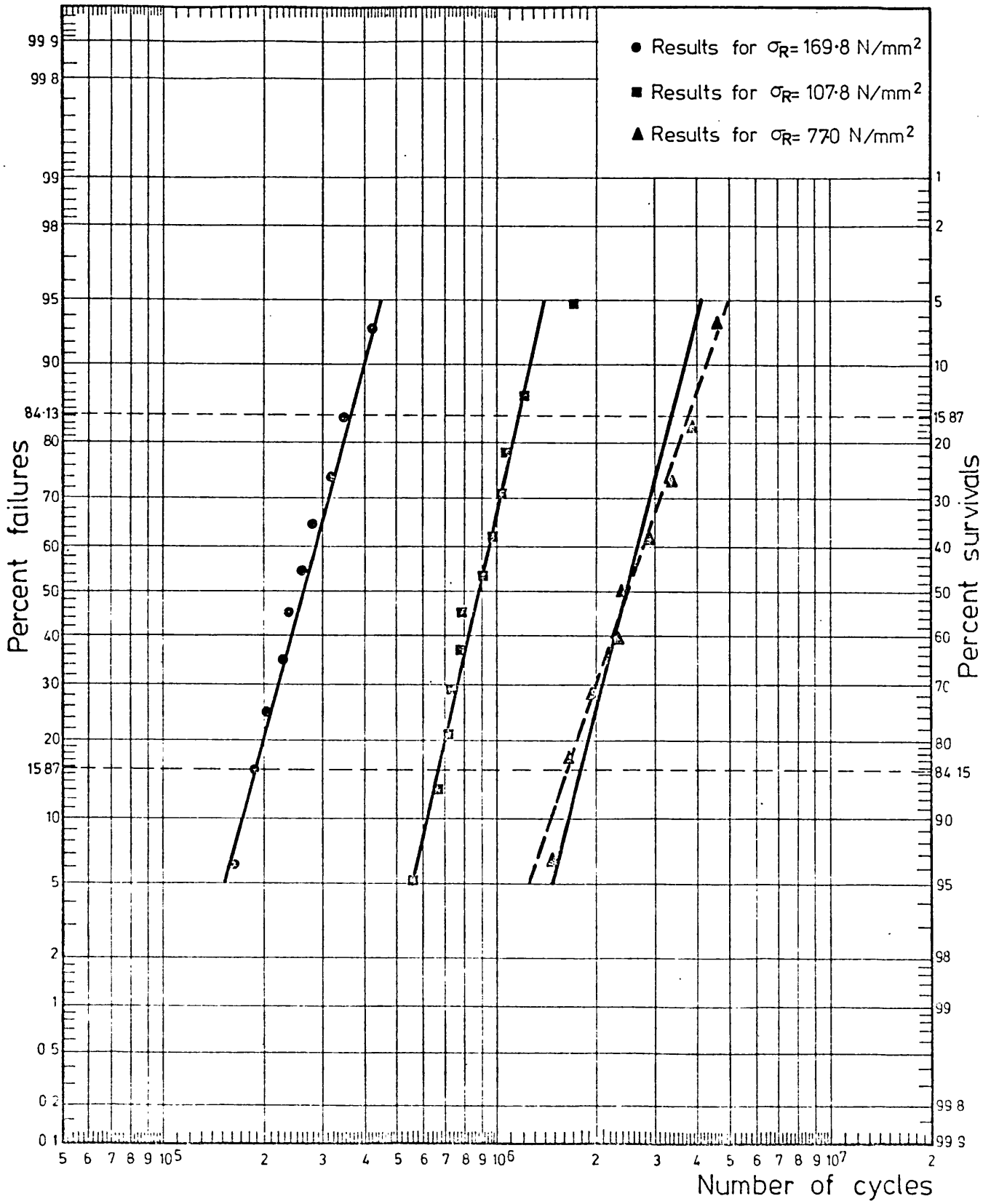


Fig. 6·11 Cumulative frequency distribution of logN for series BESFW

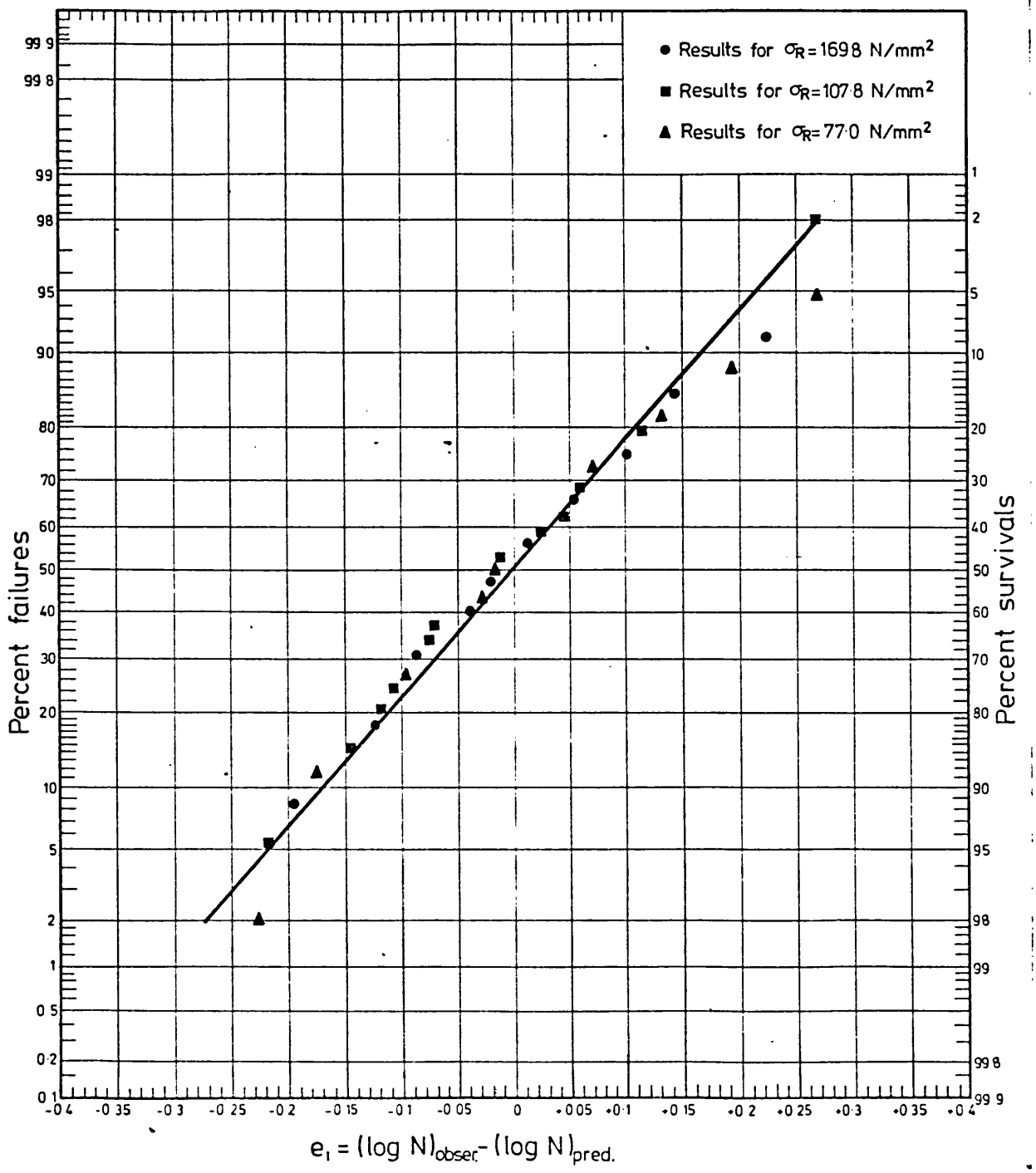


Fig. 6·12 Cumulative frequency distribution of error for series BESFW

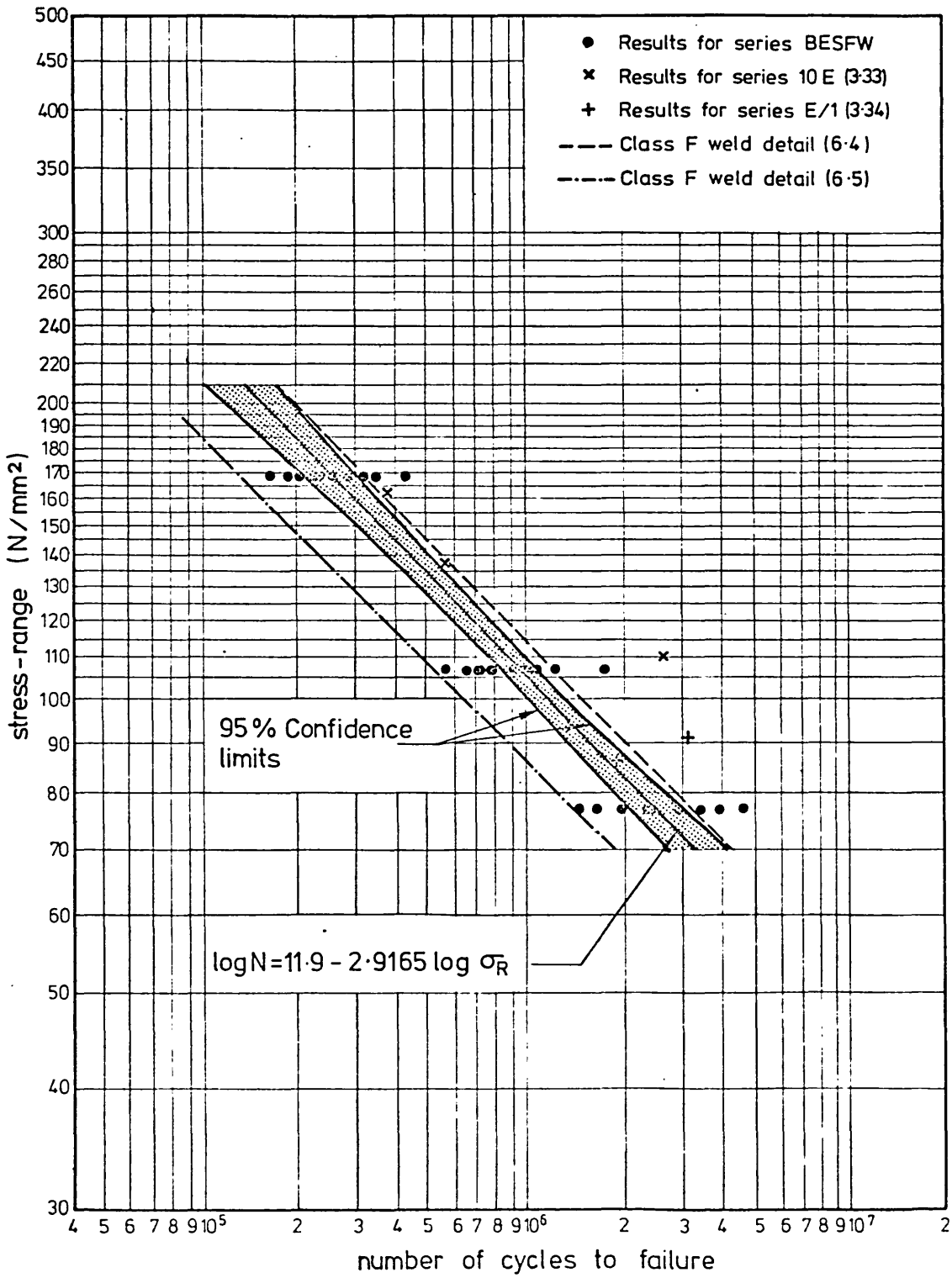


Fig. 6·13 Experimental data, mean fatigue life and 95% confidence limits for series BESFW.

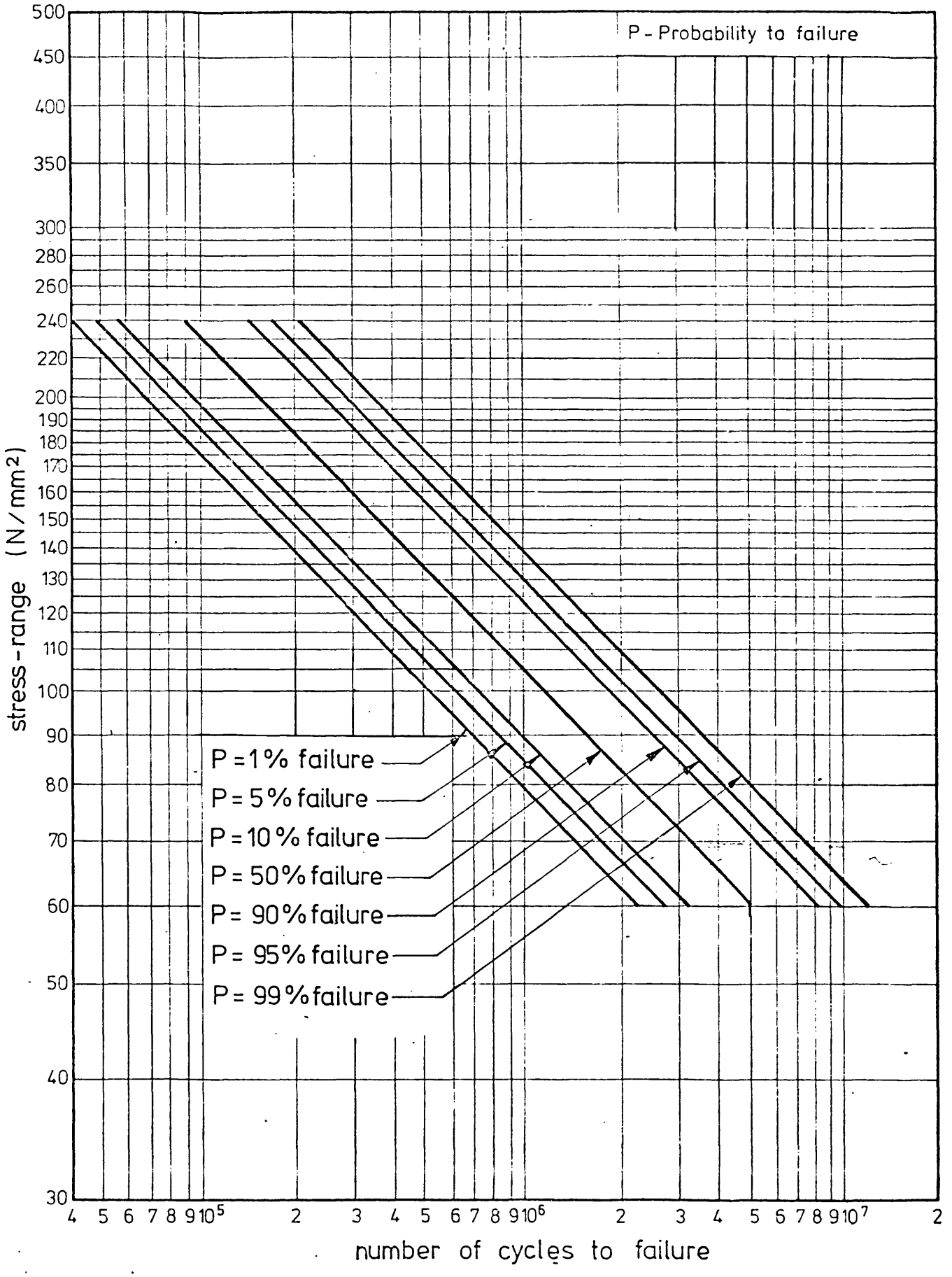


Fig. 6·14 P - S - N .Diagram for series BESFW

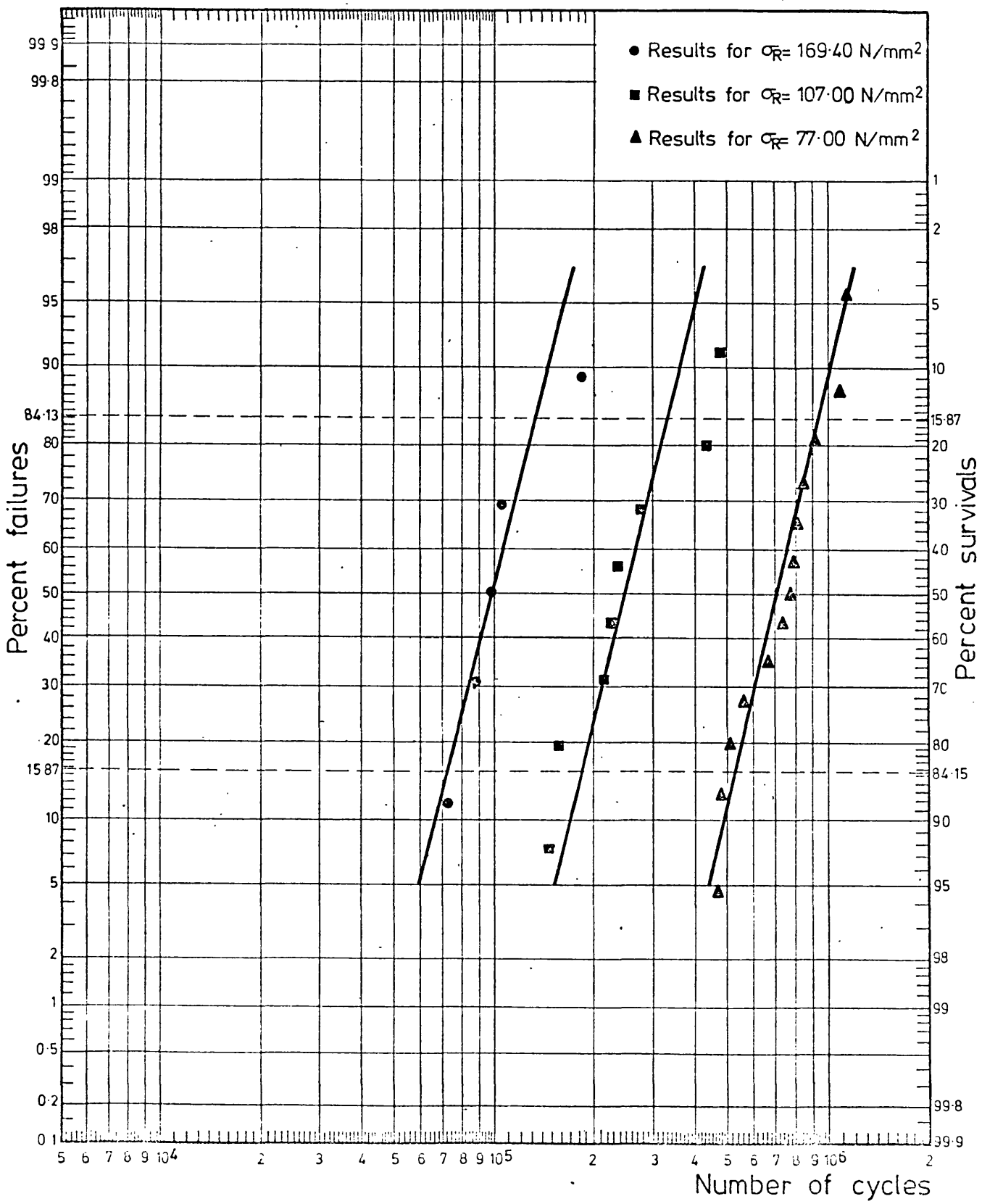


Fig. 6·15 Cumulative frequency distribution of log N for series BESFG (P - log N)

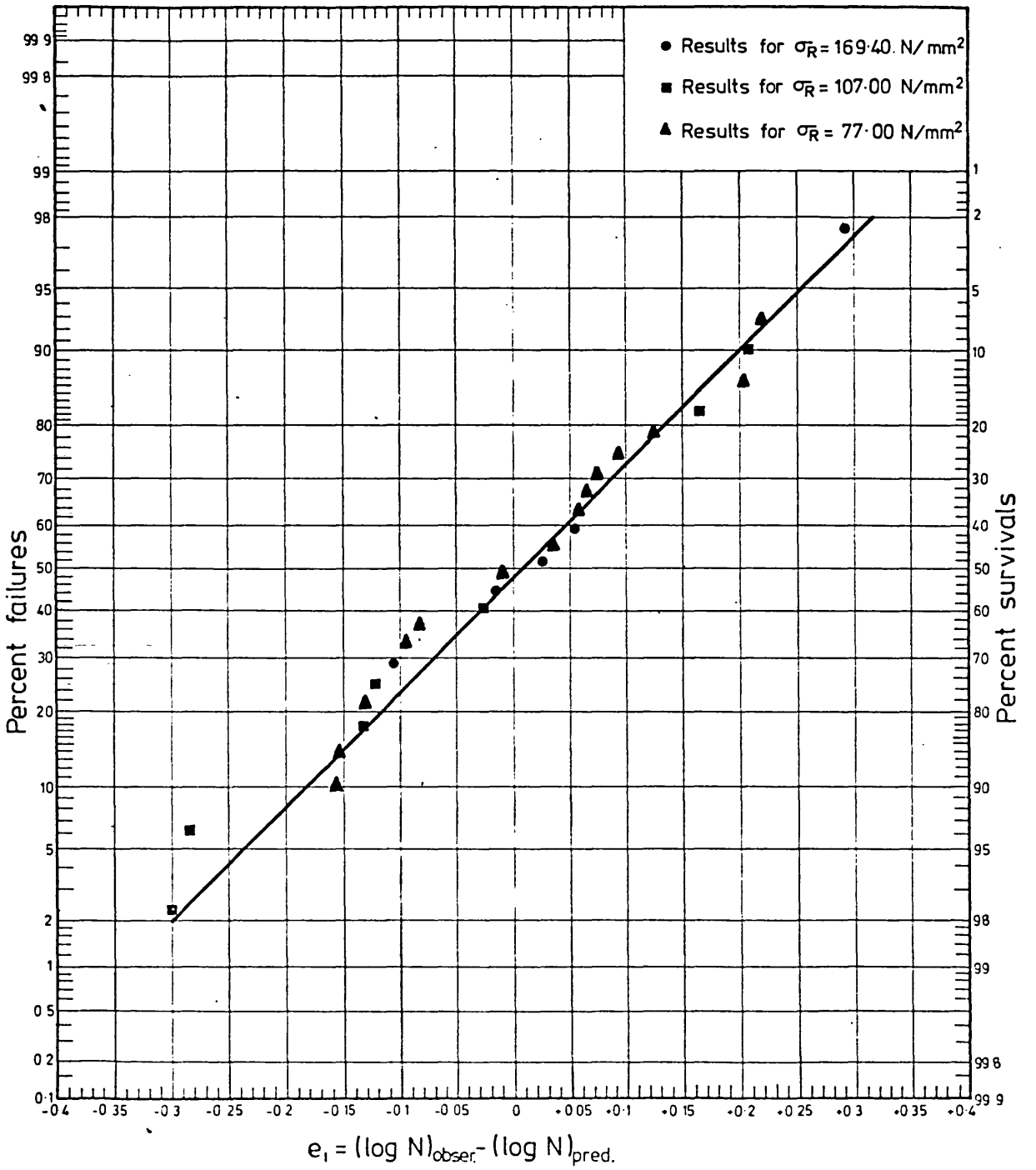


Fig. 6·16 Cumulative frequency distribution of error for series BESFG

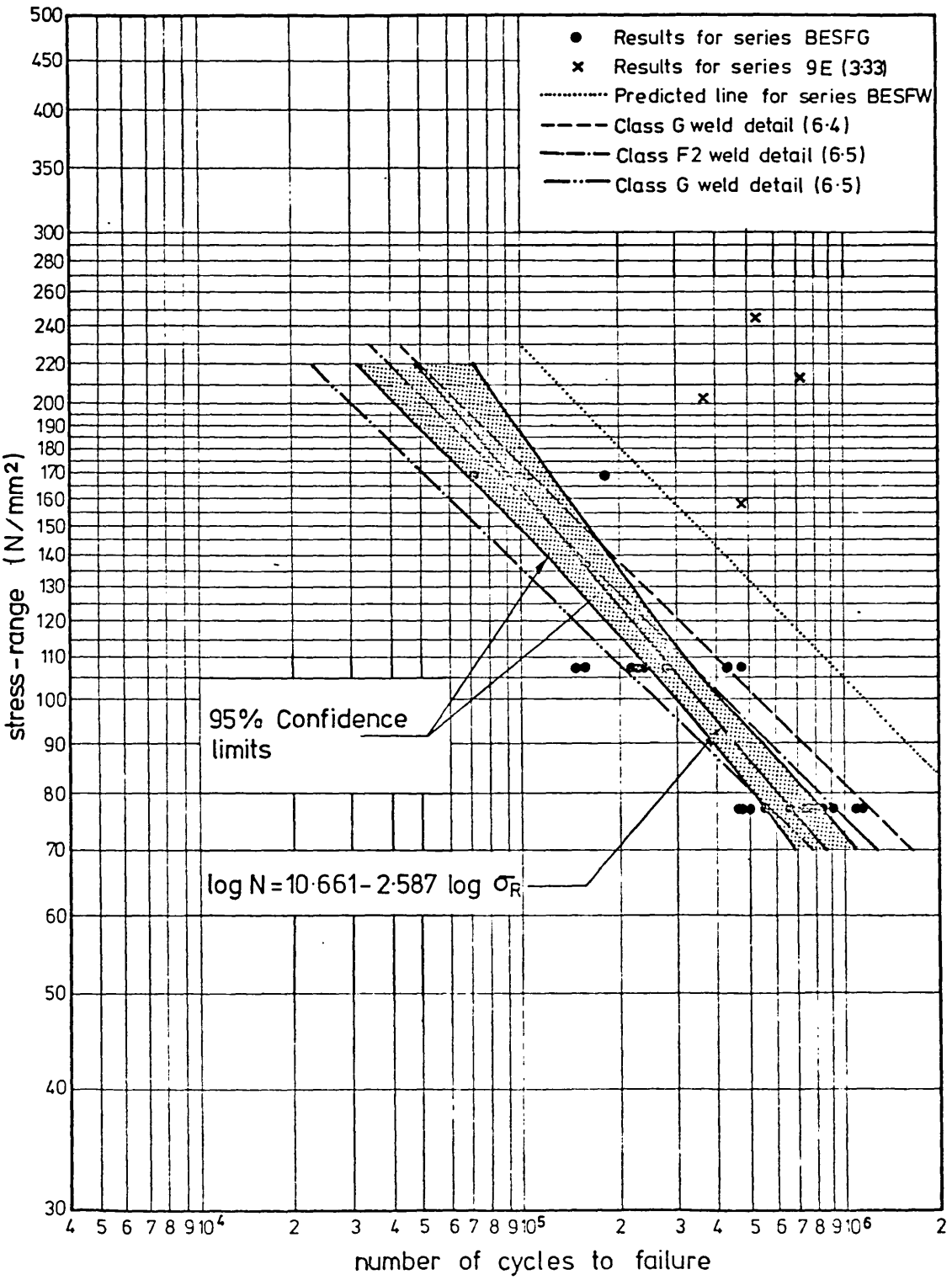


Fig. 6·17 Experimental data, mean fatigue life and 95 % confidence limits for series BESFG.

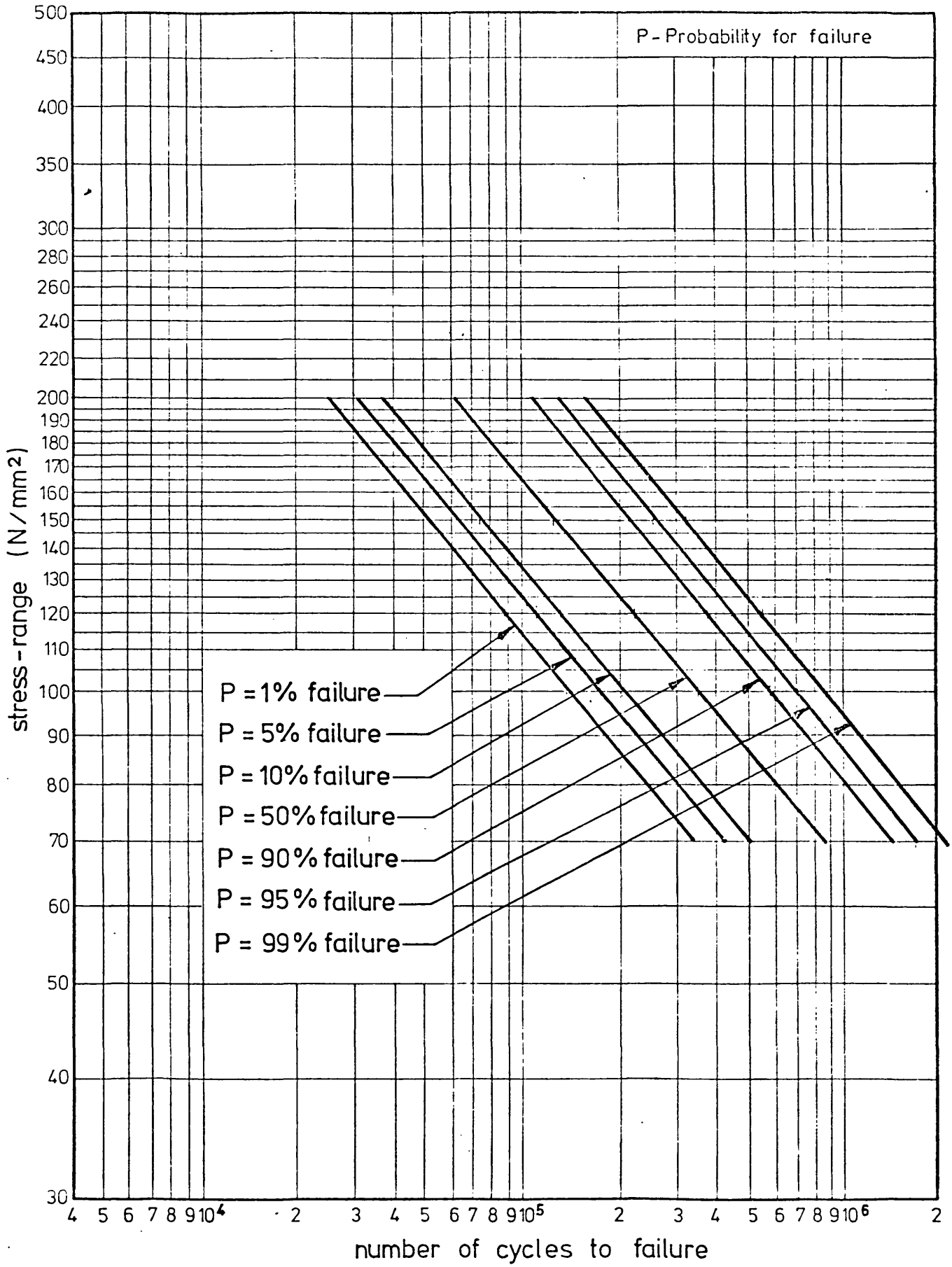


Fig. 6·18 P–S–N curves for series BESFG

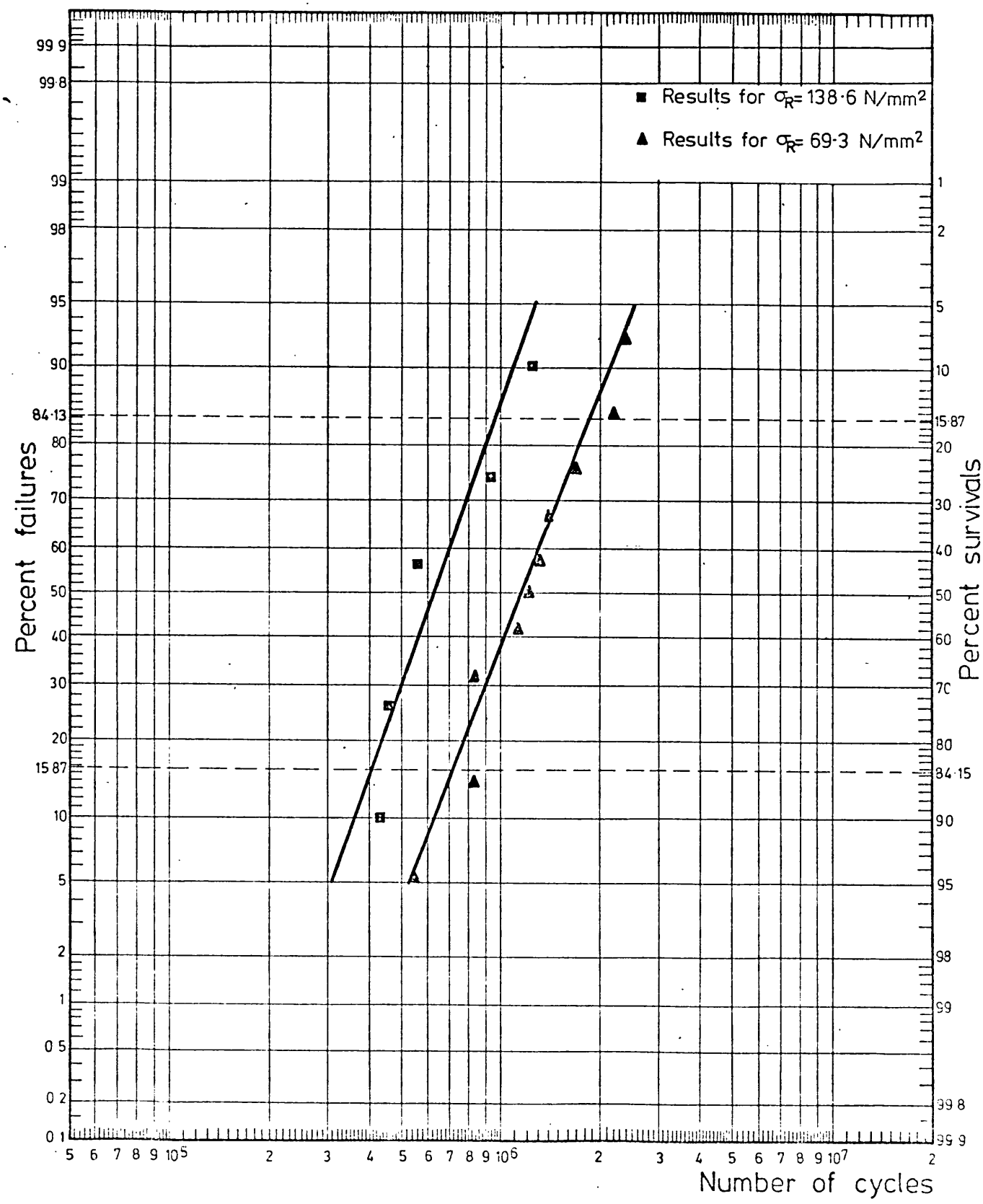


Fig. 6·19 Cumulative frequency distribution of log N for series BESFWI

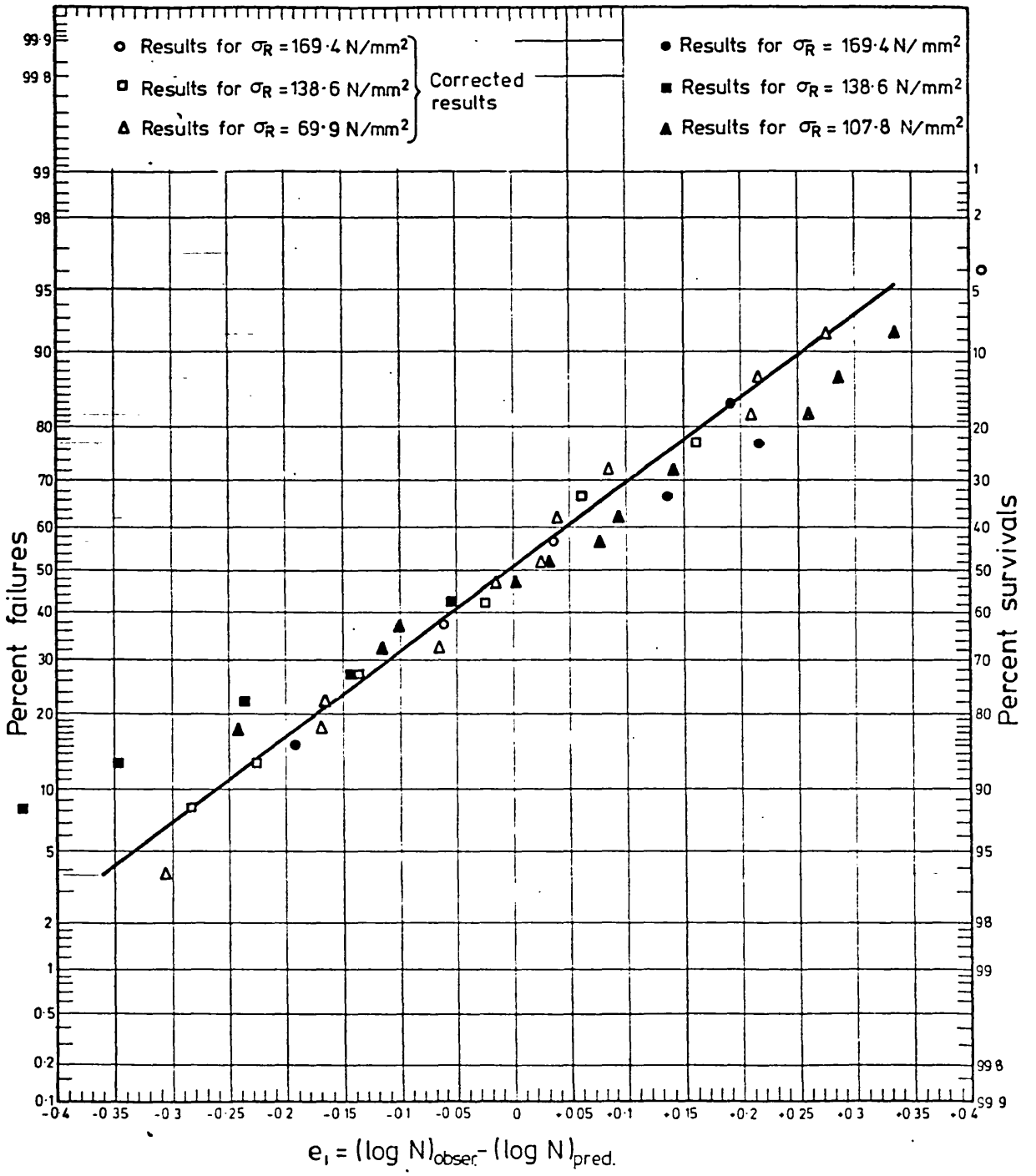


Fig. 6·20 Cumulative frequency distribution of error for series BESFWI

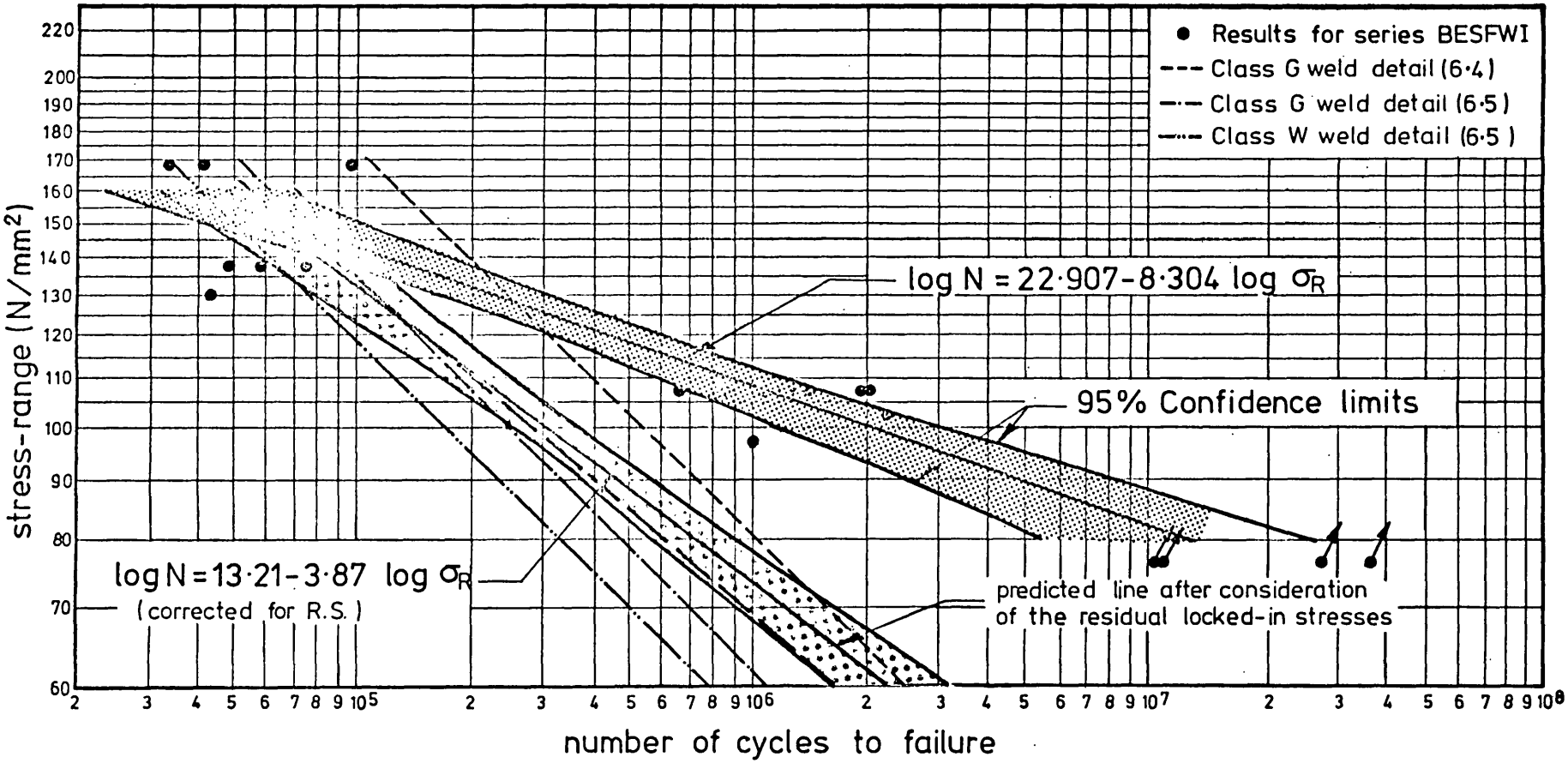


Fig. 6·21 Experimental data , mean fatigue life and 95% confidence limits of the corrected and uncorrected results of the test series BESFWI

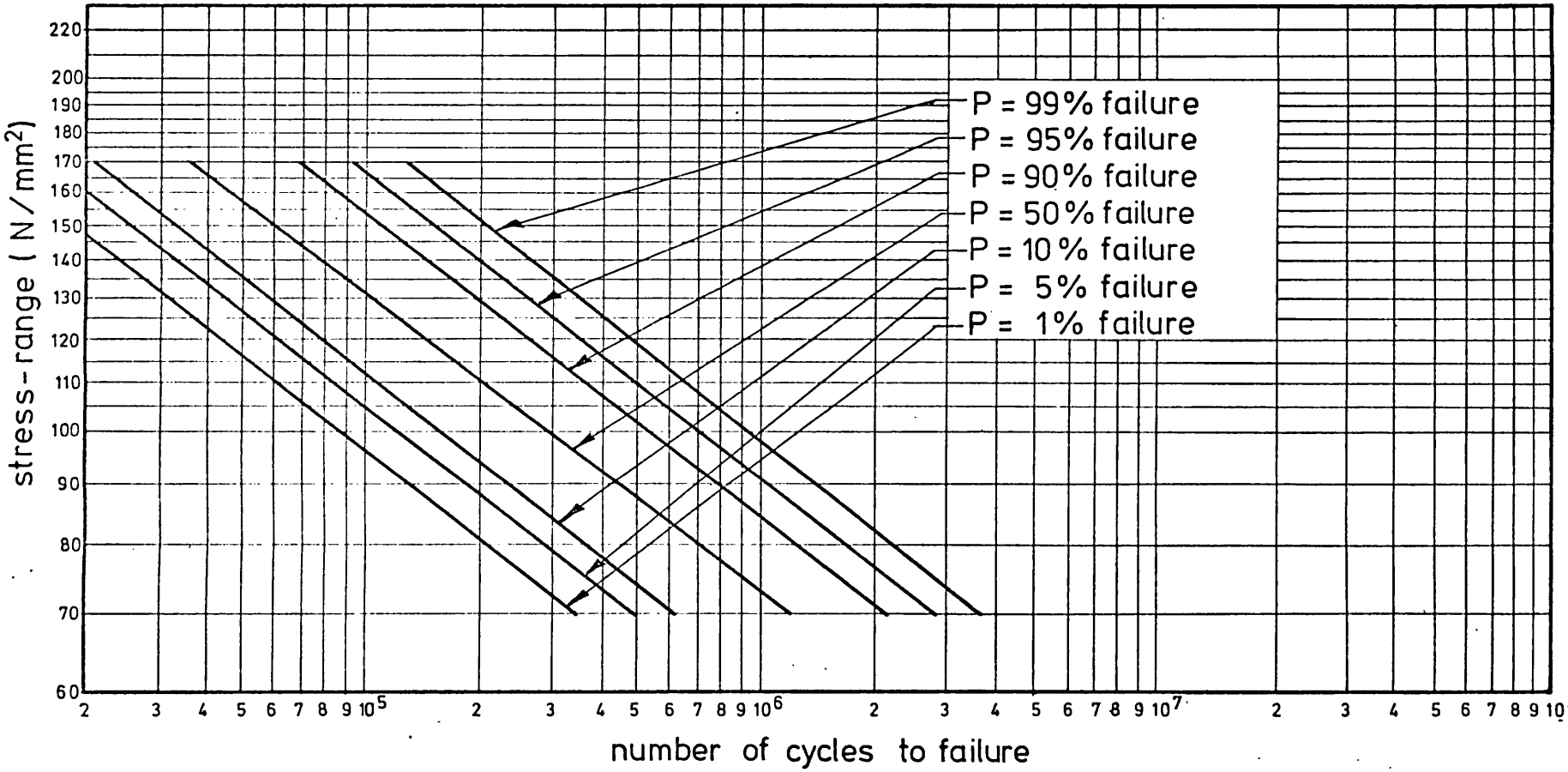


Fig. 6·22 P-S-N curves for test series BESFW I

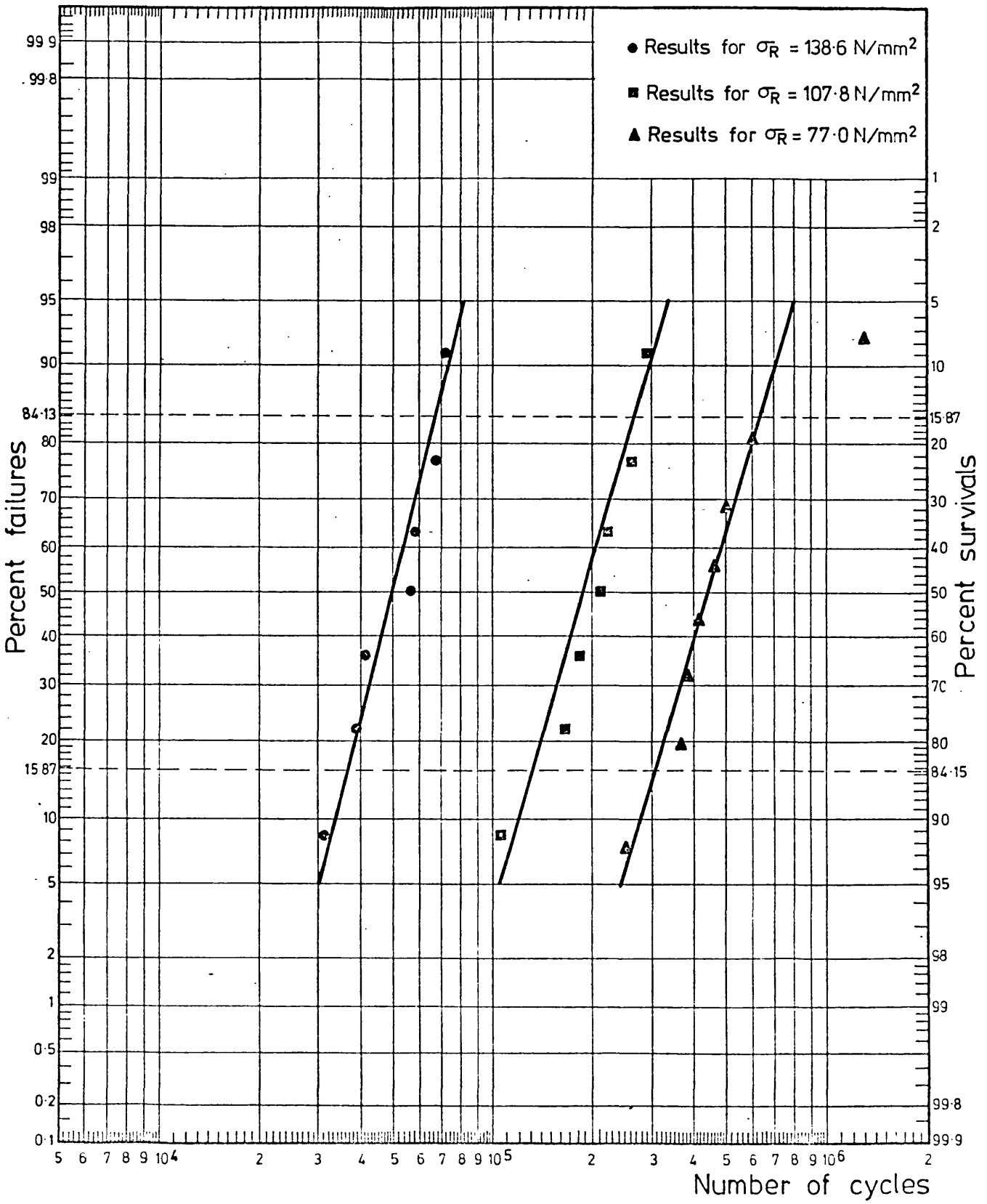


Fig. 6·23 Cumulative frequency distribution of log N for series BESFG I

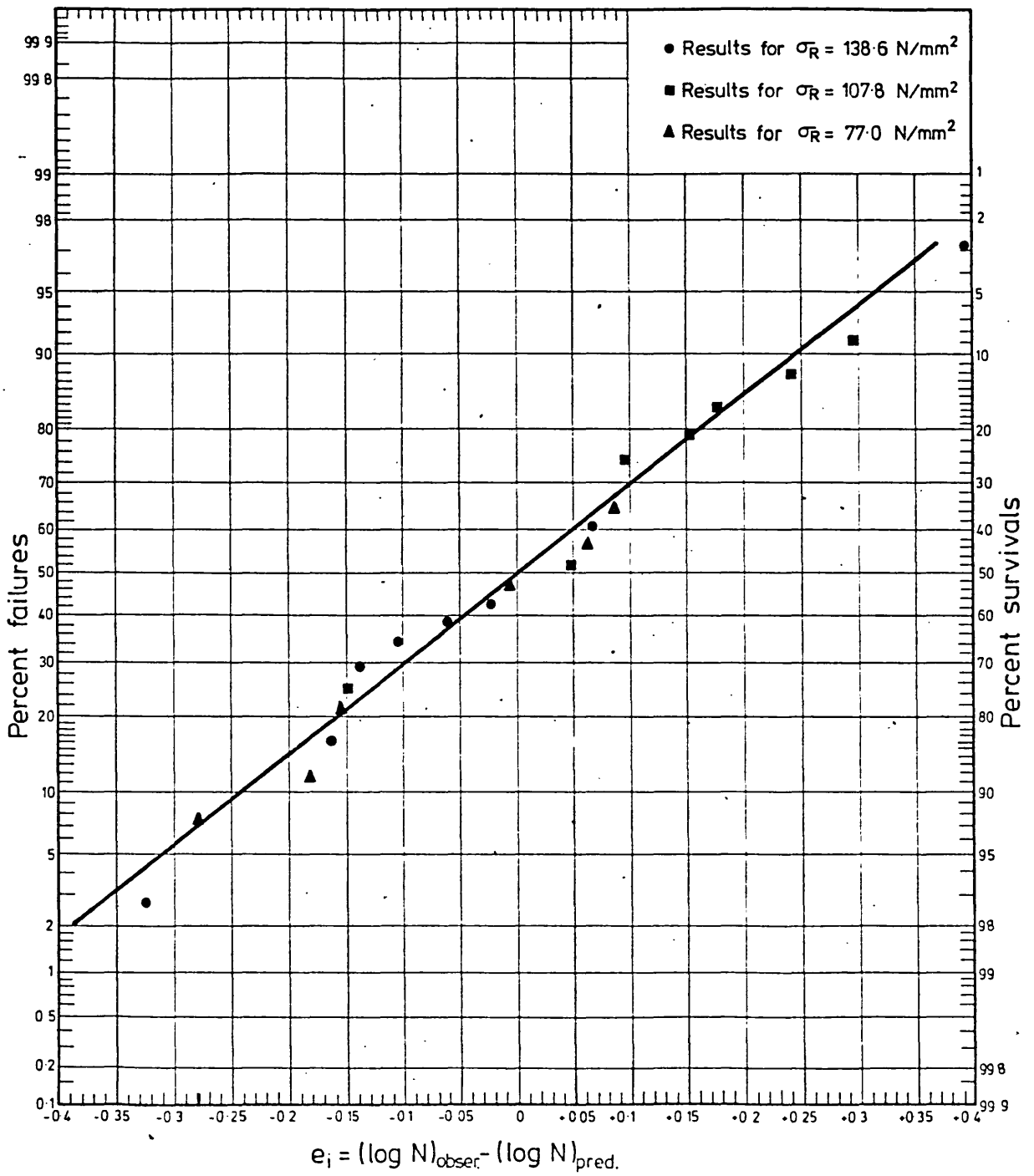


Fig. 6·24 Cumulative frequency distribution of error for series BESFGI

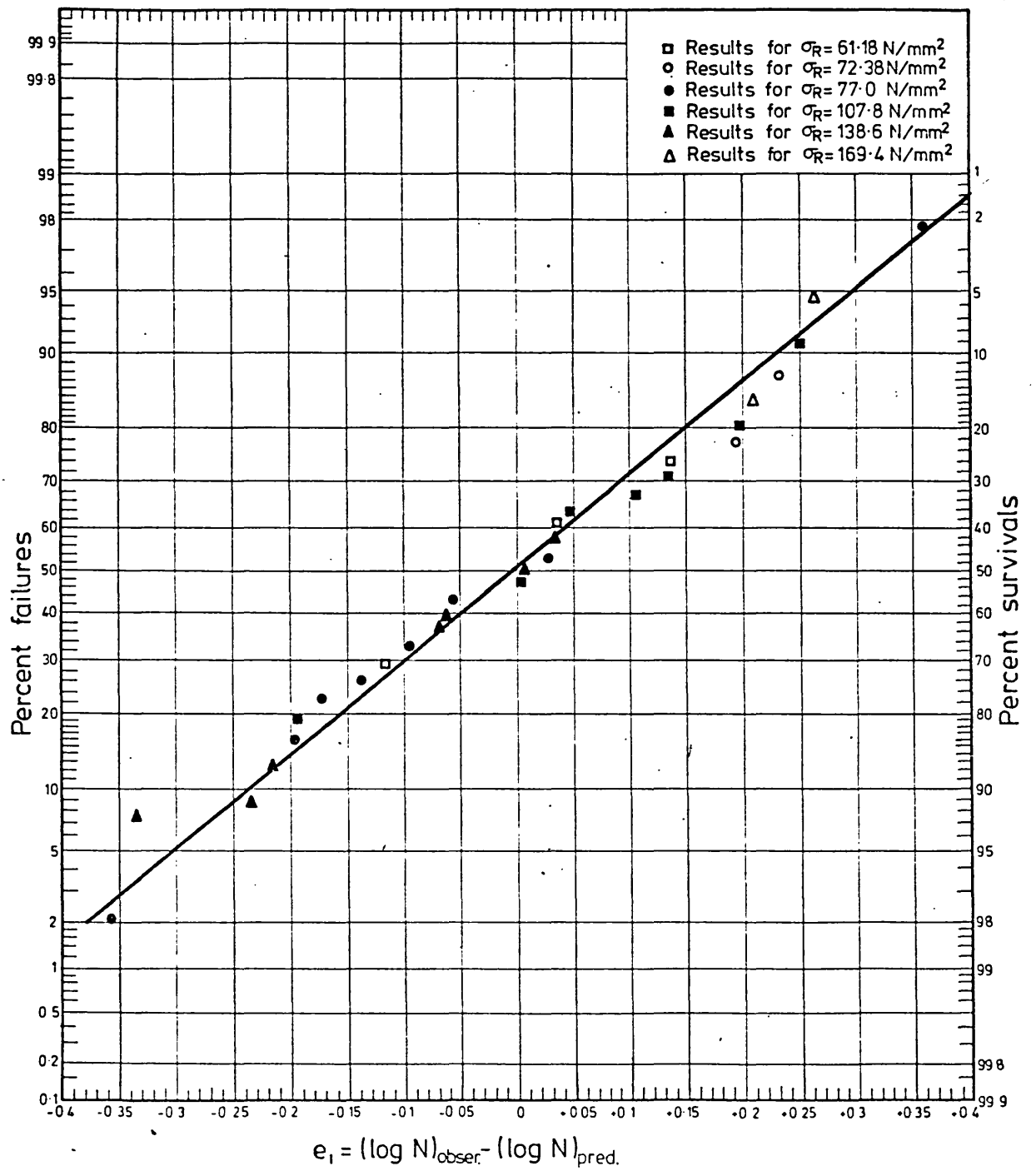


Fig. 6·25 Cumulative frequency distribution of error for series BESFG I
(Based on all experimental results)

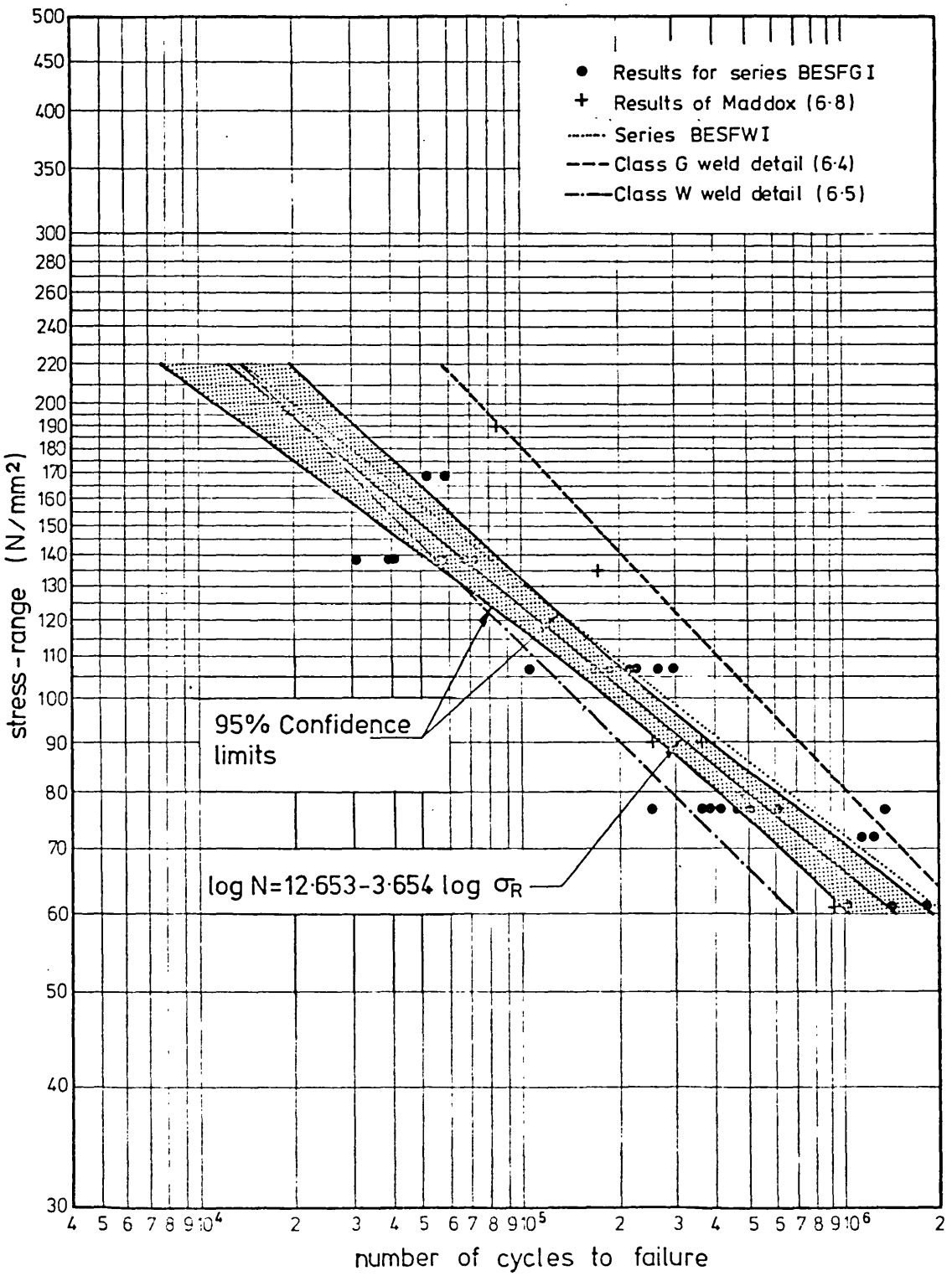


Fig. 6·26 Experimental data, mean fatigue life and 95% confidence limits for series BESFG I.

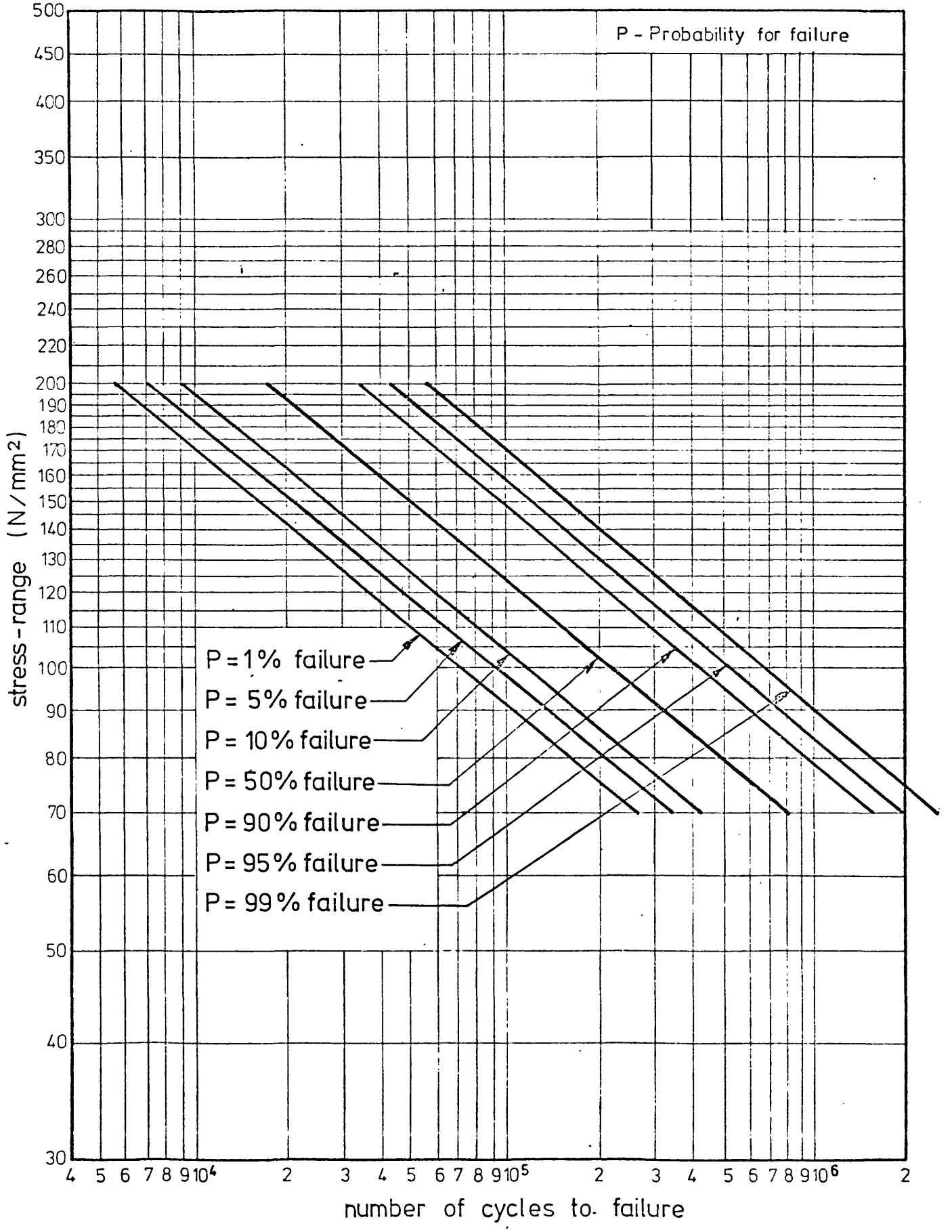


Fig. 6·27 P-S-N curves for series BESFG I

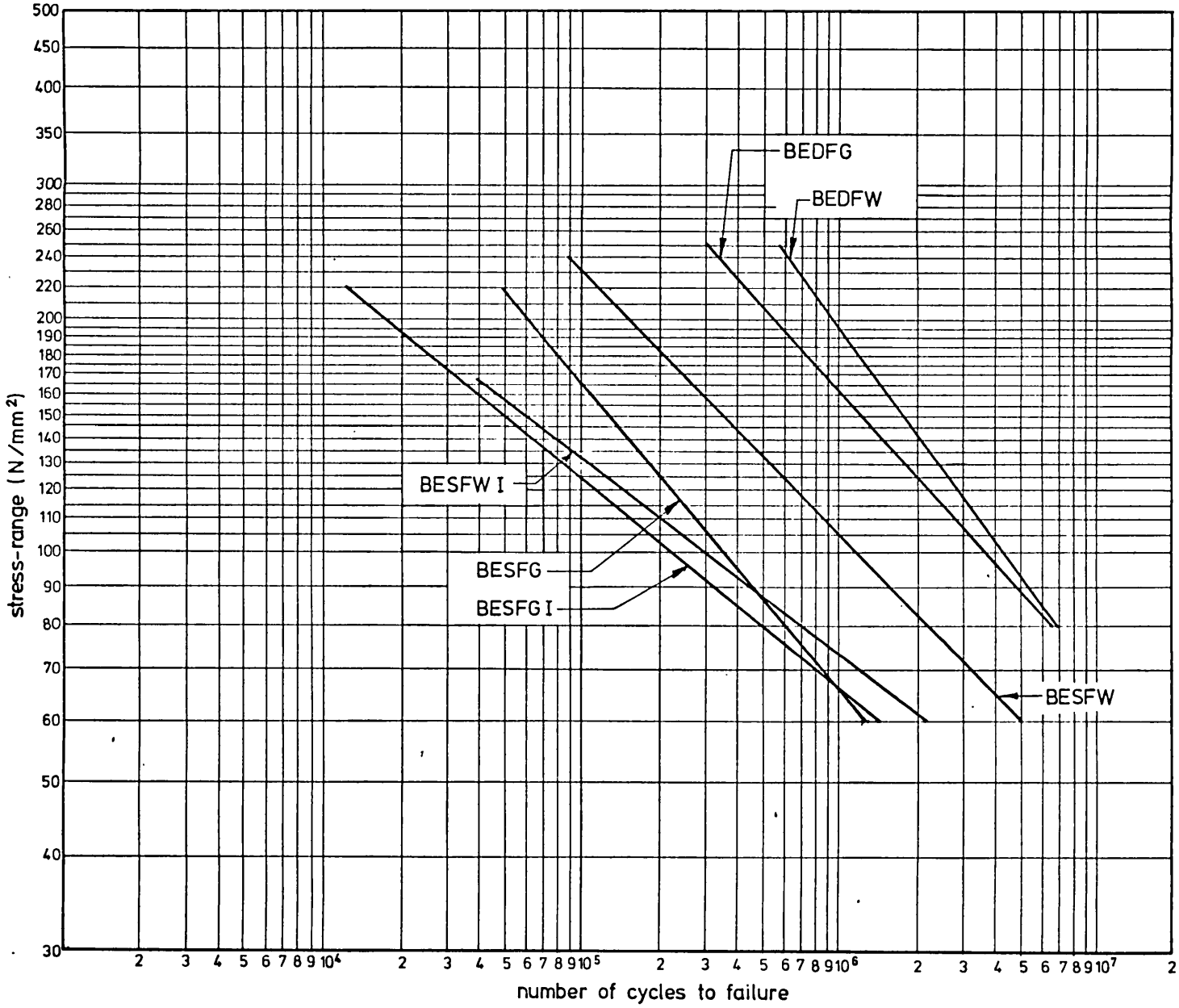


Fig. 6·28 Comparison of the mean regression lines for all fillet corner welds

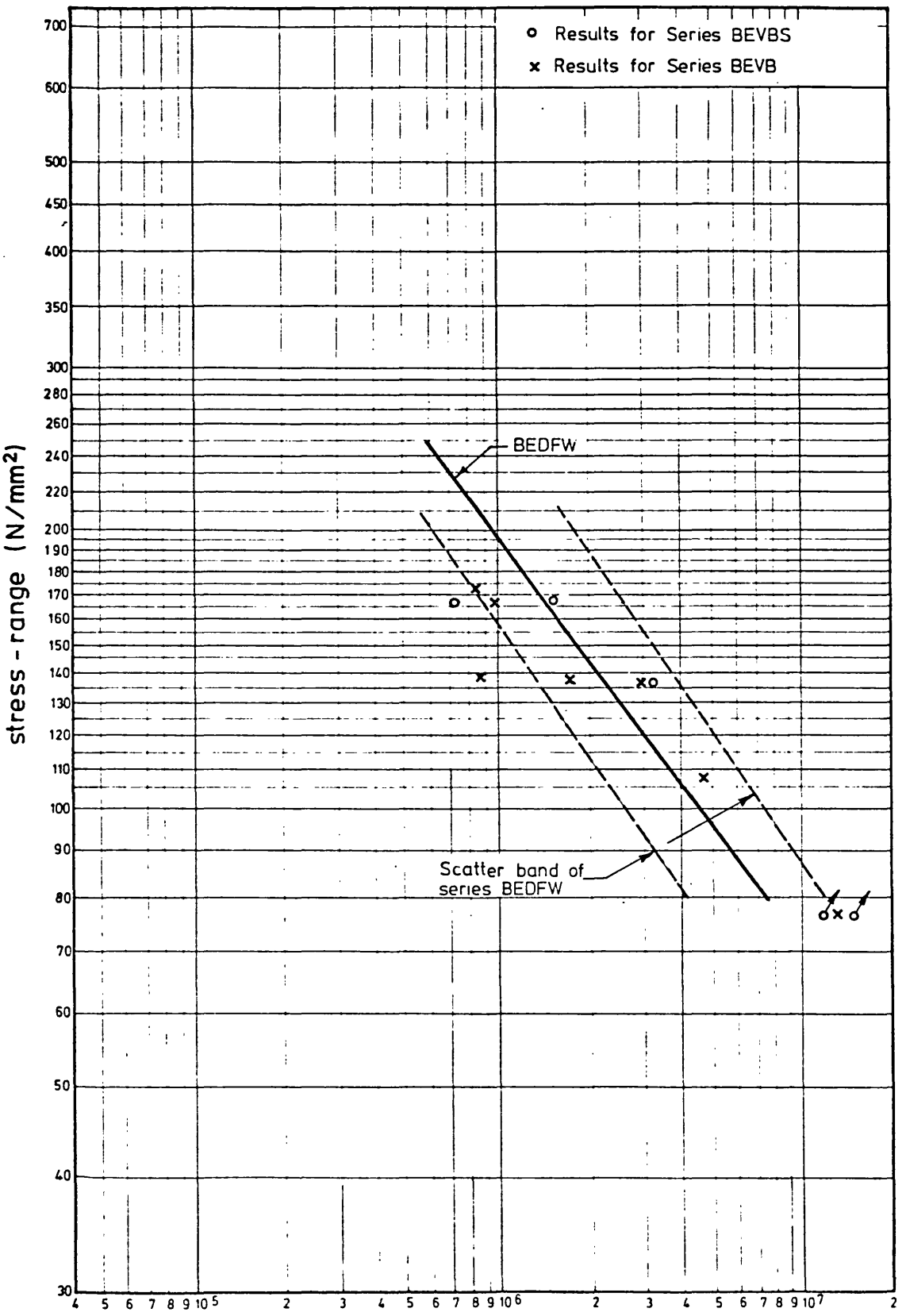


Fig. 6·29 Experiment results for V-butt welded joints

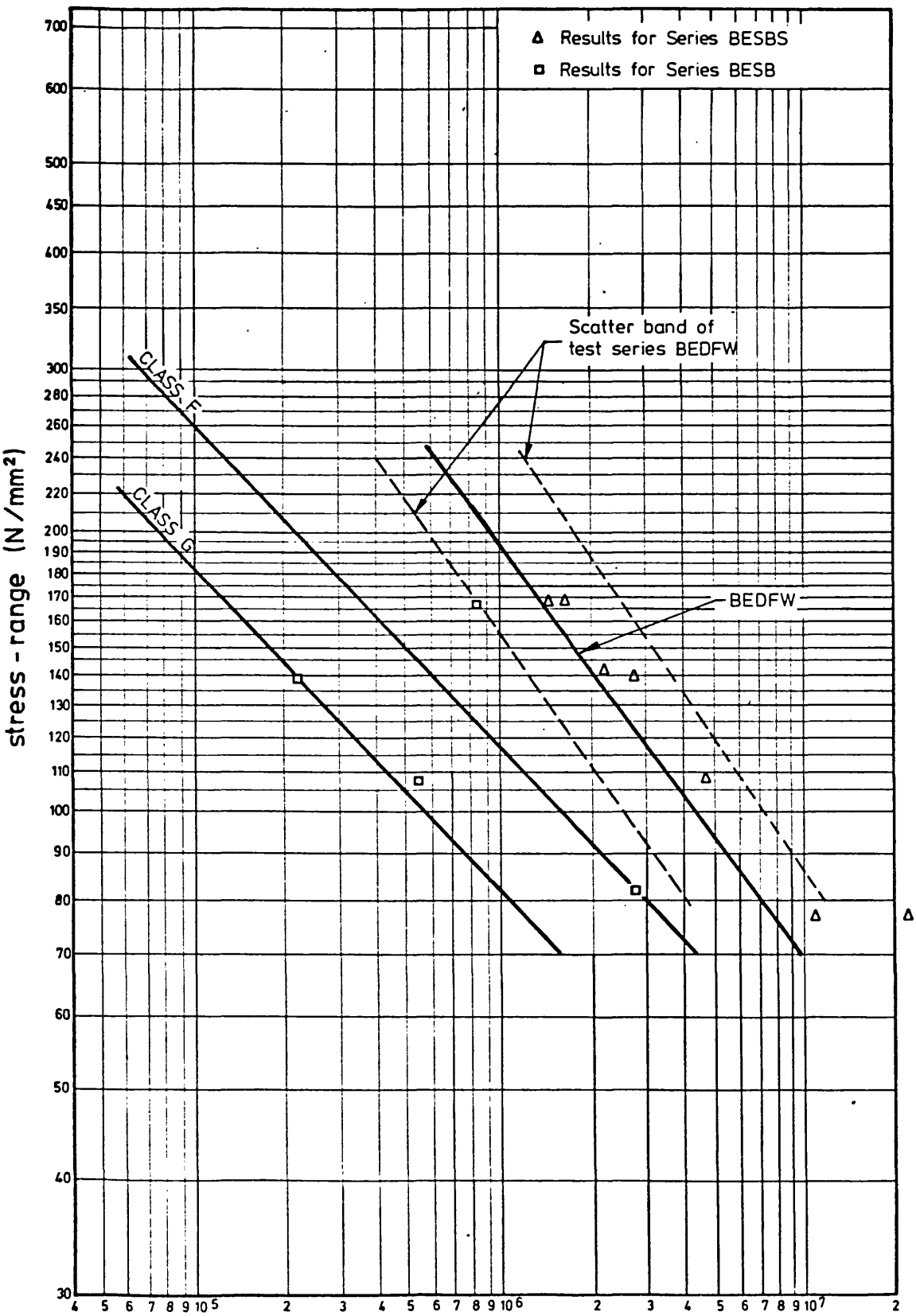


Fig. 6·30 Experimental results for single bevel V-butt weld

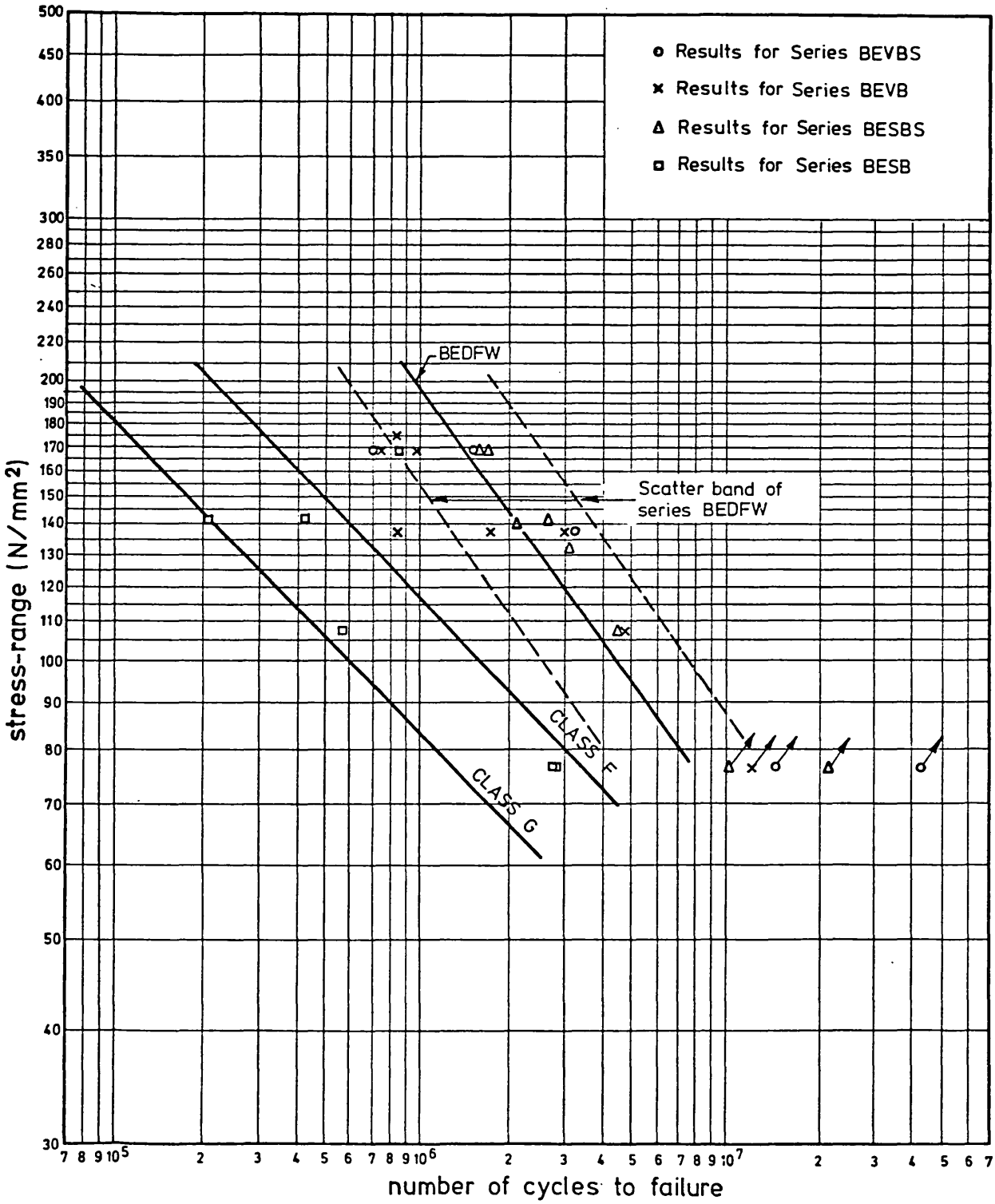


Fig. 6·31 Experimental results for different types of butt-welded joints

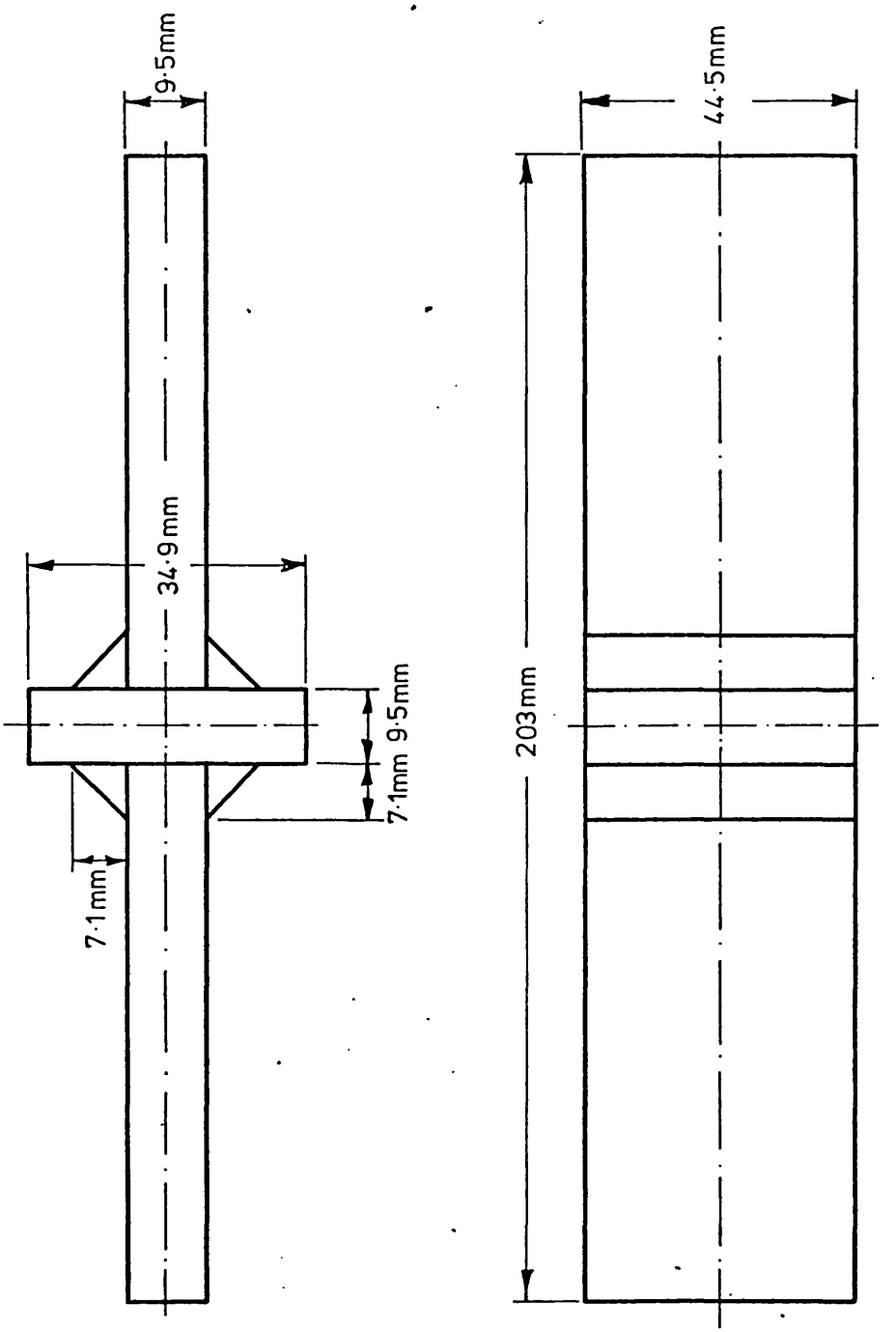


Fig. 6·32 Details of four points bending specimen (6·6)

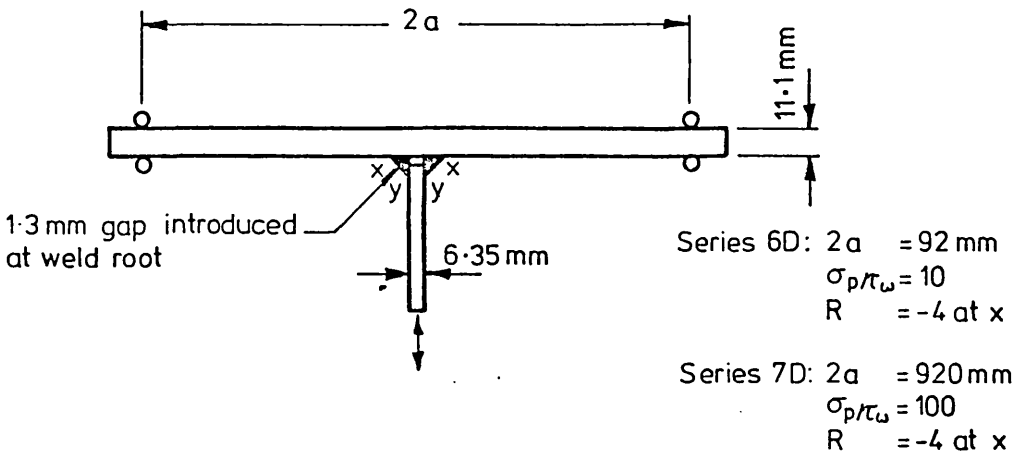


Fig. 6·33 Details of test specimens 6D and 7D (3·33)

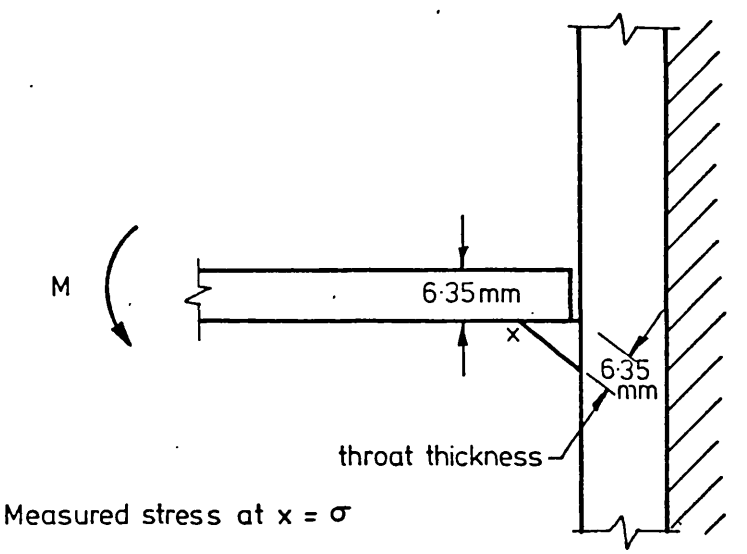
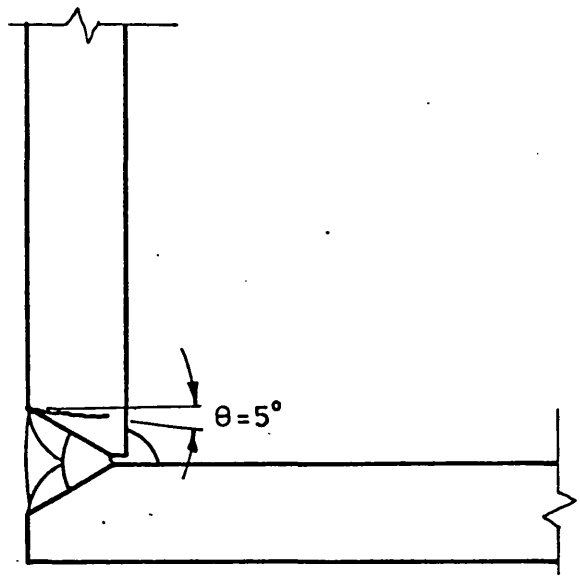
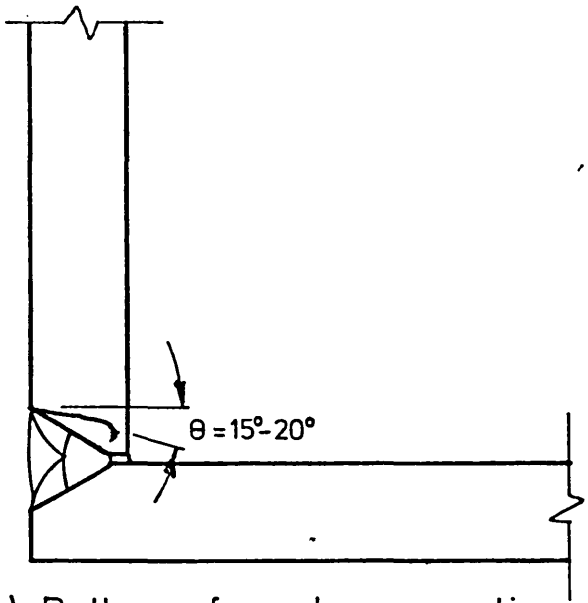


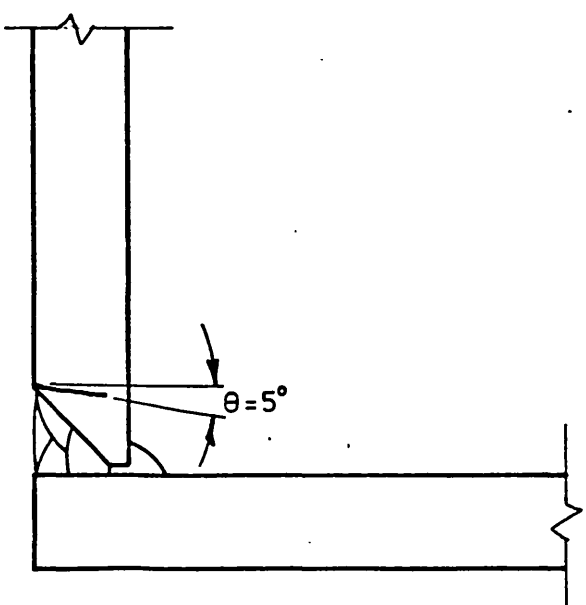
Fig. 6·34 Fillet weld in bending (6·8)



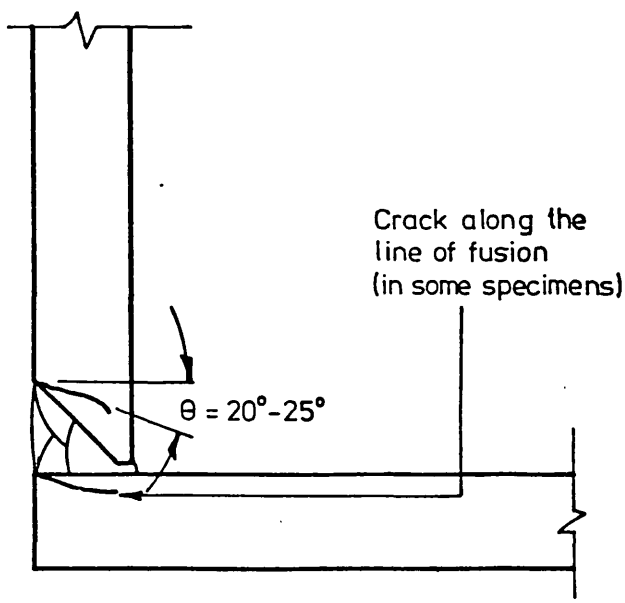
a) Pattern of crack propagation in specimen series BEVBS



b) Pattern of crack propagation in specimen series BEVB



c) Pattern of crack propagation in specimen series BESBS



d) Pattern of crack propagation in specimen series BESB

Fig. 6·35 Schematic representation of fatigue crack propagation in different types of butt corner joints.

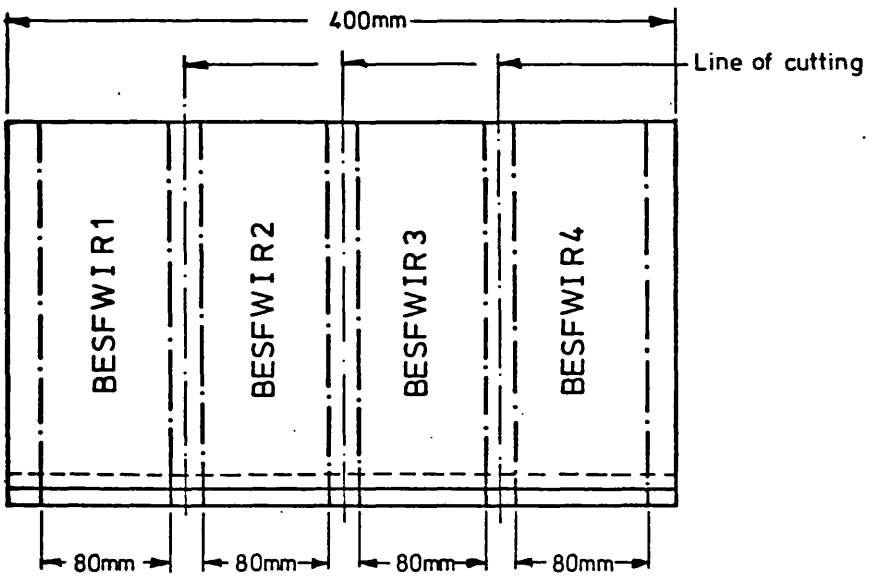


Fig. 7·1 Specimens and their designations used to investigate the effect of residual stress on fatigue.

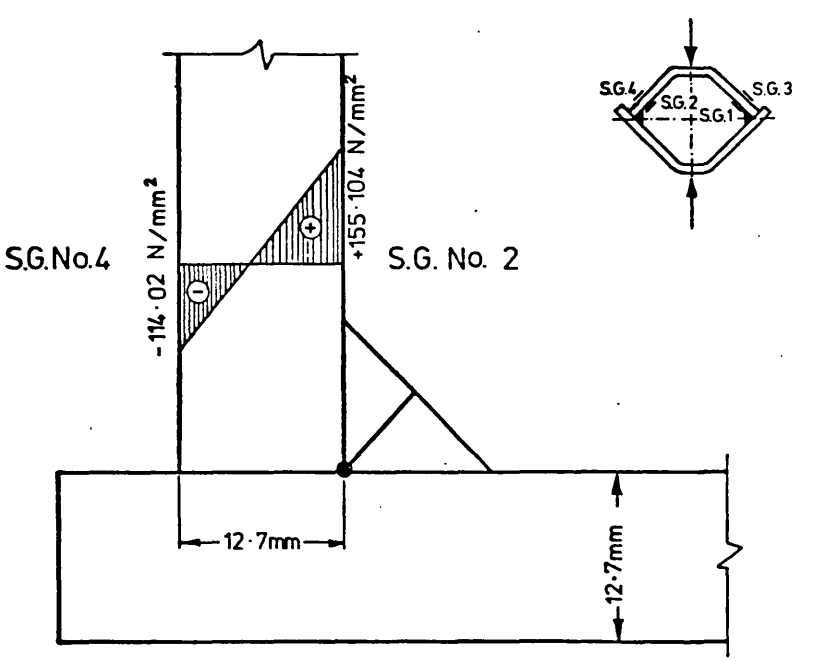


Fig. 7·2 Distribution of residual stresses across the plate thickness measured at the vicinity of the weld toe (specimen BESFWIR-2).

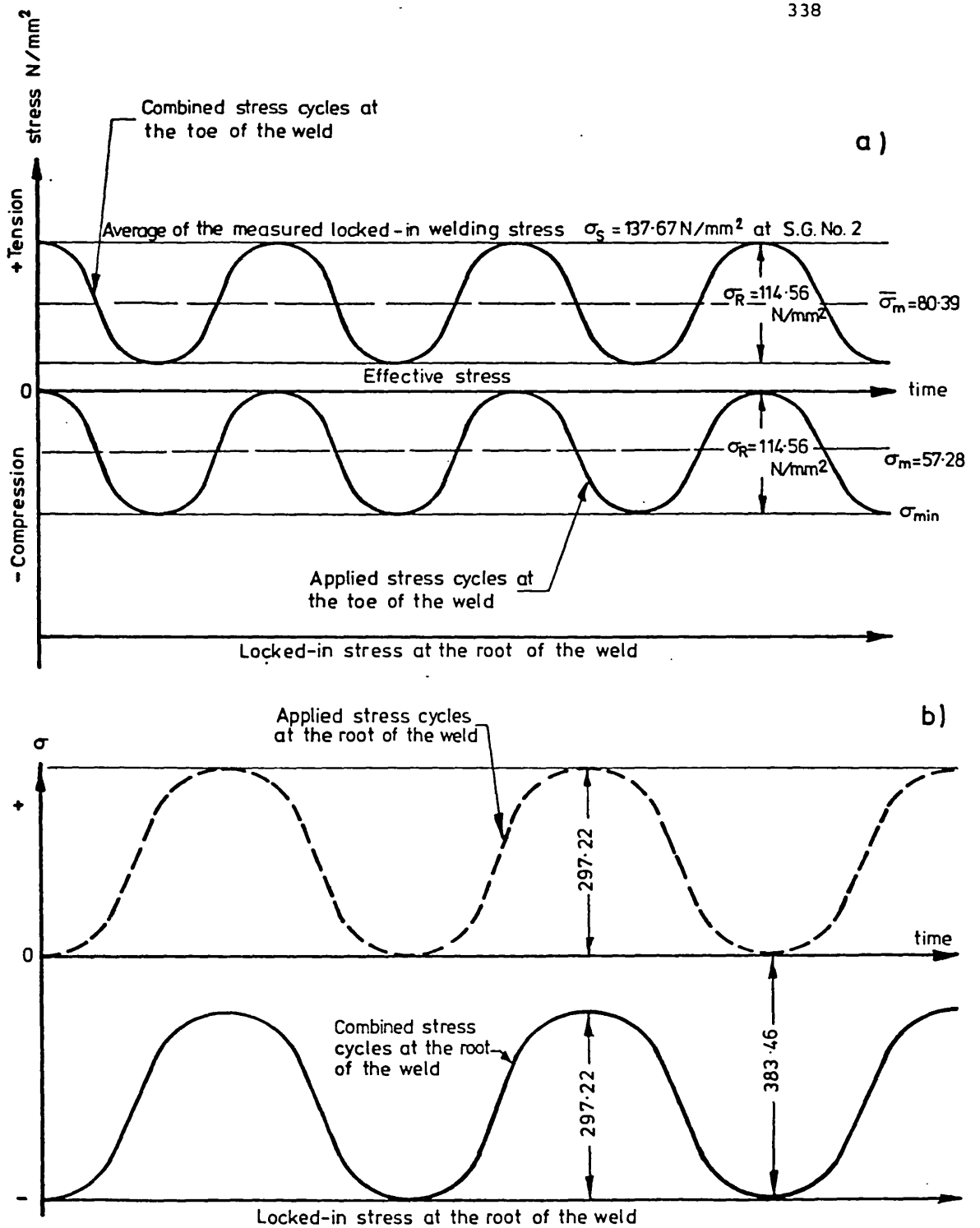


Fig. 7·3 Influence of the residual stresses on applied cyclic load
a) stresses at the toe of the weld
b) stresses at the root of the weld

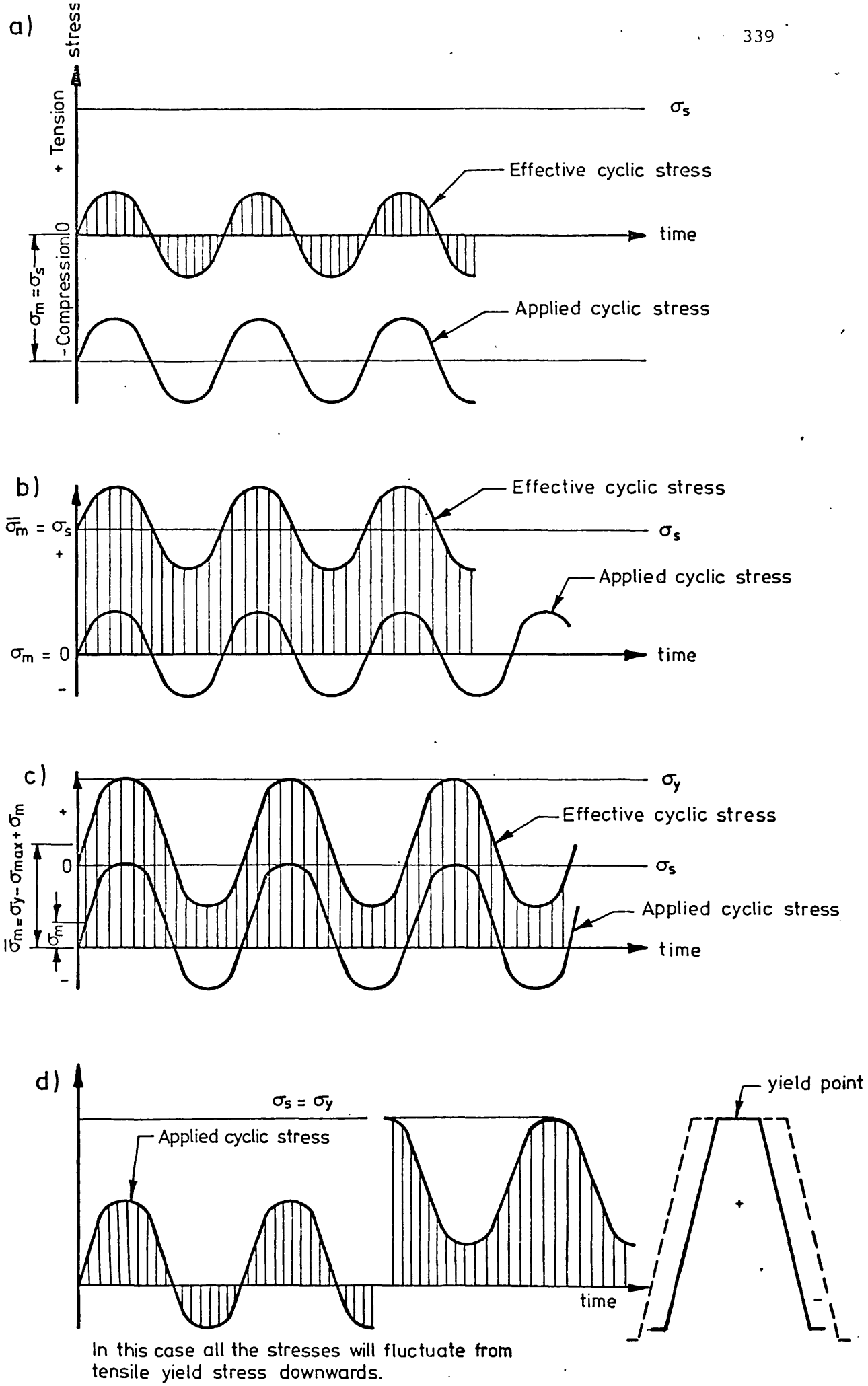


Fig. 7·4 Change of applied cyclic load due to locked-in stress

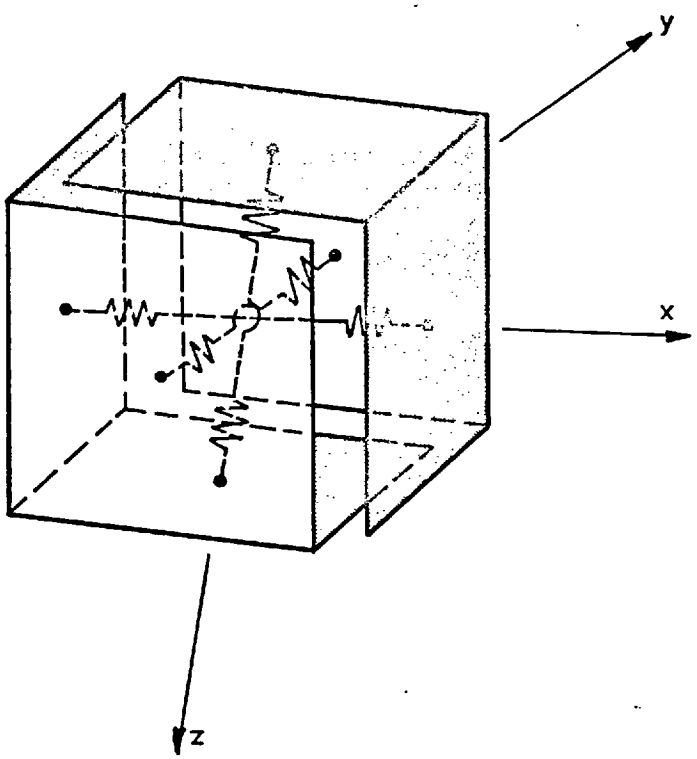


Fig. 8·1 Linkage element representation at the corner of the box.

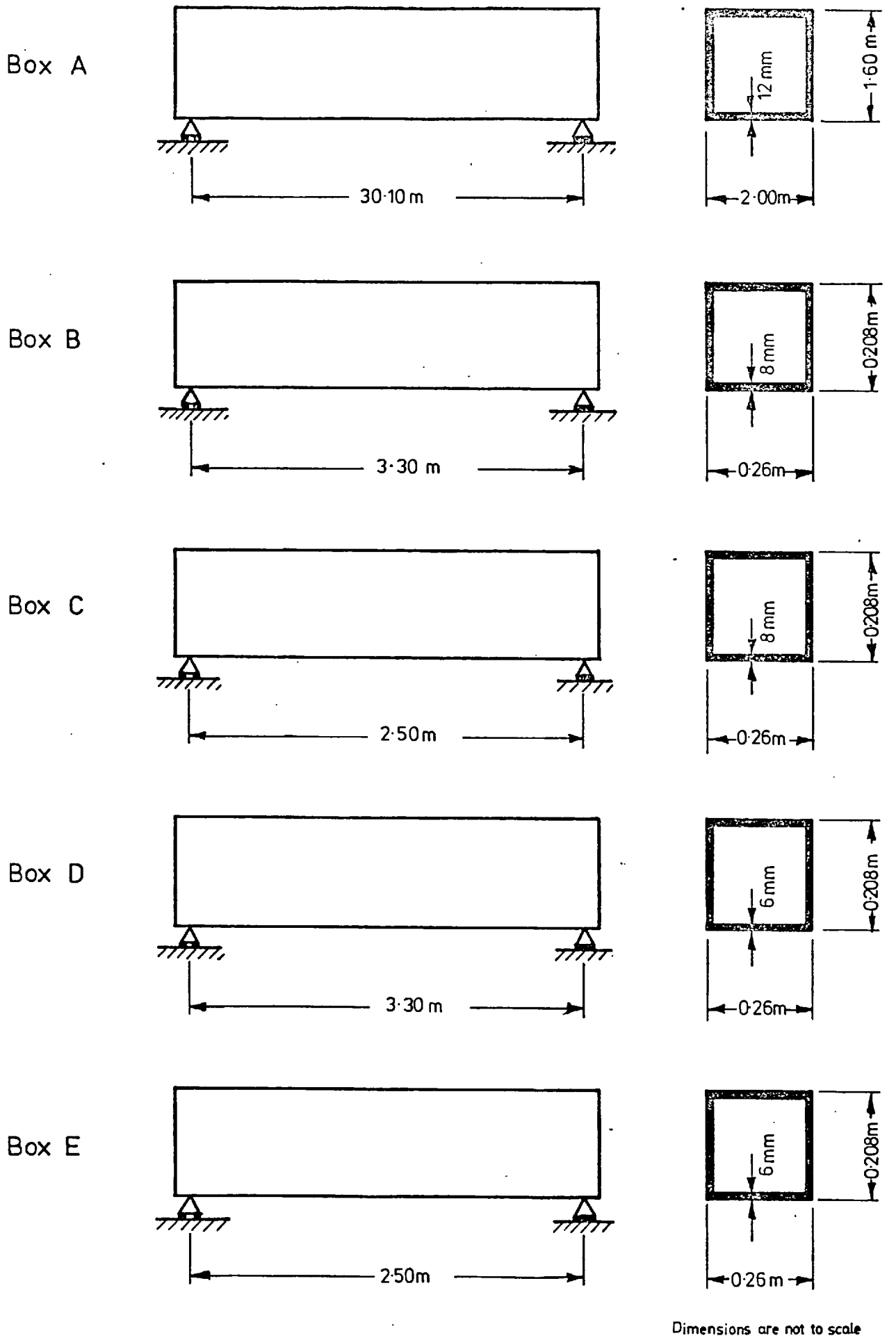


Fig. 8·2 Dimensions of the analysed boxes

DIMENSIONS SHOWN THUS *3000* ARE FOR BOX A - 12mm plate thickness
DIMENSIONS SHOWN THUS (250) ARE FROM BOX B - 8mm plate thickness - AND BOX D - 6mm plate thickness
DIMENSIONS SHOWN THUS [200] ARE FROM BOX C - 8mm plate thickness - AND BOX E - 6mm plate thickness

ALL DIMENSIONS ARE IN MILLIMETRE

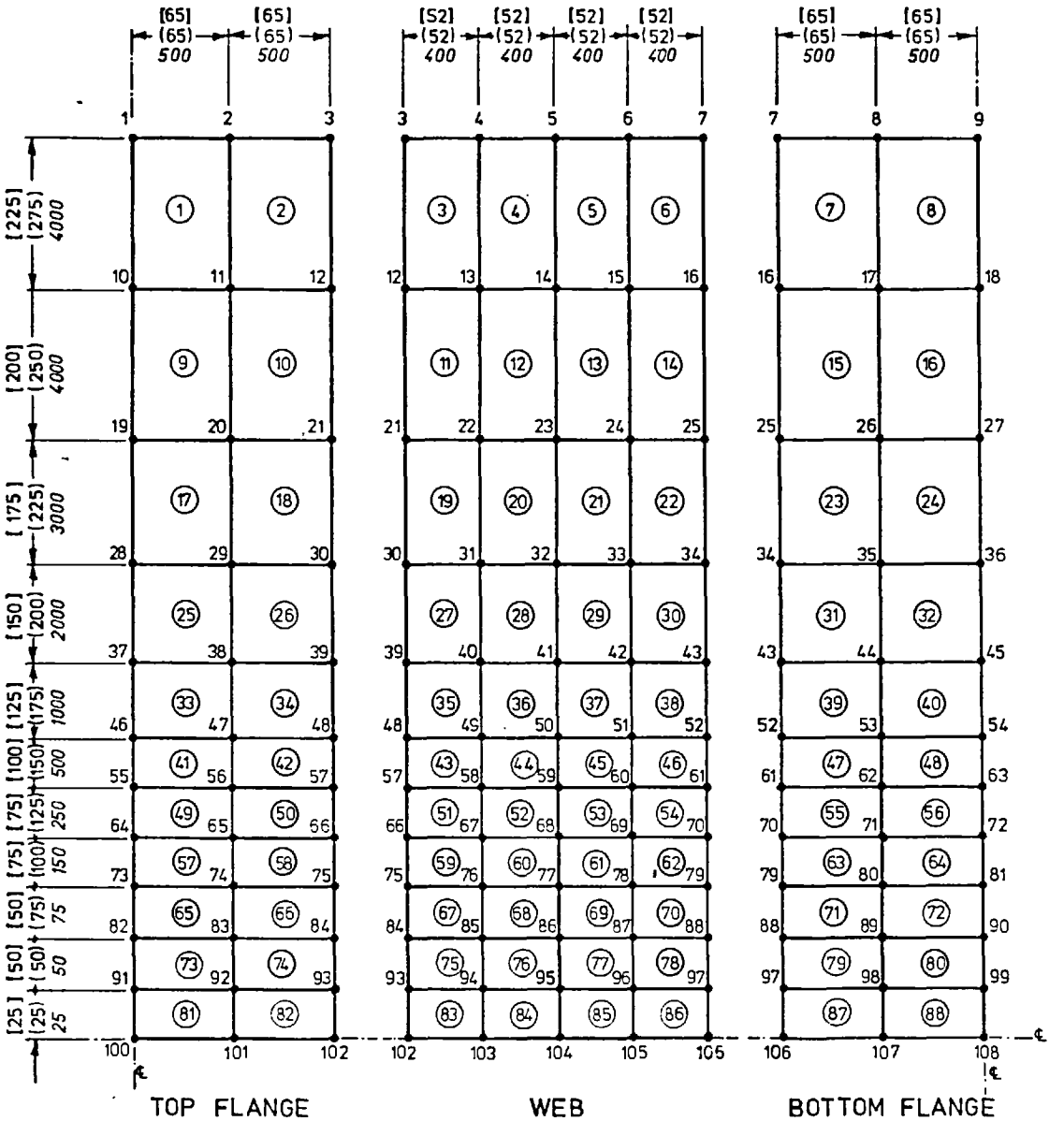


Fig. 8·3 Finite element mesh for Boxes A, B, C, D, and E without linkage elements.

DIMENSIONS SHOWN THUS *3000* ARE FOR BOX A – 12mm plate thickness
DIMENSIONS SHOWN THUS (250) ARE FROM BOX B – 8mm plate thickness – AND BOX D–6mm plate thickness
DIMENSIONS SHOWN THUS [200] ARE FROM BOX C – 8mm plate thickness – AND BOX E – 6mm plate thickness

ALL DIMENSIONS ARE IN MILLIMETRE

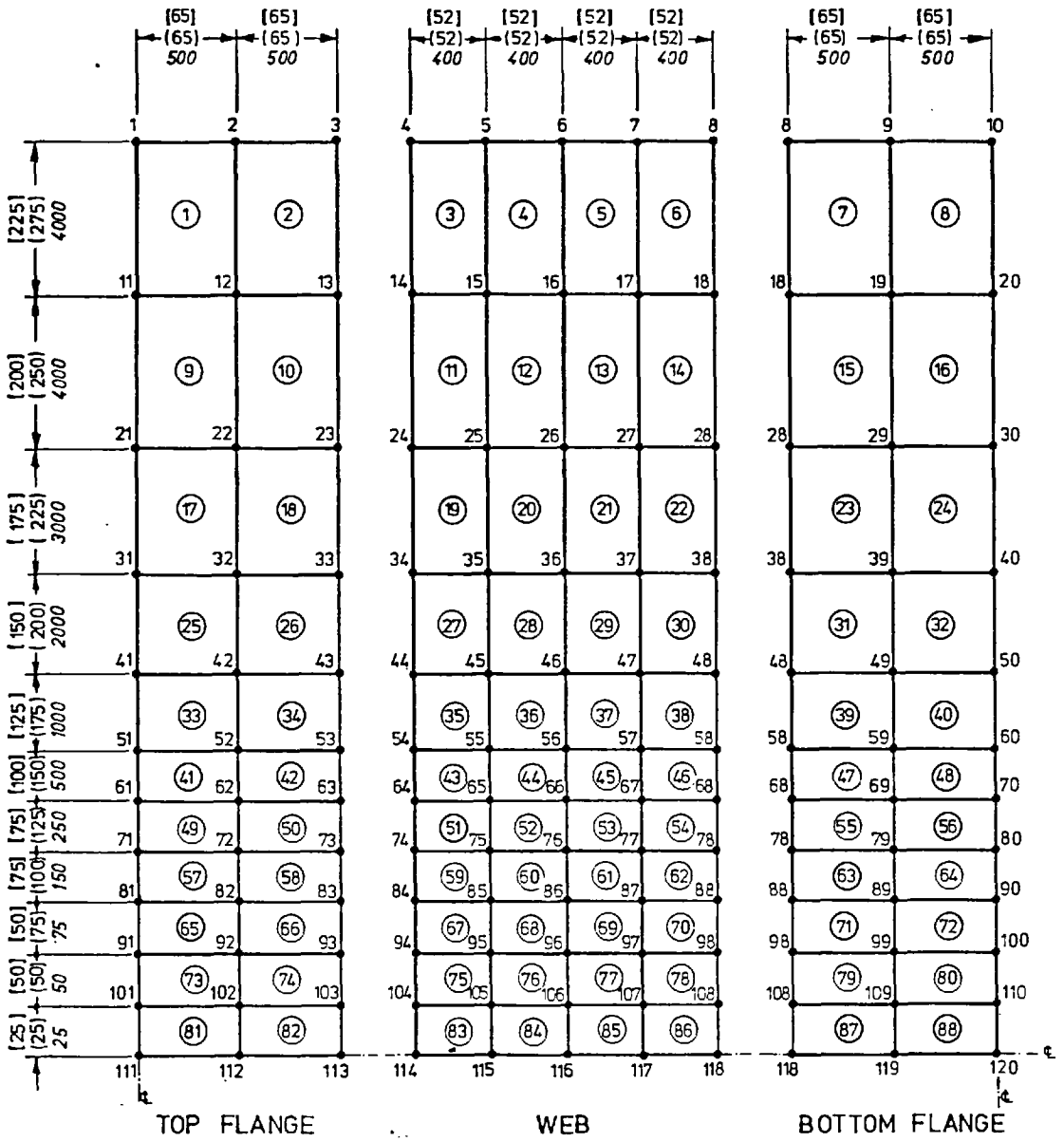


Fig. 8·4 Finite element mesh for Boxes A, B, C, D, and E with linkage elements

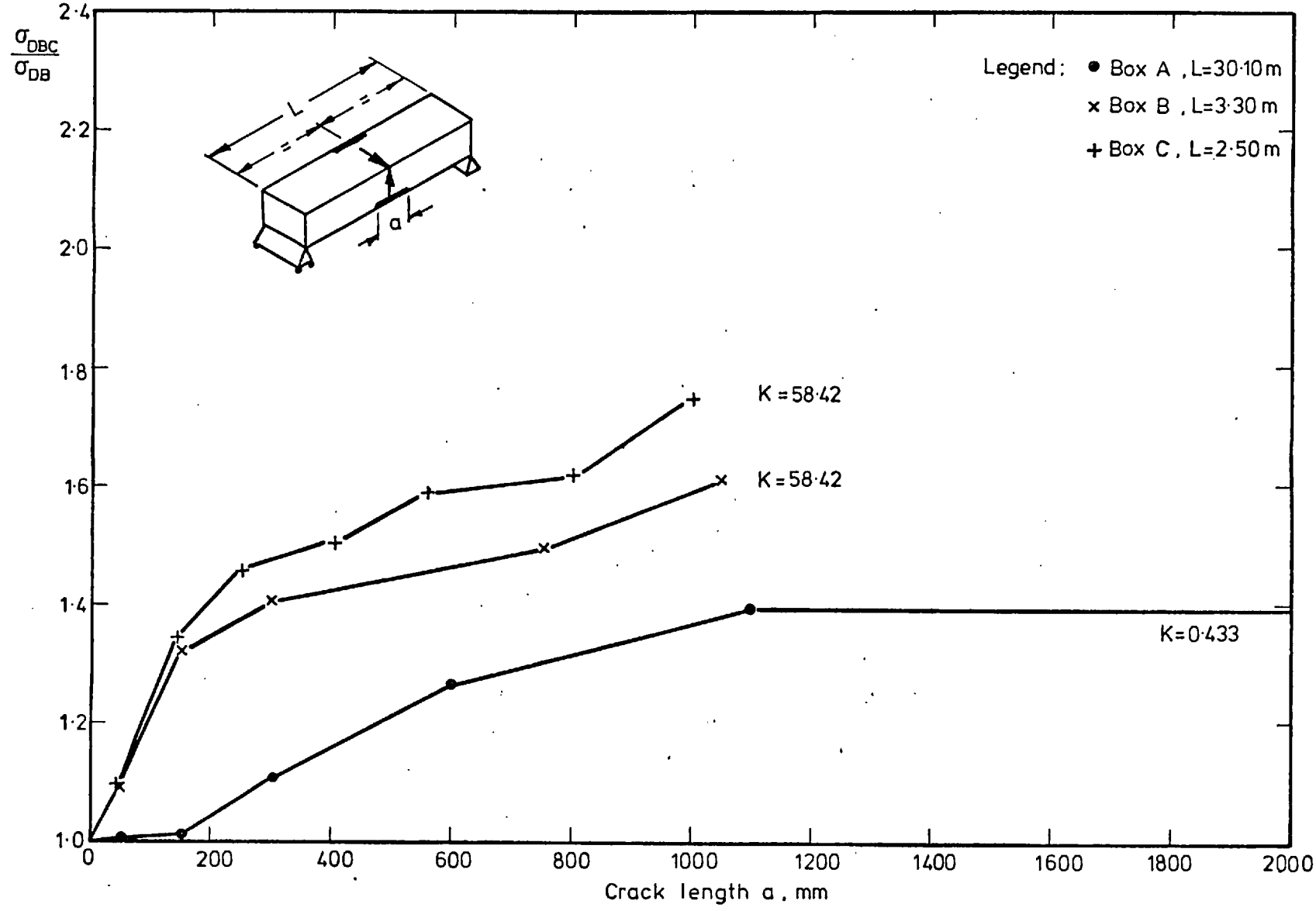


Fig. 8·5 The results for boxes A, B, and C showing the relationship between crack length and σ_{DBC}/σ_{DB} for point load at the midspan.

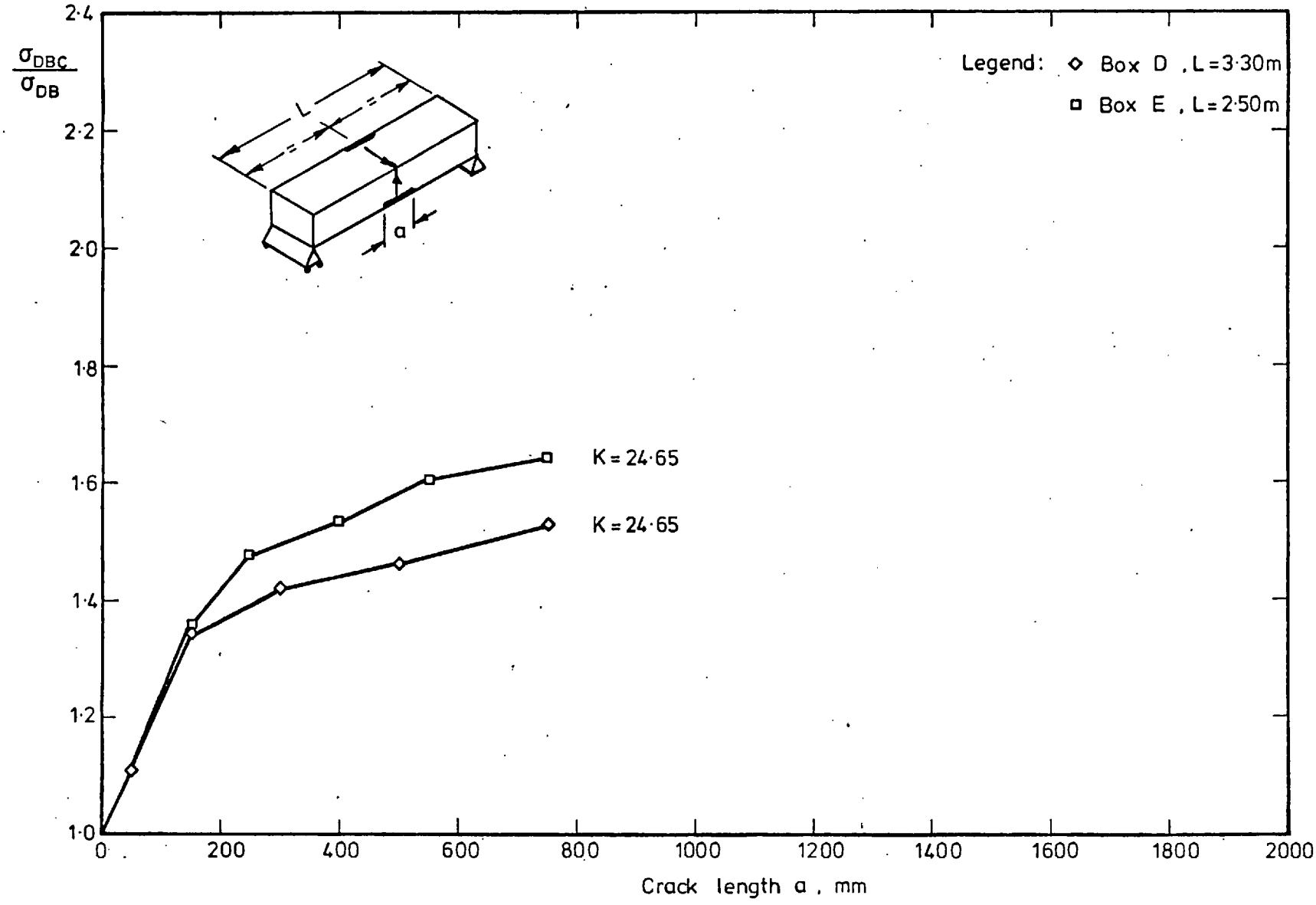


Fig. 8·6 The results for boxes D and E showing the relationship between crack length and σ_{DBC}/σ_{DB} for point load at midspan.

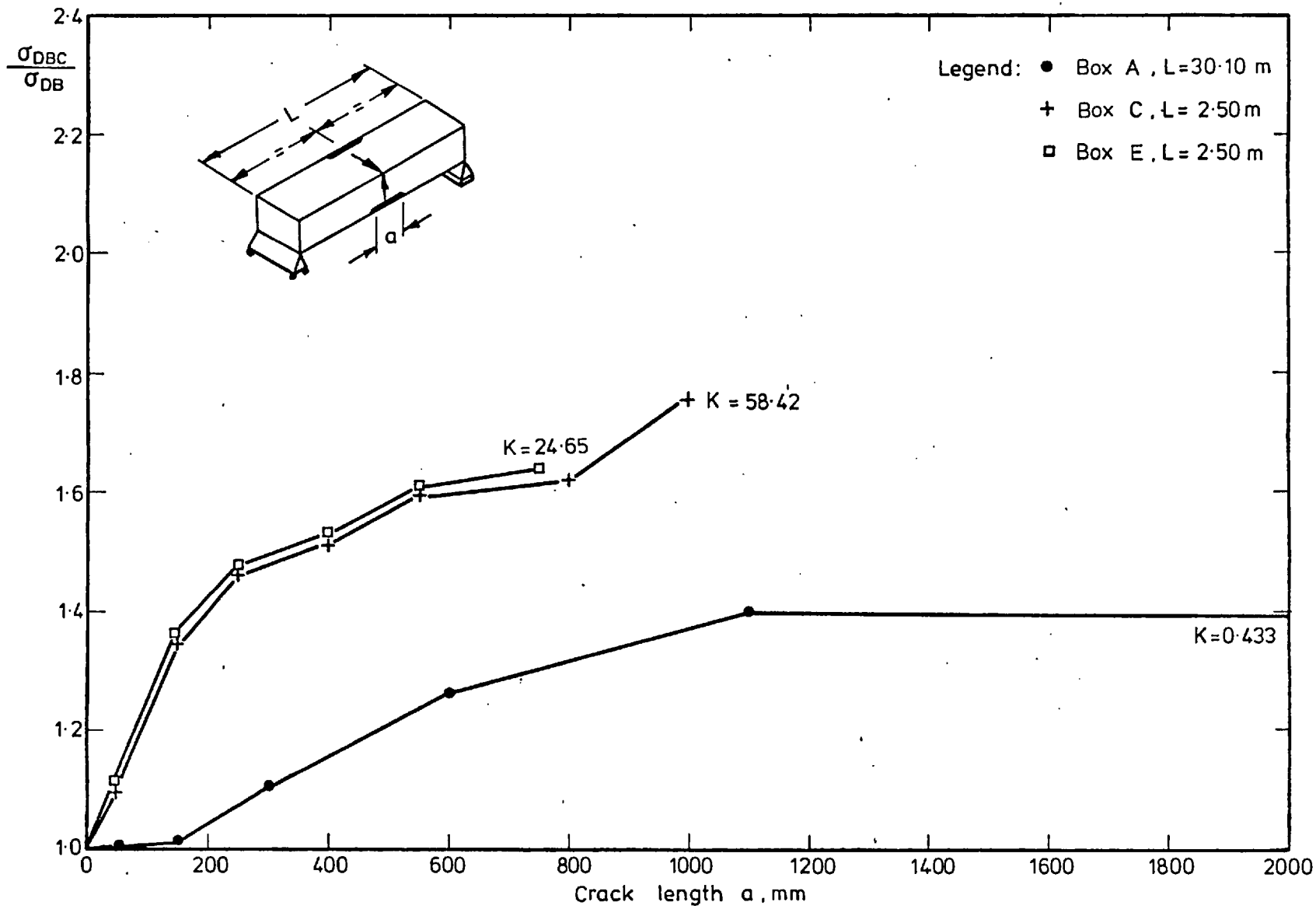


Fig. 8·7 Results for boxes A, C and E showing the relationship between crack length and σ_{DBC}/σ_{DB} for point load

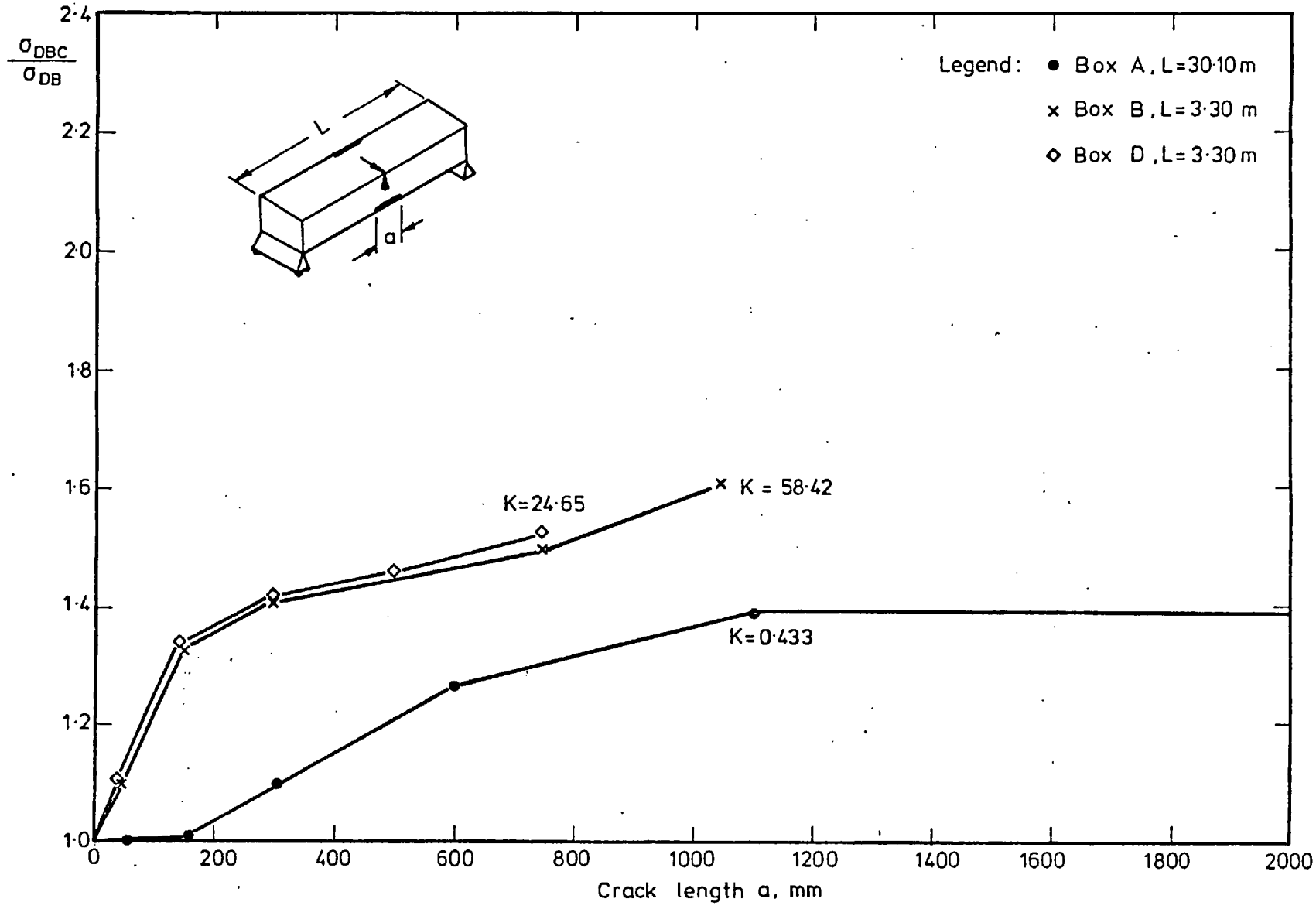


Fig. 8·8 Results for boxes A, B and D showing the relationship between crack length and σ_{DBC}/σ_{DB} for point load

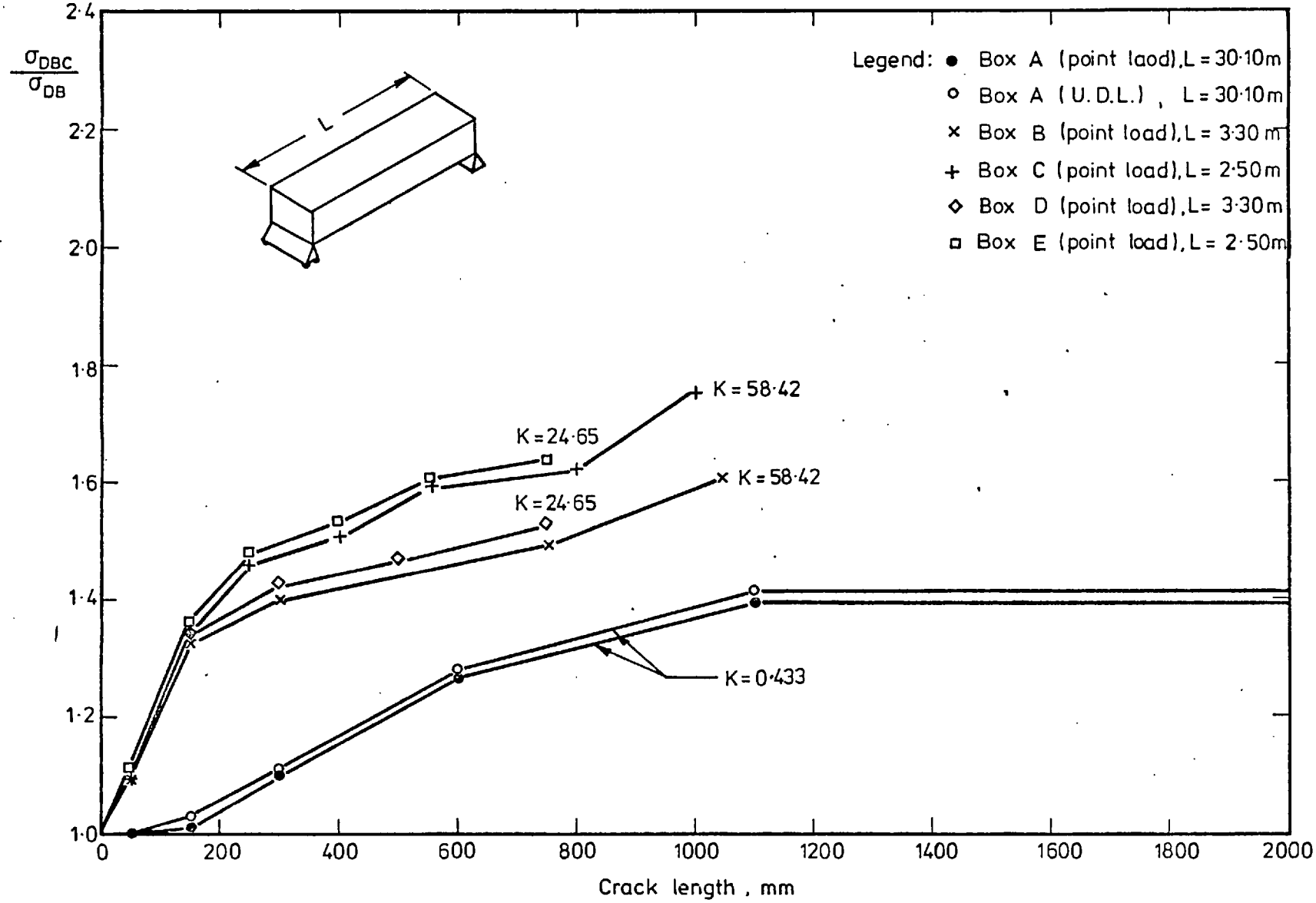


Fig.8·9 Results for all different boxes showing the relationship between crack length and σ_{DBC}/σ_{DB}

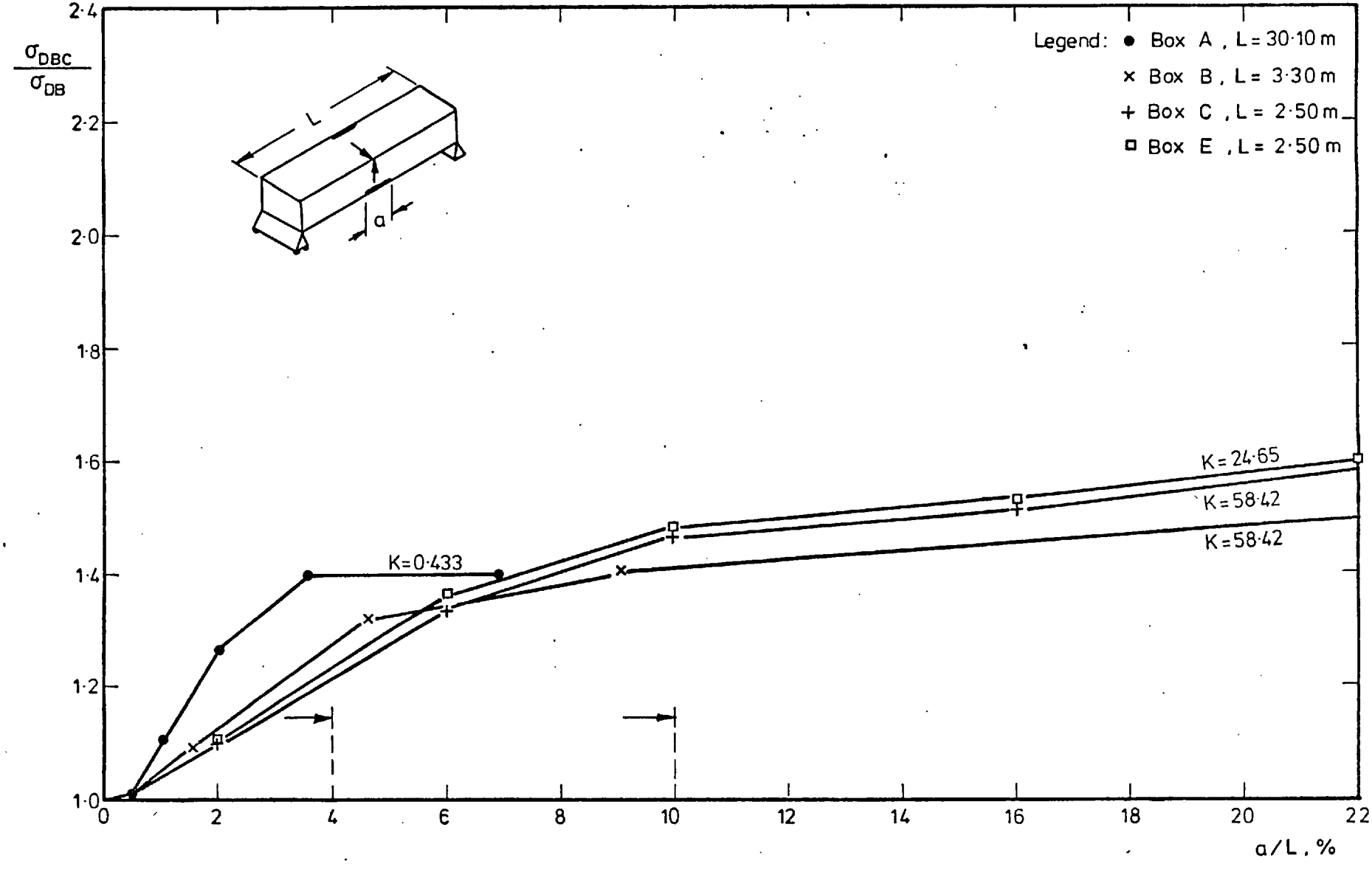


Fig. 8·10 Results for boxes A, B, C and E showing the relationship between a/L and σ_{DBC}/σ_{DB}

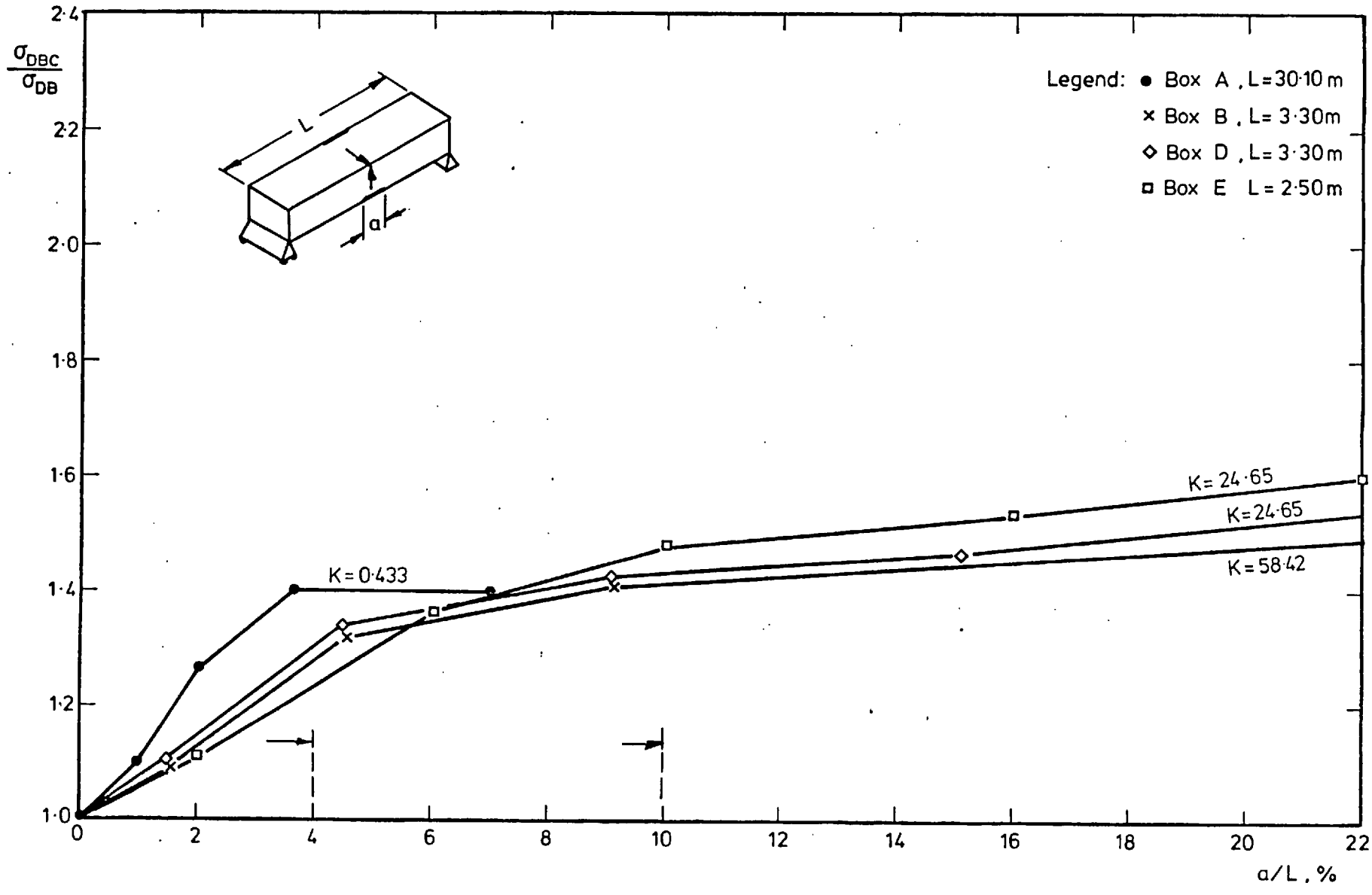


Fig. 8·11 Results for boxes A, B, D, and E showing the relationship between a/L and σ_{DBC}/σ_{DB} for point load

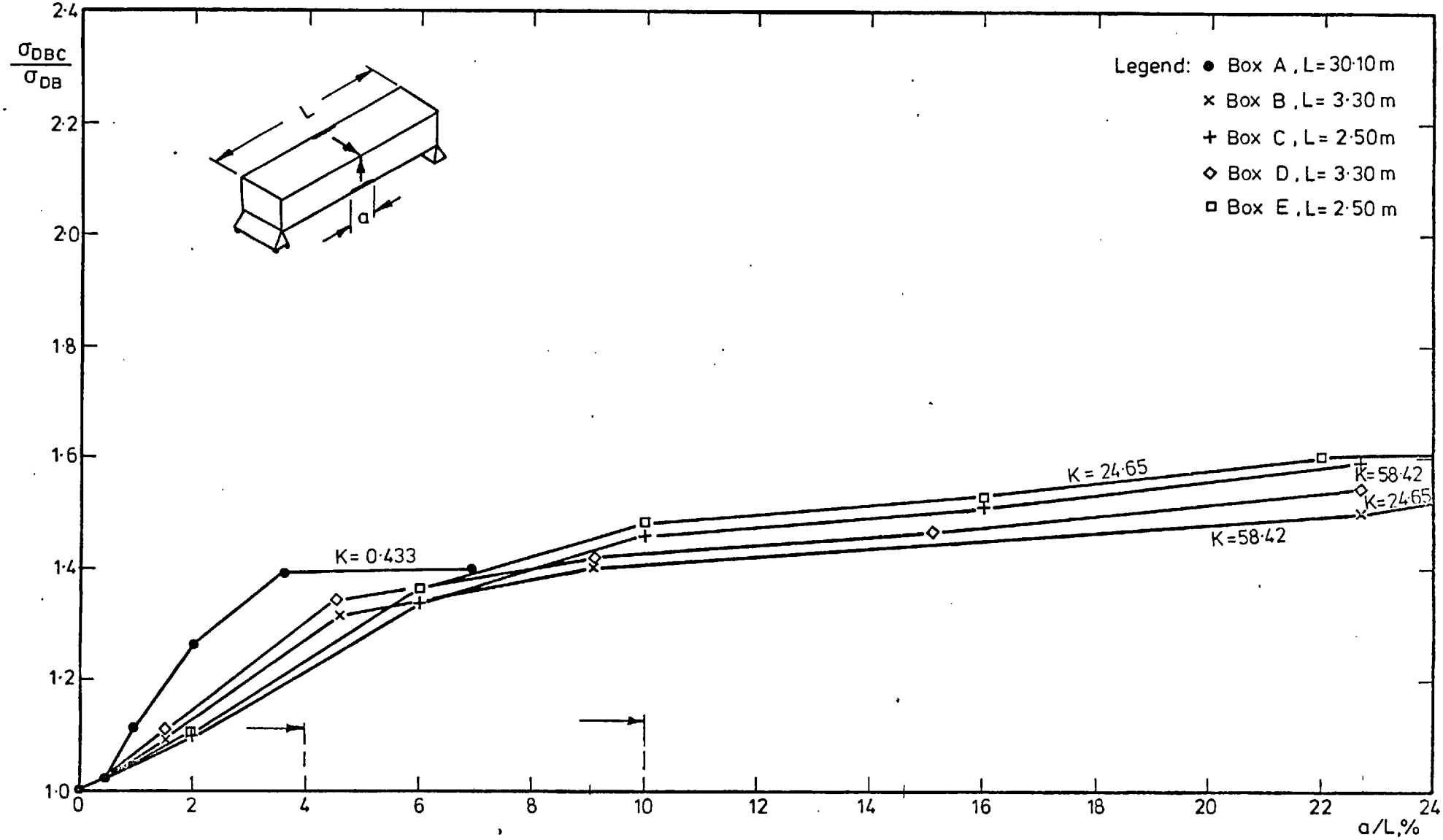


Fig.8·12 Results for all different boxes showing the relationship between a/L and σ_{DBC}/σ_{DB} for point load

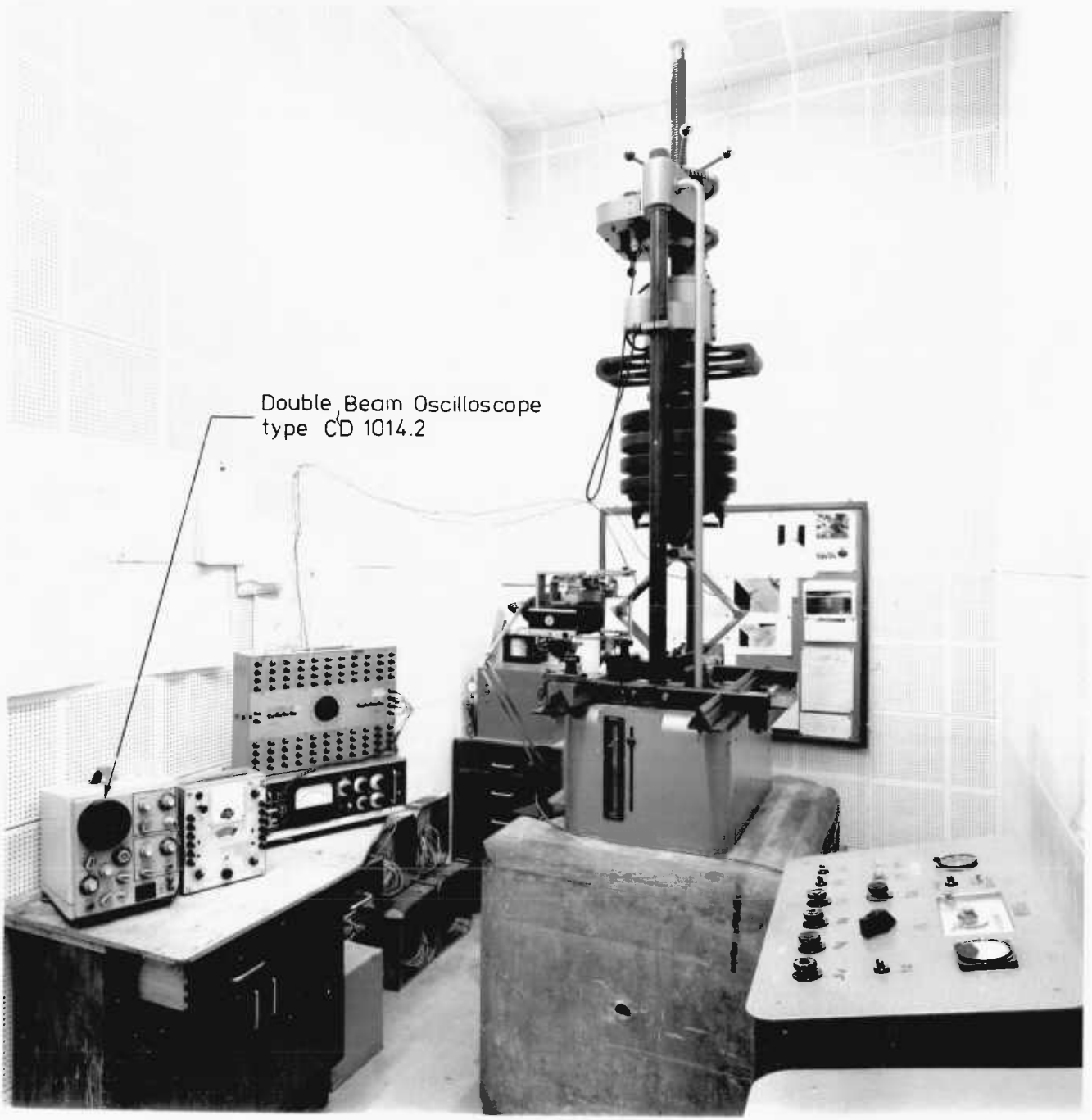


Plate 4·1 General view of the specimen in the vibrophore and the instrumentation used in the experiments

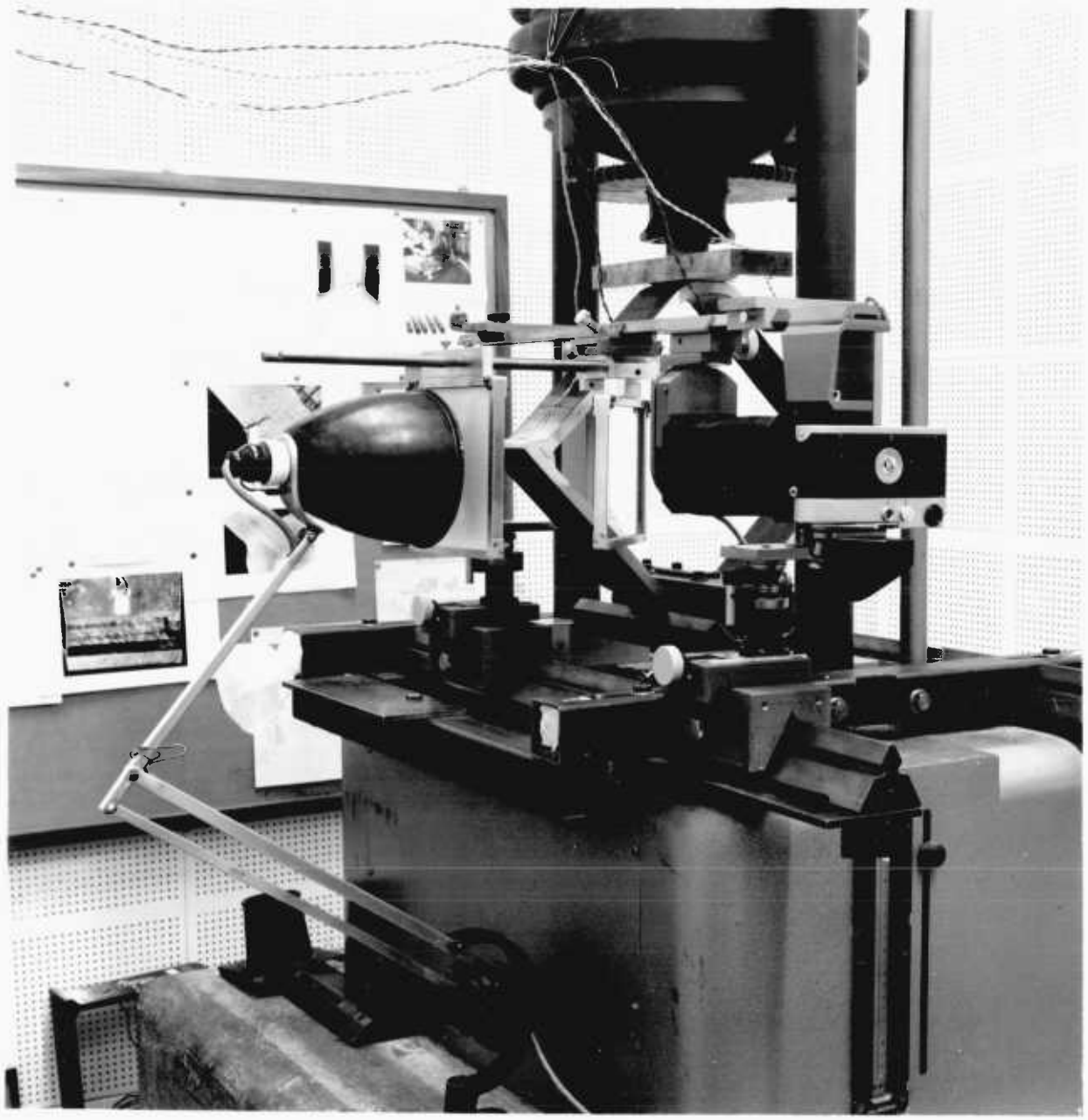


Plate 4·2 A close-up of the camera system

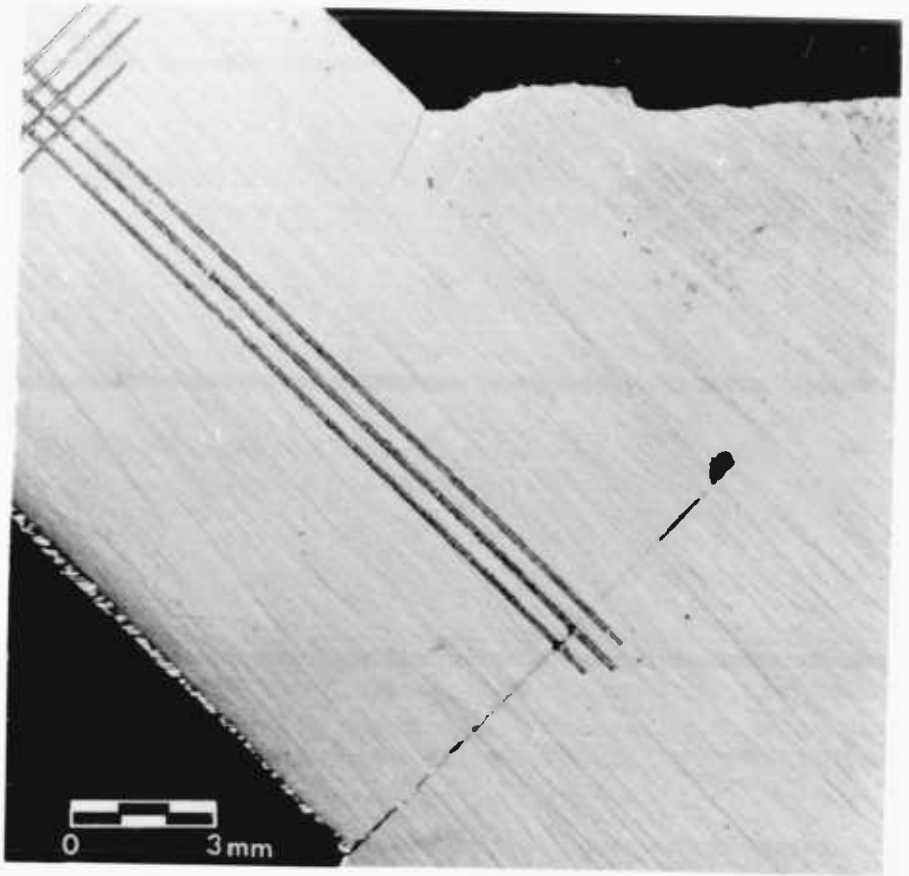


Plate 6·1 Appearance of first visible crack on the side of test series BESFW (Type 1 fatigue failure)

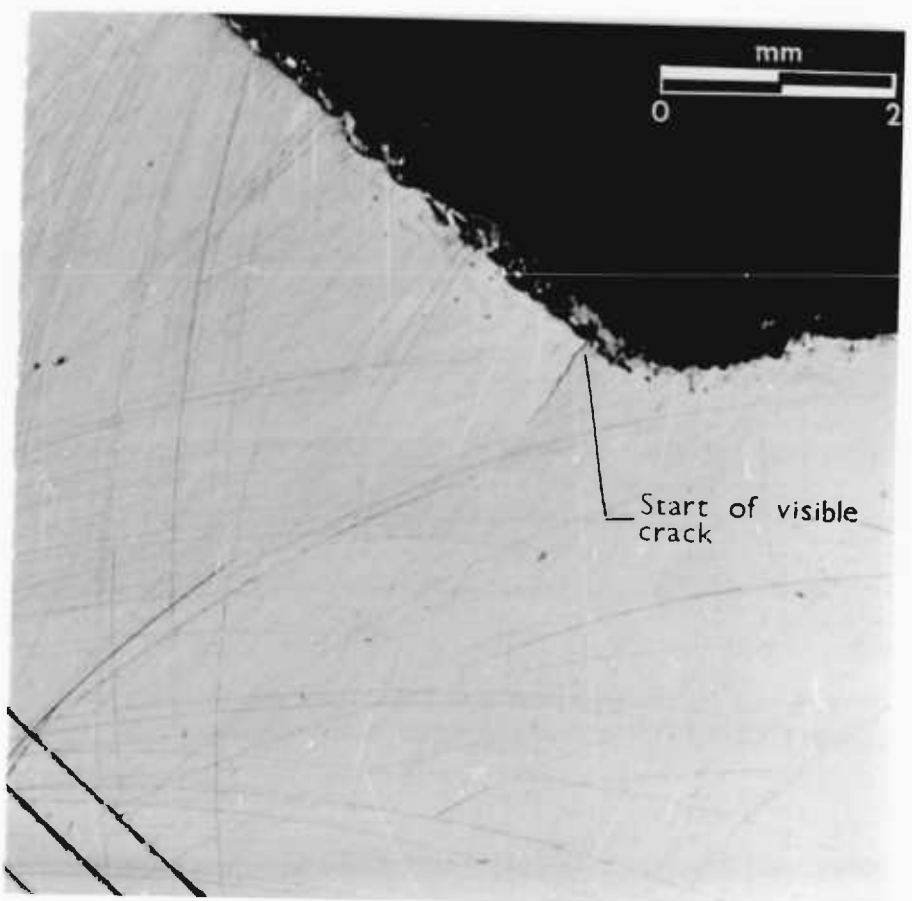


Plate 6·2 Appearance of first visible crack on the side of specimen BEDFG (Type 1 fatigue failure)

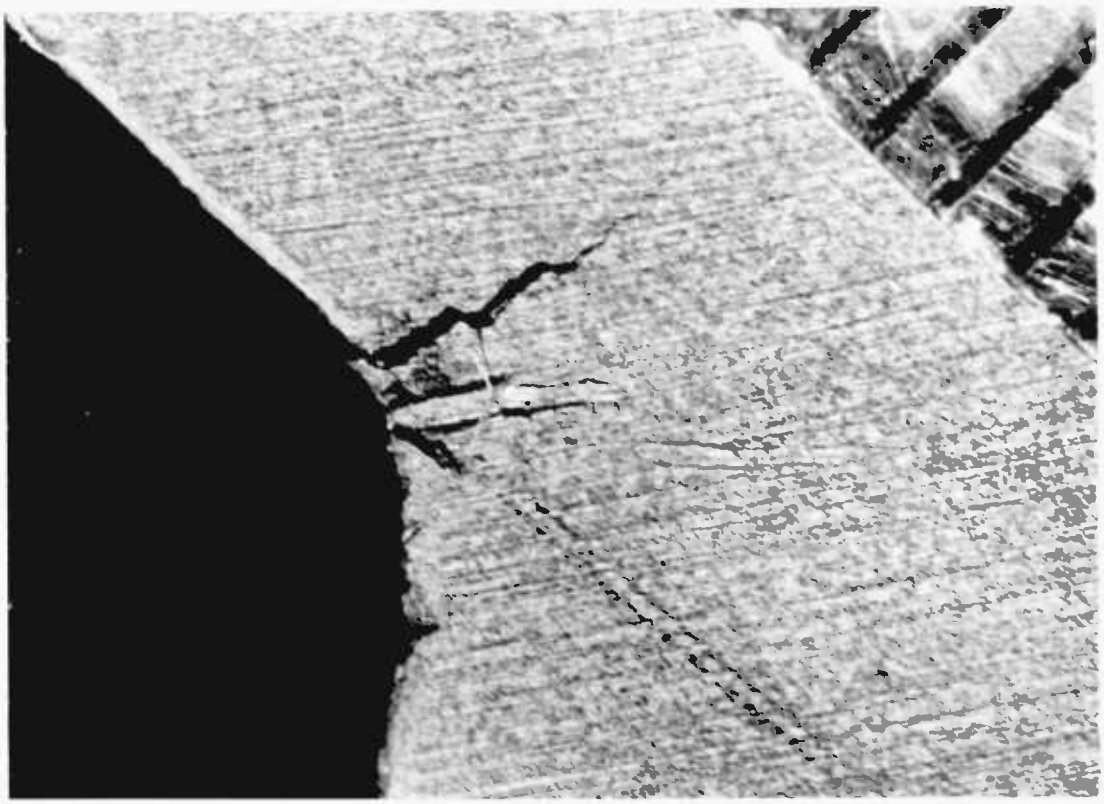


Plate 6·3 Fatigue crack in double fillet weld when sides of specimen are not polished.

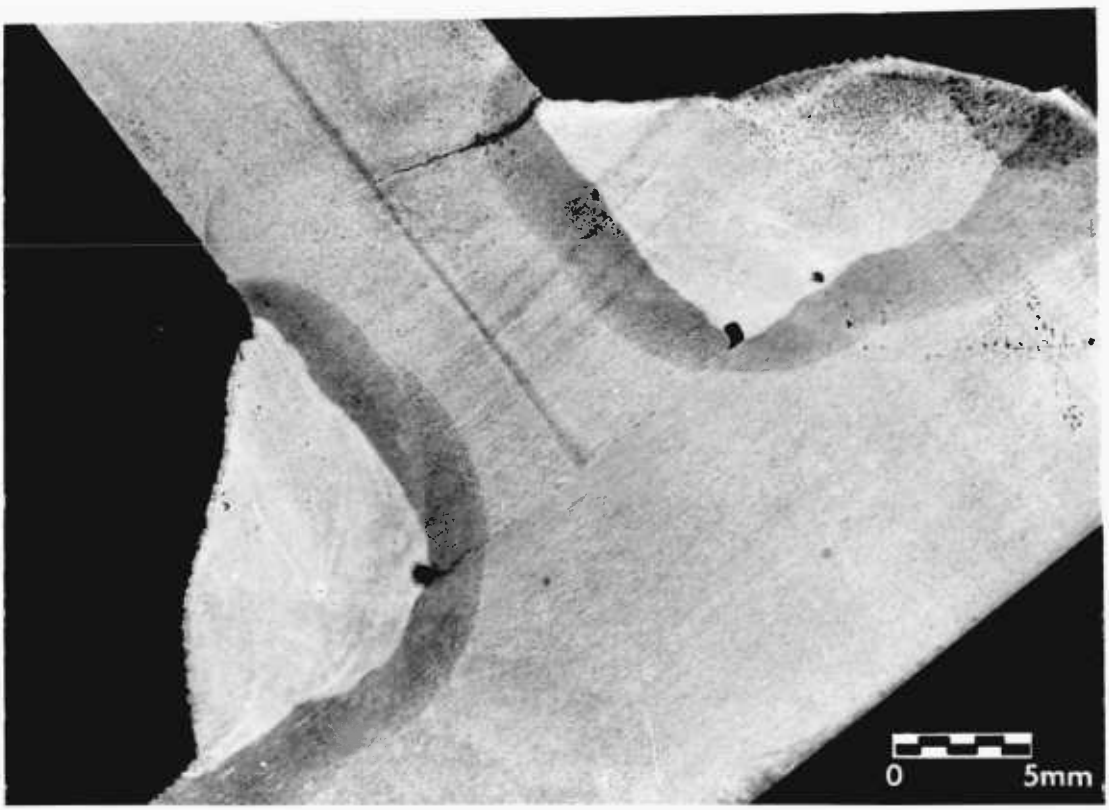


Plate 6·4 Fatigue crack in double fillet weld when sides of specimen are polished

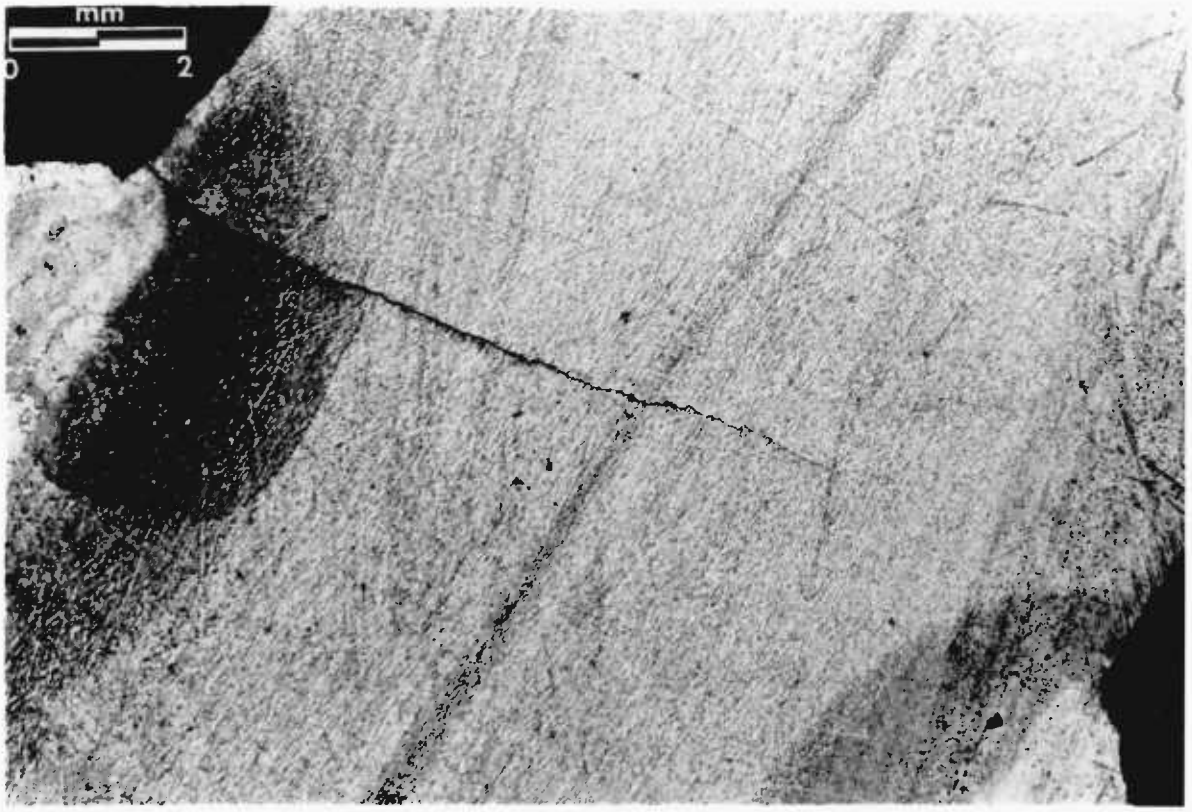


Plate 6·5 Fatigue crack propagation in specimen series BEDFW-17 (Type 1 fatigue failure)

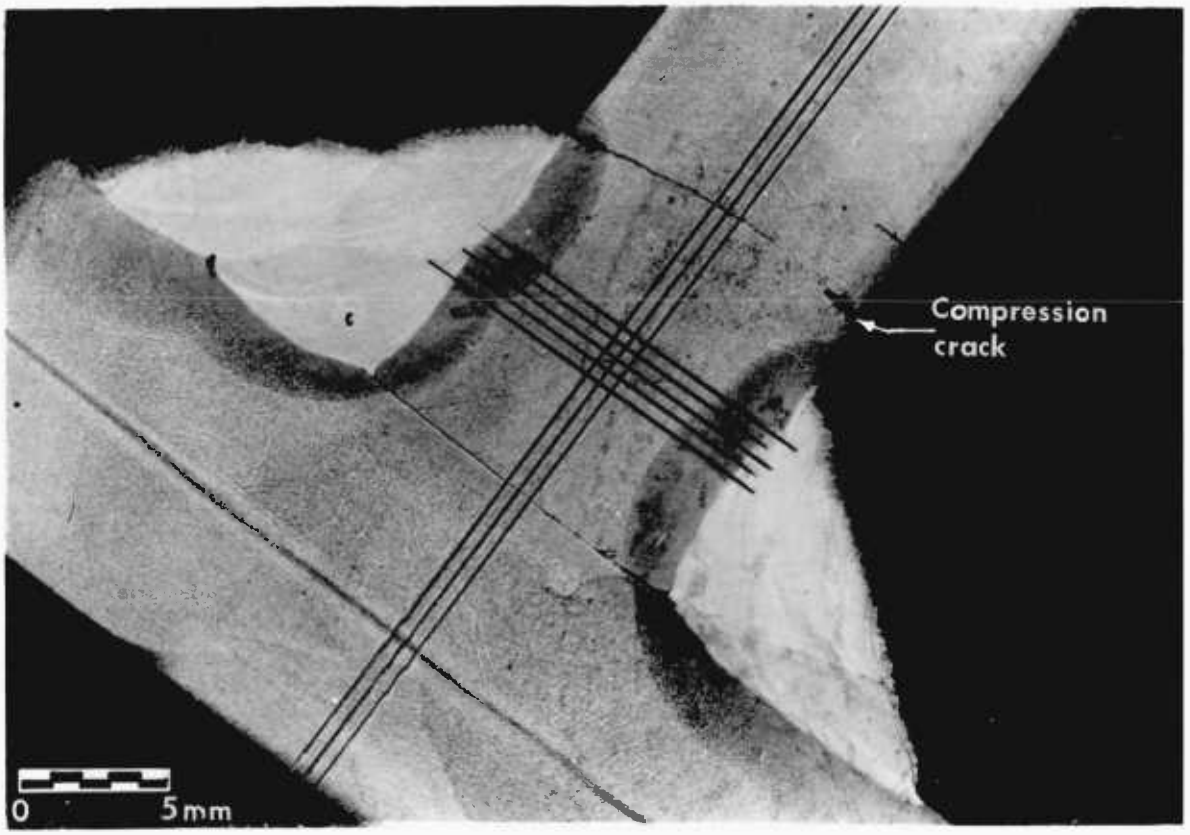


Plate 6·6 Fatigue crack propagation in specimen BEDFW-14 shows the appearance of compression crack.

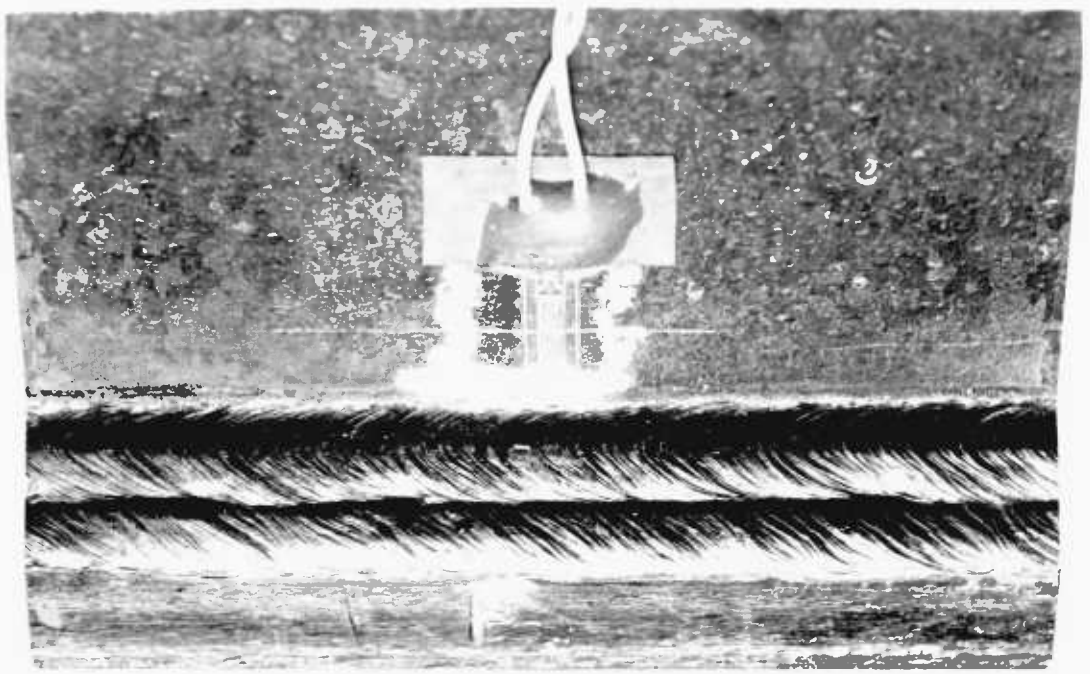


Plate 6.7 Condition of the weld surface for specimen BEDFW-3 before testing (side with strain gauge No. 4)

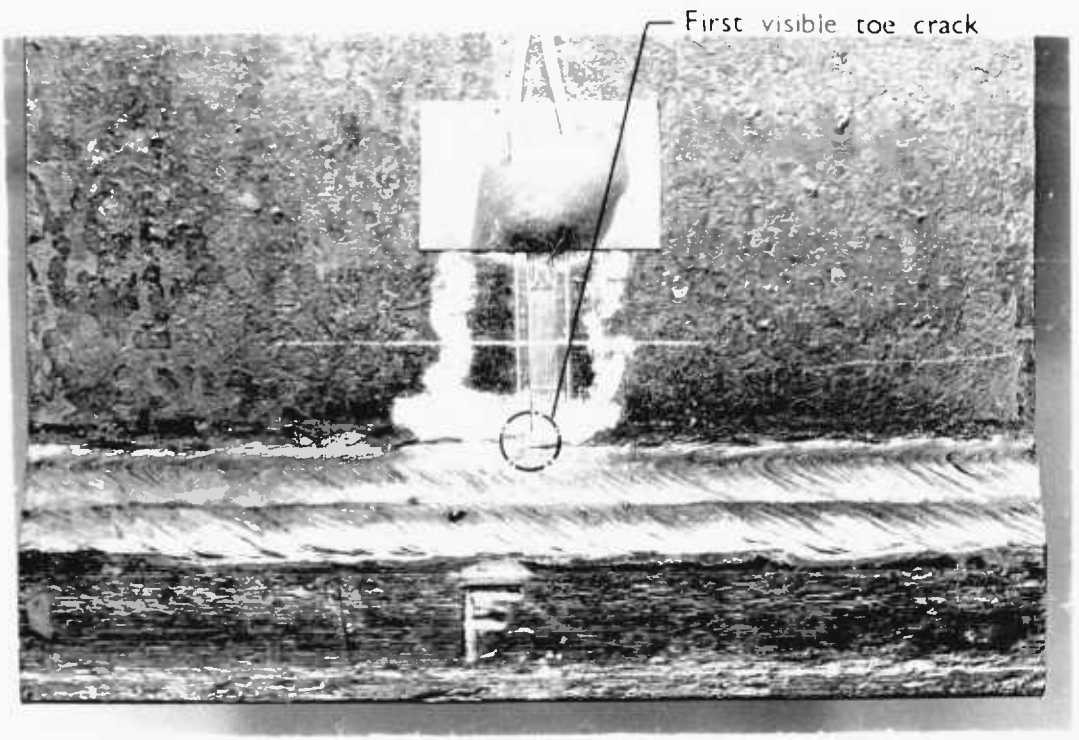


Plate 6.8 Pattern of the propagated crack along the toe of the weld in specimen BEDFW-3 (side with strain gauge No4)

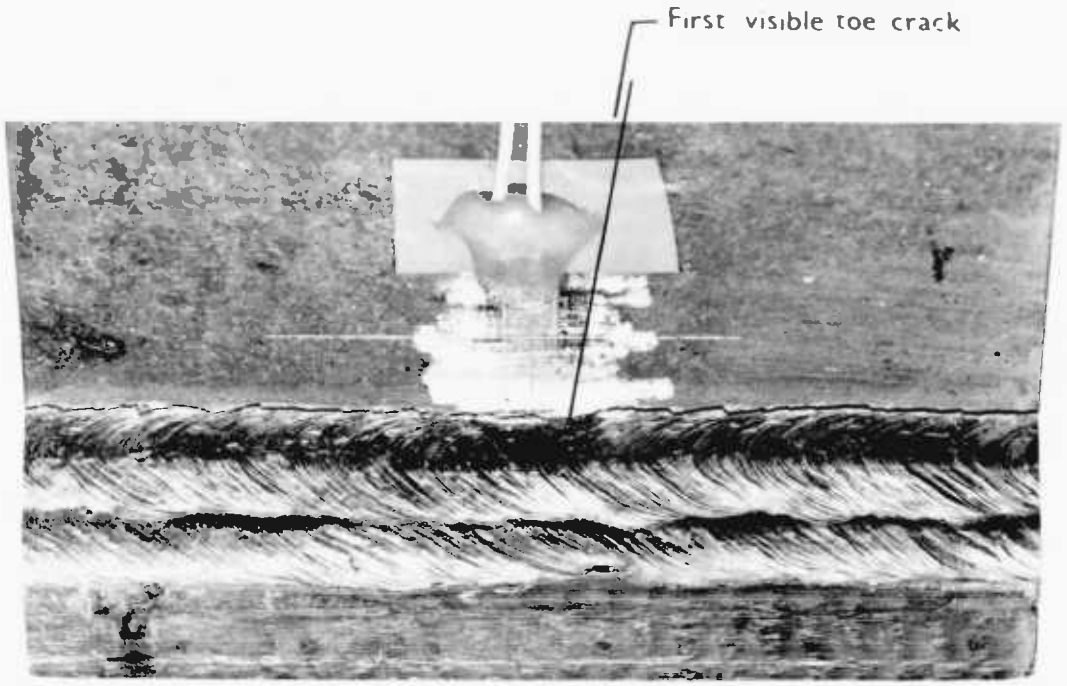


Plate 6.9 Pattern of the propagated crack along the toe of the weld in specimen BEDFW-3 (side with strain gauge No 3)

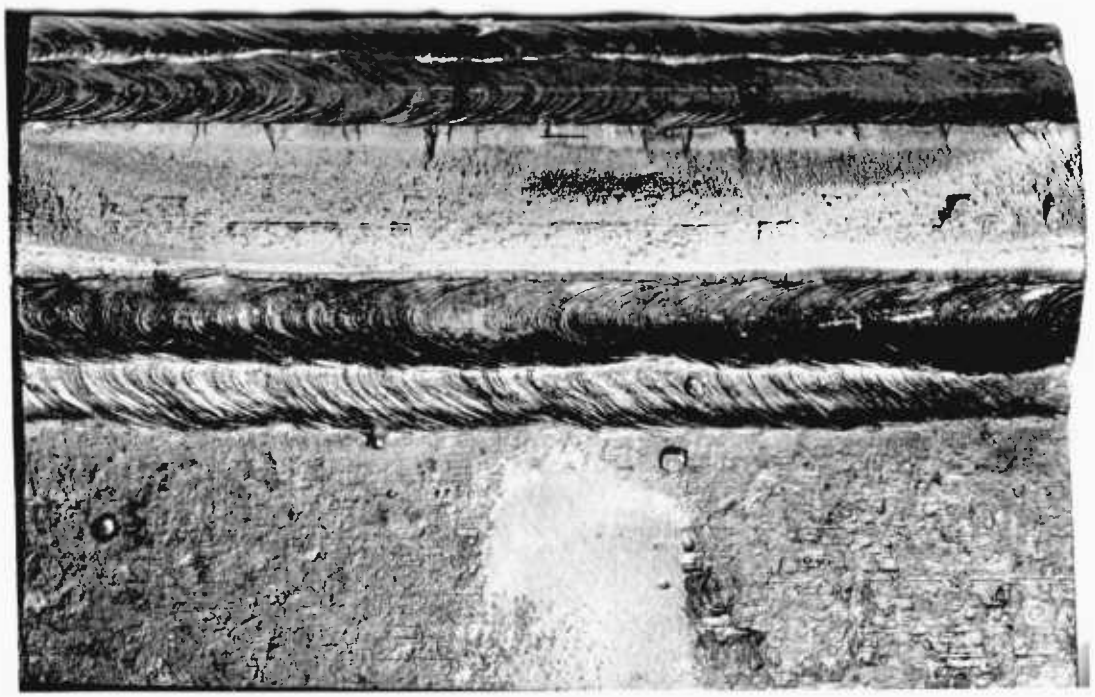


Plate 6.10 Fractured surface in specimen BEDFW-10

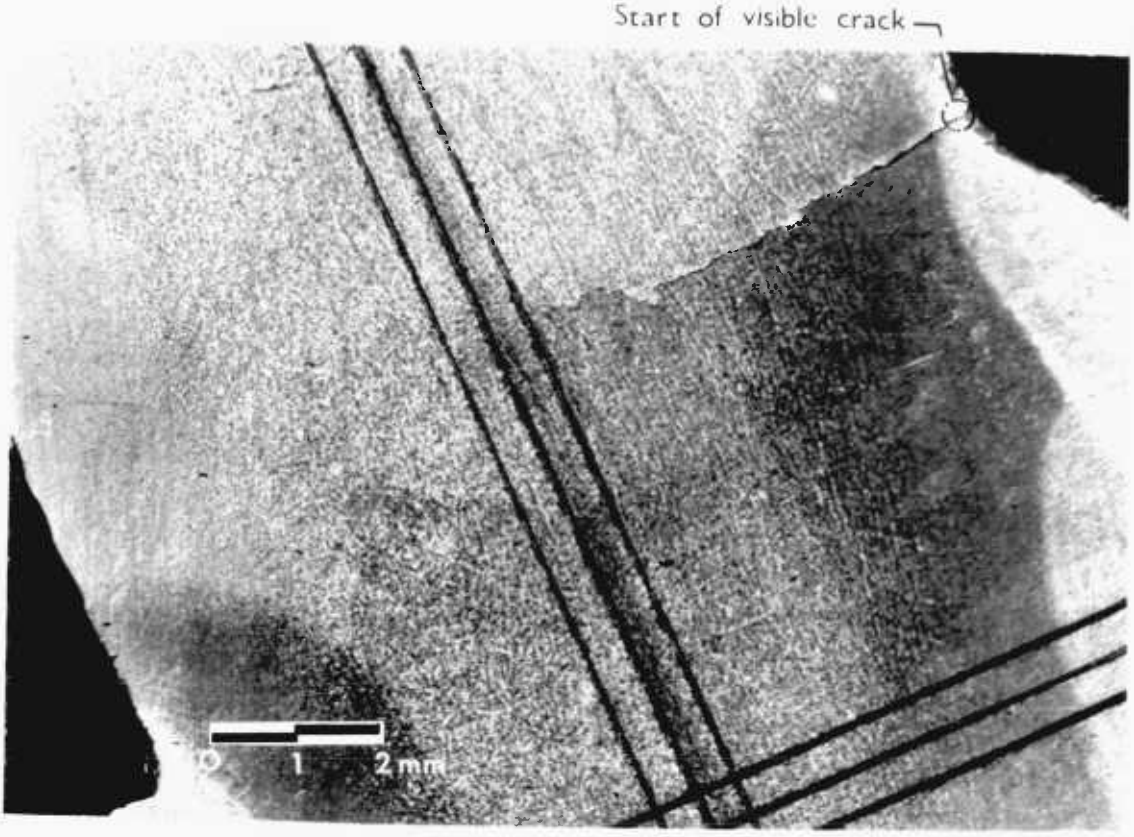


Plate 6·11 Fatigue crack propagation in specimen series BEDFG (Type 1a fatigue failure)

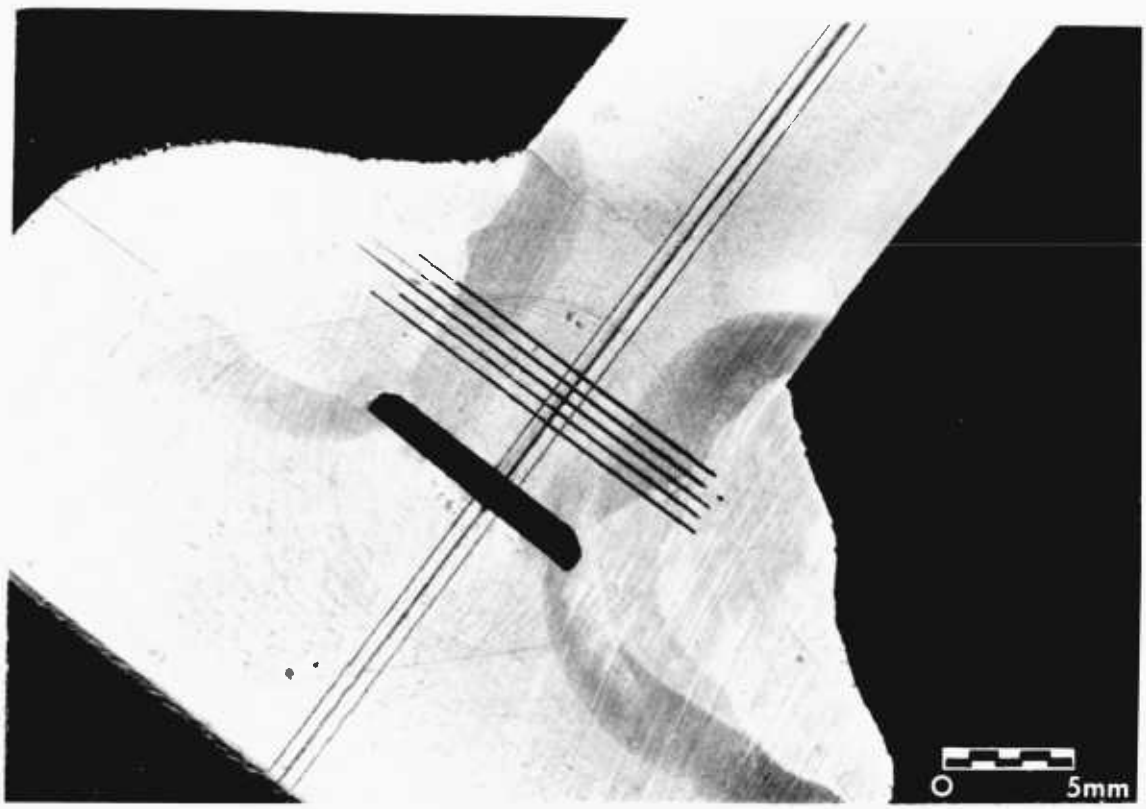


Plate 6·12 Fatigue crack propagation in specimen BEDFG-9 (Type 1b fatigue failure)

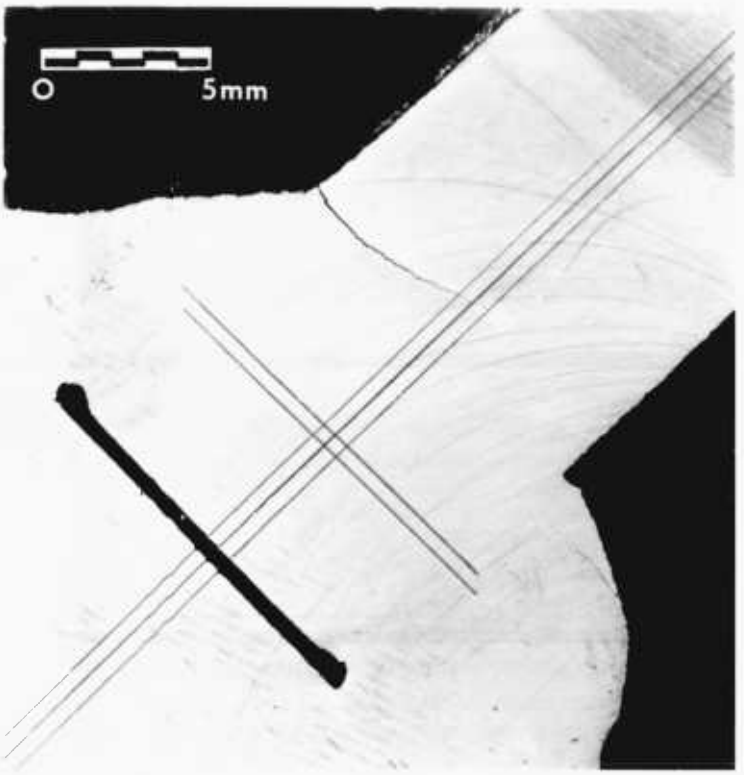


Plate 6·13 Fatigue crack propagation through the plate in specimen BEDFG-15 before appearance of compression crack

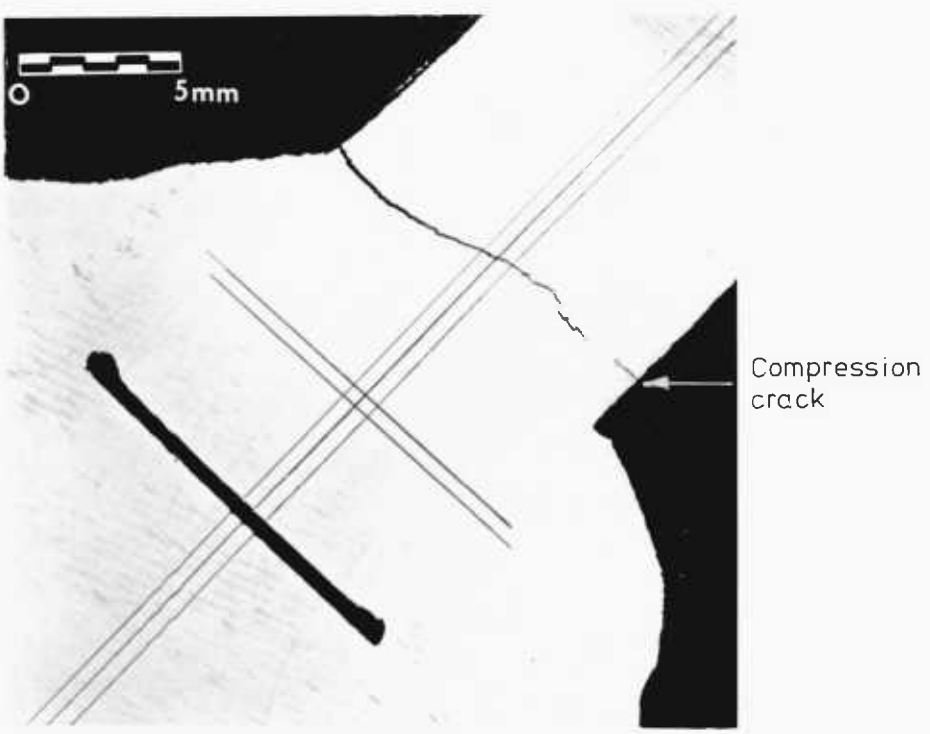


Plate 6·14 Fatigue crack propagation through the plate in speciman BEDFG-15 after appearance of compression crack

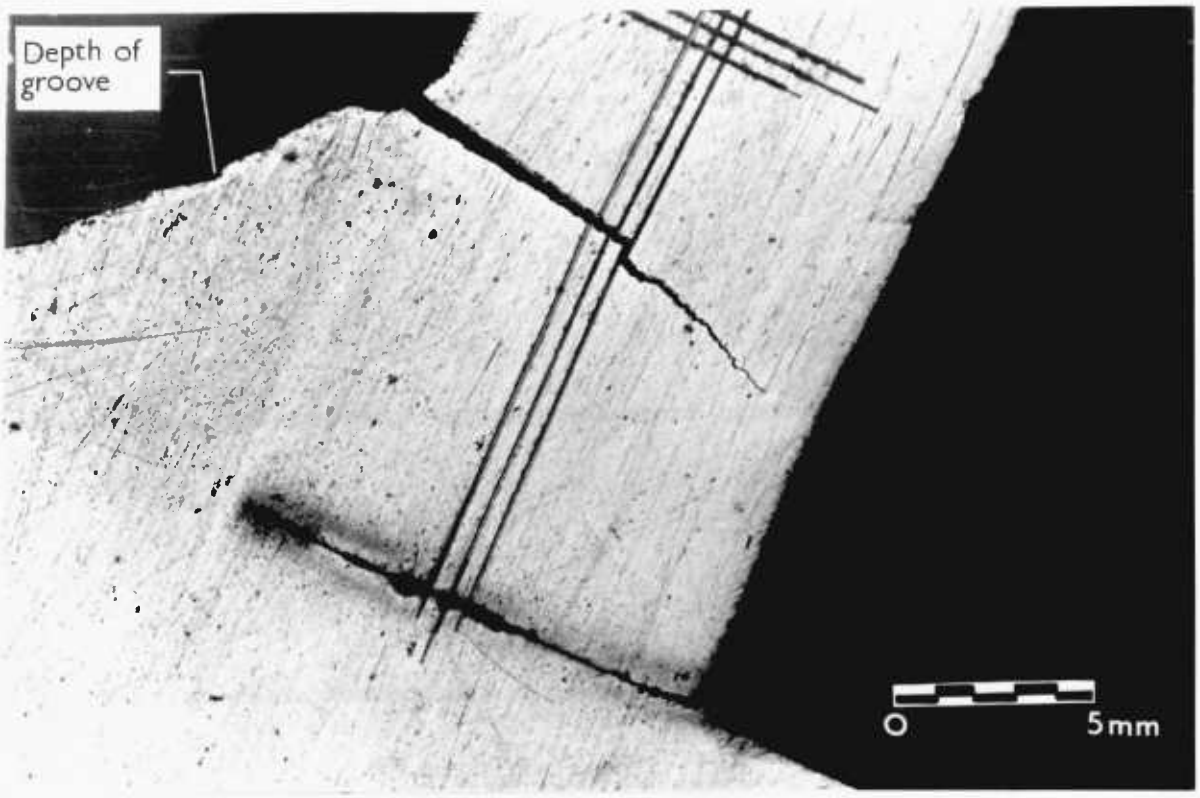


Plate 6·15 Fatigue crack propagation in specimen BESFW-10 subjected to $\sigma_R = 77{\cdot}0$ N/mm^2 (Type 1 fatigue failure)

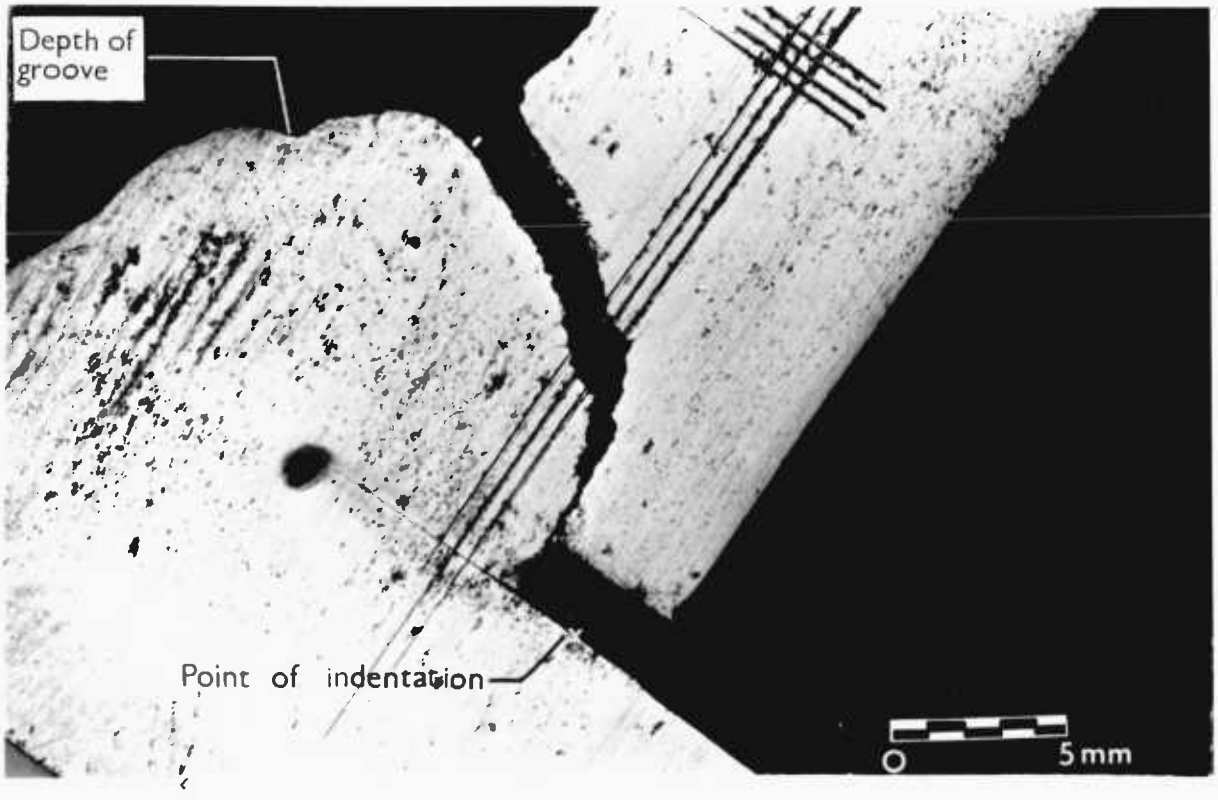


Plate 6·16 Fatigue crack propagation in specimen BESFW-9 subjected to $\sigma_R = 107{\cdot}8$ N/mm^2

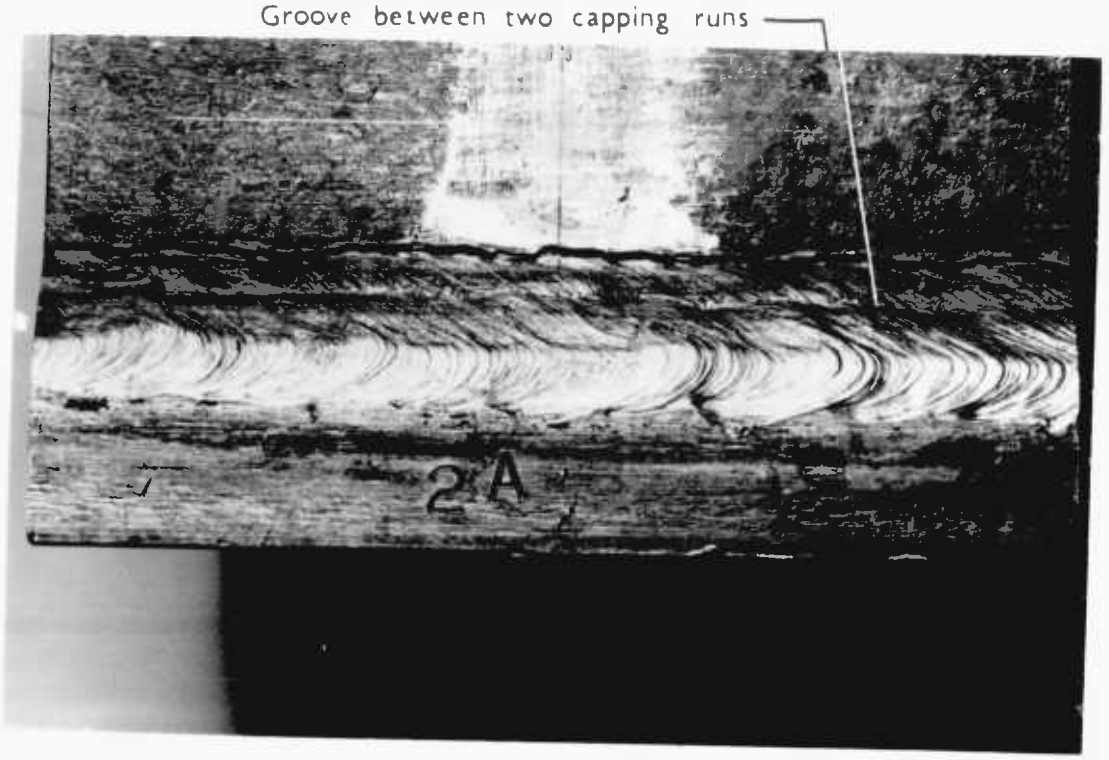


Plate 6·17 Fatigue crack propagation along the toe of the weld in specimen BESFW

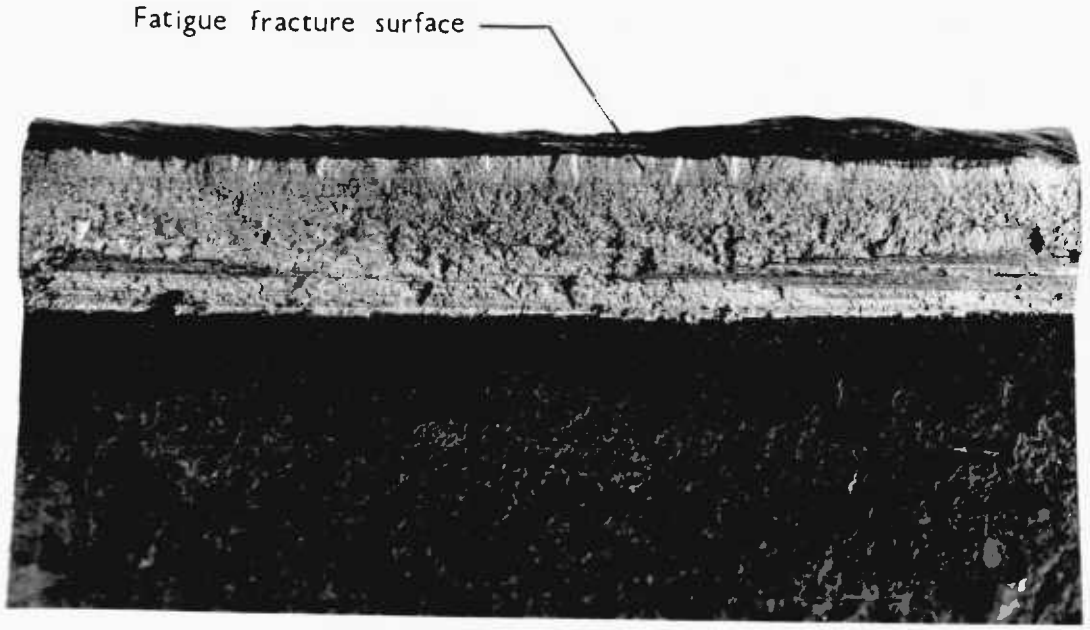


Plate 6·18 Fractured surface of specimen BESFW-9

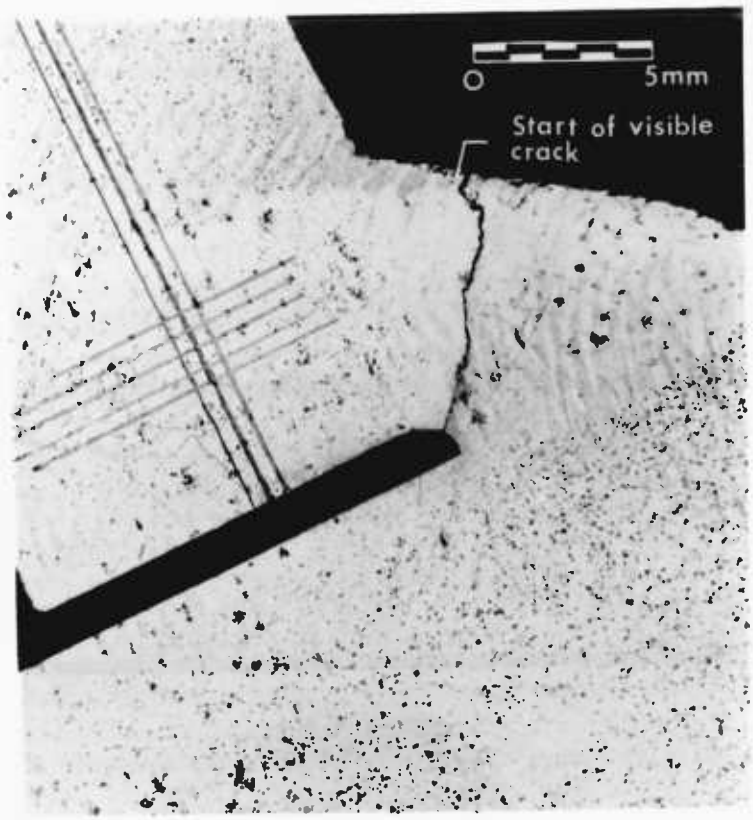


Plate 6·19 Fatigue crack propagation through the weld throat in specimen BESFG-14 (Type 2 fatigue failure)



Plate 6·20 Fatigue crack propagation in specimen BESFG-12 (Type 1 fatigue failure)

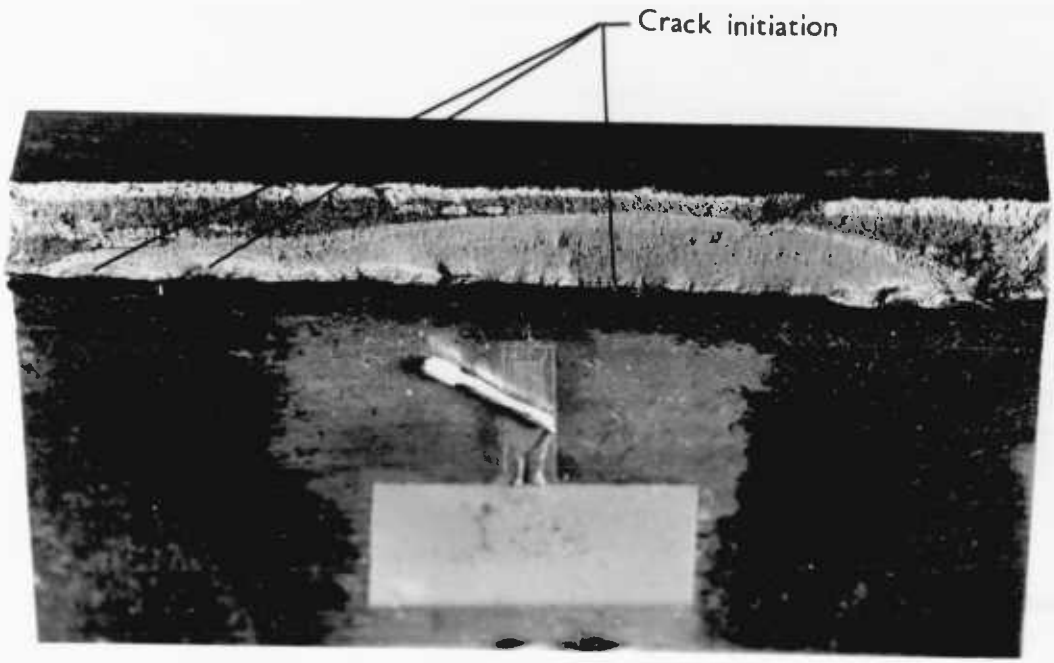


Plate 6·21 Fatigue fracture surface of specimen BESFG-6. Crack initiation from three points at weld surface.

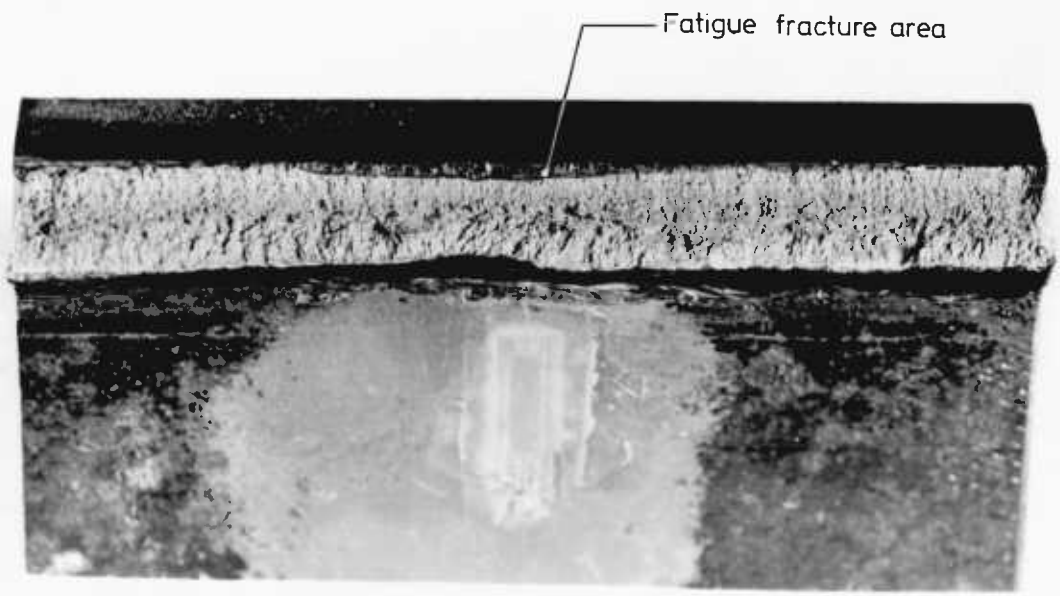


Plate 6·22 Fatigue fracture surface of specimen BESFWI

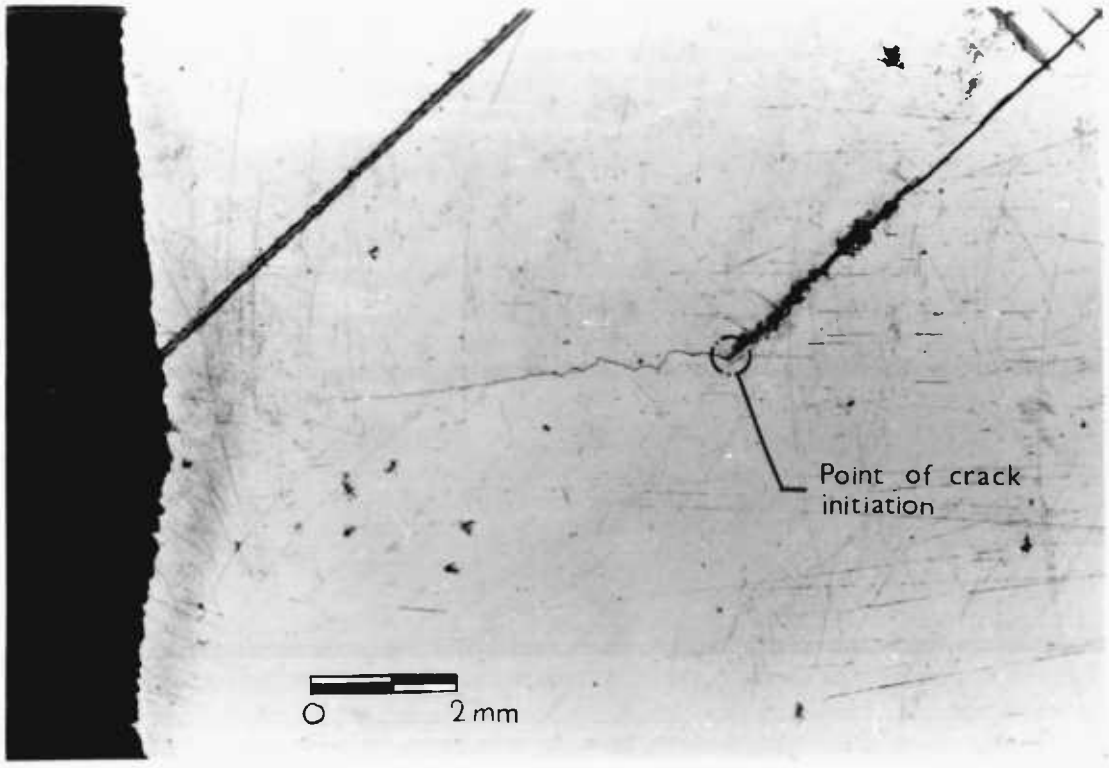


Plate 6·23 Fatigue crack propagation through the weld throat in specimen series BESFW I (Type 3 fatigue failure)

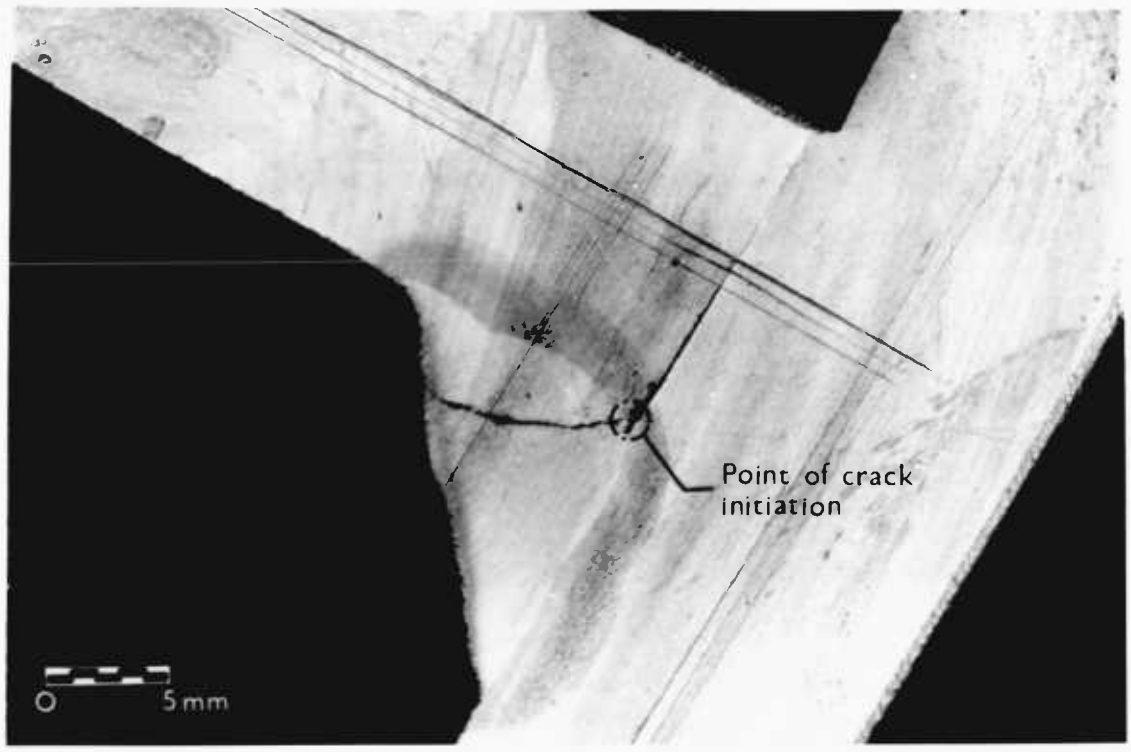


Plate 6·24 General shape of the weld after final failure in specimen BESFWI- (Type 3 fatigue failure)

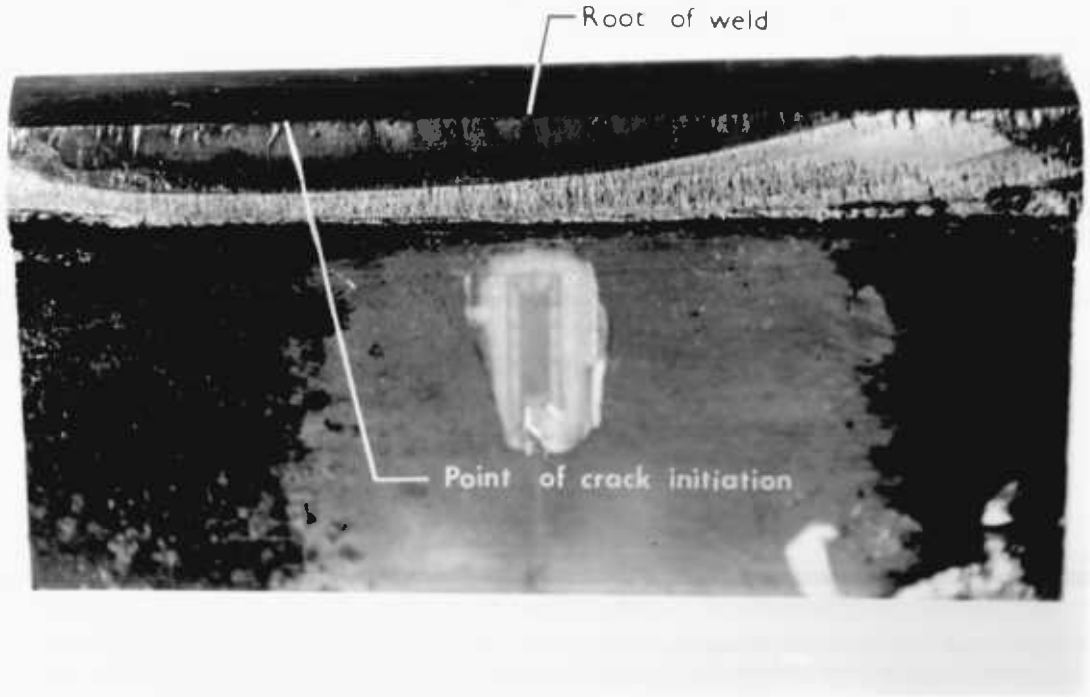


Plate 6·25 Fatigue fracture surface in specimen BESFW I
(Type 3 fatigue failure)

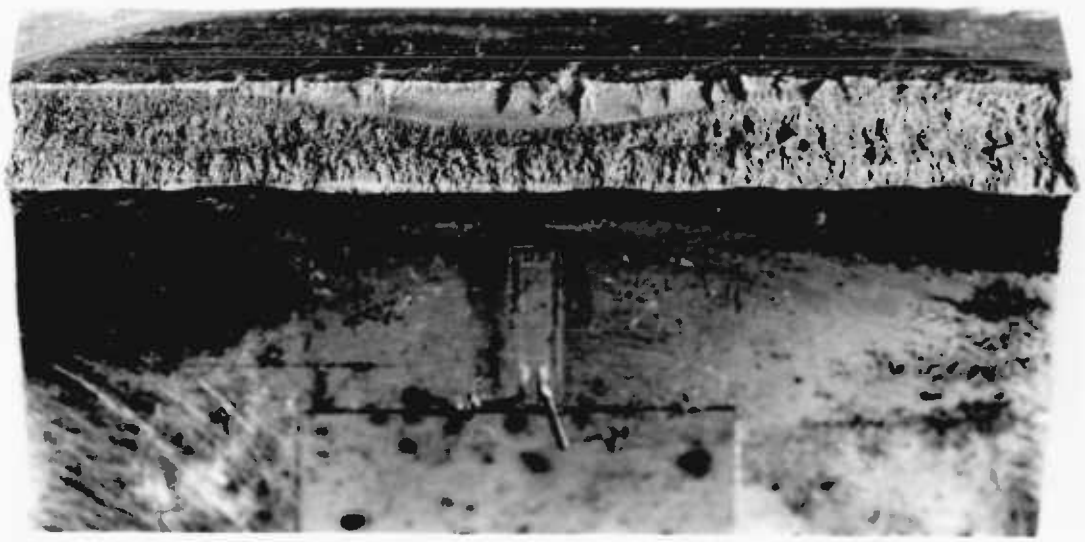


Plate 6·26 Fatigue fracture surface in specimen series BESFG I
(Type 3 fatigue failure)

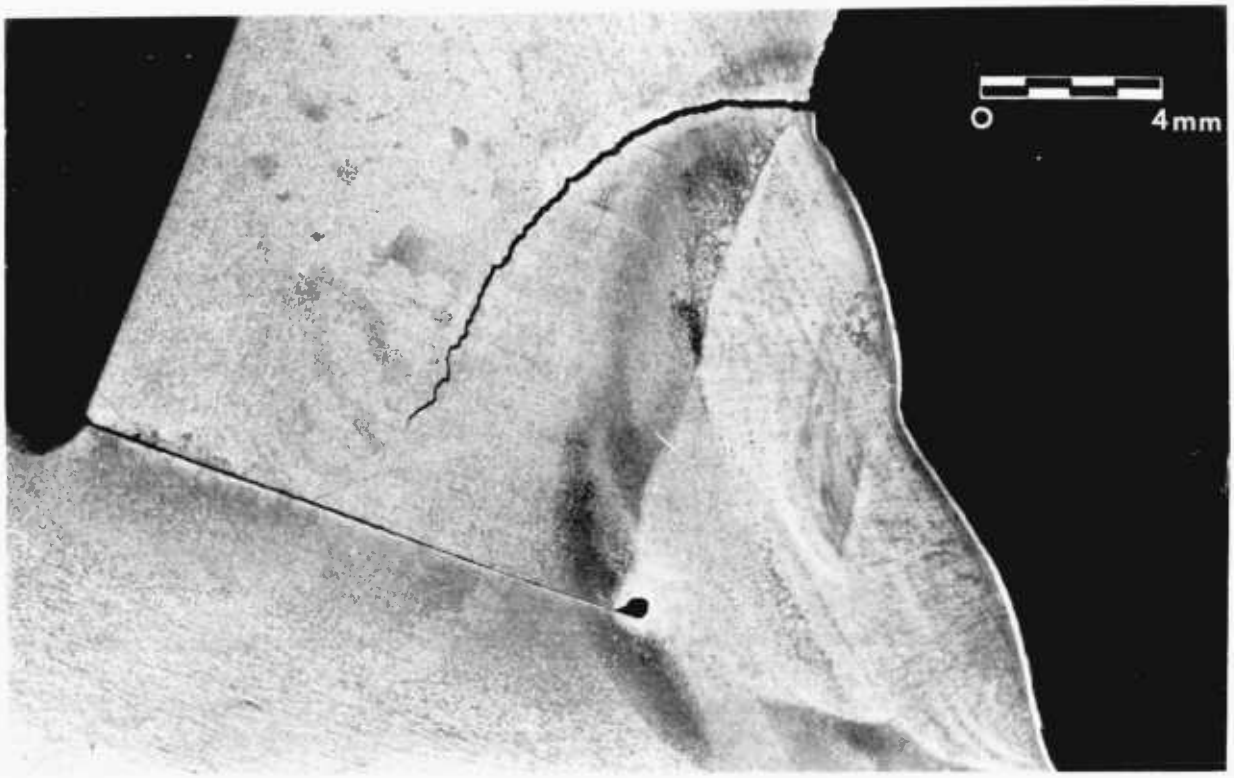


Plate 7.1 Fatigue crack pattern in specimen BESFW I R 1

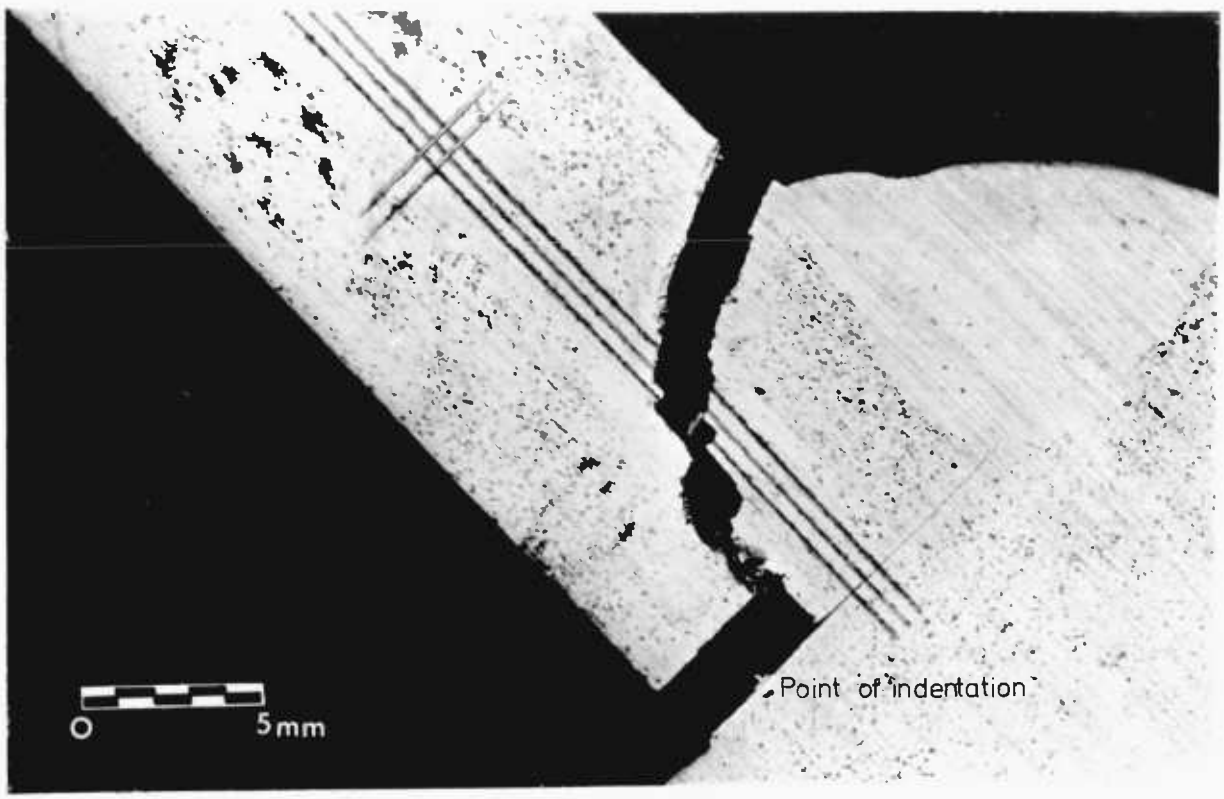


Plate 7.2 Fatigue crack pattern in specimen BESFW-8

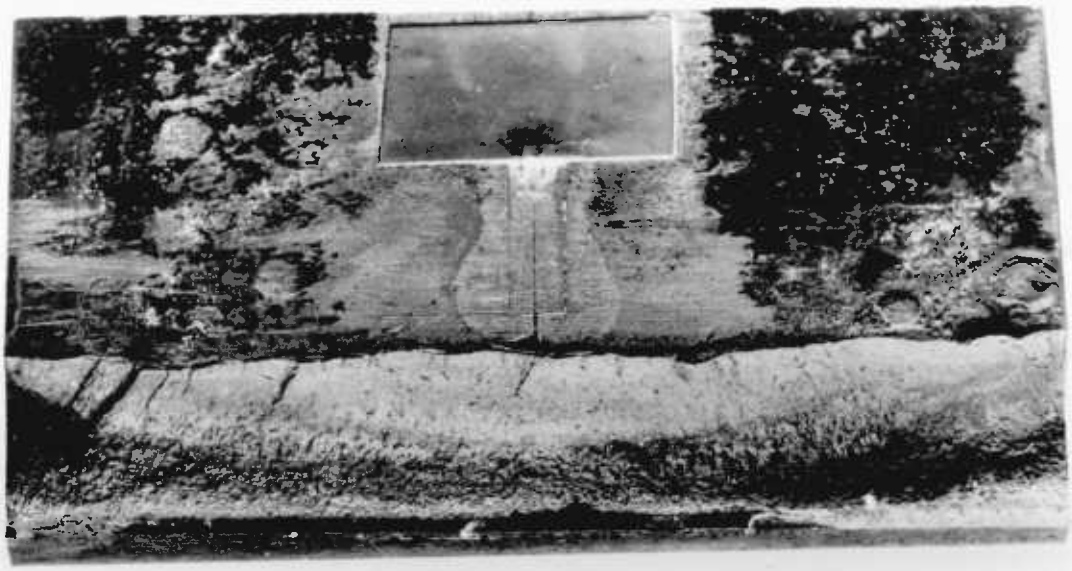


Plate 7·3 Fatigue fracture surface of specimen BESFWIR1

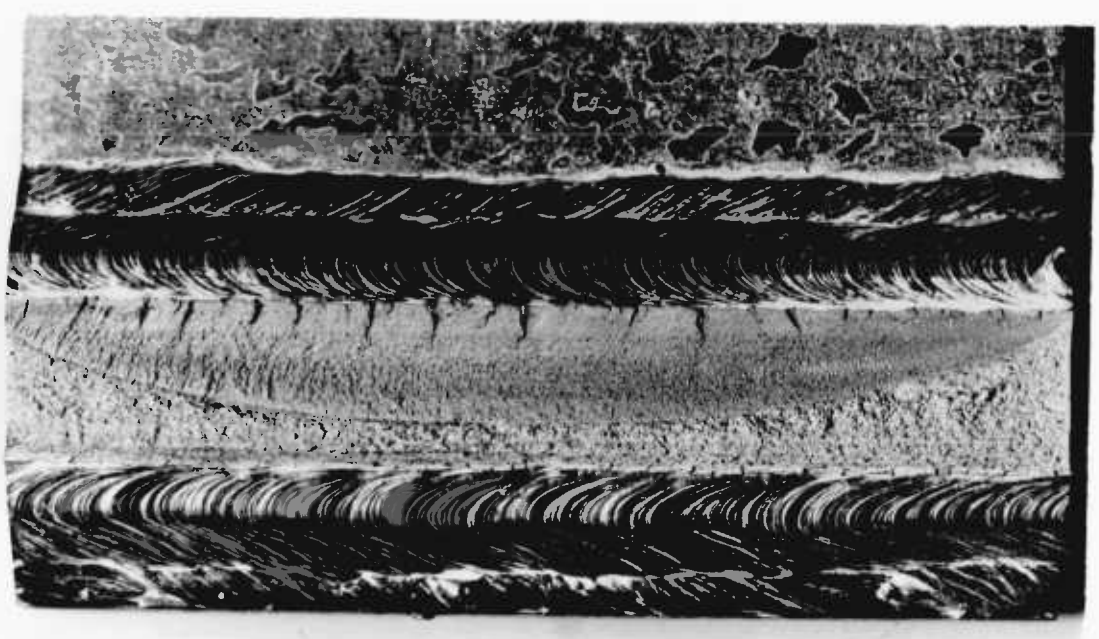


Plate 7·4 Fatigue fracture surface of specimen BEDFW